The development and application of a ChIP and MeDIP assay to determine a link between epigenetics and metabolism in ovarian cancer progression

Carmen Tse

Submitted to Swansea University in fulfilment of the requirements of the Degree of Doctor of Philosophy

Swansea University

December 2021

Abstract

Epithelial ovarian cancer (EOC) has the highest mortality rate of all gynaecological cancers globally. High-grade serous ovarian carcinomas (HGSOC) comprise 75% of EOCs and are characterised by diagnosis at advanced stages due to the late manifestation of non-specific symptoms. The majority of HGSOC cells are found to metastasise to the omentum, an adipocyte-rich membrane which can metabolise chemotherapeutic drugs. EOC patients develop malignant ascites, characterised by the high concentration of cytokines and the presence of multicellular aggregates of EOC cells known as spheroids. Both characteristics can facilitate EOC metastasis. EOC patients initially respond well to platinum-based chemotherapy, but the vast majority will relapse and eventually develop chemotherapy-resistant disease. Long-term survival for OC has shown no recent improvement which highlights the needs for new strategies that improve EOC prognosis. The dysregulation of the epigenetic landscape is a hallmark of EOC leading to the activation of oncogenes and suppression of anti-tumour genes. Ten-eleven translocation (TET) 2 is involved in DNA demethylation, playing a role in transcriptional regulation and gene expression. Oncometabolites present in EOC can inhibit TET2 which leads to aberrant gene regulation, contributing to malignant transformation and progression. Additionally, TET2 can be stabilised by metformin through activation of AMPK, a key regulator of cellular energy homeostasis. Metformin, a biguanide drug widely prescribed as first line treatment for diabetes, has shown promise as an anti-cancer drug. In EOC, metformin has been linked with an increased survival rate in addition to being able to decrease cytokine production and tumour formation in ovarian tumour cells. However, here metformin was found to increase cytokine (IL-6 and IL-8) production in chemosensitive EOC cells, under conditions of a physiological EOC tumour microenvironment (i.e., restricted glucose conditions), but not in chemoresistant EOC cells. This may be unfavourable if metformin was to be repurposed as treatment for EOC and may account for its inconsistent efficacy as a potential therapeutic drug in other cancers. Pathways including AMPK/TET2, and JAK/STAT were explored using techniques such as western Blot, Chromatin immunoprecipitation (ChIP) and methylated DNA immunoprecipitation (MeDIP) as possible mechanisms for this response. Cell viability and proliferation assays were used to explore the effect of oncometabolites on EOC cells. The results will provide insights into how metabolites affect EOC progression in addition to identifying potential therapeutic targets.

DECLARATION

This work has not previously been accepted in substance for any degree and is not being concurrently submitted in candidature for any degree.

Signed: Carmen Tse (candidate)

Date: 20/12/21

STATEMENT 1

This thesis is the result of my own investigations, except where otherwise stated. Where correction services have been used, the extent and nature of the correction is clearly marked in a footnote(s).

Other sources are acknowledged by footnotes giving explicit references. A bibliography is appended.

Signed: Carmen Tse (candidate)

Date: 20/12/2021

STATEMENT 2

I hereby give consent for my thesis, if accepted, to be available for photocopying and for inter-library loan, and for the title and summary to be made available to outside organisations.

Signed: Carmen Tse (candidate)

Date: 20/12/2021

Table of Contents

Acknowledgements

First, I would like to thank Dr James Cronin for giving me the opportunity to work with him and for his supervision and guidance. I am grateful for the knowledge and encouragement he provided throughout my studies.

Next, I would like to thank my supervisors: Dr Lewis Francis and Dr Amy Johnson for their guidance and support. I would also like to express my gratitude to post-doctoral researchers: Dr Julia Davies and Dr Marcos Quintela-Vazquez for their technical assistance as well as Porvair Ltd. for providing the kits to allow me to carry out my studies.

A big thank you to my friends/colleagues in Cronin Group and in the 4th floor office. You have made my PhD, an enjoyable and unforgettable experience. Lastly, I would like to thank my family and friends for motivating me.

Knowledge Economy Skills Scholarships (KESS 2) is a pan-Wales higher level skills initiative led by Bangor University on behalf of the HE sector in Wales. It is part funded by the Welsh Government's European Social Fund (ESF) convergence programme for West Wales and the Valleys.

List of Tables

List of Figures

Abbreviations

Abbreviation	Name
2D	Two dimensional
2-HG	2-hydroxyglutarate
3D	Three dimensional
5caC	5-carboxylcytosine
5faC	5-formylcytosine
5hmC	5-hydroxymethylcytosine
5mC	5-methylcytosine
α-KG	α-ketoglutarate
AICAR	5-aminoimidazole-4-carboxamide-1-β-D-ribofuranoside
AMP	Adenosine Monophosphate
AMPK	AMP-activated protein kinase
ANOVA	Analysis of Variance
APS	ammonium persulfate
ATCC	Adenosine Monophosphate
ATP	Adenosine triphosphate
bp	Base pairs
BSA	Bovine Serum Albumine
C	Carbon
CGI	CpG islands
ChIP	Chromatin Immunoprecipitation
CpG	Cytosine-phosphate-guanine
CO_2	Carbon Dioxide
Ct	Cycle threshold
DNA	Deoxyribonucleic acid
DNMT	DNA methyltransferase
DMEM	Dulbecco modified Eagle's minimal essential medium
DMOG	Dimethyloxaloylglycine
DMSO	Dimethylsulphoxide
dsDNA	Double stranded DNA
ECACC	European Collection of Authenticated Cell Cultures
ECM	Extracellular matrix
EDTA	Ethylenediamine tetraacetic acid
ELISA	Enzyme-linked immunosorbent assay
EMT	Epithelial-to-mesenchymal transition
EOC	Epithelial ovarian cancer
ER	Endoplasmic reticulum
Fe	Iron
GAPDH	Glyceraldehyde 3-Phosphate Dehydrogenase
GAS	Gamma-activated sequence
h	Hours
HDAC	Histone Deacetylase
HG	High glucose
HGSOC	High grade serous ovarian carcinoma
HIF	Hypoxia inducible factor
IgG	Immunoglobulin G
IL	Interleukin
IP	Immunoprecipitation

JAK	Janus Kinase
kD	Kilodaltons
LG	Low glucose
LGSOC	Low grade serous ovarian carcinoma
LPS	Lipopolysaccharides
M	Metformin
MeDIP	Methylated DNA Immunoprecipitation
mTOR	Mammalian Target of Rapamycin
mRNA	Messenger RNA
NaCl	Sodium Chloride
NADPH	Nicotinamide adenine dinucleotide phosphate
$NaHCO_3$	Sodium bicarbonate
N-cad	N-cadherin
NF-κB	Nuclear Factor Kappa-light-chain-enhancer of activated B cells
NG	Normal glucose
n.s.	Not significant
OC	Ovarian cancer
OXPHOS	Oxidative phosphorylation
PAGE	Polyacrylamide gel electrophoresis
PBS	Phosphate Buffer Saline
PCR	Polymerase Chain Reaction
PIC	Protease Inhibitor Cocktail
Q	Glutamine
qPCR	Quantitative PCR
RIPA	Radioimmunoprecipitation assay
RNA	Ribonucleic acid
ROS	Reactive Oxygen Species
RPMI-1640	Roswell Park Memorial Institute 1640
RT	Room temperature
RT-qPCR	Real time quantitative PCR
S	Serine
S.E.M	Standard error of mean
SDH	Succinate dehydrogenase
SDS	Sodium Dodecyl Sulphate
STAT	Signal Transducer and Activator of Transcription
TAE	Tris-acetate-EDTA
TBS	Tris-Buffered Saline
TCA	Tricarboxylic acid
TET	Ten-eleven translocation
TEMED	Tetramethylethylenediamine
Y	Tyrosine

Chapter 1

Introduction

In the UK, ovarian cancer (OC) is the sixth most common cancer in females and the sixth most common cause of female cancer deaths (Cancer Research UK, 2014). The high fatality ratio is due to non-specific symptoms such as abdominal, gastrointestinal, urinary, or pelvic pain which results in late detection of OC (Smolle, et al., 2014; Siegel, et al., 2018). Many women with advanced OC develop ascites which is an indicator of malignancy (Shen-Gunther & Mannel, 2002). Growth factors secreted by stromal and cancer cells are present in the ascitic fluid which provides an ideal microenvironment for tumour growth (Mills, et al., 1990). Advanced OC treatments involve tumour debulking and chemotherapy utilising a combination of taxane-based drugs or platinum-based drugs (Barnholtz-Sloan, et al., 2003). Most patients respond well initially to treatment, but the majority will relapse, displaying chemoresistant tumours (Ozols, 2005). Long-term survival for OC patients has shown no recent improvements, highlighting the need for new strategies that improve OC prognosis (Timmermans, et al., 2018).

1.1. Epithelial ovarian carcinomas

The majority of ovarian cancers are sporadic however hereditary syndromes constitute 10% of ovarian cancers, with 90% of these hereditary cancers associated with germline mutations in *BRCA1* and *BRCA2* tumour suppressor genes (Ramalingam, 2016). BRCA1 and BRCA2 are components of the homologous recombination DNA repair pathway, required to repair breaks in double-stranded DNA (dsDNA). Their deficiency results in hypersensitivity to DNA damaging agents as well as slower repair of dsDNA breaks (Rosen, et al., 2009; Botwell, 2010). Primary ovarian tumours are split into subgroups: epithelial, mesenchymal, sex-chord stromal or germ cell depending on their origin (Tanaka, et al., 2016). However, ovarian cancers of epithelial origin are the most common, constituting over 90% of ovarian neoplasms (Rosen, et al., 2009). There is a controversy concerning the origins of EOC. One theory comprises EOC arising from neoplastic conversion of normal ovarian surface epithelium (OSE) stemming from ovulatory rupture and post-ovulatory healing, requiring frequent transitions between mesenchymal and epithelial cell phenotype for migration and proliferation to regenerate the epithelial surface. The conversion of the OSE to a cuboidal/columnar phenotype is indicative of tubal metaplasia and is often accompanied by the acquisition of epithelial markers and the suppression of mesenchymal markers. Inclusion cysts may also initiate OSE metaplasia and malignant transformation due to overcrowding as OSE trapped in the underlying stroma are exposed to more growth

factors, providing cues for neoplastic progression. Another potential site of EOC origin is the distal fimbriae of the fallopian tube. Serous tubal intra-epithelial carcinomas develop via the acquisition of preneoplastic lesions known as “p53 signatures” in tumour initiating cells in distal oviduct fimbriae, which then shed and invade the ovary (Klymenko, et al., 2017b).

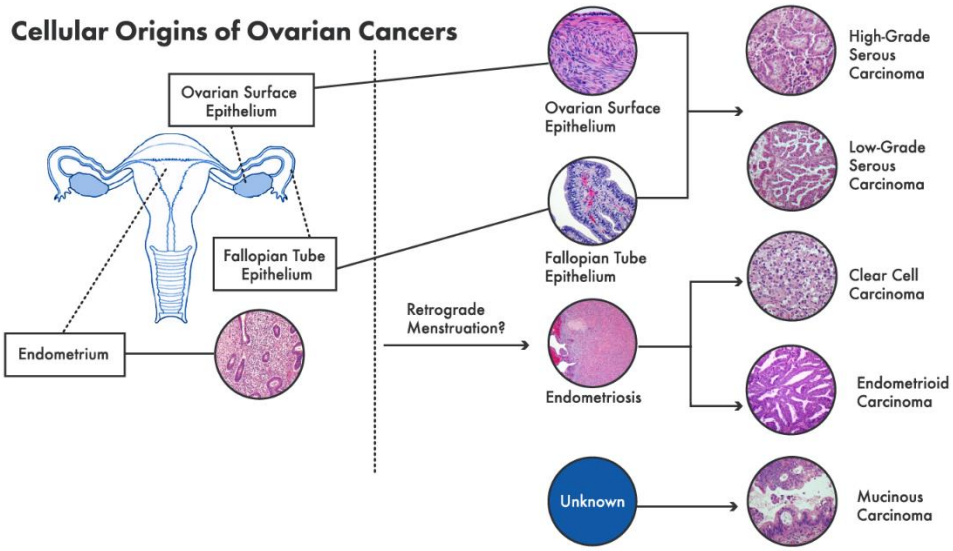

Figure 1. Cellular origins of ovarian carcinomas
Ovarian cancers can originate from locations outside the ovaries including the fallopian tube or endometrium. Figure obtained from: (National Academies of Sciences, Engineering, and Medicine, 2016).

EOCs are a heterogenous group of diseases subclassified into histological subtypes: serous, endometrioid, clear cell and mucinous carcinomas (Figure 1), which can then be further categorised, by distinct molecular characteristics, into two groups designated as Type I (low-grade) and Type II (high-grade). Low-grade serous, low-grade endometrioid, clear cell and mucinous carcinomas are Type I tumours. Type II tumours include high-grade serous, high-grade endometrioid and undifferentiated carcinomas. Type I tumours are genetically stable in comparison to Type II tumours with a specific pattern of mutations (e.g., *KRAS, BRAF, ERBB2* and *PTEN*) whereas Type II tumours are genetically unstable with a high frequency of *TP53* mutations. Type II tumours also show higher levels of morphological and molecular homogeneity (Kurman & Shih, 2010). Serous carcinoma is the most frequent subtype, making up approximately 70% of EOCs. The next most common subtypes are clear

cell carcinomas (10%) and endometroid carcinomas (10 – 15%). Mucinous carcinomas make up around 3% of EOCs (Ramalingam, 2016).

1.1.1. High Grade Serous Carcinomas vs. Low Grade Serous Carcinomas

The most common histological subtype, high-grade serous ovarian carcinoma (HGSOC) comprises 75% of ovarian cancers whereas low-grade serous carcinoma (LGSOC) accounts for 5% to 10% (Grisham, 2016; Labidi-Galy, et al., 2017). The majority of HGSOC cases are diagnosed at advanced stages when the tumour has already metastasised, contributing to the low 5-year survival rate of 31% (Kim, et al., 2012). LGSOCs may arise from the progression of serous cystadenoma or adenofibroma to non-invasive serous borderline tumours before becoming invasive. Many LGSOC are characterised by mutations in *KRAS*, *BRAF* or *ERBB2* whilst maintaining wild type *BRCA* and *TP53* (Botwell, 2010). *BRCA* dysfunction and *TP53* mutations in addition to high levels of chromosomal instability with the absence of *KRAS*, *BRAF* or *ERBB2* are observed in HGSOC. (Botwell, 2010). The loss of BRCA1/2 may predispose the development of sporadic and hereditary HGSOC (Rosen, et al., 2009). *In vivo* monitoring of HGSOC in *Dicer-Pten* double-knockout mice shows tumour development from lesions in the fallopian tube before spreading to the ovaries and metastasising throughout the peritoneum, causing ascites and then death (Kim, et al., 2012). Both HGSOC and LGSOC are positive for paired box gene 8, WT1, oestrogen receptor and progesterone receptor expression. LGSOC manifests in younger women and shows resistance to chemotherapy but the overall survival is better than HGSOC patients. HGSOC responds well initially to chemotherapy, but patients often experience recurrence before succumbing to the disease (Ramalingam, 2016).

1.2. EOC metastasis

EOC can metastasise through extension from tumours in the ovary or fallopian tube to neighbouring organs such as the bladder or colon, or the shedding of cancer cells from the primary tumour, which are carried throughout the peritoneum by peritoneal fluid, before dissemination in the abdominal cavity (Lengyel, 2010). EOC metastases are usually restricted to the peritoneal cavity and the omentum where components of the tumour microenvironment guide malignant cells into niches which allow the growth of secondary lesions (Pourgholami, et al., 2013). The peritoneum is a serous organ that is composed of

layers of mesothelial cells, basal lamina, submesothelial stroma (van Baal, et al., 2018). The omentum is a fat pad that covers the abdominal cavity and is often transformed during OC metastasis from adipocyte-rich to a tumour that is adipocyte deficient (Lengyel, 2010; Nieman, et al., 2011). EOC tumorigenesis relies on changes in cadherin expression in EOC cells to acquire a mesenchymal phenotype which allows EOC spheroids to overcome anoikis, a type of programmed cell that is induced upon detachment from the extracellular matrix (ECM). EOC cells are carried to the peritoneum or omentum where they regain their epithelial phenotype, attach, and proliferate.

1.1.2. Ascites pathophysiology and constituents

An accumulation of fluid in the peritoneal cavity is known as an ascites. EOC patients develop malignant ascites as a result of the tumour spreading to the peritoneum (Smolle, et al., 2014). The cellular components of ascitic fluid of OC patients consists of lymphocytes, mesothelial cells, macrophages, and adenocarcinoma cells (Kipps, et al., 2013). The ascitic fluid accumulates to volumes between 500 ml to > 2 L, containing components and growth factors including, secreted ECM, cytokines, chemokines, proteases, and vascular permeability factors which are implicated in facilitating tumour growth (Burleson, et al., 2006; Klymenko, et al., 2018). Tumour cells secrete vascular endothelial growth factor (VEGF) which enhances vascular permeability and has a role in ascites pathogenesis by altering the permeability of the peritoneal membrane (Kipps, et al., 2013; Matte, et al., 2017). VEGF induces cell proliferation, migration, angiogenesis and permeabilization of blood vessels in endothelial cells, in addition to inhibiting apoptosis (Kipps, et al., 2013). Overexpression of VEGF in EOC patients was associated with poor prognosis and ascites development (Paley, et al., 1997; Zebrowski, et al., 1999). Inflammatory cytokines, chemokines, in addition to decreased clearance of peritoneal fluids and blockage of lymphatic channels, causes peritoneal fluid build-up (Kipps, et al., 2013; Zhang, et al., 2008). This leads to the formation of ascites as a result of an imbalance between the production and the draining of peritoneal fluid via the diaphragmatic lymphatic system (van Baal, et al., 2018). The ascites facilitates EOC dissemination as EOC cells shed from the primary tumour exist as single cells or multicellular aggregates (termed “spheroids”) in the peritoneal fluid (Bilandzic & Stenvers, 2014).

In the peritoneal cavity, EOC cells are exposed to physical shear stress from tumour formation and the build-up of ascites. Normal intraperitoneal fluid pressure in mammals is sub-atmospheric (~5 mmHg) (Henriksen, et al., 1980) whereas in EOC patients with ascites, the intraperitoneal pressure is averaged at 22.1 mmHg (Gotlieb, et al., 1998). The exposure to fluid shear stress has been implicated in changes in benign cells, associated with transformation and ovarian cancer progression. It was also found that spheroids grown under shear stress showed an increased metastatic capability as well as enhanced chemoresistance, suggesting a role in facilitating invasion and metastasis (Ip, et al., 2016; Hyler, et al., 2018).

1.1.3. Multicellular spheroids

After detaching from the primary tumour, EOC cells exist in the ascites as single cells or multicellular spheroids (Lengyel, 2010). In the ascites, multicellular aggregates can range from 50 – 750 µM in diameter (Sodek, et al., 2009). Free-floating tumour and stromal cells in ascitic fluid can interact to form heterotypic spheroids allowing tumour cells to avoid anoikis by maintaining cell-cell contact (Figure 2) (Matte, et al., 2017). Aggregation of EOC cells may be important for anchorage-independent cell survival and growth which may be a survival mechanism which facilitates EOC dissemination (Kantak & Kramer, 1998; Shield, et al., 2007). ECM secreted by the mesothelial lining is implicated in aggregate formation and survival by facilitating cell-cell and cell-substrate interactions (Bilandzic & Stenvers, 2014). Spheroids can attach and disaggregate on mesothelial monolayers and ECM substrates – especially collagen I which is a major component of the sub-mesothelial stroma and the preferred substrate for OC cell attachment (Moser, et al., 1996; Sodek, et al., 2009). Upon adherence to the mesothelial cells by spheroids, spreading is initiated. Spreading cells exhibit protrusions which penetrate under mesothelial cell matrix, allowing the cells to migrate (Iwanicki, et al., 2011). Matrix metalloproteinases (MMPs) such as MMP-2 and MMP-9 in addition to fibronectin, vitronectin and integrin receptors play a role in the adhesion of EOC cells to the mesothelial lining (Matte, et al., 2017).

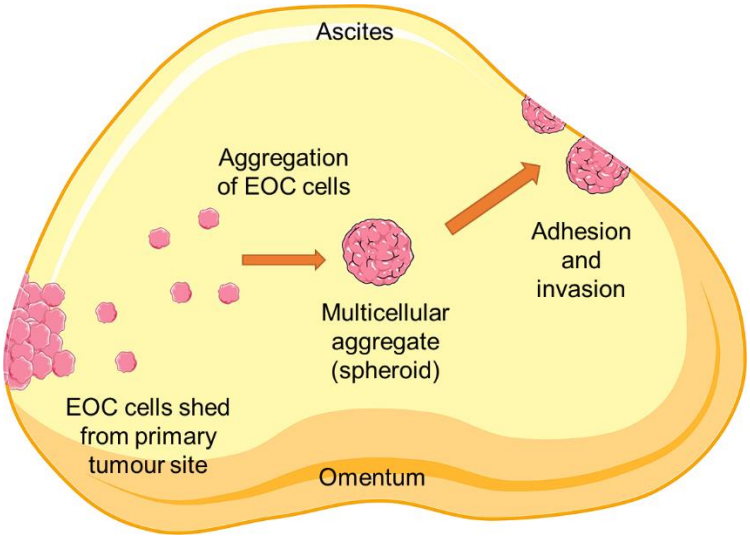

Figure 2. Model of spheroid formation and tumour metastasis.
EOC cells lose cell-cell contact and are shed into the peritoneal cavity before aggregating and forming spheroids. Peritoneal fluid carry spheroids to secondary site where they adhere and form secondary tumours. Images in this figure were modified from Servier Medical art (http://smart.servier.com). Servier Medical Art by Servier is licensed under a Creative Commons Attribution 3.0 Unported License Figures.

Spheroid size and media composition influences viability and growth due to the development of oxygen and nutrient gradients (Riffle & Hegde, 2017). Hypoxia occurs as the spheroid size increases; Spheroids between 200 µm and 400 µm in diameter often exhibit an outer proliferating zone with a normoxic quiescent zone followed by a hypoxic core (Riffle & Hegde, 2017; Däster, et al., 2017). Survival signalling pathways are activated upon the development of a hypoxic core in order to maintain cell viability (Riffle & Hegde, 2017). Necrotic areas can be seen in spheroids with a diameter of approximately 500 µm (Däster, et al., 2017). Through increasing glycolytic activity via the Warburg effect (discussed in 1.4), cancer cells can resist oxidative stress and adapt to hypoxia. Spheroids can metabolise glucose through anaerobic glycolysis resulting in increased resistance to apoptosis, conferring a more aggressive tumour phenotype (Liao, et al., 2014). Spheroids are an obstacle to treatment due to their putative role in disease progression, metastasis, and chemotherapy resistance (Liao, et al., 2014). The enhanced resistance to antitumour drugs such as cisplatin can be attributed to several mechanisms including decreased drug penetrance, increased signalling in pro-survival pathways as well as upregulating genes involved in drug resistance (Desoize & Jardillier, 2000). Populations of slowly growing or quiescent multicellular aggregates are resistant to therapies that target proliferating cells (Shield, et al., 2008). Spheroids also overexpress stem cell genes such as *NOTCH*, *NANOG*,

CDCP1, *CD34* and *MYC*. The tumour initiating potential ("stemness") of the spheroids is evident by their ability to create more tumour colonies after cisplatin treatment (Liao, et al., 2014).

1.1.3.1. 3D ovarian cancer models

The majority of *in vitro* cancer research is carried out on monolayer cultures which captures the proliferative traits of cancer cells. 2D cultures have been useful in the development and discovery of drugs due to its simplicity, convenience and ease when performing high throughput drug screening studies (Zanoni, et al., 2016; Däster, et al., 2017). However, 2D cultures fail to capture *in vivo* variabilities including cellular heterogeneity and interactions with the microenvironment. As a consequence, results may differ to those observed from more clinically relevant, *in vivo* models (Lal-Nag, et al., 2017). 3D tumours are exposed to conditions in the microenvironment such as hypoxia and nutrient gradients which can affect cellular fate, behaviour, and metabolism (Liao, et al., 2014). An alternative approach to using an *in vivo* system is to use 3D cell culture models where primary tissues or established cell lines are cultured within ECM gels, synthetic scaffolds, rotary cell culture systems, low/non-adherent plastics or via a hanging drop (Lee, et al., 2013). 3D systems exhibit features similar to *in vivo* tumours such as cell-cell interaction, cellular heterogeneity, hypoxia, drug resistance, through reduced penetrance, as well as the production and deposition of ECM (Zanoni, et al., 2016; Däster, et al., 2017; Cavo, et al., 2020). 3D cultures are highly advantageous over 2D cultures by better representing *in vivo* tumour growth and bridges the gap between 2D models and *in vivo* studies.

1.1.4. Epithelial – to - Mesenchymal Transition (EMT) and Mesenchymal - Epithelial Transition (MET)

During malignant transformation, EOC cells undergo epithelial-to-mesenchymal transition (EMT) where adhesion of epithelial cells to the basement membrane as well as intercellular adhesion between cancer cells are eased (Lengyel, 2010). This process is regulated by cadherins which are a family of calcium-dependent transmembrane molecules involved in cell-cell adhesion as well as maintenance of monolayer integrity and normal tissue architecture in an organism (Klymenko, et al., 2017c). The loss of E-cad expression and the gain of N-cadherin (N-cad) expression is designated as EMT (Klymenko, et al., 2017c). E-cad

expression of free-floating EOC cells in the ascites in addition to metastatic sites were found to be lower than in primary ovarian tumours. The low E-cad expression in EOC cells were observed to be more invasive (Veatch, et al., 1994; Lengyel, 2010). The loss of E-cad may be due to gene expression reprogramming driven by upregulation of ZEB, SNAIL and bHLH transcription factor family which results in the inhibition of E-cadherin gene, *CDH1* expression (Gong, et al., 2017). EMT is the process which allows epithelial cells to gain mesenchymal-like characteristics such as loss of apical-basal polarity and cell-cell adhesion. EMT leads to acquisition of the motile phenotype of mesenchymal cells allowing EOC to be shed from the primary tumour as single cells or spheroids into the ascites (Klymenko, et al., 2017b). Single cell or clusters of EOC are carried to the peritoneum and the omentum by the peritoneal fluid where they undergo mesenchymal-to-epithelial transition (MET) (Lengyel, 2010). MET involves N-cad inhibition and the re-expression of E-cad which occurs at the secondary metastatic site enabling adhered cancer cells to regain epithelial features and proliferate into larger tumours (Klymenko, et al., 2017b).

EOC tumour cells can show heterogenous cadherin expression with the expression of both E-cad and N-cad in the same tumour and in the same cell (Hudson, et al., 2008; Klymenko, et al., 2017a; Klymenko, et al., 2017c). EOC tumours may originate from the N-cad expressing ovarian surface epithelium that have undergone MET or from the epithelium of the fallopian tube that initially expressed both E-cad and N-cad (Hudson, et al., 2008). The expression of E-cad allows spheroids to avoid anoikis in addition to playing a role in chemotherapy resistance. N-cad expression is upregulated in metastatic lesions and is associated with an invasive EOC phenotype (Hudson, et al., 2008; Klymenko, et al., 2017a; Klymenko, et al., 2017b; Klymenko, et al., 2017c). Klymenko, et al., (2017c) found that the acquisition of E-cad expression led to alterations in the surface morphology in multicellular aggregates such as the loss of smooth spheroid-like appearance and the gain of a loosely aggregated phenotype. Additionally, cells that acquired E-cad showed a less aggressive phenotype, evidenced by reduced adhesion to collagen matrices and mesothelial layers in contrast to the gain of N-cad which led to the acquisition of a more aggressive phenotype such as enhanced mesothelial adhesion, submesothelial migration and invasion (Elloul, et al., 2010; Klymenko, et al., 2017c). The heterogeneity of cadherins in peritoneal lesions may be due to the seeding of multicellular aggregates in the metastatic niche or due to the

presence of cellular factors found in the peritoneal microenvironment which may induce the switching of cadherin expression in secondary lesions (Klymenko, et al., 2017c).

1.1.5. Role of inflammation in EOC

Chronic inflammation is an important environmental feature that contributes to oncogenesis (Lo, et al., 2011). Inflammation produces toxic oxidants in response to pathogens which can cause DNA damage. Rapid cell division as seen in inflammation can result in the acquisition of mutations or alter the expression of crucial tumour suppressor genes leading to cancer development (Kiraly, et al., 2015). Other components of inflammatory processes such as cytokines and prostaglandins may have a role in ovarian mutagenesis by inducing neoplasm and increasing tumour invasiveness respectively (Ness, et al., 2000). Chronic inflammation facilitates cancer cell attachment during EOC progression through alterations in the peritoneal lining (Sodek, et al., 2009). Inflammation also causes mesothelial cells to undergo mesothelial-to-mesenchymal transition (MMT), resulting in myofibroblast-like cells that are characterised by increased invasive and migrative capabilities. Cancer-associated fibroblasts (CAFs) are linked with cancer cell survival growth and progression and may originate from mesothelial cells through MMT. CAFs acquire a pro-tumorigenic role by secreting factors that facilitate further shedding of EOC cells from the primary tumour during EOC metastasis (Matte, et al., 2017).

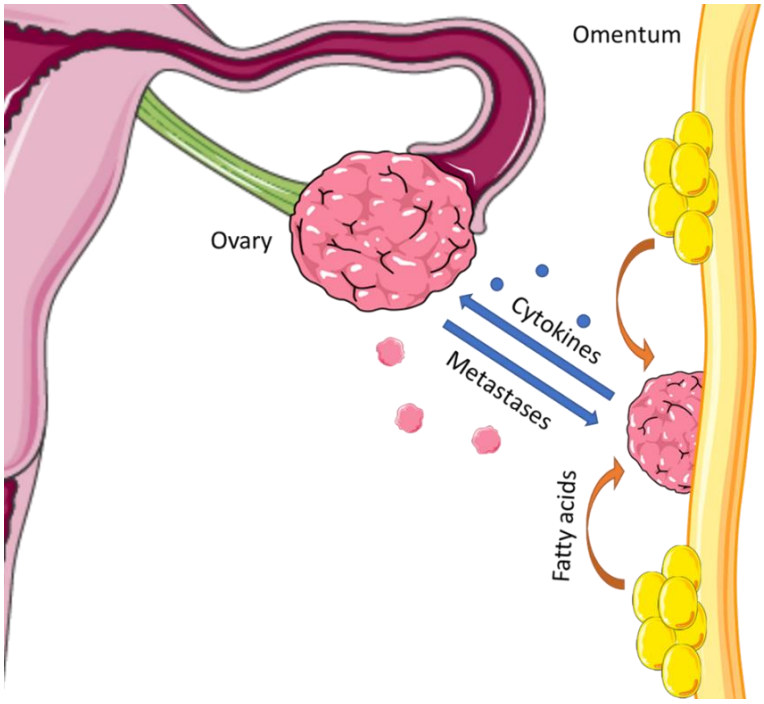

Figure 3. Model of EOC metastasis driven by the secretion of cytokines.
OC cells metastasise to the omentum where fatty acids in the omentum fuel metabolism. OC cells secrete cytokines which then attract more OC cells, promoting metastasis. Images in this figure were modified from Servier Medical art (http://smart.servier.com). Servier Medical Art by Servier is licensed under a Creative Commons Attribution 3.0 Unported License Figures.

Production of proinflammatory cytokines during initial stages of oncogenesis results in an antineoplastic effect. However, as the immune system struggles to counteract tumour growth, the inflammatory response becomes chronic which then results in deleterious effects on cell metabolism and the efficiency of the immune system (Macciò & Madeddu, 2012). The ascites is rich in cytokines and chemokines, with cytokines including IL-6, IL-8 and IL-10 present at concentrations that are two to three logs greater than serum concentration (Kryczek, et al., 2000; Penson, et al., 2000). Cytokines including IL-1β and IL-6 are produced by innate immune cells and have been implicated in the promotion of EOC growth and progression (Macciò & Madeddu, 2012). In addition to EOC tumours, omental adipocytes also secrete cytokines IL-6, IL-8 and MCP1 and TIMP1 in order to attract EOC cells to the omentum, promoting EOC cell migration and invasion (Figure 3) (Nieman, et al., 2011).

1.1.5.1. Interleukin 6 (IL-6)

Interleukin 6 (IL-6) is an immunoregulatory cytokine present in abundance in the EOC microenvironment (Lo, et al., 2011). IL-6 is produced by multiple cell types including macrophages, lymphocytes, and tumour cells (Browning, et al., 2018). In physiological conditions, IL-6 mediates processes such as haematopoiesis and platelet production (Nilsson, et al., 2005). However, IL-6 can directly stimulate cancer cells promoting EOC carcinogenesis and progression through the upregulation of pathways involved in proliferation and invasion, ultimately resulting in widespread metastatic disease (Lo, et al., 2011; Pourgholami, et al., 2013). Levels of serum IL-6 and soluble IL-6 receptor are found to be higher in malignant ascites and is associated with poor prognosis and may contribute to EOC progression (Nilsson, et al., 2005; Lo, et al., 2011). The IL-6 signalling pathway has also been implicated in the development of platinum- and taxane-based drug resistance through the upregulation of multidrug resistance-related genes (MDR1 and GSTpi), apoptosis inhibitory proteins (BCL-2, BCL-xL and XIAP) as well as the activation of Ras/MEK/ERK and PI3K/Akt signalling (Wang, et al., 2010). IL-6 can also activate pro-proliferative pathways such as JAK/STAT signalling resulting in the hyperactivation of STAT3 which has been associated with increased tumour growth and chemotherapy resistance. The activation of STAT3 by IL-6 results in the upregulation of cell cycle-promoting proteins including c-MYC and cyclins D1, D2 and B1 as well as increasing pro-survival proteins BCL-2, BCL-xL, survivin and MCL-1 which contributes to chemoresistance and survival. JAK/STAT signalling induced by IL-6 has been implicated in EOC tumour growth and resistance to anti-cancer drugs (Browning, et al., 2018).

1.1.5.2. Interleukin-8 (IL-8)

IL-8 is secreted by multiple cell types including monocytes, neutrophils, endothelial and mesothelial cells as well as tumour cells (Wang, et al., 2011). During activation of the immune system, IL-8 is mainly involved in attracting and activating neutrophilic granulocytes as well as recruiting T cells and basophils (Koch, et al., 1992; Wang, et al., 2011).

IL-8 was found to be elevated in ascites, serum, and tumour tissue of EOC patients (Ivarsson, et al., 2000; Herrera, et al., 2002; Kassim, et al., 2004; Penson, et al., 2000). Elevated IL-8 expression is associated with poor prognosis and chemoresistance (Wang, et al., 2011). IL-8 mediates its effects through the binding of two cell surface G protein-

coupled receptors CXCR1 and CXCR2 (Long, et al., 2016). Both of these receptors are expressed on most tumour cells in addition to endothelial cells (Murdoch, et al., 1999; Xu & Fidler, 2000). Expression of IL-8 was reported to be regulated by a number of stimuli including inflammatory responses and environmental stresses such as low nutrients and hypoxia – all of which are observed in the EOC microenvironment (Brat, et al., 2005; Kipps, et al., 2013; Matte, et al., 2017). IL-8 signalling results in the activation of pathways including Ras/MEK/ERK and PI3K/Akt signalling cascades which has been implicated in EOC chemoresistance (Wang, et al., 2010). The anti-apoptotic activity of IL-8 was associated with the upregulation of the expression of apoptosis inhibitor proteins including BCL-2, BCL-xL and XIAP which may contribute to chemotherapy resistance (Wang, et al., 2011). Additionally, IL-8 has been implicated in promoting EOC cell growth as well as inducing the overexpression of VEGF which contributes to the transformation and progression of EOC (Xu & Fidler, 2000; Kassim, et al., 2004).

1.3. Epigenetic modifications in ovarian cancer

Epigenetics is defined as heritable DNA modifications which occur without the alteration of the primary base-coding sequences by modulating DNA accessibility and chromatin structure resulting in the regulation of gene expression patterns (Jones, et al., 2016). Epigenetics has been strongly implicated in the development and progression of EOC whereby alterations in epigenetic states are associated with ovarian tumorigenesis (Balch, et al., 2009). Epigenetic changes in cancer cells can perturb gene expression via DNA methylation, histone modification and non-coding microRNA (miRNAs) (Nguyen, et al., 2014).

1.3.1. Histone modifications

Chromatin consists of complexes of chromosomal DNA packaged around the octameric core of histone proteins, forming units of nucleosome. The histone octamer is made up of two H3-H4 dimers surrounded by two H2A-H2B dimers. The histone tails of the N-terminal protrude from the nucleosomes into the nuclear lumen. H1 histone associates with linker DNA between the nucleosomes. Modification to DNA and histone tails regulate gene accessibility to transcriptional machinery and chromatin structure which is divided into two states: closed (heterochromatin) and open (euchromatin). Histones can be post-

translationally modified to alter chromatin structure in many ways including phosphorylation, ubiquitination, acetylation, and methylation. Histones may be mono-, di- or trimethylated which can activate or repress gene expression depending on the number of methyl groups incorporated and the residue modified (Kinnaird, et al., 2016). Histone lysine methylation patterns and subsequent transcriptional effects are more complex as some methylation sites are associated with euchromatin and some are repressive, adapting a heterochromatin state (Handy, et al., 2011). Marks such as histone H3 lysine 4 di – and trimethylation (H3K2me2 and H3K4me3) in addition to methylation of H3K79 and H3K36 are associated with active transcription and an open state of chromatin. Methylation of H3K9, H3K27 and H4K20 are lined with transcriptional repression and a closed chromatin conformation (Barski, et al., 2007). The acetylation of histones is associated with open chromatin structure and allows transcription. This is regulated by histone acetyltransferases (HATs) and histone deacetyltransferases (HDACs). Acetylation neutralises the positive charge on the lysine residues on the histone tails which leads to the unfolding of DNA, allowing access of the transcription machinery (Marsh, et al., 2014).HDACs are recognised as important regulators of cell growth, differentiation, and apoptosis with HDACs 1-3 was found to be overexpressed in OC tissues, playing a role in ovarian oncogenesis (Jin, et al., 2008).

The histone methyltransferase, Enhancer of Zeste Homolog 2 (EZH2) forms the catalytic unit of the Polycomb repressive complex 2 (PRC2) and generates H3K27 methylation mark. EZH2 was found to be overexpressed in EOC and cancer-associated stromal cells (Li & Zhang, 2013). OC cells with stem-cell properties were reported to require EZH2 expression for maintenance (Rizzo, et al., 2010). Silencing by H3K27me3 through the overexpression of EZH2 could result in populations of cells acquiring stem-cell characteristics, driving tumorigenesis (Chapman-Rothe, et al., 2013). A decrease in H3K27me3 expression correlated with poor survival and a more aggressive phenotype in OC patients (He, et al., 2015). Loss of repressive histone marks, HSK27me3 and H4K20me3 was associated with the expression of cancer-promoting genes *CLDN3* and *CLDN4* in EOC cells which could also contribute to ovarian tumorigenesis (Kwon, et al., 2010).

1.3.2. microRNA (miRNAs)

Non-coding microRNAs (miRNAs) are a class of small noncoding RNAs, 19-25 nucleotides in length that are cleaved from 70-100 nucleotide hairpin pre-miRNA precursors (Iorio, et al., 2007). miRNAs can inhibit translation by binding to the 3'UTR region of target genes and cause transcript degradation through the formation of RNA-induced silencing complexes (Gregory & Shiekhattar, 2005). Whilst miRNA is required for essential processes such as differentiation, cell growth and death, aberrant miRNA expression has been associated with carcinogenesis (Miska, 2005). In OC samples, upregulation of *miR-200a*, *miR-200b*, *miR-200c*, and *miR-141* were observed whereas *miR-199a*, *miR-140*, *miR-145*, and *miR-125b1* were the most significantly downregulated miRNAs (Iorio, et al., 2007). The miRNA signatures of OC may be used to identify tumours based on the histological subtypes as well as low- and high-grade diseases (Iorio, et al., 2007). In patients with *BRCA1* and *2* mutations, increased expression of *miR-29a* and *miR-29b*, and significant downregulation of *miR-34c*, *miR-422b*, *miR-143* were observed (Lee, et al., 2009; Corney, et al., 2010). The miR-34 family appears to play a role in EOC pathogenesis as the downregulation of *miR-34b*/c* may be important for OC progression (Corney, et al., 2010). miRNAs have also been implicated in the regulation of apoptosis in OC (Mezzanzanica, et al., 2011).

1.3.3. DNA Methylation

DNA methylation plays an important role in many biological processes such as genomic imprinting, X chromosome inactivation, B-cell development, and neuronal development (Paulsen & Ferguson-Smith, 2001; Lio, et al., 2016; Zhang, et al., 2016). During such processes, DNA methylation patterns are established through a regulated process that involves the methylation and demethylation pathway (Chen, et al., 2003). DNA methylation occurs by the addition of a methyl group to the C5 position of the cytosine residue in cytosine-guanine (CpG) dinucleotides forming 5-methylcytosine (5-mC) by DNA methyltransferases (DNMTs) (Nguyen, et al., 2014; Gong, et al., 2017). Over 50% of the genes in the vertebrate genome comprise of approximately 1kb long CpG-rich regions known as CpG islands (CGIs) (Jones, 2012). CGIs are constitutively unmethylated in somatic cells and are preferentially localised to the start site of human genes (Antequera, et al., 1990). DNMTs can add methylation marks, known as *de novo* methylation, as well as maintain the methylation marks during replication (Kohli & Zhang, 2013). There are three active DNMTs: DNMT1, DNMT3a and DNMT3b. DNMT1 is expressed in proliferating cells

and functions as a maintenance methyltransferase which is responsible for copying methylation patterns from the parent-strand to the daughter strand during each round of DNA replication in addition to restoring symmetrical methylation to hemimethylated CpGs (Chen, et al., 2003; Ooi, et al., 2009). DNMT3a and DNMT3b are expressed in embryonic stem cells and developing germ cells. DNMT3a and DNMT3b have a role in establishing and maintaining methylation patterns (Chen, et al., 2003). Generally, the presence of 5mC is associated with a transcriptionally repressed chromatin conformation (Kohli & Zhang, 2013).

DNA methylation and histone modifications can function independently or together in order to determine cell fates (Kong, et al., 2016). Methylation of CpG can suppress transcription as a methyl group at a specific CpG and can block DNA recognition and binding of transcription factors, however other factors may preferentially bind to methylated DNA to block transcription factor access by recruiting HDACs leading to transcriptional repression. Histone deacetylation promotes chromatin condensation and further represses transcription (Handy, et al., 2011). DNA hypermethylation is associated with decreased gene expression, so hypermethylation of tumour suppressor gene promoters can lead to gene silencing and inactivation of pathways such as DNA repair (Natanzon, et al., 2017). Promoter CGIs hypermethylation is an early epigenetic alternation in tumour progression associated with gene silencing leading to loss of cell cycle control, altered regulation of transcription factors as well as genetic instability (Nguyen, et al., 2014). Patterns of CGI methylation may result from clonal expansion of cells with silenced tumour suppressor genes. Therefore, accumulation of CGIs hypermethylation could result in malignant transformation of cells (Ahluwalia, et al., 2001). In ovarian tumours, methylation of CGIs is associated with silencing of tumour suppressor genes such as *RASSF1A*, *LOT1* and genes involved in DNA repair including *hMLH1* (Balch, et al., 2004). The widely studied *BRCA1* gene is involved in DNA repair and associated with hereditary EOC. Hypermethylation of the *BRCA1* promoter was associated with poorer survival and disease-free progression in OC patients (Wilcox, et al., 2005; Chiang, et al., 2006).

1.3.4. DNA Demethylation

DNA demethylation can occur actively where enzymes such as the ten-eleven translocation (TET) family catalyse the removal of a methyl group from 5mC, or passively via DNMT inhibition (Gong, et al., 2017). Hypermethylation of promoter CGIs in tumour suppressor genes have been observed in various malignancies. Aberrant methylation patterns in cancers may be due to initial random methylation resulting in proliferative advantages, facilitating the recruitment of DNMTs to their target sites by, for example, oestrogen receptor α or histone methyltransferases (Rawluszko-Wieczorek, et al., 2015).

1.3.4.1. TET enzymes

Mammalian DNA methylation was initially thought to be a passive process by the dilution of the methylation mark during DNA replication and the absence of DNMT1 maintenance. However, passive demethylation appears to be insufficient for the rate of DNA demethylation that occurs, independent of cell division during specific stages of development (Yin & Xu, 2016). TET enzymes are involved in the active demethylation process. Oxidation of 5mC has been shown to be catalysed by TET enzymes (Tahiliani, et al., 2009; Ito, et al., 2011). The TET enzymes are a family of large multidomain enzymes consisting of three members: TET1, TET2 and TET3. TET enzymes were first identified in acute myeloid leukaemia (AML), where TET1 was first identified as a fusion partner of the mixed lineage leukaemia (*MLL*) gene (Ono, et al., 2002). *TET2* and *TET3* were identified through homology searches of *TET1* (Nakajima & Kunimoto, 2014).

1.3.4.1.1. TET Enzyme Structure

TET enzymes share a conserved double-stranded β-helix (DBSH) domain which shows oxidative activity against 5mC as well as containing the binding sites for Fe(II) and α-ketoglutarate (α-KG) cofactors which are essential for their catalytic function (Figure 4) (Nakajima & Kunimoto, 2014). Omission of α-KG completely abolishes TET activity in the conversion of 5mC to 5hmC (Xu, et al., 2011). The function of the cysteine-rich domain located before the DBSH domain is not yet known (Nakajima & Kunimoto, 2014). TET1 and TET3 has an N-terminal CXXC zinc finger domain that can bind DNA with unmethylated CpG sequences (Rasmussen & Helin, 2016). TET2 lacks a CXXC domain due to chromosomal inversion during evolution (Huang, et al., 2014). The CXXC-type domain of TET2 is located

on a separate gene known as inhibition of the Dvl1 and axin complex (*IDAX*/*CXXC4*), located at the 5'- end of *TET2*. (Nakajima & Kunimoto, 2014). The CXXC domain in TET1 binds to CpG motifs irrespective of their cytosine modification whereas TET3 CXXC binds to cytosine irrespective of the guanine position. TET2 CXXC-type domain shows binding preference to 5mC derivatives (Rawluszko-Wieczorek, et al., 2015).

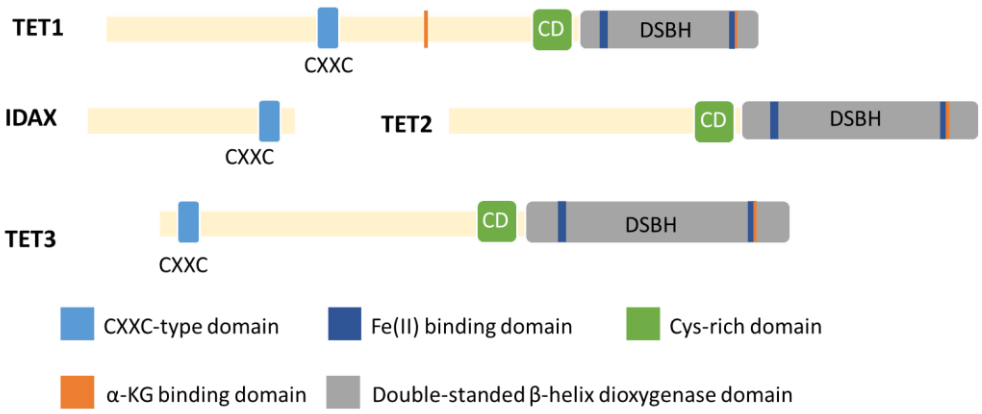

Figure 4. Structure and functional domains of the ten-eleven translocation (TET) protein family. TETs share a conserved catalytic domain consisting of a double-stranded β-helix domain (DSBH) and a cysteine (Cys)-rich domain. The DSBH domain carries catalytic motifs that interact with Fe(II) and α-ketoglutarate (α-KG). The CXXC-type zinc finger domain is located at the amino terminal of TET1 and TET3, whereas on TET2 it is encoded by the IDAX gene.

1.3.4.1.2. TET Enzyme Mechanism and Function

TET enzymes can facilitate passive DNA demethylation as well as actively affect replication-independent DNA demethylation (Huang & Rao, 2014). The TET family can erase DNA methylation by catalysing the successive oxidation of 5mC to 5-hydroxymethylcytosine (5hmC) to 5-formylcytosine (5fC) and 5-carboxylcytosine (5caC) (Figure 5) (Ito, et al., 2011). TET enzymes use molecular oxygen to catalyse the oxidative decarboxylation of α-KG to generate a reactive Fe(IV)-oxo intermediate that converts 5mC to 5hmC (Kohli & Zhang, 2013). TET proteins can further oxidise 5hmC to 5fC and to 5caC, to regenerate the Fe(II) species. The final product, 5caC cannot be converted into cytosine by TET proteins and requires other enzyme activities such as thymine-DNA-glycosylase (TDG) (Rawluszko-Wieczorek, et al., 2015); TDG is a DNA mismatch repair enzyme that shows recruitment to 5fC and 5caC. TDG catalyses base excision and yields an abasic site which is subsequently replaced by an unmodified cytosine by DNA base excision repair, leading to net DNA demethylation (Rasmussen & Helin, 2016).

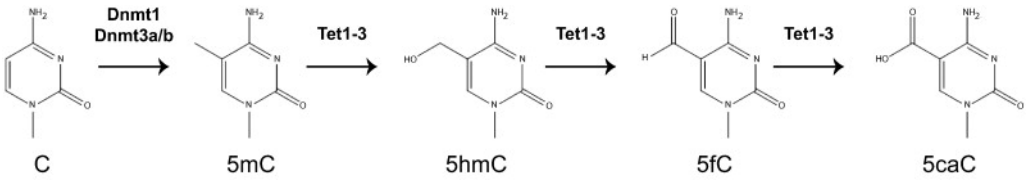

Figure 5. Epigenetic regulation through cytosine modifications.
DNMTs are involved in DNA methylation through the addition of methyl group to form 5mC (5-methylcytosine). The TET family of enzymes are involved in DNA demethylation by catalysing the successive oxidation of 5mC to 5hmC (5-hydroxymethylcytosine) to 5fc (5-formylcytosine) and 5caC (5-carboxylcytosine). Figure obtained from (Hill, et al., 2014).

DNA enriched with 5hmC generally shows an open chromatin configuration. Pluripotent cells show high levels of TET activity and 5hmC where it is required for tissue differentiation (Kafer, et al., 2016). Both *TET1* and *TET2* are expressed during early embryogenesis and in embryonic stem cells. As cells undergo differentiation and lose their pluripotency, *TET1* and *TET2* levels drop (Ficz & Gribben, 2014). TET1 is responsible for imprint erasure in embryonic germ cells as well as being involved in 5hmC production at promoter or transcription start site regions, whereas TET2 is necessary for 5hmC accumulation at the pluripotency locus in the somatic genome in addition to mostly regulating the levels of 5hmC in gene bodies (Huang, et al., 2014). Depletion of TET1 and TET2 diminishes 5hmC levels at the transcriptional start site and gene bodies respectively (Huang & Rao, 2014). TET3 has a role in the epigenetic reprogramming during fertilisation as well as having a role in neuron maintenance and neuronal transdifferentiation from fibroblasts via the activation of neuron specific genes (Gu, et al., 2011; Zhang, et al., 2016)

TET proteins have also been implicated in chromatin modifications. *TET2* is a binding partner of *O*-linked β-*N*-acetylglucosamine (*O*-GlcNAc) transferase (OGT) – an enzyme that transfers the *O*-GlcNAc group to serine or threonine residues of histone 2B which marks activating gene transcription. OGT is recruited to DNA transcriptional start sites of target genes through interaction with the TET2 catalytic domain (Nakajima & Kunimoto, 2014).

1.3.4.1.3. Role of TET enzymes and 5hmC in cancer

The exact role of 5hmC in mammalian genomes has not yet been established. During early mammalian development, the majority of the 5mC in the paternal genome is oxidised to 5hmC upon fertilisation of oocytes by sperm – catalysed by TET3. Brain tissues are very abundant in 5hmC within gene regions, at the promoter or intragenic regions. The presence of 5hmC in these regions correlate with active gene processes (Pfeifer, et al., 2013). Genomic-wide hypermethylation – associated with 5hmC depletion results in the downregulation or suppression of tumour suppressor genes and plays an essential role in tumour initiation and metastasis. (Li, et al., 2016). In addition to low 5hmC levels, some cancers often exhibit aberrant TET activity as TET-depleted cells with low 5hmC show increased errors in chromosome segregation in response to replication stress (Kafer, et al., 2016). 5hmC levels are often low in multiple cancer tissues, including EOC which also showed lower expression of *TET2* (Zhang, et al., 2015; Li, et al., 2016). Reversing the loss of 5hmC using DNMT inhibitors restored sensitivity to platinum treatment in platinum resistant EOC, increasing overall survival (Tucker, et al., 2018).

TET1 downregulation or demethylation is seen in cancer cell lines and primary tumours such as breast and cervical. TET1-mediated inhibition of CpG methylation of tumour suppressor genes such as *SLIT2* and *HOXA9* can reactivate their expression. The suppression of *TET1* is required for KRAS-induced cellular transformation, as loss of TET1 function is often seen in haematological malignancies (Li, et al., 2016). Overexpression of TET2 enzyme in platinum-resistant ovarian cancer cells can reverse the 5hmC-deficient genome, reducing the number of cells expressing cancer stem cell markers as well as restoring sensitivity to platinum (Tucker, et al., 2015). *TET2* is one of the most frequently mutated genes in haematological malignancies such as chronic myelomonocytic leukaemia (CMML, ~50%), acute myeloid leukaemia (AML, ~20%) and myelodysplastic syndromes (MDS, ~20%). In some cases of AML, translocation mutation results in the fusion of N-terminal H3K4 methyltransferase MLL1 to the TET1 DBSH domain. The TET1-MLL regulates the expression of transcription factors *HOXA9*, *MEIS1* and *PBX3* which are implicated in haematopoiesis (Kohli & Zhang, 2013). In human melanoma, TET2 and TET3 were found to be significantly decreased, their knockdown induced an EMT-like process via upregulation of transcription factors including *SNAIL1*, *SNAIL2*, *ZEB1, ZEB2*, *TWIST* and *ID4* suggesting they are potential suppressors of the EMT-like process. TET1 is a suppressor of KRAS-

mediated transformation and suppresses breast cancer invasion by the activation of tissue inhibitors of metalloproteinases. TET1 is upregulated by hypoxia and functions as a co-activator in EMT regulation and the hypoxia-response program. Regulation of *TET* genes are dependent on tissue type or different conditions that induce EMT. TET1 is involved in tumour initiation, whilst TET2 and TET3 are involved in cancer metastasis (Gong, et al., 2017).

1.3.5. Epigenetics in Chemoresistance

Platinum-derived compounds such as cisplatin and carboplatin are some of the most commonly employed drugs, used alone or in combination with other antitumour drugs in cancer chemotherapy (Li, et al., 2009). Improving the survival rate of OC patients is a challenge due to the development of chemotherapy resistance: platinum resistance in particular. Cisplatin's mechanism of action is dependent on DNA damage in proliferating cells by DNA adduct formation and disrupting DNA structure. DNA lesions then accumulate, blocking DNA replication and DNA-binding proteins, leading to apoptosis (Cepeda, et al., 2007). Drug resistance arises *de novo* via drug inactivation, increased resistance to apoptosis, decreased recognition of DNA damage and increased DNA repair (Stewart, 2007). Chemotherapy resistance is associated with methylation via the silencing of genes involved in DNA repair, apoptosis, and drug response (Esteller, 2008; Li, et al., 2009). Additional pathways involved in platinum resistance include the silencing of cell adhesion and tight junction pathways through hypermethylation and the activation of pathways involved in cell growth such as PI3K/Akt, TGF-β and cell cycle progression through hypomethylation (Li, et al., 2009).

Methylation and subsequent silencing of the mismatch repair gene *MLH1*, was associated with platinum resistant OC (Gifford, et al., 2004). Silencing of *DAPK*, a gene involved in apoptosis was also found in chemotherapy-resistant cancer as a result of methylation (Lehmann, et al., 2002). Taxane resistance has been linked to the hypermethylation of the *TUBB3* gene, which is a class III β-tubulin (Izutsu, et al., 2008). Loss of expression of the methylation controlled DNAJ (*MCJ)* gene through hypermethylation was associated with drug resistance in OC (Strathdee, et al., 2005). Hypomethylation has also been implication in the induction of drug resistance, such as through the upregulation of myelin and

lymphocyte (MAL) protein expression which accompanies platinum resistance in EOC (Lee, et al., 2010). Tumour suppressor miRNA, *let-7i* was found to be significantly downregulated in EOC (Yang, et al., 2008). Another miRNA, *miR-214* was reported to target tumour suppressor, PTEN and was linked to platinum resistance (Iorio, et al., 2007; Yang, et al., 2008).

1.3.6. Epigenetic therapy

Unlike genetic mutations that are irreversible, alterations in the epigenome could potentially be reversed and corrected (Esteller, 2008). DNMT inhibitors have shown promise and act through covalent and irreversible binding to the DNMT active site leading to genome wide hypomethylation (Lyko & Brown, 2005). DNA hypomethylation and resensitising of platinum-resistant OC to chemotherapy treatment was observed in pre-clinical studies with DNMT inhibitors suggesting potential in the treatment of chemotherapy-resistant OC (Plumb, et al., 2000; Balch, et al., 2007; Li, et al., 2009). Supporting this, a clinical study by Fu *et al.,* (2011) reported that use of a DNMT inhibitor, azacytidine enhanced the responsiveness to platinum in patients with platinum-resistant OC (Fu, et al., 2011). Other DNMT inhibitors, decitabine and zebularine also resensitised cisplatin-resistant OC cells to platinum treatment through the demethylation of *RASSF1A* and *MLH1* (Balch, et al., 2007). Another silencing mechanism is histone deacetylation by HDACs. Using HDAC inhibitors could reverse epigenetic repression of tumour suppressor genes. HDAC inhibitors have been reported to induce cell cycle arrest, differentiation, or apoptosis in cancer cells (Secrist, et al., 2003). HDAC inhibitor, belinostat showed potent anti-tumour activity in OC cell lines and xenografts (Plumb, et al., 2003). Other novel HDAC inhibitors, R306465 inhibited tumour growth in OC xenografts and Scriptaid, inhibited OC cell proliferation (Takai, et al., 2006; Arts, et al., 2007). A combination of decitabine and belinostat appeared to be more effective at sensitising drug-resistant tumours to platinum treatment compared to when decitabine was used alone (Steele, et al., 2009). Thus, a combination of both DNMT and HDAC inhibitors, along with conventional therapies, may be the most effective treatment for clinical use (Lyko & Brown, 2005; Balch, et al., 2009).

1.4. Metabolic reprogramming

The two main nutrients to support mammalian cell growth and survival are glucose and glutamine. The catabolism of glucose and glutamine replenishes the pools of carbon intermediates which are used for assembly of macromolecules (Pavlova & Thompson, 2016). Metabolic reprogramming of cancer due to metabolic dysregulation is required to sustain proliferation as well as influencing the tumour microenvironment and immune response (Sciacovelli & Frezza, 2016). Tumour-specific altered metabolism was first discovered by Otto Warburg who observed that cancers preferentially took up glucose and produced more lactic acid than normal tissue, even when oxygen was present, giving rise to the phenomenon that is the "Warburg effect" or aerobic glycolysis (Warburg, et al., 1927). Studies performed with real-time ^{13}C NMR analysis show that a significant amount of glutamine carbon is converted into lactic acid and secreted from the cells, consistent with Warburg's observations (DeBerardinis, et al., 2007). Increased glucose metabolism allows cancer cells to achieve maximal growth through the fast production of ATP and synthesis of nucleotides, proteins, and fatty acids. Cancer cells show preference to aerobic glycolysis despite being an inefficient process as oxidative phosphorylation (OXPHOS) produces 34 more ATP molecules from one molecule of glucose (Nowicki & Gottlieb, 2015). Due to the increased glucose uptake, the local tumour environment is often hypoglycaemic (Kellenberger, et al., 2010). Plasma glucose concentrations below 4 mM are considered hypoglycaemic (Tourkmani, et al., 2018). Glucose concentrations in malignant ascites are <3.3mM, whereas plasma glucose concentrations in OC patients range between 3.3 mM to 17 mM (Lamkin, et al., 2009; Kipps, et al., 2013).

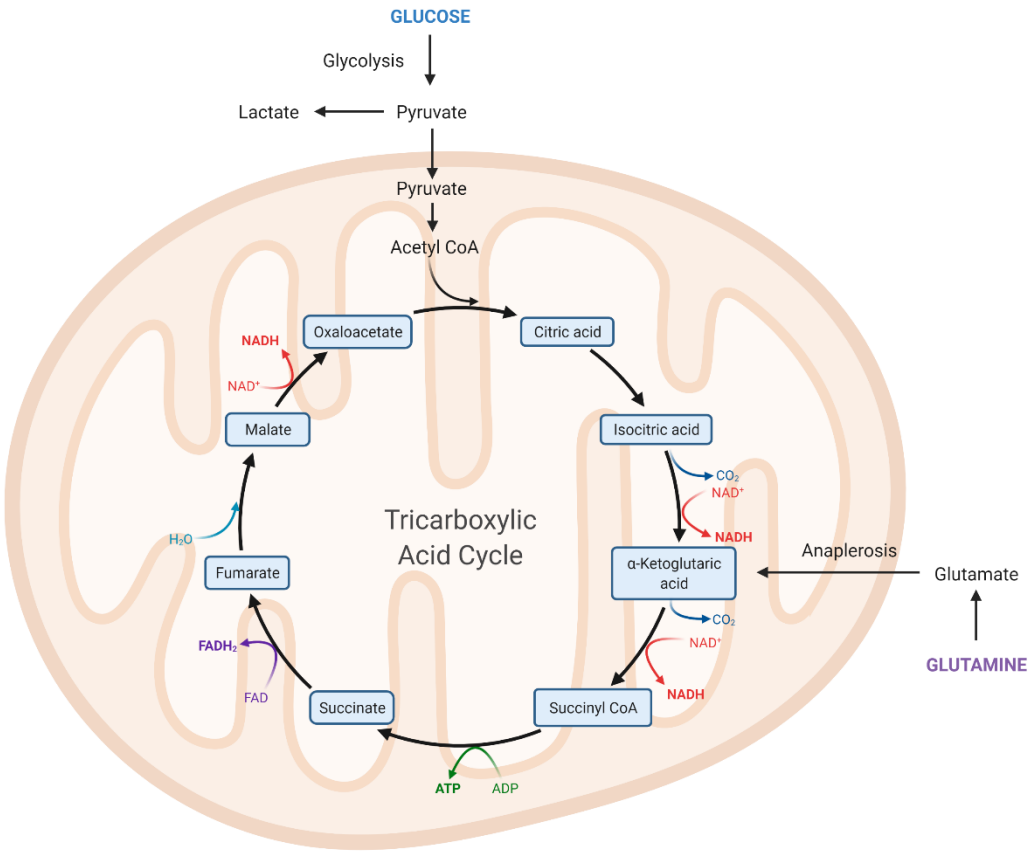

Figure 6. Glucose and glutamine metabolism in cancer cells.
Adapted from "Krebs Cycle" by BioRender.com (2021). Retrieved from https://app.biorender.com/biorender-templates

Glutamine metabolism acts as an alternative metabolic pathway in a glucose-depleted microenvironment (Helmlinger, et al., 2002). Malignant ascites exhibits higher levels of glutamine (Bharti, et al., 2017). Cancer cells consume glutamine at a higher rate than any other amino acid. Glutamine loses its amide group to produce glutamate, catalysed by glutaminase (GLS). Glutamate acts as a substrate for glutamate dehydrogenase (GDH), producing α-KG (Wise & Thompson, 2010). α-KG has several roles in different metabolic and cellular pathways such as being an intermediate in the tricarboxylic acid (TCA) cycle and a glutamine formation precursor for amino acid synthesis (Xiao, et al., 2012). Glutamine is essential for anaplerosis in the TCA cycle and cell survival in highly invasive cancers (Figure 6) (Yang, et al., 2014). Glutamine metabolism is promoted by the oncogene *MYC* (Wise, et al., 2008). Elevated *MYC* expression is observed in cancers, such as EOC which harbour a high frequency of *MYC* amplification. MYC regulates the expression of target genes involved in cell growth and proliferation (Kalkat, et al., 2017). Increased

glutamine uptake and glutamine flux due to the induction of glutamine transporter (SLC1A5), glutaminase (GLS1) and lactate dehydrogenase A (LDHA) were seen upon MYC induction in glioma cells (Wise, et al., 2008). The metabolic tumour microenvironment can inhibit function of anti-tumour immune effectors, whilst attracting inflammatory cells that are involved in tumour progression. High lactate levels in the tumour microenvironment can inhibit natural killer cells as well as suppress proliferation, cytokine production and cytolytic activity of cytotoxic T lymphocytes (Kroemer & Pouyssegur, 2008).

1.4.1. Oncometabolites in ovarian cancer

To support cancer cell survival and proliferation, cancer cells undergo metabolic reprogramming for energy and biomass (Pavlova & Thompson, 2016). Epigenetic modifications such as acetylation and methylation require metabolites as substrates. When these metabolites accumulate to the levels whereby, they act as oncogenic signalling molecules, they are termed "oncometabolites". The abundance of oncometabolites can depend on the reprogramming of cellular metabolism due to oncogenic mutations as well as environmental cues such as hypoxia (Sciacovelli & Frezza, 2016). Oncometabolites can aberrantly modify the epigenome and contribute to malignant transformation and progression (Seeber & van Diest, 2012). Mutations in metabolic genes such as succinate dehydrogenase (*SDH*) lead to cancer, supporting the link between alterations in metabolism and tumorigenesis. Cells deficient in SDH show an accumulation of succinate – an oncometabolite, due to its role in tumorigenesis (Sciacovelli & Frezza, 2016). Cancers with mutations in IDH can produce oncometabolite, 2-hydroxyglutarate (2-HG). At elevated concentrations, 2-HG can affect the epigenome to drive a malignant phenotype (Sciacovelli & Frezza, 2016). Analysis of The Cancer Genome Atlas (TCGA) dataset for ovarian cancer shows SDH genomic deletions in 67% of serous ovarian cancer patient samples with 39% of the samples showing heterozygous deletion of *SDHB* (Aspuria, et al., 2014). Consequently, HGSOC patient samples show elevated concentrations of succinate (Sans, et al., 2017). Despite having no IDH mutations, HGSOC patients also show high levels of 2-HG (Zand, et al., 2016).

1.4.1.1. L- and D-2-hydroxyglutarate

2-HG is a minor by-product of metabolism in normal cells and exists in two forms: L-2HG and D-2HG. Concentrations of these metabolites are kept low by the activity of L/D-2-

hydroxyglutarate dehydrogenases (L2HGDH and D2HDGH) which convert 2-HG to α-KG (Sciacovelli & Frezza, 2016). Mutations in isocitrate dehydrogenase genes *IDH1* and *IDH2* are found in over 75% of low-grade gliomas and approximately 20% of AML. IDH mutations lead to the abolishment of its normal catalytic activity and gain the ability to produce elevated levels of D-2HG (Xu, et al., 2011). Glutamine is a source of α-KG which is further converted to 2-HG by mutant IDH (Matre, et al., 2016). Cancers without *IDH* mutations such as breast and ovarian still accumulate 2-HG, this may be as a result of promiscuous enzyme activity. *L*-2HG can be produced in a promiscuous reaction when α-KG is reduced by L-dehydrogenases such as malate dehydrogenase (MDH) or lactate dehydrogenase (LDH) (Sullivan, et al., 2016). Human D-3-phosphoglycerate dehydrogenase (PHGDH) has also been implicated in the conversion of α-KG to D-2HG in breast cancers with no IDH mutations (Fan, et al., 2015). ADHFE1 produces D-2HG from α-KG as a result of 2-hydroxybutyrate metabolism in breast tumours (Terunuma, et al., 2014). Furthermore, ADHFE1 expression is found to be increased in ovarian cancer (Ramakrishna, et al., 2010).

2-HG and α-KG are structurally similar as in 2-HG, the oxygen atom linked to the second carbon (C2) in α-KG is replaced by a hydroxyl group. 2-HG can function as a competitor of dioxygenases that utilise α-KG as a co-substrate such as the TET family. Both 2-HG enantiomers act as weak antagonists of α-KG to inhibit TET1 and TET2 with D-2HG being significantly less potent than L-2HG. 2-HG has a lower binding affinity than α-KG due to the hydroxyl moiety being the weaker ligand of the catalytic Fe (II) centre than the keto group in α-KG. D-2HG binds to the catalytic core close to Fe(II) adopting a similar orientation as α-KG, except the Fe(II) is coordinated by two oxygen atoms in the keto carboxyl end of α-KG; whereas, Fe(II) is coordinated by one oxygen atom and a hydroxyl group in D-2HG. The weak activity of D-2HG may be responsible for tumour cells needing to accumulate and tolerate high levels of D-2HG (Xu, et al., 2011). Accumulation of 2-HG can also inhibit ATP synthase in the mitochondria, leading to the suppression of mTOR (Fu, et al., 2015). The direct targeting of D-2HG production by inhibiting conversion of glutamine to α-ketoglutarate using small molecule inhibitors such as bis-2-[5-phenyl-acetamido-1,2,4-thiadiazol-2-yl] ethyl sulphide or GLS inhibitor C-839 can slow the growth rate of *IDH* mutated cancers via the reduction of 2-HG production and induce differentiation (Menendez, et al., 2014; Matre, et al., 2016). Telaglenastat (CB-839) is a bioavailable GLS

inhibitor that was shown to have antiproliferative activity in triple negative breast cancer cell lines (Matre, et al., 2016).

1.4.1.2. Succinate

Succinate is structurally similar to α-KG and 2-HG, sharing the same acetate end with two oxygen atoms linked to C5 used by α-KG and 2-HG to interact with conserved residues in dioxygenases (Xiao, et al., 2012). Succinate can inhibit TET enzymes. (Laukka, et al., 2016). SDH is an enzyme in the TCA cycle, involved in the conversion of succinate to fumarate. The enzyme consists of four subunits, SDHA, SDHB, SDHC and SDHD in addition to two assembly factors SDHF1 and SDHF2 (Sciacovelli & Frezza, 2016). SDH has a role as tumour suppressors. Loss of SDH leads to accumulation of succinate as well as the induction of pseudohypoxia – classified as the activation of hypoxia-inducible factor (HIF) in normoxic conditions (MacKenzie, et al., 2007). HIF transcription factor is a heterodimer consisting of HIF-α subunit which is the oxygen-inducible component and HIF-β subunits. HIF promotes the adaption of cells to low oxygen by inducing neovascularisation and glycolysis (Selak, et al., 2005). SDH forms complex II of the electron transport chain, dysfunction of SDH leads to enhanced neovascularisation and glycolysis that supports cancer formation. The overaccumulation of succinate may have tumorigenic effects via the overproduction of reactive oxygen species (ROS) leading to irreversible DNA modification and protein oxidation by the succination of cysteine residues, promoting tumorigenesis by enhancing ROS detoxification and promoting cell survival and proliferation (Menendez, et al., 2014). Succinate was identified as a potential metabolic urinary biomarker in ovarian cancer, indicating that altered SDH activity may be important in ovarian cancer progression (Zhang, et al., 2013). SDH members, especially *SDHB* are often dysregulated in serous ovarian cancer. Knocking down *Sdhb* leads to a hypermethylated epigenome sufficient to promote EMT as well as reprogrammed carbon source utilisation and mitochondrial dysfunction. *Sdhb* knockdown cells had elevated levels of succinate and decreased levels of fumarate and malate relative to control cells (Aspuria, et al., 2014).

1.4.2. The use of metformin in the treatment of ovarian cancer

Due to the emergence of chemoresistant EOC and the demand for new therapeutic strategies, drug repurposing is an attractive method for new drug development. Drug repurposing involves the identification of new uses for approved drugs. One widely studied

drug for the treatment of cancer is biguanide, metformin. In the liver of diabetic patients, metformin inhibits gluconeogenesis by impairing oxidative phosphorylation leading to the imbalance of AMP/ATP ratio which activates AMPK and results in the reduction in blood glucose and insulin levels (Rattan, et al., 2011). Several studies suggest that patients undergoing metformin treatment show a better prognosis of ovarian cancer (Kumar, et al., 2014; Bar, et al., 2016). Long term treatment of metformin may decrease OC recurrence, risk, and death (Bodmer, et al., 2011; Wang, et al., 2017).

The exact anti-cancer mechanism of metformin has not yet been established; however, the activation of AMPK may be central to this. Metformin accumulates in the mitochondria and inhibits complex I of the electron transport chain, inhibiting mitochondrial ATP production (Owen, et al., 2000). The activation of AMPK by metformin leads to the inhibition of the mTOR pathway which regulates the expression of p21, p27 and cyclin D1 which can lead to the inhibition of proliferation of cancer cells (Shackelford & Shaw, 2009; Rattan, et al., 2011). Through the activation of AMPK, metformin is able to reduce inflammation by suppressing NF-κB signalling (Guma , et al., 2015). In ovarian cancer cell lines, low concentrations of metformin showed little effect on proliferation rate but supressed the expression of *snail2*, *twist*, and *vimentin* in addition to inhibiting the secondary and tertiary tumour spheroid formation (Zhang, et al., 2015). Additionally, metformin exhibits an anti-proliferative effect as opposed to cytotoxic effect in OC by inducing cell cycle arrest at the G1 phase leading to a suppression in tumour growth and reduction in the number of proliferating cells when used in combination with cisplatin (Shank, et al., 2012). In other cancer cell lines, the anti-cancer effect of metformin and other AMPK agonists on proliferation and metabolism appear to be independent of AMPK activation (Vincent, et al., 2015). The activation of AMPK by metformin leading to metabolic reprogramming and inhibition of proliferation in cancer cells may be context and cell type specific (Vincent, et al., 2015). Limiting nutrient utilisation appears to be the main canonical mechanism of metformin's anticancer effect (Zakikhani, et al., 2006).

1.4.3. Tumour microenvironment and the efficacy of metformin

1.4.3.1. Glucose

The efficacy of metformin to induce cell death in ovarian cancer cell lines was reduced in hyperglycaemia as high glucose concentrations acts as a fuel for glycolysis, in order to maintain ATP levels, despite the inhibition of mitochondrial oxidative phosphorylation by metformin (Rogalska, et al., 2018). Metformin was found to be most effective under hypoglycaemic conditions. Thus, decreasing the concentration of glucose could enhance the cytotoxicity of metformin in ovarian cancer cells. Metformin was found to induce a decrease in ATP levels in cells cultured in restricted glucose medium but could activate AMPK in relatively high glucose medium, stimulating glycolysis. The activation of AMPK and glucose availability allows for efficient glycolysis. The depletion of ATP in restricted glucose medium treated with metformin is due to the failure to maintain or activate AMPK, leading to cytotoxicity. However, non-cancer cells do not exhibit the cytotoxic effect of metformin under restricted glucose conditions as non-cancer cells can rely on other glycolytic substrates to maintain ATP levels and are less dependent on glucose (Zhuang, et al., 2014). Glutamine does not exacerbate the effect of metformin as the generation of ATP from glutamine depends on the mitochondria, relying on the TCA cycle and oxidative phosphorylation whereas glucose can provide ATP via glycolysis or oxidative phosphorylation therefore metformin can inhibit the growth of those cells that rely on glutamine as a carbon source (Javeshghani, et al., 2012). Metformin treatment under restricted glucose conditions showed a dose-dependent decrease in cell viability in endometrial cancer cell lines. High glucose may encourage cancer cells to undertake the glycolytic pathway to protect against drugs that target OXPHOS (Sivalingam, et al., 2020). Metformin treatment with low glucose conditions also strongly induced cell cycle G1 arrest in endometrial cancer cells (Guo, et al., 2019). In ovarian cancer cells, the low glucose and metformin-induced apoptosis was due to the accumulation of ROS, leading to mitochondrial damage. ROS accumulation induced the activation of ASK1 which triggered the mitochondrial localisation of pro-apoptotic protein, NOXA. Apoptosis was initiated by mitochondrial dysregulation (Ma, et al., 2019).

1.4.3.2. Aspartate, pyruvate, and serine

Complex I of the mitochondria supports proliferation by regenerating NAD+. The antiproliferative effect of metformin may also be due to the inhibition of aspartate

biosynthesis and the loss of NAD+/NADH homeostasis. Cells cultured in media without pyruvate were more sensitive to metformin treatment, requiring lower concentrations for inhibition of proliferation. The presence of pyruvate or the addition of exogenous pyruvate in the environment can help maintain the NAD+/NADH ratio in the absence of complex I activity. Pyruvate allowed the regeneration of NAD+ via its conversion to lactate in addition to the increase in cellular aspartate levels. Aspartate plays a role in purine synthesis, metformin causes nucleotide insufficiency due to decreased aspartate levels (Gui, et al., 2016). Serine metabolism supports cancer cell proliferation through the facilitation of amino acid transport, nucleotide synthesis and folate metabolism (Mattaini, et al., 2016). The deprivation of serine potentiated the antiproliferative effect of metformin on transformed cells compared to non-transformed cells (Gravel, et al., 2014).

1.4.3.3. Galactose

Galactose is a by-product of lactose conversion to glucose by the enzyme lactase and is important for the biosynthesis of glycoproteins and glycolipids which are required for cellular functions in cancer such as cell-cell recognition, metastasis, and receptor signalling (Tang, et al., 2016). Replacing glucose with galactose forces cells to rely on mitochondrial respiration (OXPHOS). Metformin was able to reduce cell growth for breast cancer cell lines MDA-MB-468 but not MCF7, and MDA-MB-231 under hyperglycaemic conditions (25 mM glucose). However, metformin treatment in glucose free media supplemented with galactose led to the inhibition of all three cell lines (Lord, et al., 2020). These studies highlight the importance of the levels of metabolites present in the tumour microenvironment and its effect on the efficacy of metformin.

1.5. Aims and Objectives

The aim of this thesis was to investigate the importance of metabolism on EOC progression through the regulation of epigenetics and immune response with a focus on metformin as a potential anti-cancer drug. Additionally, the influence of oncometabolites and the OC tumour microenvironment on OC cell lines was also explored. The following chapters will discuss the objectives which were:

1. Establish the effect of metformin on the immunological response in chemosensitive and chemoresistant HGSOC cell lines in cell culture conditions and physiological OC conditions.
2. Determine what pathway is involved in the immune response to metformin at an epigenetic level using the chromatin immunoprecipitation (ChIP) and methylated DNA immunoprecipitation (MeDIP) assay.
3. Investigate the effect of oncometabolites on OC cell line proliferation in cell culture conditions and physiological OC conditions

Chapter 2

Methods and Materials

2.1. Cell lines and culture conditions

Two ovarian cancer cell lines SKOV3 (ATCC; Cat#HTB-77) and OVCAR3 (ATCC; Cat#HTB-161) were obtained from American Type Culture Collection (ATCC). Two ovarian cancer cell lines PEO1 (ECACC; Cat#10032308) and PEO4 (ECACC; Cat#10032309) were obtained from European Collection of Authenticated Cell Cultures (ECACC). SKOV3 cells were maintained in McCoy's 5A (Modified) medium (Gibco; Cat#26600-023) and 10% foetal bovine serum (FBS) (Biosera; FB-1001). PEO1 and PEO4 cells were maintained in RPMI-1640 medium (Gibco; Cat#31870-025) with 10% FBS, and 1% L-glutamine (Gibco; Cat#25030-024). OVCAR3 cells were maintained in RPMI-1640 medium with 20% FBS, 1% L-glutamine and 0.5% bovine insulin (Sigma; Cat#I0516-5ML) All cell lines were supplemented with 1% Antibiotic-Antimycotic (ABAM) solution (100x) (Merck; Cat#A5955) and cultured in a T-75 flask at 37°C in a humidified atmosphere at 5% CO_2.

DMEM was used for the experimental culture media with 10% FBS and 1% ABAM. Experimental culture media was made by combining different volumes of DMEM containing 5.5 mM glucose (Gibco; Cat#31053028) with DMEM glucose-free medium glucose (Gibco; Cat#A1443001) to obtain the different glucose concentrations ('Low' - 1mM, 'Normal' - 10 mM, 'High' - 25 mM). FBS used is not dialysed therefore exact glucose concentrations are higher than reported. The media was also supplemented with L-glutamine and sodium lactate (Sigma; Cat#L7022) depending on the culture condition listed in Table *1*.

Table 1. Experimental culture conditions

Media condition		For 50 mL of Media			
		DMEM, High Glucose (25 mM) (mL)	DMEM, No Glucose (mL)	L-glutamine [200 mM] (mL)	Sodium Lactate [1 M] (mL)
Low Glucose (1mM) + (2mM) Glutamine	LG + Q	2	48	0.5	0
Normal Glucose (10 mM)	NG	30	20	0	0
Normal Glucose (10 mM) + (2mM) Glutamine	NG + Q	30	20	0.5	0
Normal Glucose (10 mM) + (2 mM) Glutamine + (10 mM) Lactate	NG +Q + Lac	30	20	0.5	0.5
High Glucose (25 mM) + (2 mM) Glutamine	HG + Q	50	0	0.5	0

2.2. Cell line maintenance

Upon reaching 70-80% confluency, cells were gently washed with PBS (Gibco; Cat#10010023) and detached using Accutase (Merck; Cat#A6964) for 15 min at 37^{o}C. Accutase was deactivated by the addition of complete cell culture media before subculturing the cells at a ratio of 1:3 media for OVCAR3 and PEO4 cell lines and 1:5 media for SKOV3 and PEO1 cell lines to ensure cells maintained sub-confluency. The media was changed, or cells were subcultured every 2 - 3 days.

2.2.1. Preparing and thawing cryostocks

Cells stocks were prepared after detaching and counting the cells using the Coulter Counter (BR-9723A, USA) and centrifugation at 500 x g for 5 min. The cell pellet was resuspended in a freezing solution (5% DMSO (Merck; Cat#D5879-1L-M) and complete cell culture media) at a density of 1 x 10^6 cells/mL. The cell suspension was aliquoted into cryovials (Elkay; Cat#127-T310-200) and stored at -80^{o}C for 24 h before transferring to the liquid nitrogen for long term storage. To revive frozen cells, cryovials were thawed at 37^{o}C. The cell suspension was diluted with complete medium and centrifuged at 500 x g for 5 min to remove freezing media. The cell pellet was then washed 2 times before culturing in a T-25 flask with fresh medium.

2.3. Spheroid preparation

2.3.1. Hanging drop

2.3.1.1. Methylcellulose preparation

Preparation of spheroid media was adapted from Ware, et al., (2016). A 2.4% methylcellulose stock solution was prepared by dissolving 12 g of autoclaved methylcellulose powder (Merck; Cat#M0512) to preheated 500 mL cell media (60^{o}C) for 20 min before the addition of double the percentage amount of FBS for each cell line. The final stock solution was mixed overnight at 4^{o}C prior to centrifugation at 5000 x g for 2 h at room temperature. The clear and viscous supernatant was used to make 20% stock and 80% culture media solution corresponding to 0.48% methylcellulose solution.

2.3.1.2. Preparation of the hanging droplets

The cell suspension was diluted to 2.5 x 10 cells/mL with 20% of the 0.48% methylcellulose and 80% of complete culture medium solution. After gently mixing the diluted cell suspension solution, 20 µL droplets were pipetted onto a lid of a petri dish (Greiner bio-one; Cat#688161) and inverted over dishes containing 10 mL PBS.

2.4. Statistical Analysis

All experiments were repeated using at least three different passages, unless otherwise stated. Results are displayed as the mean and standard error of the mean (SEM). GraphPad Prism 8.0.2 was used to generate graphs. R was used to perform statistical analysis. Shapiro-Wilk's test was used to test for normality. Students t-test, One Way ANOVA, Two-Way ANOVA were used where stated in *Results*.

Chapter 3

Repurposing metformin for the treatment of ovarian cancer

3.1. Introduction

Platinum-based treatments are the first-choice chemotherapeutic drugs used to treat epithelial ovarian cancer (EOC). Patients initially respond well to treatment, but the majority will relapse due to the development of chemotherapy resistant tumours; therefore, highlighting the need for new therapeutic options (Ozols, 2005). Drug repurposing is the process of investigating existing drugs for new therapeutics, outside of their original purpose. As the traditional method of drug development can take many years with a high rate of failure, there are many advantages to drug repurposing. For example, the data regarding safety and toxicity has already been established and it is also economical as the cost for repurposing drugs is less than the development of new drugs. Furthermore, established medicines are cheaper than novel therapies as well as being readily available world-wide.

Metformin is a biguanide drug which is a widely prescribed first line treatment for Type 2 diabetes. Studies have found that metformin treatment is associated with improved cancer prognosis, in addition to a reduced incidence and mortality seen across many cancer types, such as gastric adenocarcinoma (Zheng, et al., 2021), lung cancer (Brancher , et al., 2020) and head and neck cancers (Rego, et al., 2015; Saraei, et al., 2019). EOC patients with a co-morbidity of Type 2 diabetes, who used metformin, showed an increase in progression-free survival (Romero, et al., 2012; Kumar, et al., 2014). Additionally, long-term use of metformin was associated with a decreased risk in EOC (Bodmer, et al., 2011). *In vitro,* metformin was found to inhibit the formation of ovarian tumour spheroids and potentiated the anti-proliferative effect of cisplatin cytotoxicity (Gotlieb, et al., 2008; Rattan, et al., 2011; Shank, et al., 2012). Furthermore, in a randomised clinical trial, non-diabetic women with EOC receiving 1500 mg alongside carboplatin/paclitaxel showed a lower rate of recurrence compared to control EOC patients who received standard chemotherapy without metformin (Hamedi, et al., 2018). Metformin is able to inhibit multiple pathways which may reduce the risk of inducing chemotherapy resistance. Additionally, metformin treatment was able to inhibit the proliferation of most HGSOC cell lines but did not affect fallopian tube secretory cell lines, which were used as a control for normal cells, making it desirable as a candidate for drug repurposing for OC treatment (Hodeiba, et al., 2017). However, despite showing promising results, the use of metformin in some tumour types is

controversial as it failed to improve outcomes in patients of certain types of cancer (Lega, et al., 2013; Lee, et al., 2019; Skinner, et al., 2021).

Metformin has been shown to exhibit anti-inflammatory effects and can decrease inflammatory cytokine production such as IL-6, IL-8, TNF-α and VEGF by inactivating NF-κB and HIF-1α (Ersoy, et al., 2008; Huang, et al., 2009; Guo, et al., 2019). Patients undergoing metformin treatment showed lower IL-6 protein expression in ovarian cancer tumour stroma (Xu, et al., 2018). Despite metformin reportedly showing an anti-inflammatory effect in EOC (Xu, et al., 2018; Yang, et al., 2021), an MSci student under my mentorship showed that metformin appeared to induce a significant increase in IL-6 production (Figure 7A) and a non-significant increase in IL-8 production (Figure 7B) in the chemosensitive ovarian cancer PEO1 cell line. This increase was observed at a physiological concentration of 0.625 mM in low glucose (1 mM) media supplemented with glutamine (2 mM) at 96 h (Kellenberger, et al., 2010; Tourkmani, et al., 2018). If considering the use of metformin in the treatment of EOC, this effect could be detrimental and worsen the pathological state as cytokines IL-6 and IL-8 can promote migration and invasion of EOC through chemotaxis (Nieman, et al., 2011). The mechanism behind the increased IL-6 production is not yet known but potential pathways include JAK/STAT3 signalling (Johnson, et al., 2018) and AMPK/TET2 signalling (Wu, et al., 2018).

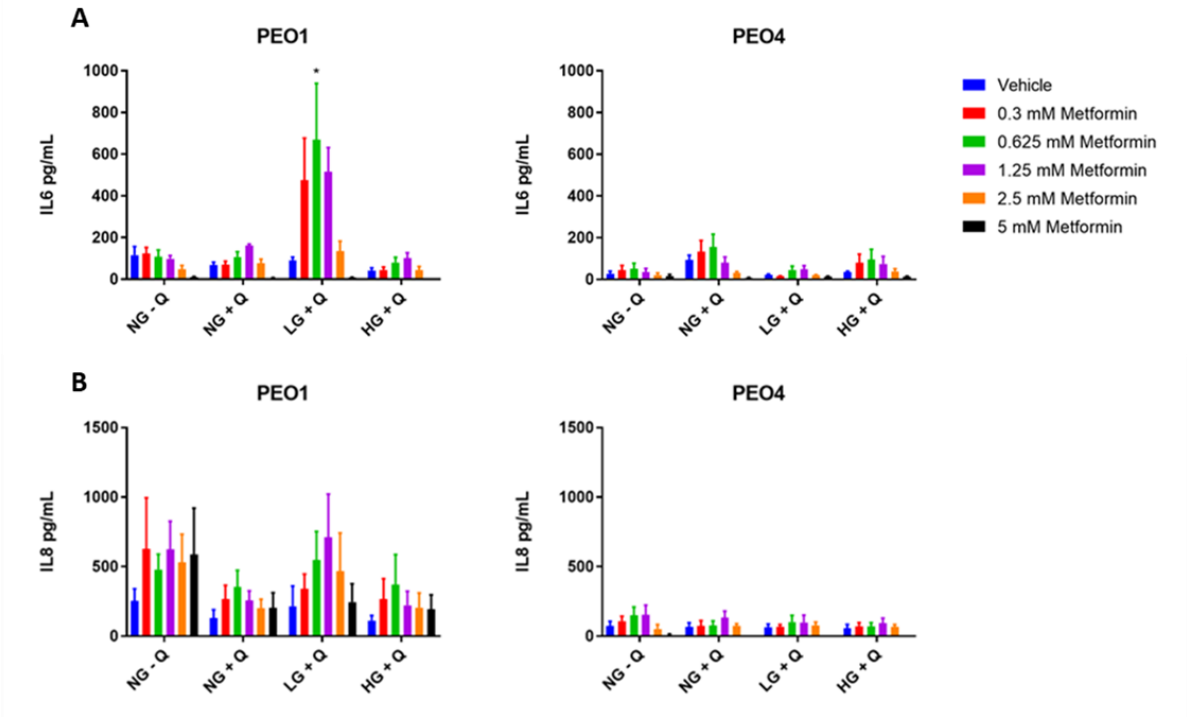

Figure 7. ELISA assay performed on the supernatants of PEO1 and PEO4.
IL-6 (A) and IL8 (B) secretion were measured after 96 h. Different concentrations of metformin (0 mM – 5 mM) and experimental conditions (NG – Q: 10 mM glucose, NG + Q: 10 mM glucose, 2 mM glutamine, LG + Q: 1mM, 2 mM glutamine, HG + Q: 25 mM glucose, 2mM glutamine) were used. In PEO1 cells, treatment with 0.625 mM in LG + Q showed a significant increase in IL-6 production and a non-significant increase in IL8 production. Statistical analysis by Two-way ANOVA: $p < 0.05$ (*). (n = 3 independent cell passages, error bars represent ± S.E.M.). (Data generated by an MSci student under my mentorship, unpublished)

Cytokines are produced by multiple cell types including tumour infiltrating immune cells, stromal cells as well as the tumour cells themselves. Cytokine signalling, including IL-6 and IL-8, stimulates the hyperactivation of JAK/STAT signalling. The cytokines then act directly on the tumour cells to induce expression of STAT3 target genes that encode proteins that drive tumour proliferation and/or survival (Johnson, et al., 2018). STAT3 is constitutively activated in many cancers and *in vitro* and *in vivo* human cancer models (Berishaj, et al.,

2007; Lee, et al., 2019). STAT3 can become phosphorylated upon the binding of JAK proteins to the cytokine receptor, which then leads to the translocation of the phosphorylated STAT3 (pSTAT3) dimers to the nucleus, leading to the transcription of downstream genes (Wang, et al., 2013). STAT3 can induce the expression of genes for pathways that drive tumorigenesis such as cyclin D1 (*CCND1*), angiogenesis (*VEGF*), invasiveness and metastasis (MMPs) (Johnson, et al., 2018).

Interleukin-6 signalling is mediated by two different pathways: classic signalling and *trans*-signalling (Figure 8). Classical signalling involves the binding of IL-6 to the IL-6 receptor (IL-6R) on the cell surface followed by the interaction of the complex with gp130. In *trans*-signalling, IL-6 binds to the secreted form of IL-6R (sIL-6R), which then binds to gp130. The formation of the IL-6, IL-6R and gp130 hexamer leads to the phosphorylation of STAT3 through JAKs before translocation to the nucleus and upregulation of target genes, including *IL6* and *IL8* (Nilsson, et al., 2005; Johnson, et al., 2018).

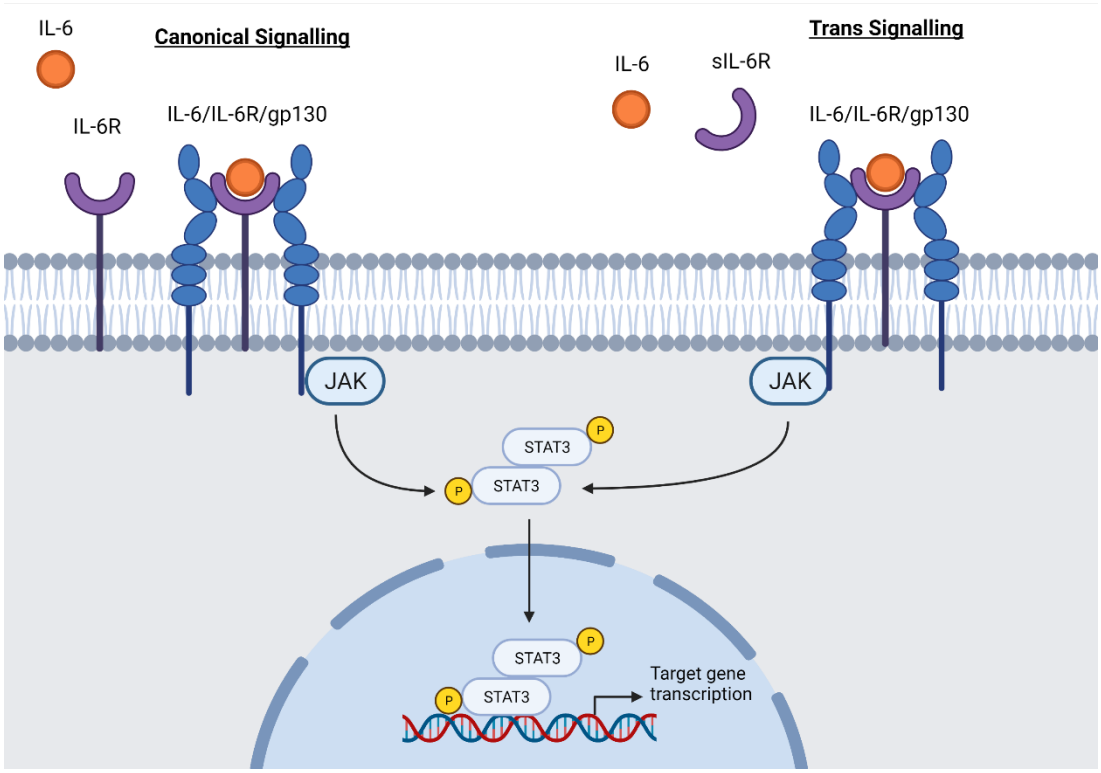

Figure 8. Canonical IL-6 signalling vs IL-6 trans-signalling.
Canonical IL-6 involves the binding of IL-6 to the IL-6 receptor (IL-6R) which then interacts with gp130. Trans signalling involves the binding of IL-6 to the secreted form of the IL-6R (sIL-6R) before binding to gp130. Formation of the hexamer results in the phosphorylation of STAT3 through JAKs

Phosphorylated STAT3 translocates to the nucleus to drive downstream gene expression. Created with BioRender.com

In turn, IL-8 secreted from the tumour cells can bind to two cell-surface G-protein coupled receptors known as CXCR1 and CXCR2, which promotes the activation of JAK/STAT signalling and the nuclear translocation of STAT3 (Figure 9) (Long, et al., 2016). The presence of IL-6 or IL-8 in the tumour microenvironment could form a positive feedback loop though the autocrine/paracrine activation of JAK/STAT signalling, increasing their expression (Wang, et al., 2013; Jin, et al., 2017).

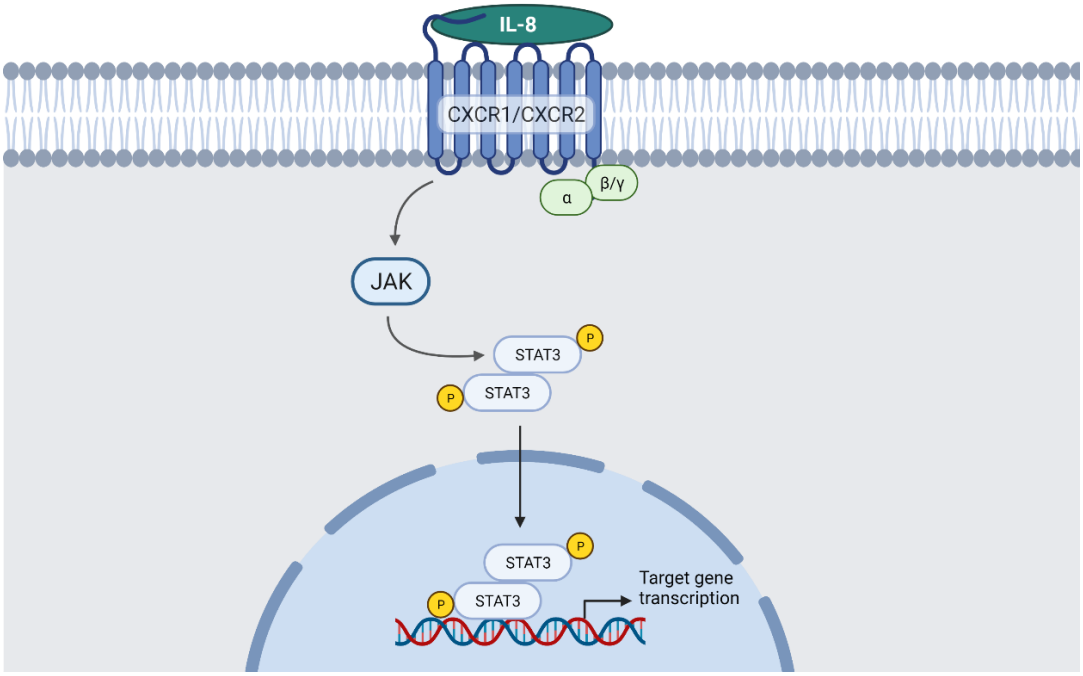

Figure 9. IL-8 activation of the JAK/STAT3 signalling pathway.
IL-8 binds to the G-coupled receptors CXCR1/CXCR2 which results in the phosphorylation of STAT3 through JAK. Phosphorylated STAT3 translocates into nucleus to drive target gene expression. Created with BioRender.com

STAT3 phosphorylation is correlated with cisplatin resistance. Metformin enhanced the cytotoxic effect of cisplatin and inhibited STAT3 phosphorylation in a dose-dependent manner (Lin, et al., 2013). STAT3 can be phosphorylated at the tyrosine 705 (Y705) residue as well as the serine 727 (S727) residue. The phosphorylation of STAT3 Y705 is responsible for processes that lead to malignant transformation by promoting cell proliferation, angiogenesis, and immune evasion (Lee, et al., 2019). STAT3 S727 phosphorylation may be

involved in the modulation of mitochondrial respiration (Lee, et al., 2019). *In vitro,* metformin reduced the expression of phosphorylated STAT3 S727 and total STAT3 and its target genes, leading to the inhibition of cell proliferation, survival, and migration in endometrial cancer. *In vivo*, metformin also reduced STAT3 (phosphorylated and total) and target proteins, leading to a decrease in tumour weight (Wallbilich , et al., 2017). In glioblastoma cells, metformin inhibited STAT3 phosphorylation and could potentiate the antiproliferative effect of Stattic, a STAT3 small-molecule inhibitor (Leidgens, et al., 2017).

The tumour suppressor, TET2 is a substrate of AMP-activated protein kinase (AMPK). AMPK is involved in energy conservation and its activation leads to the inhibition of anabolic processes involved in growth and proliferation (Shackelford & Shaw, 2009). TET2 can become stabilised by its phosphorylation by AMPK. Metformin treatment protected the AMPK-mediated phosphorylation of serine residue 99 (S99) on TET2 which increased TET2 stability and 5hmC levels. The phosphorylation of S99 may protect TET2 from degradation by calpain (Figure 10). Hyperglycaemia caused the destabilisation of TET2 which resulted in the dysregulation of 5hmC and the tumour suppressive function of TET2. Glucose-responsive cells - peripheral blood mononuclear cells (PBMC), human endothelial cells (HUVEC) and erythroleukemia cells (TF-1) showed a decrease in TET2 in hyperglycaemic conditions (Wu, et al., 2018). During myogenesis, AMPK stabilises murine TET2 protein by phosphorylation at serine residue 77 leading to an increase in 5hmC (Zhang, et al., 2019).

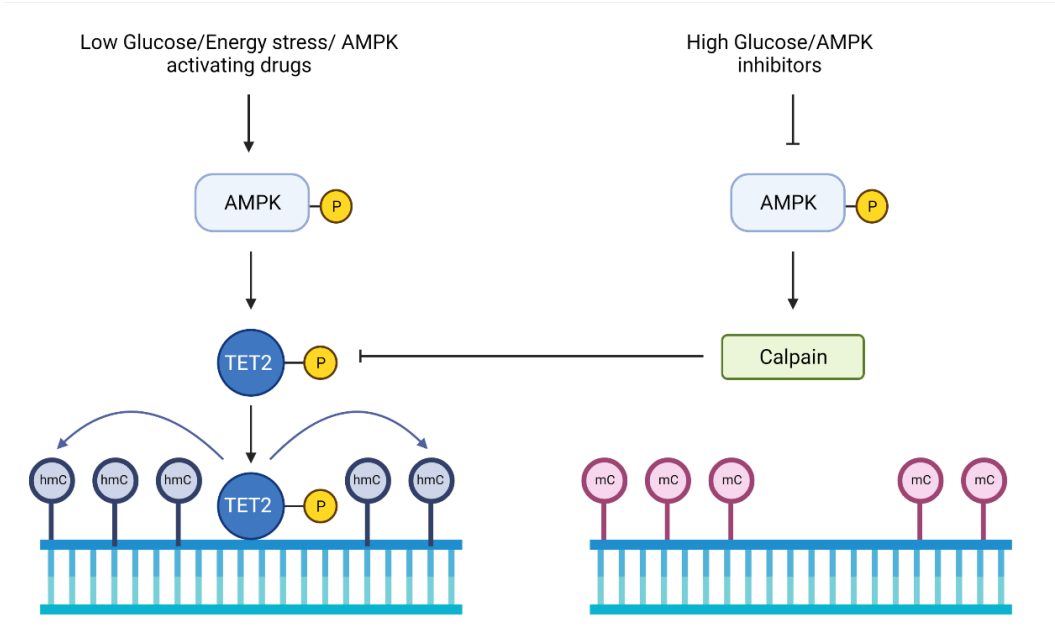

Figure 10. AMPK/TET2 signalling forms the link between metabolism and the epigenome. Under low glucose conditions, AMPK stabilises TET2 through the phosphorylation of the serine 99 residue. In high glucose conditions, calpain degrades TET2 resulting in aberrated regulation of DNA methylation. Figure adapted from (Wu, et al., 2018). Created with BioRender.com

TET2 has been reported to play a role in the regulation of the inflammatory response. In innate myeloid cells (including dendritic cells and macrophages), TET2 controls the repression of *IL6* transcription during inflammation. An IL-6 specific transcription factor, IκB controls the targeting of TET2 to the *IL6* promoter during the initial and resolution phases of inflammation. In LPS-activated dendritic cells, TET2 and HDAC2 formed a complex which bound directly to the *IL6* promoter leading to the repression of *IL6* transcription through histone deacetylation (Zhang, et al., 2015). Despite its role as a tumour suppressor, TET2 also exhibits pro-oncogenic roles in osteosarcoma cells through the demethylation of the *IL6* promoter leading to increased *IL6* expression – promoting lung metastasis. TET2 may be essential for *IL6* expression in osteosarcoma cells at the primary site. *In vivo*, TET2 activity appears to have little effect on the proliferation rate of tumour cells but is associated with increased metastatic capacity in osteosarcoma cells (Itoh, et al., 2018).

OC patients show a plasma glucose concentration range of approximately 3.3 mM to 17 mM (Lamkin, et al., 2009). Whereas, in malignant ascites, the glucose concentrations were <3.3 mM (Kipps, et al., 2013); plasma glucose concentrations below 4 mM are considered

hypoglycaemic (Tourkmani, et al., 2018). The local EOC tumour microenvironment (TME) in the ascites is often hypoglycaemic as a result of tumours taking up large volumes of glucose, so to better represent the TME, a glucose concentration of 1 mM was used in this study, to represent the hypoglycaemic conditions (Kellenberger, et al., 2010; Tourkmani, et al., 2018). Glutamine is maintained in circulation at 0.6 – 0.9 mM in healthy patients (Bergström, et al., 1974). Glutamine concentration is increased in OC showing a 2-fold change compared to borderline tumours (Denkert, et al., 2006) and 0.46-fold change compared to healthy controls (Hilvo, et al., 2016). Therefore, a higher concentration of glutamine (2 mM) was used for this study to represent this. The significant increase in cytokine response to metformin in OC cell lines was only observed in the low glucose conditions supplemented with glutamine (Figure 7), conditions which corresponds with what is observed physiologically.

3.2. Aims and objectives

The aims of this Chapter were to explore the effect of metformin on 2D and 3D cultured HGSOC cells under differing glucose conditions over long time-periods. The differences between 2D and 3D cultured cells will also be explored as 3D aggregates better represent the conditions found *in vivo*. Additionally, the work in this Chapter aimed to assess whether JAK/STAT3 signalling or AMPK/TET2 signalling was involved in the increase in inflammation under specific conditions. The objectives were:

1. Examine the morphology, cell viability, proliferation, and inflammatory response of 2D and 3D HGSOC cells treated with a physiological concentration (0.625 mM) of metformin under differing glucose conditions every 48 h until 144 h using brightfield microscopy, MTT, DC assay and ELISAs.
2. Establish the expression levels of phosphorylated and total STAT3 and AMPK using Western blotting to determine the potential pathway involved in the inflammatory response.

3.3. Methods and Materials

3.3.1. MTT (3-(4,5-Dimethyl-2-thiazolyl)-2,5-diphenyl-2H-tetrazolium bromide) Assay

To determine cell viability, cells were seeded at a density of $7x10^4$ cells per well in a 12-well cell culture plate and incubated under cell culture conditions for 24 h without treatment. After 24 h, 2 mL of LG + Q (1 mM + 2 mM, respectively) or NG + Q (10 mM + 2 mM, respectively) experimental cell media containing a final concentration of 0.625 mM metformin or vehicle was added to each well. The MTT assay was run over 48 h, 96 h and 144 h. The media was changed every 48 h with or without the addition of metformin.

At each time point, a stock solution of MTT (Merck; Cat#M2128) at 5 mg/ml in PBS was diluted to 0.5 mg/mL with cell culture medium. The MTT/media solution was added at 250 µL to each well and the plate incubated at 37°C for 2 h. The MTT/media solution was then removed, and the purple formazan crystals were dissolved in 300 µL of DMSO and incubated at room temperature for 15 min. After the resuspension of the crystals, 100 µL of the solution was pipetted in triplicate into a 96-well plate and then analysed on a microplate reader at 570 nm.

3.3.2. Treatments

3.3.2.1. 2D cultures

PEO1 and PEO4 cells were seeded at a density of 3 x 10^5 cells/mL in a T-25 flask. Cells were allowed to grow for 24 h before treatment. Metformin-HCL (Cat# 2864/100) was purchased from R & D Systems and made up as a stock solution of 150 mM in nuclease-free water (Invitrogen; Cat#AM9937). A final concentration of 0.625 mM metformin or the vehicle (ddH_2O) was diluted in LG + Q or NG + Q experimental cell culture media (**Table *1***). Experimental culture media was changed every 48 h with or without metformin. The cells and supernatants were collected at 48 h, 96 h and 144 h for further experiments.

3.3.2.2. 3D spheroids

PEO1 and PEO4 spheroids were made following the protocol mentioned in 2.3. Briefly, cells were resuspended in LG + Q or NG + Q media with the addition of ddH_2O or a final

concentration of 0.625 mM metformin before seeding on the lid of a petri dish. Approximately 100 spheroids were made per treatment condition. After 48 h, an additional 10 µL of experimental media containing the vehicle or 3 times the concentration of 0.625 mM metformin was added to each spheroid at the 96 h and 144 h condition. After 48 h – for the 144 h time point, an additional 10 µL of experimental media containing the vehicle or 4 times the concentration of 0.625 mM metformin was added to each spheroid. The spheroids were harvested after another 48 h by careful collection into a 1.5 mL tube using a bulb pipette before pelleting at 500 x g for 5 min. The supernatants and cells were collected for further experiments.

3.3.3. Enzyme-Linked Immunosorbent (ELISA) assay

Human IL-6 (RnD Systems; Cat#DY206-05) and IL-8 ELISA assays (RnD Systems; Cat#DY208-05) were performed on the supernatants, according to the manufacturer's protocol. All incubations were performed at RT. The aspiration step was performed 3 times. Half-area 96-well plates (Greiner bio-one, Cat#675001) were coated with the capture antibody and incubated overnight with gentle rocking. After incubation, each well was aspirated using wash buffer (0.5% PBS (Thermo Fisher; Cat#10010023) TWEEN 20 (Sigma; Cat#SLBS7729)). The plates were then blocked for 1 h before aspiration with wash buffer and the addition of 50 µL standard or sample and incubated for 2 h. The plates were aspirated again, and the detection antibody was added and incubated for 1 h. After incubation, the wash and aspiration step were repeated and the Streptavidin-HRP was added and incubated for 20 min in the dark. The wash and aspiration step were then repeated before the addition of the substrate solution and further incubation for 20 min. The stop solution was added to each well and the plate was read at 570 nm using the microplate spectrophotometer (POLARstar omega; BMG labtech, Offenburg, Germany).

3.3.4. Western blotting

3.3.4.1. Protein extraction

3.3.4.1.1. 2D cultures

The supernatant was removed from the T-25 flasks and stored at -20^{o}C for ELISA assay (3.3.3). The cells were washed with 1 mL of PBS to remove any residual media. To each flask, the lysis mix containing 600 µL of 1 x RIPA lysis buffer (1:10 dilution from 10 x RIPA

buffer - Merck; Cat#20-188), 0.6 µL Protease Inhibitor Cocktail (PIC) (Merck; Cat#P8340-1ML), 0.6 µL Phosphatase Inhibitor Cocktail 2 (Merck; Cat#P5726-1ML) and 0.6 µL Phosphatase Inhibitor Cocktail 3 (Merck; Cat#P0044-1ML) before incubation for 20 min at 4°C. After the incubation period, the cells were scraped using a cell scraper and collected into a 1.5 mL tube. The cells were centrifuged in a Microfuge at maximum speed at 4°C for 10 min. The supernatant was then transferred to a clean 1.5 mL tube and stored at -20°C.

3.3.4.1.2. 3D spheroids

Spheroids were carefully collected into a 1.5 mL tube using a bulb pipette and pelleted at 500 x g for 5 min. After collecting the supernatant, the spheroids were resuspended in PBS to wash and centrifuged at 500 x g for 5 min. The pellet was resuspended in 100 µL of the lysis mix (as mentioned in Section 3.3.4.1.1) before incubation for 20 min at 4°C. After incubation, the suspension was mixed by pipetting to aid in spheroid disaggregation and cell lysis and then centrifuged in a Microfuge at maximum speed at 4°C for 10 min. The supernatant was transferred to a clean 1.5 mL tube and stored at – 20°C.

3.3.4.2. DC Assay and protein preparation

Bovine serum albumin (BSA) (Sigma; Cat#A7906-500) standards were prepared at concentrations from 0–2.5 mg/mL. To a 96-well plate (Nunc, Thermo Fisher #161093), 5 µL of sample or standard was added to wells in duplicate. To each well, a combination of 25 µL of reagent A (alkaline copper tartrate solution; Bio-Rad, Cat #5000113) and 0.5 µl reagent S (surfactant solution; Bio-Rad Cat#5000115) was added and then 200 µl of reagent B (dilute Folin reagent; Bio-Rad Cat#5000114), before a 15 min incubation at room temperature. The plate was then read at 750 nm using a microplate spectrophotometer (POLARstar omega; BMG labtech, Offenburg, Germany).

Sample concentrations were determined from the standard curve. A protein concentration of 10 µg per well was used and prepared for loading by mixing the sample with 2x Laemmli buffer (Sigma, Cat#S3401) at a 1:1 ratio.

3.3.4.3. SDS-PAGE

A 10% sodium dodecyl sulphate-polyacrylamide gel was used to analyse the samples. The sample/Laemmli buffer mix was heated at 95°C for 5 min in a T100 thermal cycler (Bio-Rad) and loaded into a gel with a 5 µL dual colour ladder (Bio-Rad, Cat#1610374). Gels were run in 1x running buffer (100 ml of a 10x running buffer (25 mM Tris, 190 mM glycine, 0.1% SDS) made up to 1L with ddH_2O) for 60-70 min at 120 V.

3.3.4.4. Immunoblotting

The gels were transferred to the polyvinylidene difluoride membrane (GE Healthcare Life Sciences, Cat#10600023) using the Trans-blot turbo transfer system (Bio-Rad) using 1x transfer buffer (100 mL of 10x transfer buffer (25 mM Tris, 192 mM glycine) and 200 mL methanol made up to 1L with ddH_2O). Membranes were blocked using 5% non-fat milk in TBS-Tween (20 mM Tris, 150 mM NaCl, 0.1% Tween 20) for 1 h at room temperature. The membranes were then incubated with primary antibodies (Table 2) at 1:1000 concentration in 5% BSA in TBS-Tween, overnight at 4°C. Membranes were washed 3 times with TBS-Tween with a 5 min incubation between washes before incubation with secondary anti-rabbit IgG (Cell Signalling Technology; Cat#7074S) for 1 h at room temperature. The membranes were then washed again 3 times in TBS-Tween with a 5 min incubation between washes before developing in ECL solution (Clarity western peroxide reagent and Clarity western luminol/enhancer reagent, 1:1; Bio-Rad, Cat#1705061). The ChemiDoc XRS+ (Bio-Rad) was used to image the membranes using the Quantity One software.

Table 2. Primary antibodies used for western blotting.
The antibodies are rabbit monoclonal antibodies, purchased from Cell Signalling Technology.

Antibody	Catalogue number
TET2	#18950S
Phospho-Stat3 (Ser727)	#9134S
Phospho-Stat3 (Tyr705)	#9145s
Stat3	#12640S
p-AMPK	#2535S
AMPK	#5831S
α-Tubulin	#2125S

3.4. Results

3.4.1. The effect of metformin on the morphology, cell viability, proliferation and the inflammatory response in 2D ovarian cancer cells

The 2D cell cultures were treated with metformin under normal and low glucose media conditions, to better replicate the harsh tumour microenvironment. A concentration of 0.625 mM metformin was used due to previously showing a significant increase in inflammatory mediators and being within a physiologically achievable concentration (He & Wondisford, 2015; Kajbaf, et al., 2015) (Figure 7). Metformin appeared to inhibit the growth of PEO1 cells in both low glucose and normal glucose conditions compared to the normal glucose control (Figure 11A). The low glucose condition alone also inhibited the growth of PEO1 cells upon which the addition of 0.625 mM metformin further reduced the growth. After 144 h, the growth number of PEO1 cells treated with metformin in normal glucose conditions appeared comparable to the normal glucose control. In the PEO4 cell line, the low glucose control also inhibited the growth with the addition of metformin only slightly reducing the growth further (Figure 11B). The addition of metformin to the normal glucose condition inhibited the growth of PEO4 cells at 48 h but cells recovered with the growth being comparable to the control at 96 h and 144 h. PEO4 cells treated with metformin in the low glucose media appear show some recovery in growth after 144 h when compared to the low glucose control.

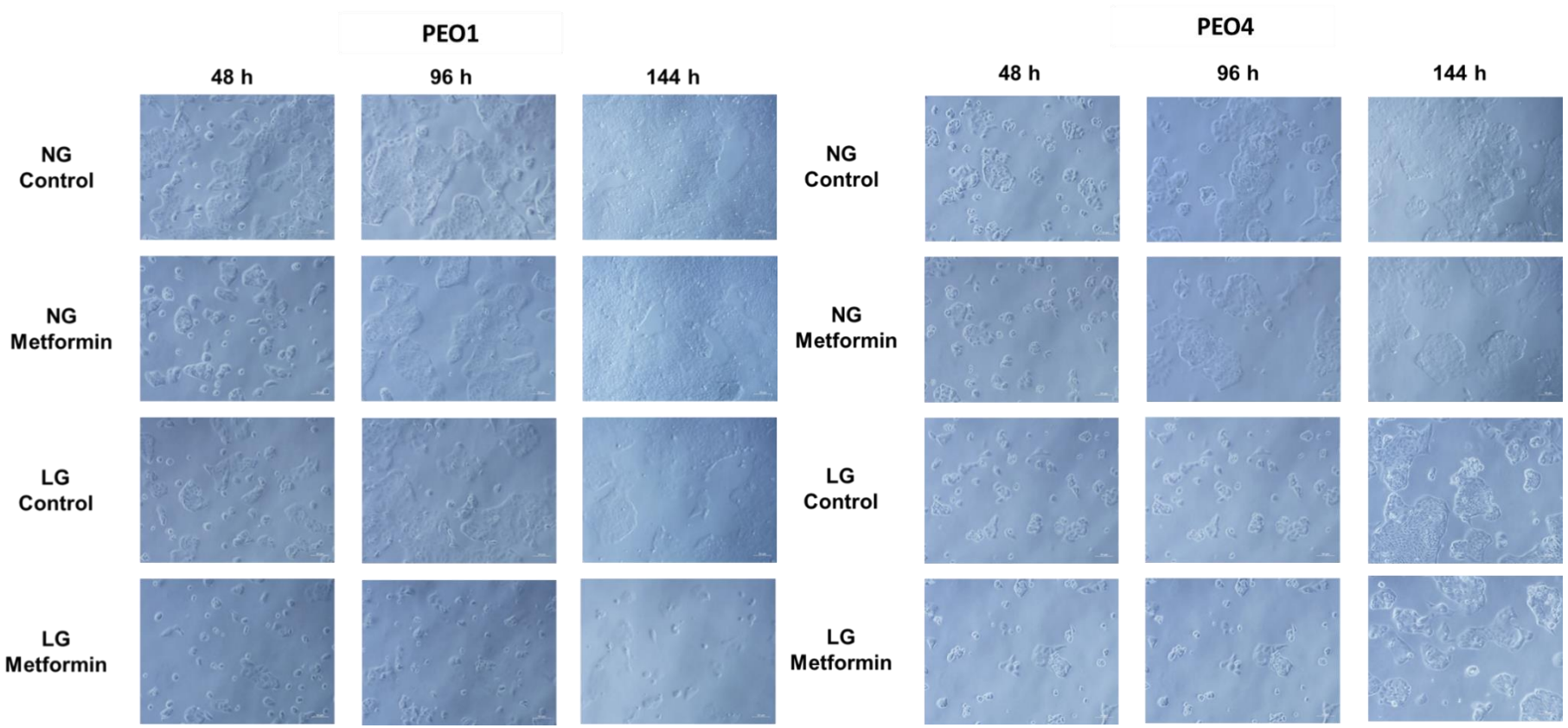

Figure 11. Brightfield microscopy of 2D PEO1 and PEO4 cells treated with metformin.
PEO1 (A) and PEO4 (B) cells were treated with metformin (0.625 mM) and ddH_2O vehicle (control) in media with 10 mM glucose and 2 mM glutamine (NG) or 1 mM glucose and 2 mM glutamine (LG) for 48 h, 96 h and 144 h (Magnification 10x). Scale bar: 50 µM.

The MTT assay was performed on 2D PEO1 and PEO4 cells to determine cell viability. PEO1 cells grown in low glucose media showed a decrease in cell viability which was further reduced when metformin was added (Figure 12). Despite the initial decrease (when compared to the normal glucose control), the low glucose control PEO1 cells showed a gradual increase in cell viability, comparable to the normal glucose and metformin treated cells at 144 h. Metformin treated PEO1 cells in normal glucose media cells appeared to show no noticeable changes in cell viability across all time points. In PEO4 cells, the addition of metformin to low glucose media reduced the cell viability at 96 h which then increased at 144 h. Low glucose control media and normal glucose media with metformin did not appear to significantly affect PEO4 cell viability.

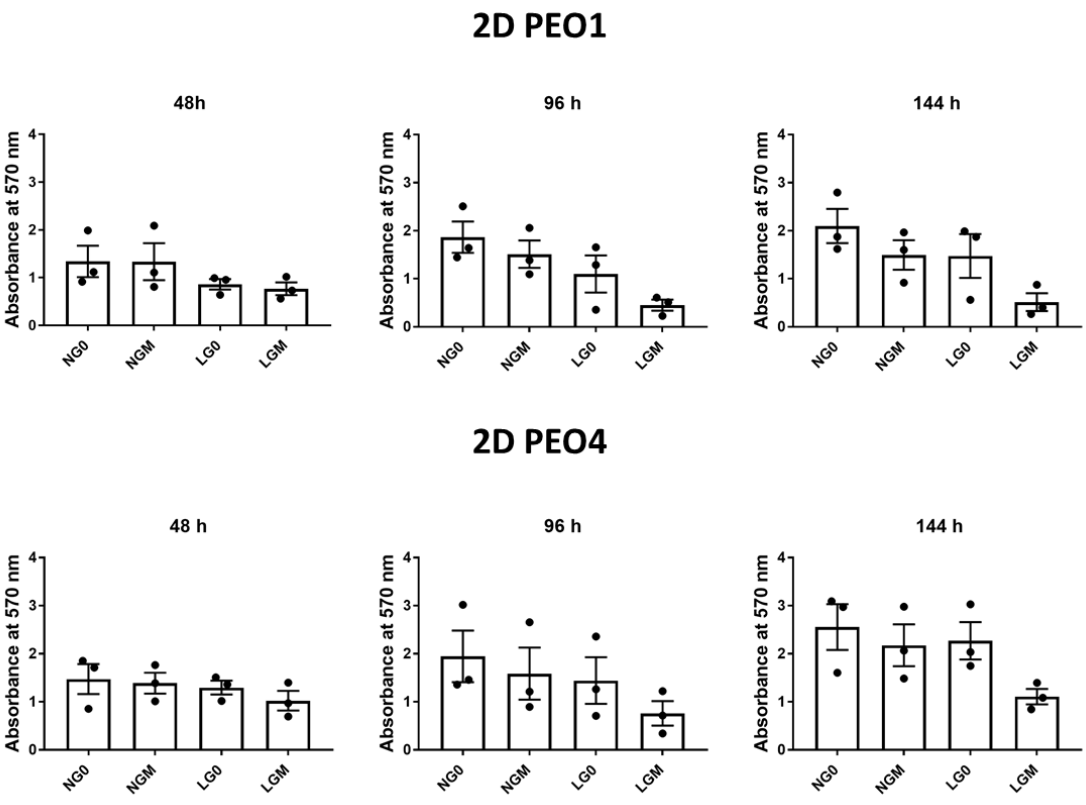

Figure 12. MTT assay of 2D PEO1 and PEO4 cells treated with metformin.
Cells were treated with ddH_2O vehicle (0) or with metformin (M; 0.625 mM) under experimental media conditions (NG – normal glucose (10 mM) + 2 mM glutamine; LG – low glucose (1 mM) + 2 mM glutamine) for 48 h, 96 h and 144 h. Statistical analysis by two-way ANOVA: $p > 0.05$ (n.s.). (n = 3 independent cell passages, error bars represent ± S.E.M.)

As metformin inhibits complex I in the mitochondria, and MTT being a mitochondrial assay (Owen, et al., 2000; Rai, et al., 2018), the DC assay was used as an indirect measurement of cell proliferation by measuring protein concentration in both 2D and 3D cells in addition to validating the MTT data for 2D cells. In 2D PEO1 cells, the addition of metformin to the low glucose media caused a reduction in protein concentration but did not appear to affect cells grown in normal glucose media when compared to the normal glucose control (Figure 13). At 96 h, there was a significant decrease in protein concentration in PEO1 cells treated with metformin grown in low glucose compared to cells treated with metformin in normal glucose conditions ($p < 0.05$). The addition of metformin to 2D PEO4 cells initially increased the protein concentration in both low glucose and normal glucose media at 48 h when compared to their respective controls. At 144 h, the low glucose condition appeared to show a decrease in protein concentration when compared to the normal glucose control. The addition of metformin did not significantly affect protein concentration.

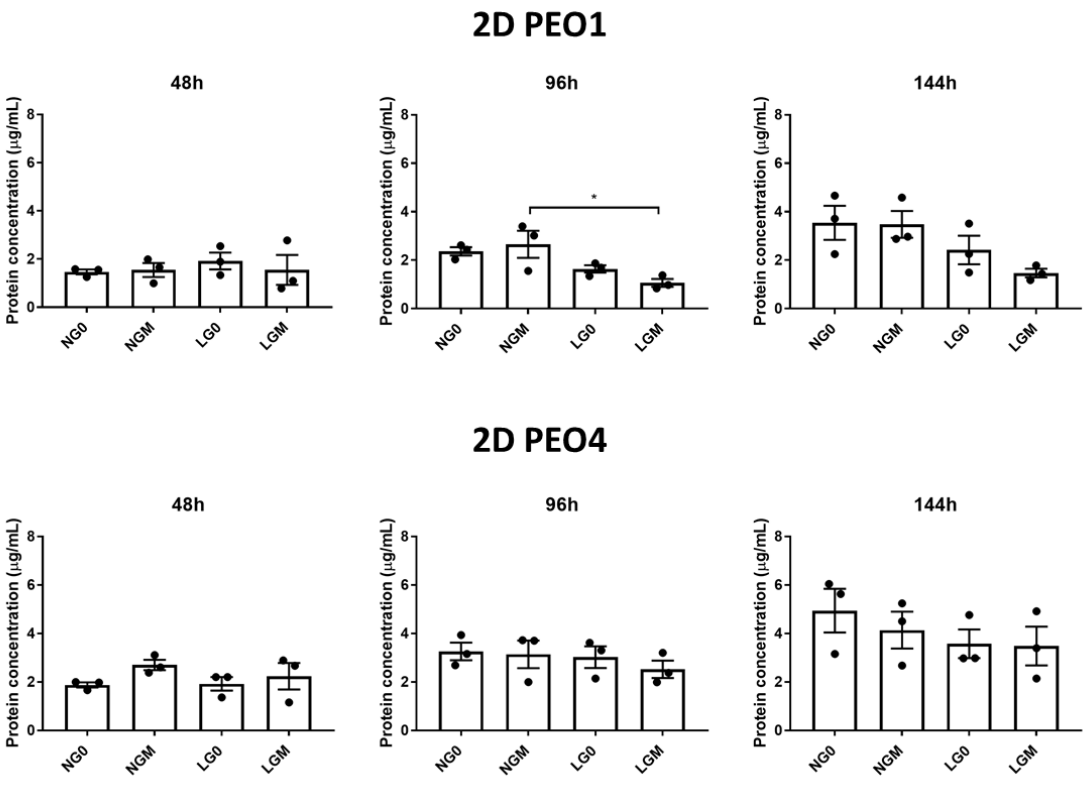

Figure 13. DC assay was performed on 2D PEO1 and PEO4 cells treated with metformin.
Cell lines were treated with ddH_2O vehicle (0) or metformin (M; 0.625 mM) under experimental media conditions (NG – normal glucose (10 mM) + 2 mM glutamine; LG – low glucose (1 mM) + 2 mM glutamine) for 48 h, 96 h and 144 h. Statistical analysis by two-way ANOVA: $p < 0.05$ (*.). (n = 3 independent cell passages, error bars represent ± S.E.M.)

The effect of glucose concentration and metformin on the secretion of inflammatory cytokines was explored. Cytokines IL-6 and IL-8 levels were measured using ELISA. In 2D PEO1 cells, the low glucose media supplemented with metformin caused a significant increase in IL-6 levels compared to the normal glucose media supplemented with metformin ($p < 0.01$) and the low glucose control ($p < 0.05$) at 48 h (Figure 14A).At 96 h, the low glucose media with metformin showed a significant increase in IL-6 production compared to the low glucose control ($p < 0.05$). . In 2D PEO4 cells, IL-6 production was relatively low compared to the 2D PEO1 cells. In contrast to PEO1 cells, the low glucose control resulted in a significant decrease in IL-6 production at 144 h ($p < 0.05$) when compared to the normal glucose control in PEO4 cells.

PEO1 cell line produced more IL-8 than the PEO4 cell line (Figure 14B). The low glucose metformin condition caused a significant increase in IL-8 levels compared to the normal glucose metformin media in 2D PEO1 cells at 48 h ($p < 0.05$). A significant increase in IL-8 production can be seen in cells grown in the low glucose metformin media compared to the normal glucose metformin media at both 96 h ($p < 0.001$) and 144 h ($p < 0.05$). At 96 h, the low glucose metformin media caused a significant increase in IL-8 production compared to the low glucose control media ($p < 0.001$). Additionally, at 144 h, the low glucose control media also caused a significant increase ($p < 0.01$) in IL-8 levels compared to the normal glucose control. Little change in IL-8 production was observed with 2D PEO4 cells at 48 h. At 96 h, the low glucose metformin media caused a significant increase in IL-8 production compared to the low glucose control ($p < 0.05$) and normal glucose metformin media ($p < 0.01$). The low glucose metformin media caused a non-significant increase in IL-8 levels when compared to the low glucose control and the normal glucose condition with metformin at 144 h.

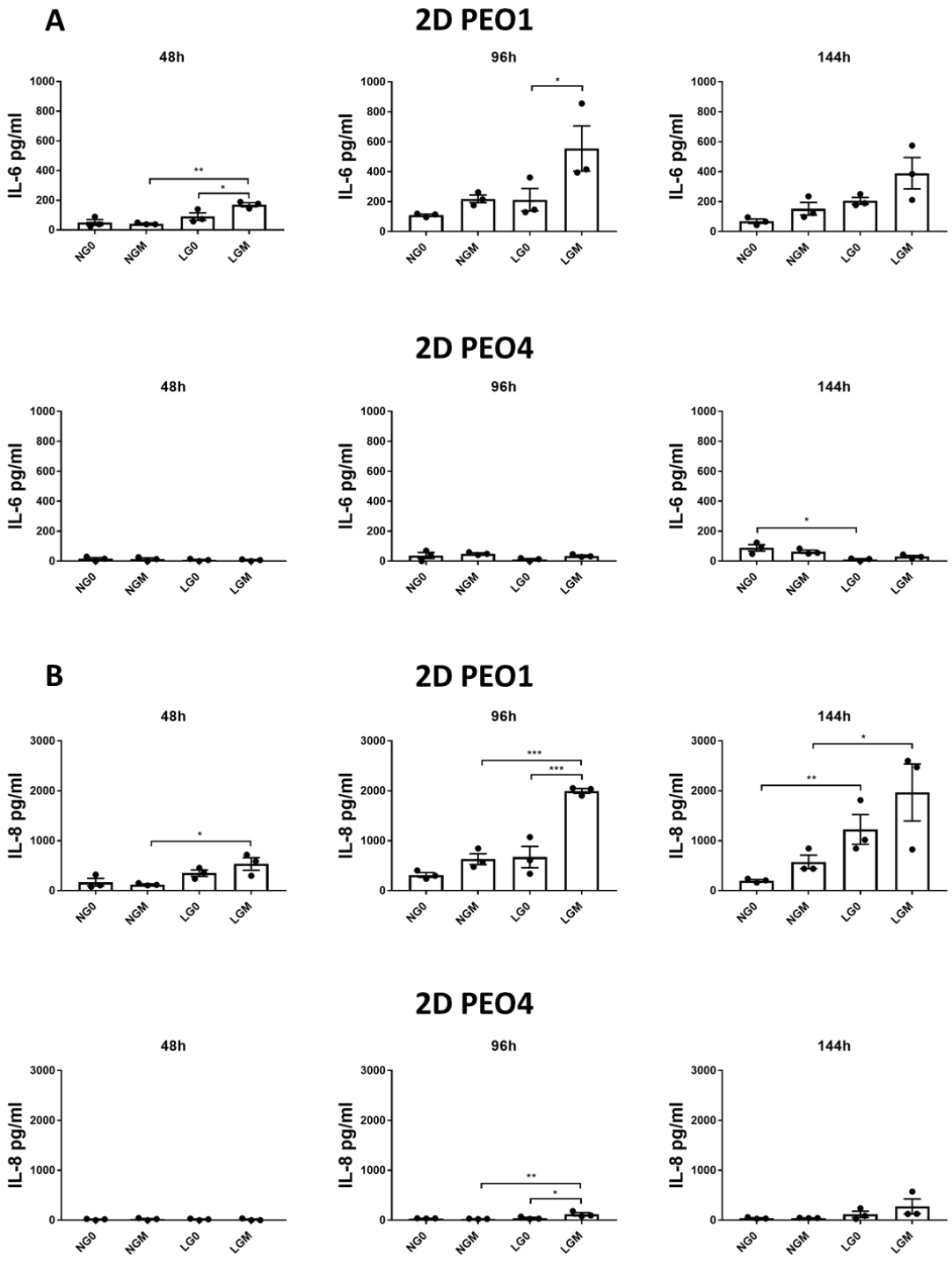

Figure 14. IL-6 and IL-8 ELISA were performed on 2D PEO1 and PEO4 cell lines after metformin treatment.

Cells were treated with metformin (M; 0.625 mM) and ddH_2O vehicle (0; control) in experimental media conditions for 48 h, 96 h and 144 h. ELISA assays were performed on the supernatant to measure the secretion of IL-6 (A) and IL-8 (B). Statistical analysis by two-way ANOVA: $p < 0.05$ (*), $p < 0.01$ (**), $p < 0.001$ (***),. (n = 3 independent cell passages, error bars represent ± S.E.M).

3.4.2. Investigating protein expression of targets involved in IL-6 and IL-8 production using western blotting in 2D ovarian cancer cells

In order to identify the potential mechanism behind the significant increase in IL-6 and IL-8 levels in the PEO1 cell supernatant, expression levels of phosphorylated AMPK (pAMPK) and total AMPK (AMPK/TET2 pathway) and STAT3 (JAK/STAT pathway) were assessed. Phosphorylation of threonine (Thr) residue 172 is essential for AMPK activity (Willows, et al., 2017). At 48 h, metformin caused a non-significant increase in pAMPK in low glucose media in 2D PEO1 cells compared to the normal glucose metformin media (Figure 15A).. At 96 h and 144 h, metformin caused a significant increase in pAMPK in the low glucose media compared to the low glucose control (96 h; $p < 0.05$, 144 h; $p < 0.05$). At both time points, a non-significant increase in pAMPK was seen in the normal glucose metformin media compared to the normal glucose control. In 2D PEO4 cells, the low glucose metformin condition resulted in a significant increase in AMPK phosphorylation compared to the low glucose control ($p < 0.05$) and normal glucose metformin media ($p < 0.05$) at 96 h (Figure 15B).

Phosphorylated STAT3 (pSTAT3) status was measured at both the S727 residue as well as the Y705 residue. A non-significant increase in pSTAT3 S727 was seen in the 2D PEO1 cells cultured in low glucose metformin media when compared to the low glucose control media at 144 h (Figure 16A). Additionally, 2D PEO1 cells grown in low glucose metformin media also showed a significant decrease in pSTAT3 Y705 compared to the low glucose control at 96 h ($p < 0.05$) and 144 h ($p < 0.05$). No significant changes were seen in the levels of STAT3 phosphorylation in 2D PEO4 cells. The addition of metformin appeared to reduce the levels of pSTAT3 S727 at 48 h and 96 h as well as reducing the levels of pSTAT3 Y705 at 96 h and 144 h in both glucose conditions (Figure 16B).

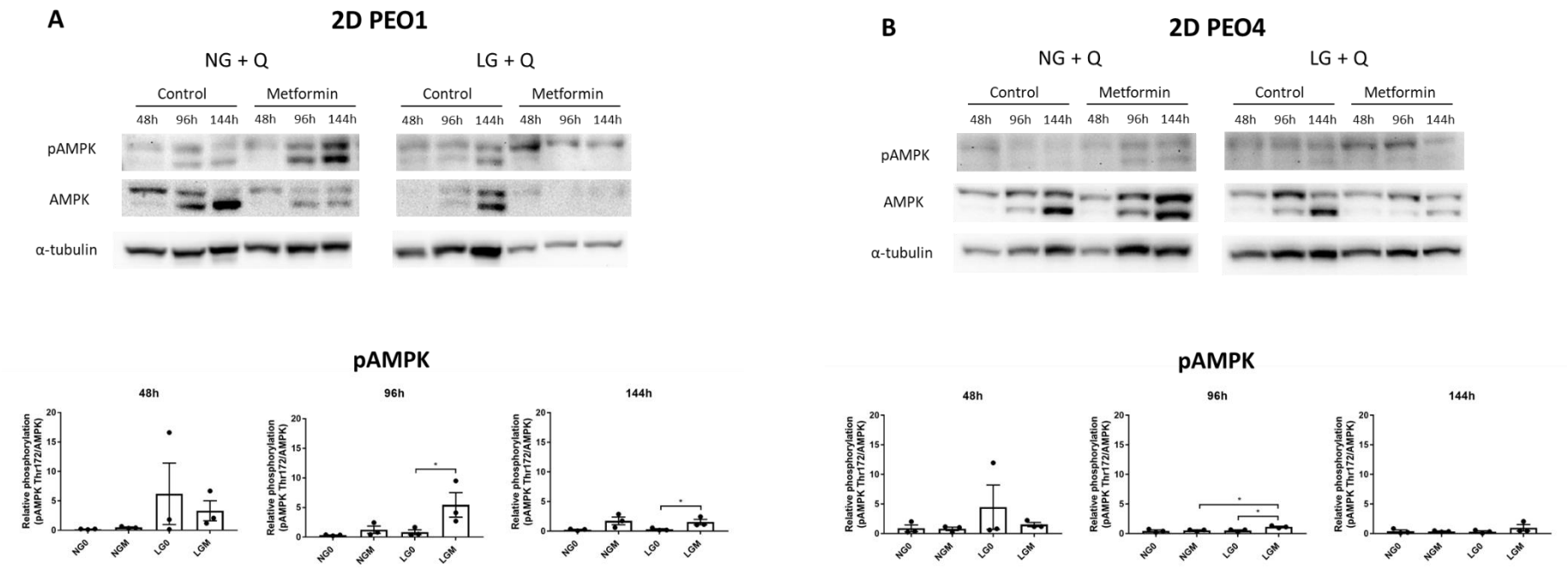

Figure 15. Western blot of AMPK was performed on 2D cultures of PEO1 and PEO4 cells after metformin treatment.
PEO1 (A) and PEO4 (B) cells were treated with metformin (M; 0.625 mM) and ddH_2O vehicle (0; Control) in experimental media conditions for 48 h, 96 h and 144 h. Western blot analysis was used to evaluate phosphorylated AMPK (pAMPK), total AMPK and α-tubulin levels. Protein bands were quantified using Image J. Bars represent relative protein qualification of pAMPK/AMPK normalised to α-tubulin. Statistical analysis by two-way ANOVA: $p < 0.05$ (*). (n = 3 independent cell passages, error bars represent ± S.E.M).

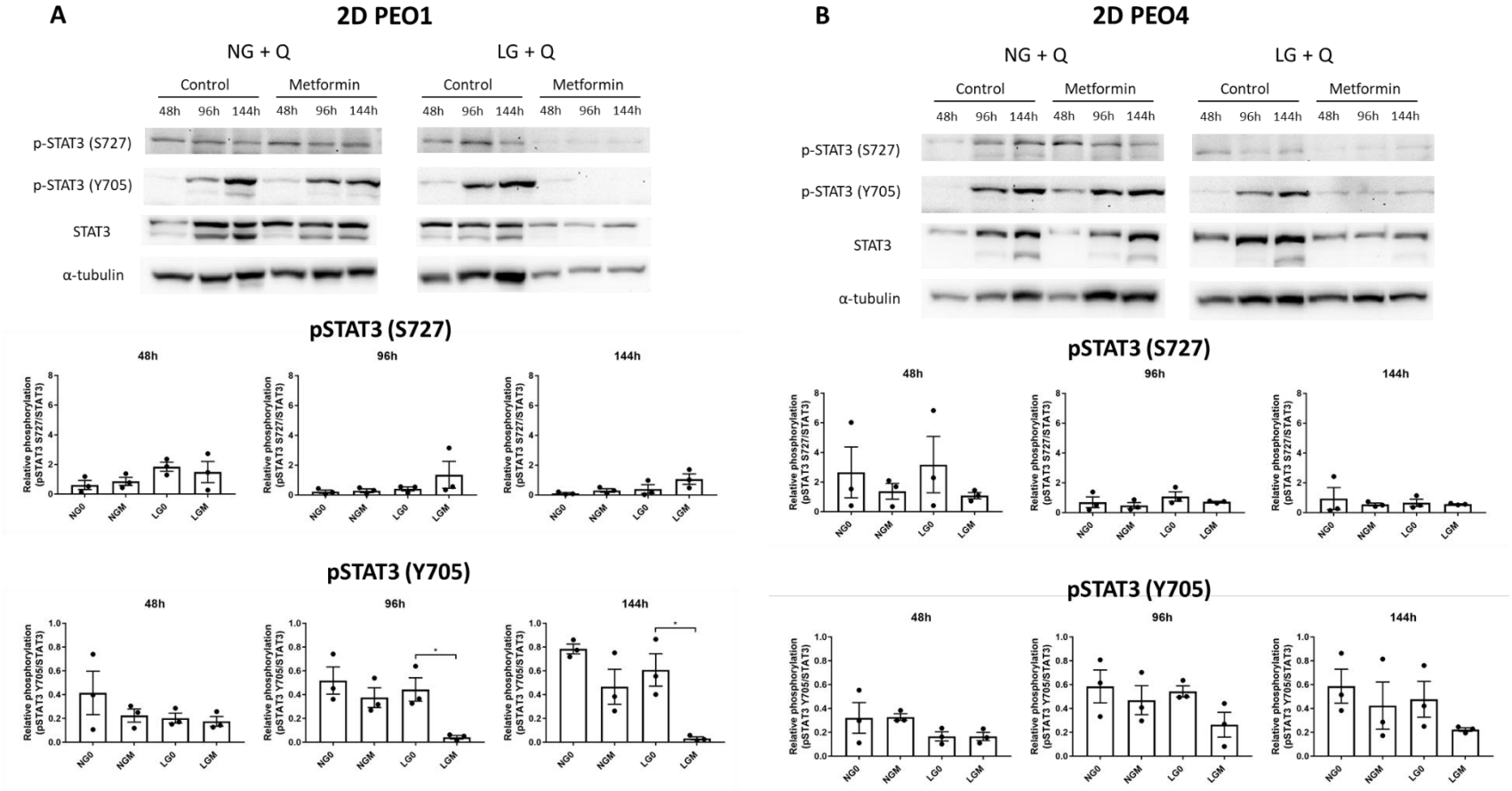

Figure 16. Western blots of pSTAT3 were performed on 2D cultures of PEO1 and PEO4 cells after metformin treatment.
PEO1 (A) and PEO4 (B) were treated with metformin (M; 0.625 mM) and ddH_2O vehicle (0; Control) in experimental media conditions for 48 h, 96 h and 144 h. Western blot analysis was used to evaluate phosphorylated STAT3 serine 727 (pSTAT3 S727), phosphorylated STAT3 tyrosine 705 (pSTAT3 Y705), total STAT3 and α-tubulin levels. Protein bands were quantified using Image J. Bars represent relative protein qualification of pSTAT3/STAT3 normalised to α-tubulin. Statistical analysis by two-way ANOVA: $p < 0.05$ (*)(n = 3 independent cell passages, error bars represent ± S.E.M).

3.4.3. The effect of metformin on the morphology, cell proliferation, , and the inflammatory response in 3D ovarian cancer cells

The addition of metformin in low glucose or normal glucose media did not result in any noticeable changes between each condition in PEO1 spheroid shape and size (Figure 17A). Spheroids under normal glucose conditions (both control and metformin treated) showed less shedding of aggregates at 48 h compared to the rest of the conditions. The control and metformin treated spheroids in low glucose media showed more shedding of cells/aggregates compared to the normal glucose conditions at all time points (48 h, 96 h and 144 h). In PEO4 cells, the addition of metformin to the aggregates grown in normal glucose media did not appear to affect the morphology of the spheroids compared to the normal glucose control (Figure 17B). The aggregates under normal glucose conditions also became more compact after 96 h. Spheroids in low glucose media appear to be less compact than the spheroids grown in normal glucose media. When spheroids grown in low glucose media were treated with metformin, there were more areas of dark and dense cells. Both PEO1 and PEO4 spheroids in low glucose media treated with metformin were easily disaggregated whilst being transferred and processed for further experiments.

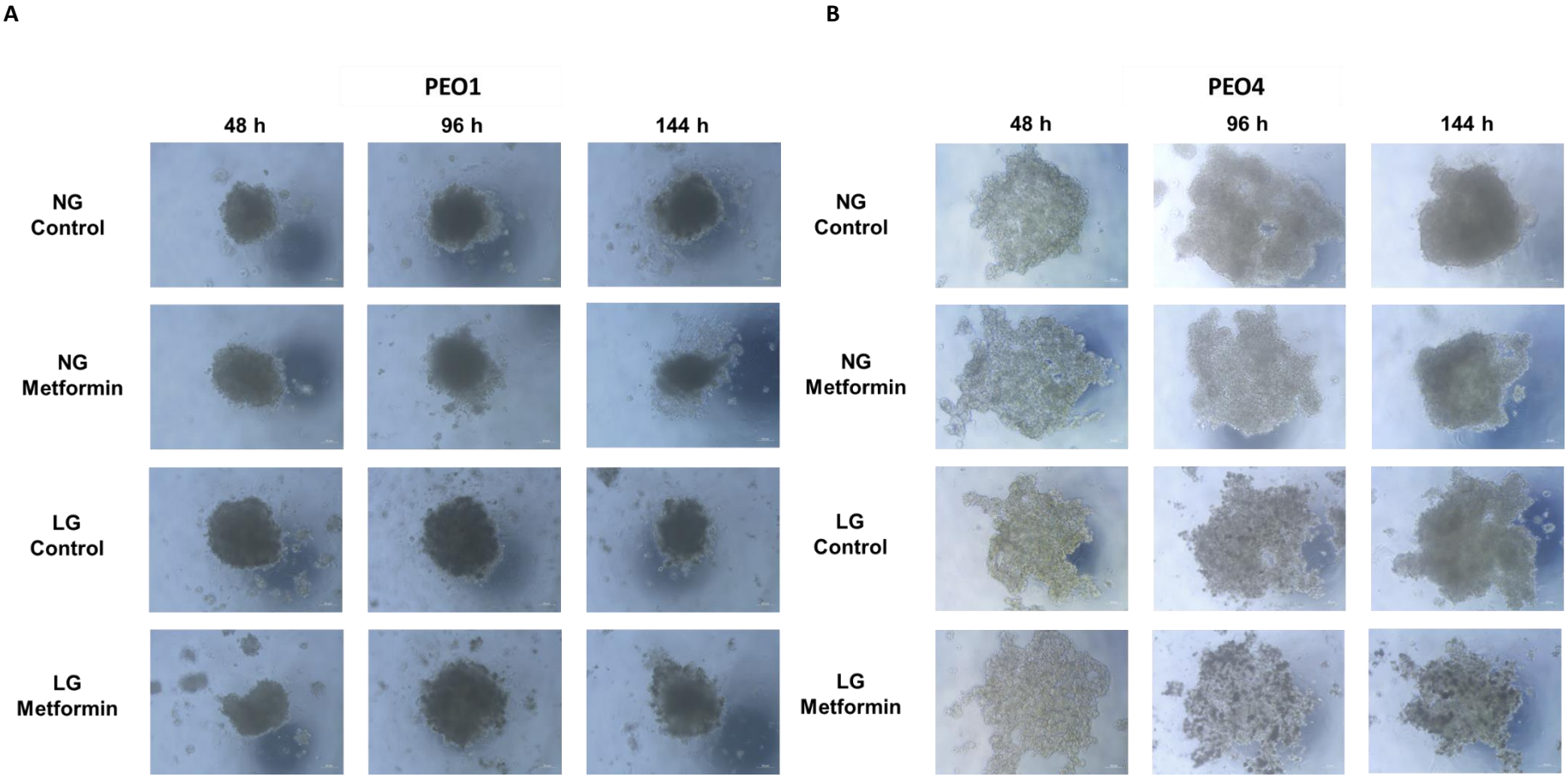

Figure 17. Brightfield microscopy of 3D PEO1 and PEO4 spheroids treated with metformin.
PEO1 (A) and PEO4 (B) spheroids were prepared using the hanging drop method. Brightfield microscopy was used to image the spheroids which were treated with metformin (0.625 mM) and ddH_2O vehicle (control) in experimental media conditions for 48 h, 96 h and 144 h (Magnification 10x). Scale bar: 50 µM.

MTT assay was not performed on the aggregates/spheroids as it would not penetrate the core, therefore only the DC assay was performed. No significant changes were seen in protein concentration with 3D PEO4 aggregates in experimental conditions (Figure 18). Metformin initially increased protein concentration in 3D PEO1 spheroids in normal glucose and low glucose media (48 h). However, the spheroids grown in low glucose media metformin showed a significant decrease in protein concentration at 144 h compared to the spheroids in normal glucose metformin condition ($p < 0.01$). In 3D PEO4 spheroids, metformin caused a non-significant decrease the protein concentration in both normal glucose and low glucose media at 144 h.

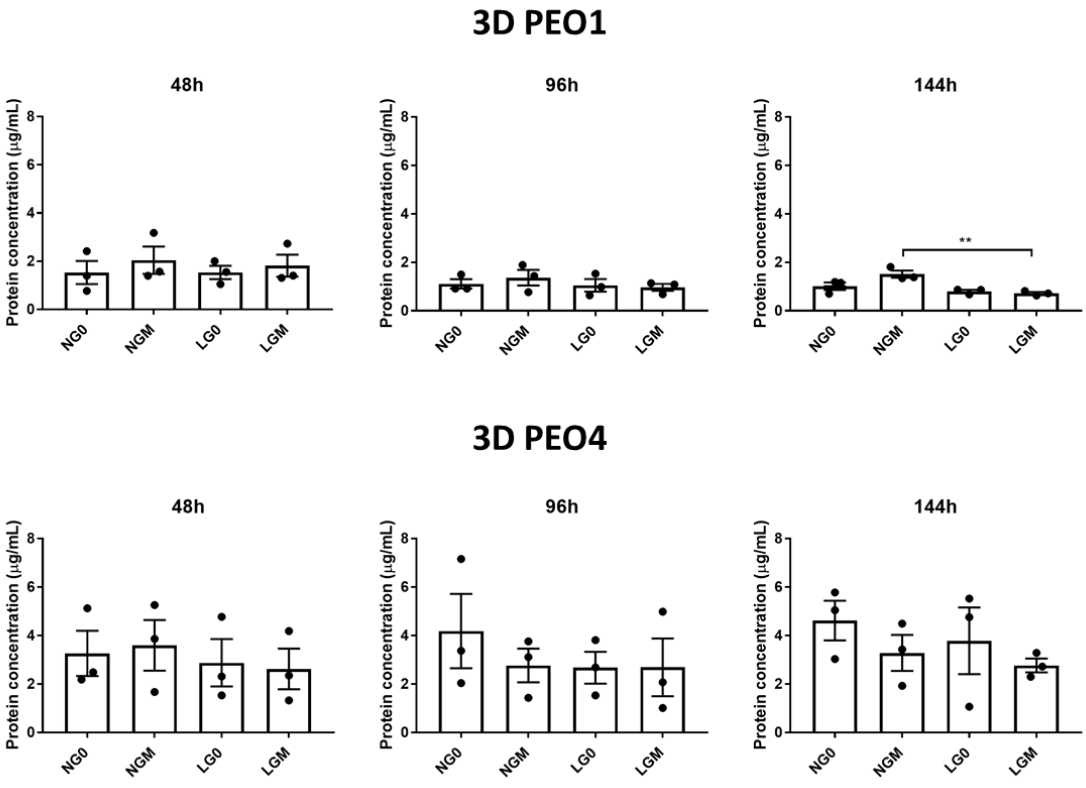

Figure 18. DC assay was performed on 3D PEO1 and PEO4 cells treated with metformin.
Cell lines were treated with metformin (M; 0.625 mM) and ddH_2O vehicle (0; control) in experimental media conditions (NG – normal glucose (10 mM) + 2 mM glutamine; LG – low glucose (1 mM) + 2 mM glutamine) for 48 h, 96 h and 144 h. Statistical analysis by two-way ANOVA: $p < 0.01$ **) . (n = 3 independent cell passages, error bars represent ± S.E.M.)

Metformin resulted in a non-significant increase in IL-6 levels in low glucose media when compared to the low glucose control at 144 h in 3D PEO1 spheroids (Figure 19A). At 48 h,

3D PEO4 spheroids in low glucose metformin media showed a significant increase in IL-6 production ($p < 0.05$) compared to the normal glucose metformin media. The low glucose condition (control and metformin) also showed a non-significant decrease in IL-6 levels when compared to the normal glucose condition at 144 h. PEO4 showed relatively low IL-6 production in comparison to the PEO1 cell line.

No significant effect on IL-8 production was observed in 3D PEO1 and PEO4 (Figure 19B). In 3D PEO1 cells, there was a slight increase in IL-8 levels in the low glucose metformin media at 96 h and 144 h when compared to the normal glucose metformin media. Whereas minimal IL-8 was produced by 3D PEO4 spheroids.

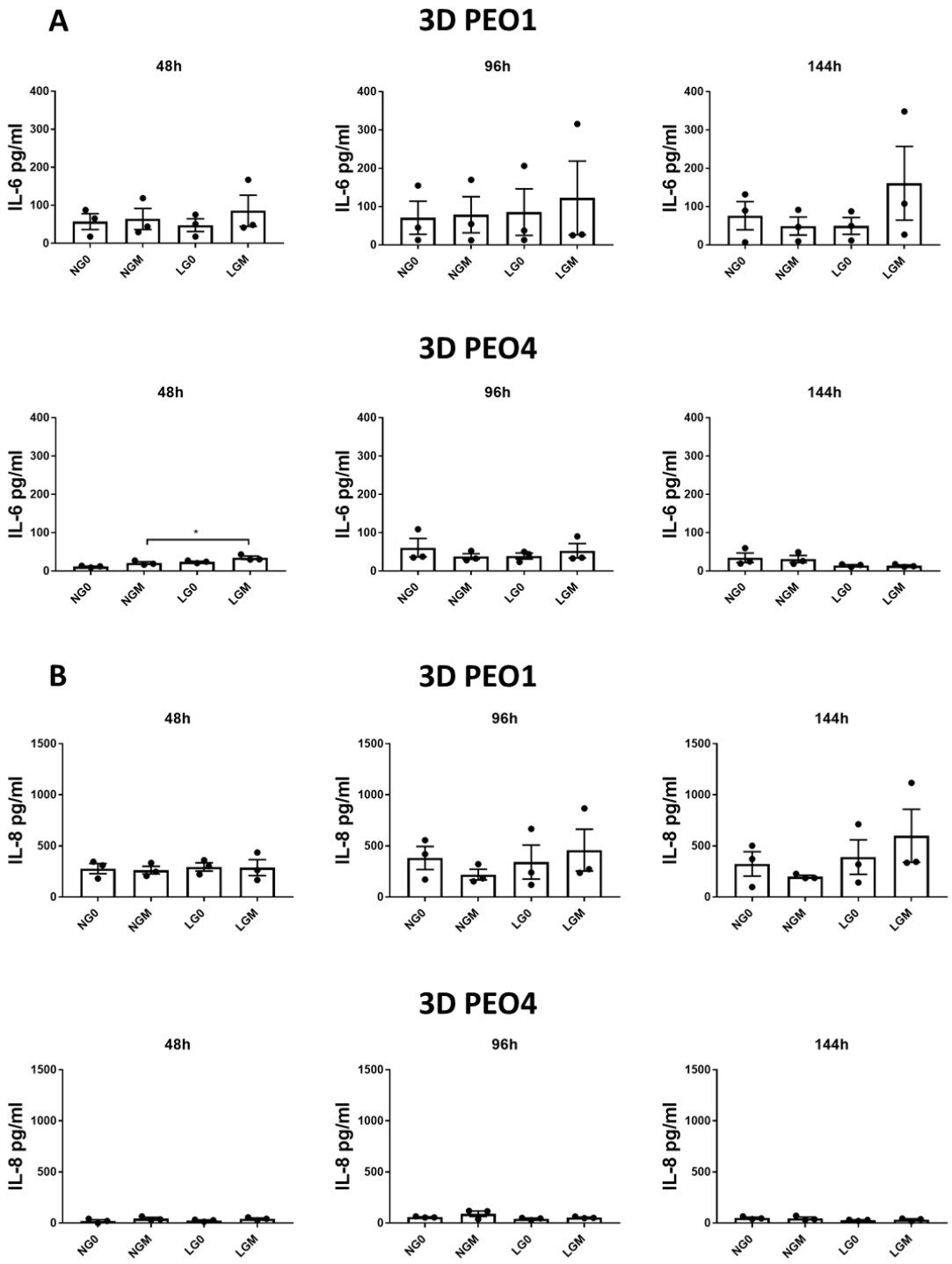

Figure 19. IL-6 and IL-8 ELISA were performed on 2D PEO1 and PEO4 cell lines after metformin treatment.

Cells were treated with metformin (M; 0.625 mM) and ddH_2O vehicle (0; Control) in experimental media conditions for 48 h, 96 h and 144 h. ELISA assays were performed on the supernatants to measure the secretion of IL-6 (A) and IL-8 (B). Statistical analysis by two-way ANOVA: $p < 0.05$ (*) (n = 3 independent cell passages, error bars represent ± S.E.M).

3.4.4. Investigating protein expression of targets involved in IL-6 and IL-8 production using western blotting

In 3D PEO1 spheroids, no significant changes in AMPK phosphorylation were observed. A non-significant increase in pAMPK levels could be seen across all time points in the low glucose metformin media compared to the normal glucose metformin media and low glucose control (Figure 20A).. A non-significant increase in pAMPK levels was observed in 3D PEO4 spheroids cultured in low glucose metformin media compared to the low glucose control and normal glucose metformin condition at 48 h and 96 hr (Figure 20B). At 144 h, a significant increase in AMPK phosphorylation was seen in the low glucose metformin condition compared to the low glucose control ($p < 0.05$) and normal glucose metformin media ($p < 0.05$).

A decrease in pSTAT3 S727 levels was seen in 3D PEO1 spheroids in low glucose metformin media compared to normal glucose metformin media and the low glucose control across all time points (Figure 21A).. Similarly, 3D PEO1 spheroids in low glucose metformin media also showed a significant decrease in pSTAT3 Y705 levels compared to normal glucose metformin media at 48 h ($p < 0.05$) and 96 h ($p < 0.01$).. The addition of metformin to the normal glucose media significantly reduced pSTAT3 Y705 levels compared to the control at 96 h ($p < 0.01$) and 144 h ($p < 0.05$). In the low glucose media, the addition of metformin also significantly decreased pSTAT3 Y705 levels compared to the control at 96 h ($p < 0.001$) and 144 h ($p < 0.05$). With 3D PEO4 spheroids, no significant changes were seen in pSTAT3 levels (Figure 21B). However, the addition of metformin caused a decrease in pSTAT3 S727 expression in both normal and low glucose media, compared to their respective control at 96 h and 144 h. A non-significant decrease of pSTAT3 Y705 was observed in 3D PEO4 spheroids in low glucose media treated with metformin compared to the low glucose control at 96 h and 144 h.

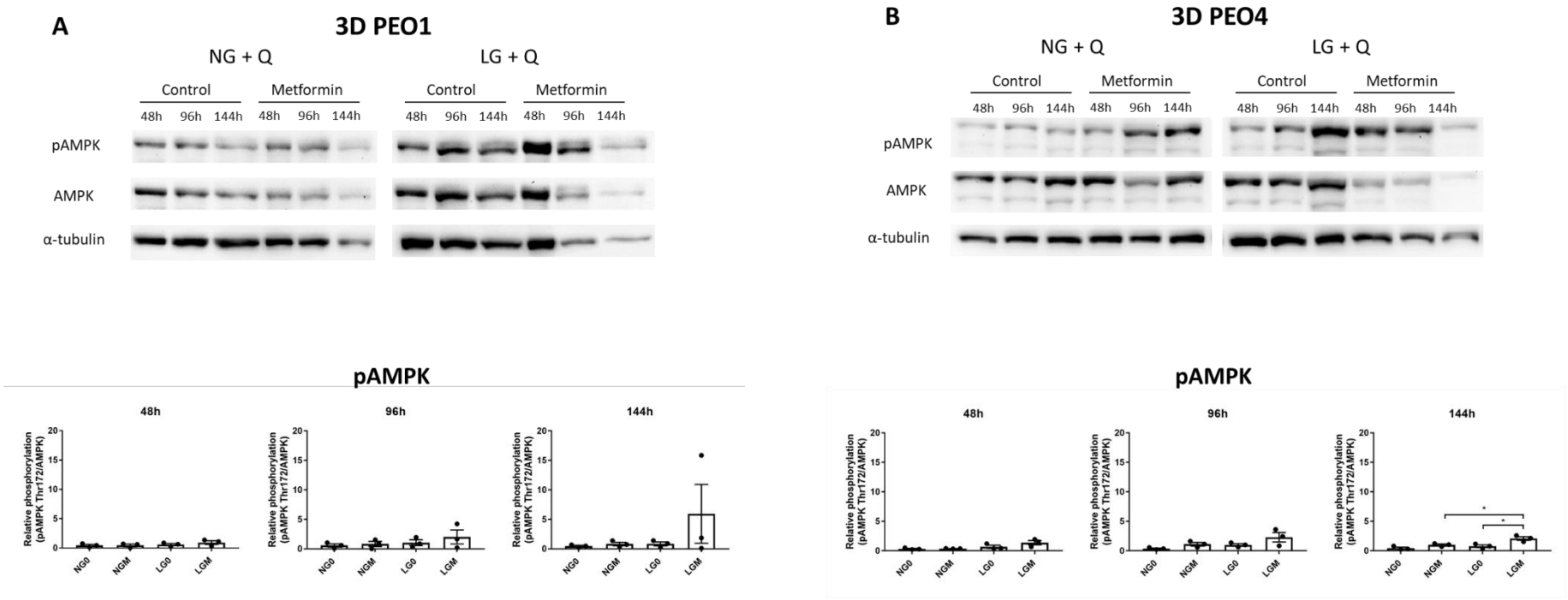

Figure 20. Western blot of AMPK was performed on 2D cultures of PEO1 and PEO4 cells after metformin treatment.
PEO1 (A) and PEO4 (B) spheroids were treated with metformin (0.625 mM) and ddH_2O vehicle (0; Control) in experimental media conditions for 48 h, 96 h and 144 h. Western blot analysis was used to evaluate phosphorylated AMPK (pAMPK), total AMPK and α-tubulin levels. Protein bands were quantified using Image J. Bars represent relative protein qualification of pAMPK/AMPK normalised to α-tubulin. Statistical analysis by two-way ANOVA: $p < 0.05$ (*) (n = 3 independent cell passages, error bars represent ± S.E.M).

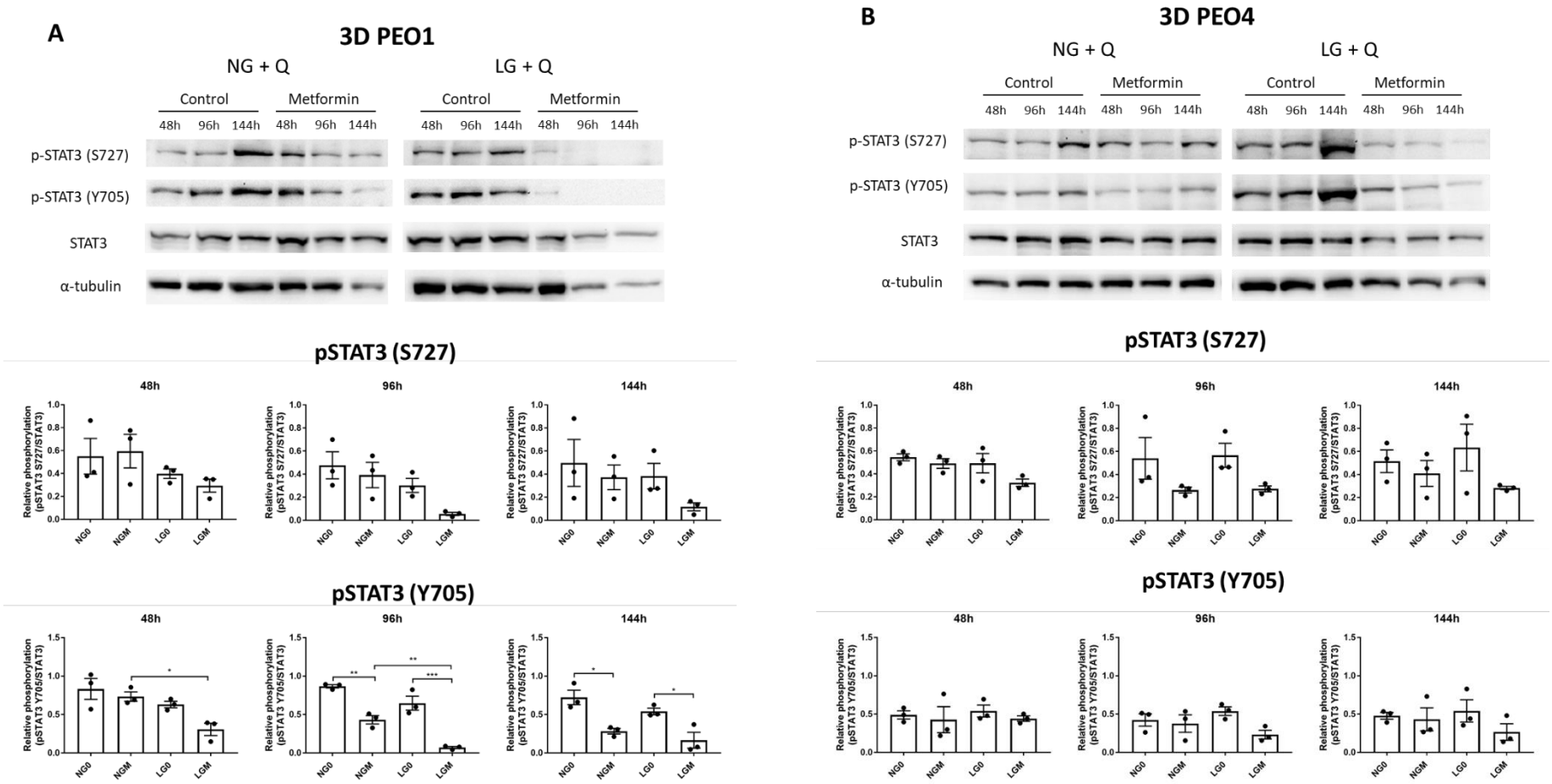

Figure 21. Western blots of pSTAT3 were performed on 3D cultures of PEO1 and PEO4 cells after metformin treatment.

PEO1 (A) and PEO4 (B) spheroids were treated with metformin (M; 0.625 mM) and ddH_2O vehicle (0; Control) in experimental media conditions for 48 h, 96 h and 144 h. Western blot analysis was used to evaluate phosphorylated STAT3 serine 727 (pSTAT3 S727), phosphorylated STAT3 tyrosine 705 (pSTAT3 Y705), total STAT3 and α-tubulin levels. Protein bands were quantified using Image J. Bars represent relative protein qualification of pSTAT3/STAT3 normalised to α-tubulin. Statistical analysis by two-way ANOVA: $p < 0.05$ (*), $p < 0.01$ (**), $p < 0.001$ (***)(n = 3 independent cell passages, error bars represent ± S.E.M).

3.5. Discussion

This study aimed to explore the effects of prolonged exposure to metformin, under physiological conditions of restricted glucose, in order to determine the impact on the inflammatory response in a chemosensitive and a chemoresistant ovarian cancer cell line. Whilst mentoring a previous MSci student, we observed that metformin at a concentration of 0.625 mM caused a significant increase in IL-6 and IL-8 production in PEO1 cells (Figure 7), this concentration was further used for this study and also falls within the therapeutic range (He & Wondisford, 2015; Kajbaf, et al., 2015).

Studies have shown that the activation of AMPK may bidirectionally modulate inflammation, acting as a link between inflammation and metabolic regulation, and vice versa. AMPK agonists, AICAR and metformin are also able to decrease the secretion of various proinflammatory cytokines including IL-6 and IL-8 through AMPK activation and the downregulation of the phosphorylation of NF-κB and STAT3 (Myerburg, et al., 2010; Kohn, et al., 2013; Tan, et al., 2015; Leidgens, et al., 2017). In several cell types, AMPK is involved in the induction of IL-6 and IL-8 production. For instance, in mouse cardiac fibroblasts, AICAR and metformin both elevated AMPK activation and promoted IL-6 production through p38 MAPK which could increase NF-κB binding to the *IL6* promoter leading to induction (Du, et al., 2005). Exposure of human primary airway epithelial cells to cigarette smoke extract activated AMPK signalling as a result of NADPH oxidase-dependent elevation of intracellular ROS. The activation of AMPK led to an increase of IL-8 production through NF-κB (Tang, et al., 2011). AICAR and metformin are able to inhibit the phosphorylation of STAT3 Y705 (Nerstedt, et al., 2010; Mancini, et al., 2017; Esparza-López, et al., 2019). AMPK activation by agonists can promote or suppress inflammation depending on the cell type and the various stimuli.

We observed that the 2D chemosensitive PEO1 cell line exhibited a significant increase in IL-6 and IL-8 production in the low glucose and metformin media as well as a significant increase in pAMPK and a significant decrease in pSTAT3 Y705. The significant decrease in pSTAT3 Y705 was also seen in the 3D PEO1 spheroids when cultured in low glucose and metformin media but the increase in cytokine production and AMPK activation was not as pronounced, probably due to

penetration of the metformin and reduced secretion of cytokines from cells situated deeper in the spheroids. Metformin caused a decrease in STAT3 phosphorylation in both the 2D and 3D PEO4 cells. Additionally, PEO4 cells produced relatively low amounts of cytokines. These results suggest that the induction of IL-6 and IL-8 upon the addition of metformin in low glucose condition is STAT3 independent, with AMPK possibly playing a role in the regulation of cytokine induction.

Where the effect of metformin was potentiated by the low glucose condition in PEO1 cells, the chemoresistant PEO4 cell line was less sensitive to the anti-proliferative effects of metformin. It is possible this may be due PEO4 cell lines not expressing the metformin transporters, *OCT3* and *OCTN1* which are present in the PEO1 cell line (Coscia, et al., 2016; Jackson, et al., 2017). OCT3 is expressed ubiquitously in most tissues. Deletion of *Oct3* in mice showed a reduction in the bioavailability and tissue accumulation of metformin. *Oct3* knockout mice showed higher pAMPK/AMPK ratios when treated with metformin compared to those treated with saline. No difference was seen in total AMPK (Chen, et al., 2015). OCTN1 is localised to the apical membranes of small intestine and may have a bidirectional role as *Octn1* knockout mice showed higher plasma concentration of metformin compared to wildtype at low oral dose but lower at the higher oral dose (Nakamichi, et al., 2013).

PEO4 cells also lack *LKB1* which regulates AMPK function (Coscia, et al., 2016). Under energy stress, *LKB1* encodes a serine/threonine kinase that directly phosphorylates and activates AMPK. *LKB1* deletion mice showed a decrease in AMPK activation in the liver but unimpaired AMPK activation in muscle (Shaw, et al., 2005). The combination of the loss of *OCT3*, *OCTN1* and *LKB1* in PEO4 cells may contribute to the lower sensitivity to metformin treatment and the different levels of AMPK activation and total AMPK. Future work could involve the use of another AMPK agonist phenformin which is more lipophilic, therefore does not rely on transporters in order to enter the cell. Phenformin could be more potent as an anti-tumour drug than metformin and may be effective against cancer cells that lack the transporters (Jackson, et al., 2017).

STAT3 Y705 phosphorylation is constitutively expressed in patient ascites-derived ovarian cancer cells whereas STAT3 S727 is not (Saini, et al., 2017). STAT3 expression appears to be influenced by glucose concentration, as STAT3 showed a concentration dependent increase in endometrial cancer cells cultured in media containing increasing concentrations of glucose, which was inhibited by metformin (Wallbilich , et al., 2017). Interestingly, 2D PEO1 cell lines show a non-significant increase in pSTAT3 S727 but showed a decrease of pSTAT3 Y705 in the 3D spheroids grown in low glucose metformin media. This increase could be due to pSTAT3 S727 playing a role in the negative regulation of STAT3 tyrosine phosphorylation (Chung, et al., 1997). In breast cancer, metformin increased phosphorylation of AMPK in DMEM media without glucose. In glucose depleted conditions, metformin suppressed cell proliferation, disintegrated tumour spheroids and reduced cell survival (Bizjak, et al., 2019). We also found that under similar conditions, 3D PEO1 and PEO4 spheroids were easily disaggregated when slightly agitated. Malignant transformation involves the loss of E-cad in favour of N-cadherin (Cerezo, et al., 2013). Metformin could also increase E-cad and reverse the expression of mesenchymal markers vimentin and SNAIL in addition to decreasing STAT3 Y705 phosphorylation in IL-6 induced EMT (Esparza-López, et al., 2019). An increase in E-cad expression was also seen in metformin treated ovarian cancer stem cells (Zhang, et al., 2015). The deletion of *STAT3* in ovarian cancer cell lines inhibited spheroid formation capability and reduced viability. Knock-out spheroids were small and showed loosely associated aggregates (Lu, et al., 2019). As metformin could inhibit STAT3 Y705 phosphorylation, which was further potentiated by the low glucose conditions, the JAK-STAT3 signalling of cytokine induction may not be involved. The weakly formed spheroids under low glucose and metformin condition could be a result of STAT3 inhibition.

Unfortunately, due to time constraints and limited availability of consumables as a result of COVID-19, the effect of metformin and glucose on the protein status of TET2 or phosphorylated/total NF-κB could not be explored in addition to further validating the role of AMPK in this immune response by using AMPK agonists such as AICAR. As JAK-STAT pathway does not appear to be involved in the cytokine production, it is possible that the production may be induced through the AMPK/TET2 pathway (our original hypothesis). This novel

signalling pathway first shown by Wu *et al.,* (2018), defining the link between metabolism and epigenetics.

3.6. Conclusion

In this chapter we found that PEO1 cells were more sensitive to the antiproliferative effect of metformin. The significant increase in inflammatory cytokines which was seen in 2D conditions was not seen under 3D conditions, although the trend remained. We also found that metformin decreased the phosphorylation of STAT3 Y705 in both 2D and 3D PEO1 and PEO4 cells which suggests that JAK/STAT3 signalling was not involved in induction of inflammatory cytokines under low glucose metformin conditions. However, there was a significant increase in AMPK phosphorylation in 2D PEO1 cells under the same condition, which suggests that AMPK/TET2 may be involved. Thus, the next chapter will explore the link between epigenetic regulation of cytokine expression and metabolism.

Chapter 4

Optimisation and use of Chromatin Immunoprecipitation (ChIP) to explore a link between metabolism and epigenetics in 2D and 3D ovarian cancer cell lines

4.1. Introduction

The metabolic state of a cell is important in the regulation of epigenetic modifications as many metabolites can serve as substrates, cofactors or inhibitors for enzymes that modify the genome. The epigenome can also affect the transcription of metabolic genes (Lu & Thompson, 2012; Wong, et al., 2017). The metabolic environment plays a role in immune cell phenotype. The trigger for inflammatory events following metabolic dysfunction has not yet been established but epigenetic changes appear to be the precursor. Environmental cues such as nutrient levels can induce epigenetic changes which can lead to the activation or repression of gene transcription in response to environmental stimuli. Furthermore, epigenetics plays an important role in the relationship between genetics and the microenvironment that drive inflammatory changes in metabolic diseases such as cancer (Raghuraman, et al., 2016).

The rapid proliferation of cancer cells creates a demand on protein synthesis until it exceeds the protein-folding capacity of the endoplasmic reticulum (ER) leading to the accumulation of misfolded proteins, resulting in ER stress. Chronic inflammation is often associated with protein misfolding and ER stress (Hasnain, et al., 2012). Activating transcription factor 4 (ATF4) is induced downstream of metabolic stresses including ER stress and promotes the adaptation of cells to the limited availability of nutrients (Wortel, et al., 2017). ATF4 activation has been detected in several human tumours in hypoxic or nutrient-deprived regions where ATF4 was associated with pro-survival and pro-proliferative effects (Sorge, et al., 2020). PERK is an ER transmembrane protein that links ER stress signals to translation inhibition. PERK phosphorylates eukaryotic translation-initiation factor 2α (eIF2α) which promotes the expression of ATFs including ATF4 (Quentin, et al., 2012). Chronic activation of ATF4 induces apoptosis indirectly though the transcription of ATF4 target, *CHOP*. Metformin was reported to upregulate ATF4 by phosphorylating PERK and induced the mRNA and protein levels of CHOP without inducing apoptosis (Quentin, et al., 2012). ATF4 has a proinflammatory effect by directly binding to the *IL6* and the *IL8* promoter, linking metabolic stress to cytokine production at the epigenetic level (Iwasaki, et al., 2014; Püschel, et al., 2020).

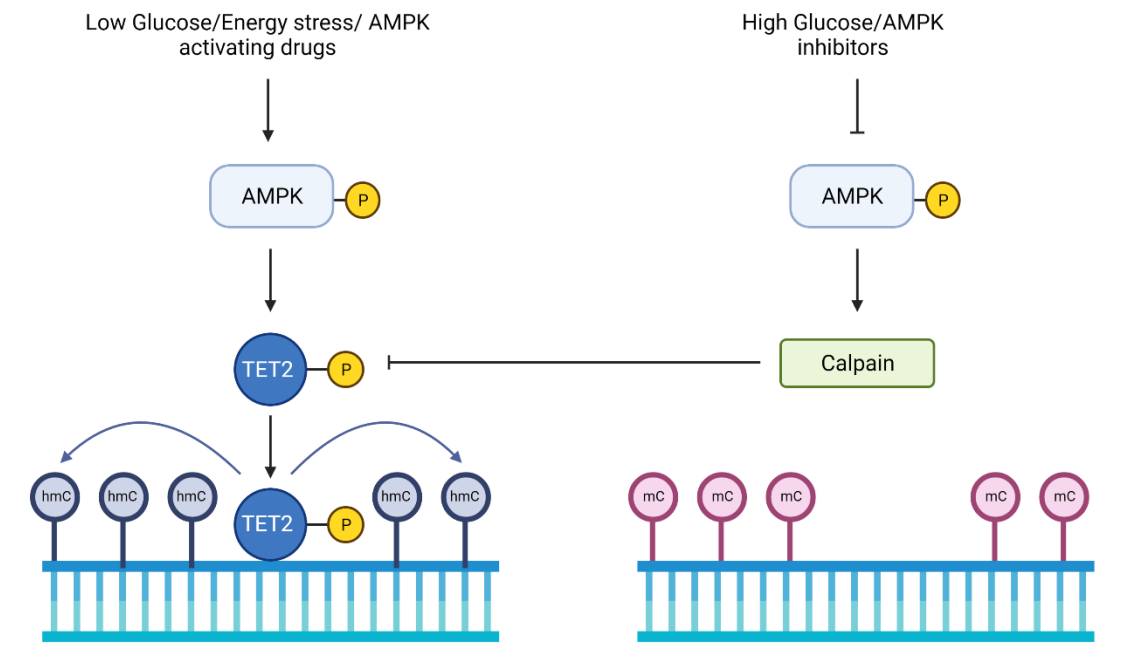

Figure 22. AMPK/TET2 signalling forms the link between metabolism and the epigenome. Under low glucose conditions, AMPK stabilises TET2 through the phosphorylation of the serine 99 residue. In high glucose conditions, calpain degrades TET2 resulting in aberrated regulation of DNA methylation. Figure adapted from (Wu, et al., 2018). Created with BioRender.com

In addition to ATF4, STAT3 and TET2 are also able to regulate the inflammatory response on an epigenetic level. STAT3 has been observed to bind to interferon gamma-activated sequence (GAS) motifs (- TTNNNGAA) (Seidel, et al., 1995). The activation of STATs is able to transactivate cytokine-responsive genes by binding to the GAS motifs in the gene promoter regions and promotes the transcription of downstream genes (Yu, et al., 2002; Sun, et al., 2017). In synovial fibroblasts, the binding of STAT3 to the GAS element of the *IL8* promoter was required for leptin-induced IL-8 production (Tong, et al., 2008). On the *IL6* promoter, STAT3 forms a complex with NF-κB in order to bind and induce *IL6* expression (Yoon, et al., 2012). Wu *et al.,* (2018) found that TET2 could be stabilised by the activation of AMPK (Figure 22). TET2 was reported to be detected on promoters of CpG islands; the binding domain of TET2, IDAX preferentially associates with CpG-rich regions (Ko, et al., 2013; Ramussen, et al., 2019). Furthermore, TET2 has been implicated in the expression of *IL6* and *IL8* by binding to the promoter (Zhang, et al., 2015; Itoh, et al., 2018; Lv, et al., 2018; Wang, et al., 2018).

Chromatin immunoprecipitation (ChIP) is an important method for studying the interactions between protein and DNA, improving our understanding of where and how gene regulatory processes occur in cells. The main steps of the ChIP procedure include the crosslinking of protein to DNA complexes in cells before the extraction and shearing of the chromatin. Immunoprecipitation of chromatin is required in order to isolate the chromatin bound by the protein of interest before reverse crosslinking to release the protein from the DNA, isolating the DNA of interest. Chromatin sample not immunoprecipitated is also set aside, designated as "input" to represent the total DNA for normalisation (Figure 23). The isolated DNA can then be analysed using downstream processes such as quantitative PCR (ChIP-qPCR), DNA hybridisation array (ChIP-chip) and genome-wide sequencing (ChIP-seq). The main disadvantages of the ChIP assay are the low sensitivity and reproducibility of the results which can be significantly influenced by several factors during preparation of the samples including formaldehyde crosslinking, efficiency of chromatin shearing, number of cells and specificity of the antibodies which all need to be optimised in order to ensure the success of ChIP experiments (discussed below).

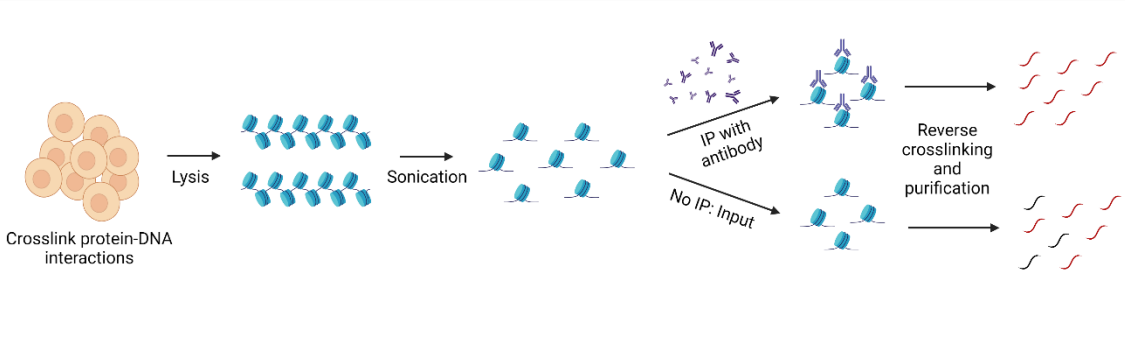

Figure 23. Principles of Chromatin Immunoprecipitation (ChIP).
Cells are treated with formaldehyde to crosslink protein-DNA interactions. Chromatin is extracted and then sonicated to achieve fragments between 100 – 500 bp. Some sample that is not immunoprecipitated, designated as "input" is used for normalisation. Samples are immunoprecipitated using an antibody targeting protein of interest. Input and immunoprecipitated samples undergo reverse crosslinking and purification before downstream processing. Created with Biorender.com

Crosslinking and shearing are important parameters for successful ChIP analyses as they influence the specificity and efficiency of the immunoprecipitation stage as well as the

resolution of the chromatin analysis. Formaldehyde is the most commonly used crosslinking agent to covalently attach proteins to DNA. Optimisation of crosslinking time is important as over-crosslinked chromatin may not be fully reversed and may be resistant to sonication. Subsequently, the large molecular weight complexes may be removed during the purification stage. Too little crosslinking results in the insufficient attachment of DNA to the nucleosome resulting in the loss of DNA during immunoprecipitation (Cheaib & Simon, 2013). Different cell types will respond differently to formaldehyde fixation so optimal times should be determined for each cell type. Sonication (hydrodynamic shearing) and enzyme digestion are the two most commonly used methods to fragment chromatin. With formaldehyde crosslinking, sonication is the preferred method as crosslinking may restrict the access of the enzyme to chromatin (Haring, et al., 2007). The number of sonication cycles required is dependent on the number of cells in the starting samples. Success was seen for chromatin with average size ranging between 200 – 250 bp (Keller, et al., 2021). Inefficient chromatin shearing can lead increased background signal, resulting in the decrease in signal to noise ratio and sensitivity of the assay (Khoja, et al., 2019). In order to improve the quality and reproducibility of ChIP, sonication conditions should be determined for each cell type, number of cells and same growth conditions or treatments should be applied as it may alter cell morphology (Keller, et al., 2021).

The amount of input material and antibody used are important and require optimisation. The specificity and the affinity of an antibody is important in ChIP assay. The final amount of DNA obtained from ChIP reactions may be very low. The cycle threshold (Ct) of positive samples may be obscured by the background signal and leads to poor fold enrichment and false negative results. Therefore, a large number of cells or tissue may be required to study certain targets (Hunter, et al., 2019). The successful use of an antibody in other experiments i.e., western blotting, does not necessarily mean the antibody is suitable for ChIP and requires testing. The affinity of epitopes varies between antibodies, affecting signal levels (Haring, et al., 2007). Furthermore, effective antibodies need to be specific and must be able to recognise epitopes that may not be sufficiently exposed in fixed chromatin (Keller, et al., 2021).

DNA that is isolated from precipitated chromatin requires analysis to determine the DNA fragments present in the precipitate. Commonly used methods of analysis are conventional PCR and quantitative PCR. DNA-dye based PCR uses the fluorescent dye, SYBR green to detect the amplicon. SYBR green fluoresces upon binding to any double stranded DNA; therefore, primer sets require optimisation as the amplification of non-target DNA fragment and formation of primer dimers will generate fluorescent signal, obscuring PCR signal (Haring, et al., 2007).

4.2. Aims and objectives

Building on the results of the previous Chapter, our aims for this Chapter were to establish if the AMPK/TET2 pathway (Figure 22) was involved in the regulation of the inflammatory response under specific metabolic conditions, by investigating TET2 binding to the *IL6* and/or *IL8* promoter. We also investigated the ER stress regulator ATF4, as it could play a pivotal role in epigenetic regulation due to it also being upregulated by AMPK. The work in this Chapter was aided by Porvair Sciences Ltd. (Wrexham, UK), who provided the ChIP assay kits (Chromatrap) and technical assistance. Our additional aim was to validate this kit for ovarian cancer cells under harsh nutrient conditions. The objectives for this Chapter are:

1. Determine the optimal sonication time and seeding density for both ovarian cancer cell lines.
2. Determine the amount of chromatin and antibody to be used for the immunoprecipitation.
3. Design primer sets encompassing the binding sites on the cytokine promoter.
4. Examine if phosphorylated STAT3 binds to the GAS motifs in the cytokine promoter and if experimental conditions influence this.
5. Investigate if TET2 and/or ATF4 has a role in ovarian cancer cytokine regulation by directly binding to cytokine promoters.

4.3. Methods and Materials

Chromatrap ChIP-seq assay kits (Porvair; Cat#500189) were used for the ChIP assay according to the manufacturer's protocol.

4.3.1. Cell lines

In addition to PEO1 and PEO4 cells, HeLa and HEK293 cells were used as potential positive controls as, according to The Human Protein Atlas (http://www.proteinatlas.org), both cell lines express TET2 (Uhlen, et al., 2017). Both cell lines were obtained from ATCC and grown in RPMI-1640 (Gibco; Cat#31870-025) and DMEM (Gibco; Cat#31053028) media, respectively. The media were supplemented with 10% FBS, 1% L-glutamine (2 mM) and 1% ABAM. The cell lines were cultured at 37°C in a humidified atmosphere at 5% CO_2.

4.3.2. Treatments

4.3.2.1. 2D cultures

PEO1 or PEO4 cells were seeded in a T-75 flask. Cell densities for seeding required optimisation for ChIP. Cells were cultured for 24 h before treatment with 0.625 mM metformin or vehicle which was diluted in low glucose + glutamine (LG + Q) or normal glucose + glutamine (NG + Q) experimental cell culture media (**Table *1***) for 48 h.

4.3.2.2. 3D cultures

3D spheroids of PEO1 and PEO4 cells were made following the protocol outlined in 2.3.1. Cell densities for seeding required optimisation for ChIP. Cells were resuspended in experimental cell media: LG + Q or NG + Q containing a final concentration of 0.625 mM before seeding on the lid of a 96-well plate. Approximately 192 spheroids (2 plates) were generated per treatment condition. Spheroids were then cultured for 48 h before harvesting.

4.3.3. Preparation of chromatin

4.3.3.1. Chromatin fixing and extraction

4.3.3.1.1. 2D cultures

Cells were gently washed with PBS (Gibco; Cat#10010056) before the addition of 6 mL basal cell media containing 1% formaldehyde (Sigma; Cat#F8775) for cell fixation and the crosslinking of DNA/protein complexes. Cells were gently agitated on a rocking platform at room temperature for 10 min. After the incubation period, the fixation solution was removed and 3 mL 0.65 M glycine solution (Chromatrap, Norfolk, UK) was added to quench the reaction and the cells were gently agitated and incubated for a further 5 min at room temperature (RT) on a rocking platform. The glycine solution was removed, and cells were collected by scraping in 10 mL ice cold PBS. Cells were then collected by centrifugation at 3500 x g for 5 min at 4^{o}C and the supernatant was discarded. The cell pellet was resuspended in 400 µL Hypotonic buffer (Chromatrap, Norfolk, UK) and incubated at 4^{o}C for 10 min. The nuclei were collected by centrifugation at 5000 x g for 5 min at 4^{o}C. The supernatant was discarded, and the pellet resuspended in 300 µL Lysis buffer and incubated at 4^{o}C for 10 min.

4.3.3.1.2. 3D spheroids

Approximately 96 spheroids were carefully collected by pipette into a 1.5 mL centrifuge tube. Spheroids were pelleted by centrifugation at 500 x g for 2 min at RT and the media was discarded. The pellet was re-suspended in PBS and centrifuged at 500 x g for 5 min before resuspending in 1 mL PBS containing 1% formaldehyde. The samples were incubated for 10 min at RT on an end-to-end rotator after which 114 µL 1.3 M glycine was added and incubated for a further 5 min. Spheroids were collected by centrifugation at 500 x g for 5 min at 4^{o}C and then resuspended in ice cold PBS. The spheroids were then pelleted again at 500 x g for 5 min, the supernatant was discarded, and the pellet was resuspended in 400 µL of Hypotonic Buffer and incubated at for 10 min on ice. Hypotonic slurry was centrifuged at 5000 x g at 4^{o}C for 5 min at 4^{o}C. The supernatant was discarded, and the pellet was resuspended in 200 µL Lysis Buffer and incubated on ice for 10 min.

4.3.3.2. Determining chromatin shearing efficiency

Samples were sonicated using a water bath sonicator set at 30 sec bursts with 30 sec rest intervals on ice for 20 min to produce fragments of 100 - 500 bp. Sonicated samples were

centrifuged for 10 min at maximum speed at 4°C and the supernatant transferred to another microcentrifuge tube before the addition of 1 µL of protease inhibitor cocktail (PIC) (Chromatrap, Norfolk, UK). In order to check the chromatin shearing efficiency, an aliquot of 25 µL of sheared chromatin was placed in a new microcentrifuge tube and 5 µL of 1M $NaHCO_3$ (Chromatrap, Norfolk, UK) and 5 µL of 5M NaCl (Chromatrap, Norfolk, UK) and nuclease free water was added to a final volume of 50 µL. Samples were incubated at 65°C for 2 h to reverse the crosslinking before the addition of 1 µL of Proteinase K solution, mixed thoroughly and incubated for 1 h at 37°C. After the incubation period, 2 µL Proteinase K stop solution was added. The DNA in the samples was quantified using a spectrophotometer, NanoDrop 1000 (NanoDrop, Wilmington, USA). The sheared DNA was visualised against 100 bp ladder (Promega; Cat#G2101) on a 1% agarose gel (Melford; Cat#A20090-100.0) with 5 µL/50 mL SYBR-Safe DNA gel stain (Invitrogen; Cat#S33102).

4.3.3.3. Preparation of slurries and column activation

Chromatin stocks were thawed at 4°C and centrifuged at maximum speed in a Microfuge for 10 min at 4°C. Only the clear supernatant was used for the preparation of the immunoprecipitation slurries and Input (Table 3). The antibodies used for ChIP can be found in Table 4.The slurries were mixed and incubated on an end-to-end rotator for 1 h at 4°C.

Table 3. Preparation of the slurries for immunoprecipitation in the spin column

Reagents	**Immunoprecipitation Slurry**	**Positive Control (H3K4me3)**	**Input**
Chromatin Stock	Up to 100 µL	Up to 100 µL	Up to 100 µL
Antibody		2 µL	-
Protease Inhibitor Cocktail	2 µL	2 µL	-
Column Conditioning Buffer	Made up to 1000 µL	Made up to 1000 µL	Made up to 100 µL

Table 4. ChIP Antibodies were all raised in rabbit and purchased from Cell Signalling Technology

Antibody	Catalogue number
TET2	#18950S
Phospho-Stat3 (Ser727)	#9134S
Phospho-Stat3 (Tyr705)	#9145S
ATF4	#11815S
Tri-Methyl-Histone H3 (Lys4)	#9751S

The spin columns were removed from the collection tube and placed on a rack before the addition of 600 µL Column Conditioning Buffer was added to each column and allowed to flow through under gravity. The flow through was discarded and 600 µL of Column Conditioning Buffer was added again and allowed to flow through. After discarding the flow through, the columns are ready for immunoprecipitation.

4.3.4. Immunoprecipitation of sheared chromatin

The slurries were briefly centrifuged after incubation and loaded onto the column and allowed to flow through the column at RT. The columns were placed into the collection tubes and washed twice with 600 µL of Wash Buffer 1, centrifuging at 4000 x g for 30 sec at RT. The columns were then washed twice with Wash Buffer 2 and Wash Buffer 3. After the wash steps, the columns were dried by centrifuging at maximum speed for 30 sec. The columns were transferred to a 1.5 mL collection tube after which, 50 µL ChIP-seq Elution buffer was added and allowed to incubate at RT for 15 min. The columns were centrifuged at maximum speed for 30 sec to collect the eluted chromatin.

4.3.5. Reverse crosslinking and DNA purification

To each sample and Input, 5 µL of 1 M $NaHCO_3$ and 5 M NaCl was added and a final volume of 110 µL was made up with DNase/RNase free deionised water. The samples were mixed and

incubated for 2 h at 65°C. After incubation, 1 µL of Proteinase K was added to each sample and Input before mixing and incubation for 1 h at 37°C. To each sample and Input, 2 µL of Proteinase K Stop Solution was added before mixing.

After reverse crosslinking, the samples were purified by adding 5 volumes of DNA binding buffer to 1 volume of sample and mixed. In order to ensure efficient DNA adsorption, 10 µL 3M Sodium Acetate pH 5 was added to reduce the pH ≤7.5. Samples were transferred to the Chromatrap® DNA purification column and centrifuged at 16,000 x g for 60 sec. The flow through was discarded and 700 µL DNA Wash Buffer wash buffer was added before centrifugation at 16,000 x g for 60 sec. The flow through was discarded again and the columns were centrifuged at 16,000 x g for 60 sec to remove the residual Wash buffer. The columns were transferred to a clean 1.5 mL microcentrifuge tube and the DNA was eluted by adding 50 µL of DNA elution buffer, incubating for 15 min and centrifugation at 16,000 x g for 60 sec.

4.3.6. DNA analysis

4.3.6.1. Primer Design

JASPAR (http://jaspar.genereg.net) was used to predict the binding motifs for STAT3 and ATF4 (Fornes, et al., 2020). The motifs were downloaded and inputted into FIMO, a part of the MEME Suite (https://meme-suite.org/meme/doc/fimo.html) and cross-referenced to the promoter sequence for *IL6* and *IL8*, which were obtained from UCSC Genome Browser (Kent, et al., 2002; Grant, et al., 2011). Primers were designed using PrimerQuest™ Tool (Integrated DNA Technologies; http://www.scitools.idtdna.com/Primerquest/). Primer dimers, hairpin formations and efficiency were analysed using OligoEvaluator™ (Sigma-Aldrich; http://www.oligoevaluator.com). A Primer-BLAST search of the primer sequences against the whole genome was performed check specificity to our region of interest (Ye, et al., 2012).

4.3.6.2. Real Time Quantitative Polymerase Chain Reaction (RT-qPCR)

Table 5 Real time qPCR primers for ChIP assay.
Primers were either designed in house following the method in 4.3.6.1 or obtained from a paper (referenced).

Target	Primer sequences	Reference
CCND2	F – GTTTCTGCTCGAGGATCACA R – GGGAGAGGTGGGTATTAGGA	(Guilhamon, et al., 2013)
STAT3 IL-6	F - CCGACTAGACTGACTTCTGTATTT R - CAAAGGTGGGCATGGATTTC	Custom
STAT3 IL-8	F – AGACATGTGCCCCTTCACTC R - GGTGAAGATAAGCCAGCCAAT	(Tong, et al., 2008)
IL-6 CpG	F – CCAGGAGAAGATTCCAAAGATGTA R - CGTCGAGGATGTACCGAATTT	(Alipour , et al., 2020)
IL-8 CpG	F - GATAAGGAACAAATAGGAAGTGTG R - TGGCTTTTTATATCATCACCCTAC	(Venza, et al., 2012)
ATF4 IL-6	F - TCCAGCCCAGCATTAACAAG R - CAAAGCCCAACAGATGCTAGA	Custom
ATF4 IL-8	F – GAGAGTCTTAGCTTGCCTACTATAA R - CTGACAACATTGAACGACTTCC	Custom

The Inputs were diluted 1 in 10. The primer pairs used for real time qPCR are found in Table 5 and used at a final concentration of 1 µM each with 2.5 µL of Input or purified sample and 5 µL of 2 x QuantiFast SYBR® Green (Qiagen; 204056). The cycle conditions used for RT-qPCR were as follows:

95°C – 5 min

95°C – 10 sec
60°C – 30 sec
72°C – 30 sec
} 35 cycles

The melt curve was obtained as follows:

60°C – 1 min

95°C – 30 sec

For the Inputs, 3.3 cycles were subtracted from the Ct values. To interpret the qPCR data, locus recovery was calculated as follows:

$$\% \text{ recovery} = 2^{\wedge} (Ct_{input} - Ct_{sample}) * \text{dilution} * 100\%$$

The % recovery for the background (IgG) was subtracted from the % recovery for the sample to calculate an overall % of Input.

4.4. Results

4.4.1. Optimisation of shearing efficiency and cell number for ChIP

Per the protocol, cells were fixed with 1% formaldehyde for 10 min. It was found that this condition was sufficient for shearing and subsequent immunoprecipitation and did not require further optimisation. To determine the optimum time to achieve the required DNA fragment range (100 – 500 bp), chromatin was sheared up to 30 min with an aliquot taken every 5 min. It was found that all intervals produced the desired fragment sizes (Figure 24). PEO1 cells produced smaller fragments after 20 min of sonication. For subsequent experiments, 20 min of sonication was used.

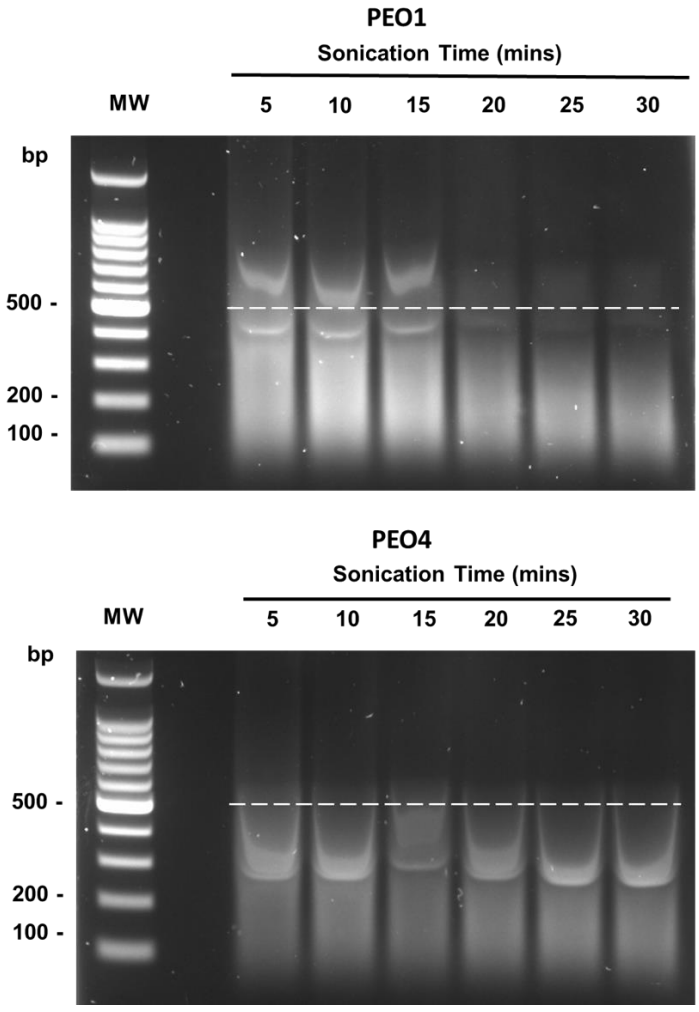

Figure 24. Comparison of chromatin shearing efficiency for PEO1 and PEO4 cells.
Both cell lines were grown under cell culture conditions at confluency (approx. 3 x 10^5 cells/mL). The fragment range desired (100 – 500 bp) was achieved at all time points.

For experimental conditions, 2D cells were initially seeded at 1 x 10^6 cells in total per flask and 3D cells at 5 x 10^3 cells per spheroid before chromatin extraction and shearing. Samples were sonicated for 20 min before the efficiency was checked on an agarose gel after reverse crosslinking (Figure 25). It was confirmed that 20 min of sonication was also sufficient for experimental conditions. Due to the anti-proliferative effect of metformin in addition to the low glucose condition, the initial amount of chromatin extracted from 2D and 3D PEO1 cells and 2D PEO4 cells was insufficient for ChIP as the smear of DNA was barely visible on the gel.

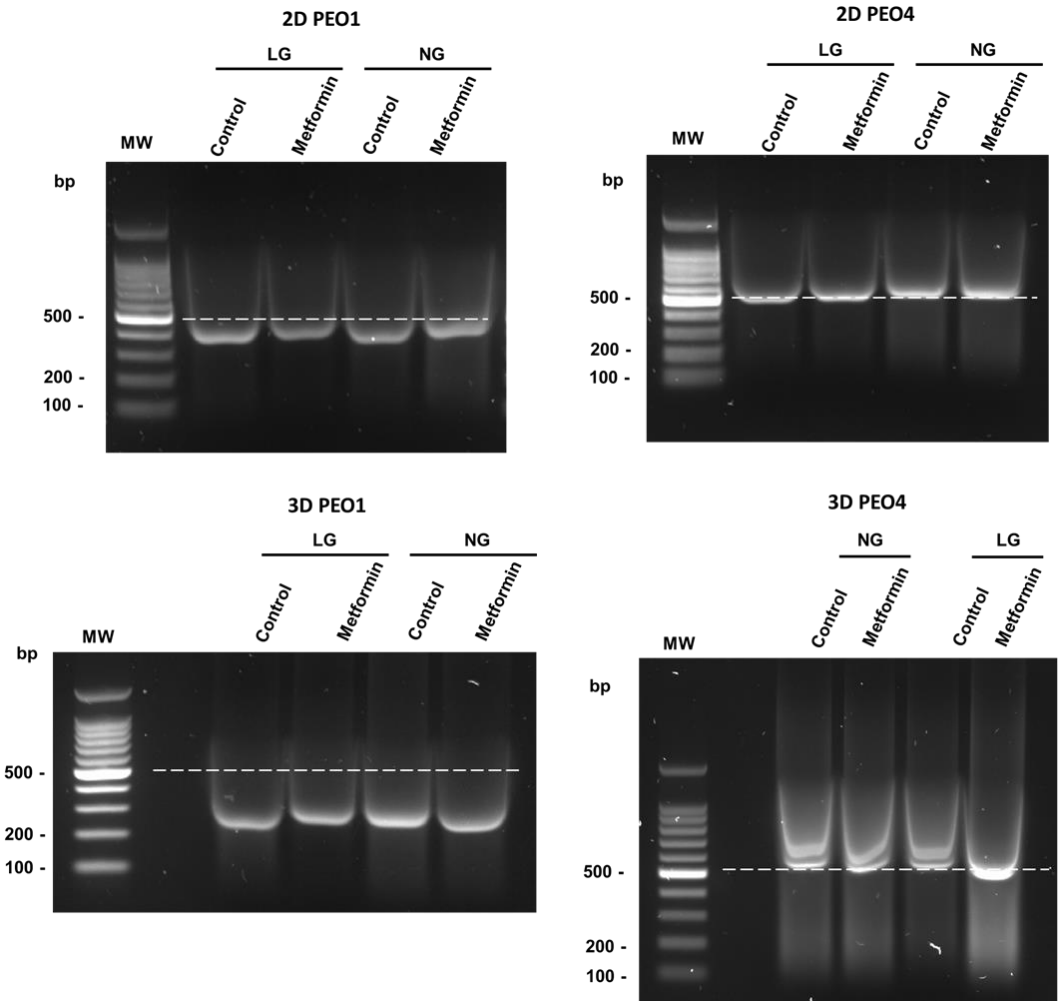

Figure 25. Checking the shearing efficiency of 2D and 3D PEO1 and PEO4 cells
2D and 3D PEO1 and PEO4 cells were sonicated for 20 min and the shearing efficiency was confirmed using gel electrophoresis. Cells were seeded at a density of 1 x 10^6 cells in total per flask for 2D cells and 5 x 10^3 cells per spheroid for 3D spheroids.

Next, the seeding density was doubled: for 2D cells 2 x 10^6 cells in total per flask and for 3D spheroids 1 x 10^4 cells per spheroid were used. Chromatin was extracted and then sonicated for 20 min. The shearing efficiency was checked by running the reverse crosslinked samples on an agarose gel (Figure 26). It was confirmed that this density produced enough chromatin, even under low glucose metformin conditions (where proliferation was reduced) for subsequent ChIP analysis. The shearing time of 20 min was also enough to produce the desired fragment size (100 – 500 bp).

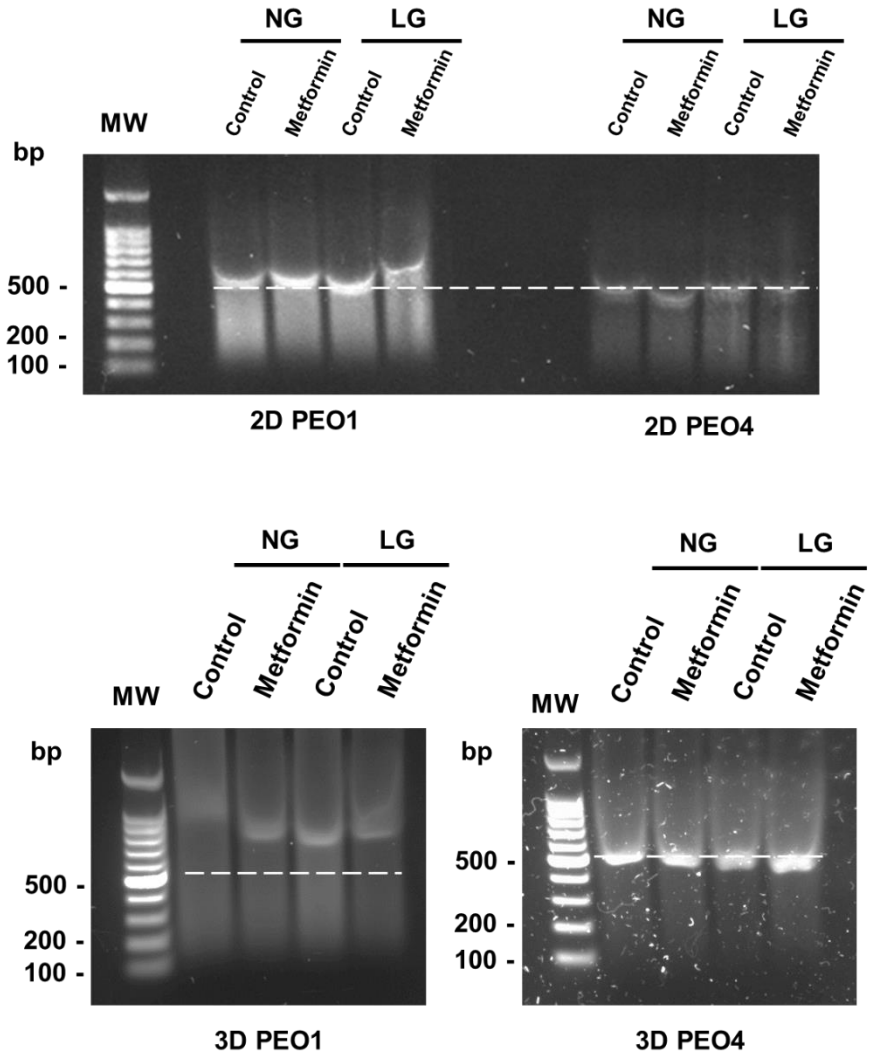

Figure 26. Checking the shearing efficiency of 2D and 3D PEO1 and PEO4 cells after doubling the seeding density.

2D and 3D PEO1 and PEO4 cells were sonicated for 20 min and the shearing efficiency was confirmed using gel electrophoresis. 2D cells were seeded at a density of 2 x 10^6 cells per flask for 2D cells and 1 x10^4 cells per 3D spheroids.

4.4.2. Validation of chromatin samples and the positive controls

Histone H3 lysine K4 (H3K4) trimethylation (H3K4me3) is a consistent mark of transcriptionally active genes (O'Neill, et al., 2006). Glyceraldehyde 3-phosphate dehydrogenase (*GAPDH*) is a housekeeping gene and a positive control for H3K4me3 (Lin, et al., 2015). Enrichment of H3K4me3 on the *GAPDH* promoter was used to validate ChIP experiments. First, the signal between the H3K4me3 antibody from the Chromatrap kit was compared to another commercial ChIP-grade H3K4me3 antibody from Cell Signalling Technology. For the immunoprecipitation, 1 µg of chromatin was incubated with 1 µg of antibody before loading into the column. RT-qPCR analysis was performed on the samples using *GAPDH* primers which were included in the Chromatrap kit. Both antibodies showed a good signal to background ratio with the Chromatrap antibody showing a higher signal for H3K4me3 enrichment compared to the Cell Signalling Technology antibody (Figure 27). Thus, the H3K4me3 antibody from Chromatrap was used to validate the experimental chromatin samples.

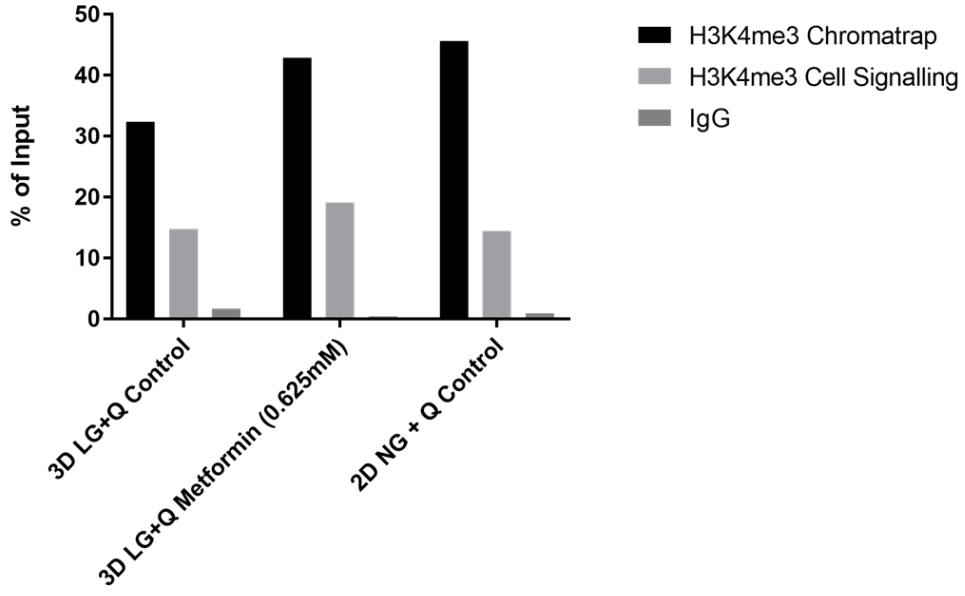

Figure 27. ChIP-qPCR analysis comparing the enrichment of H3K4me3 on the *GAPDH* promoter in PEO1 cells using H3K4me3 antibodies from different companies.
H3K4me3 antibodies from the Chromatrap kit and Cell Signalling Technology were used against the *GAPDH* promoter in PEO1 samples under various conditions. IgG was used to represent the background. For the slurry incubation, 1 µg of chromatin was incubated with 1 µg of antibody (n=1).

We found that 1 µg of Input (chromatin that was not immunoprecipitated and subsequently used for normalisation) produced a high Ct value in RT-qPCR analysis which means that a weaker signal of interest may be missed. Next, RT-qPCR analysis was performed on 1 µg, 2 µg, 3 µg and 5 µg genomic DNA (Promega; Cat#G3041) and 2D PEO1 (NG and LG control) Input with *GAPDH* primers (data not shown). We found that 5 µg of genomic DNA or Input produced a low enough Ct value (<25) for analysis (Gade & Kalvakolanu, 2012). Chromatin extracted from 2D and 3D PEO1 and PEO4 cells were validated by investigating H3K4me3 enrichment on the *GAPDH* promoter (Figure 28). For the immunoprecipitation, 5 µg of chromatin was incubated with 2 µg anti-H3K4me3 antibody and resulted in a good signal to background ratio, confirming the presence of chromatin in the samples.

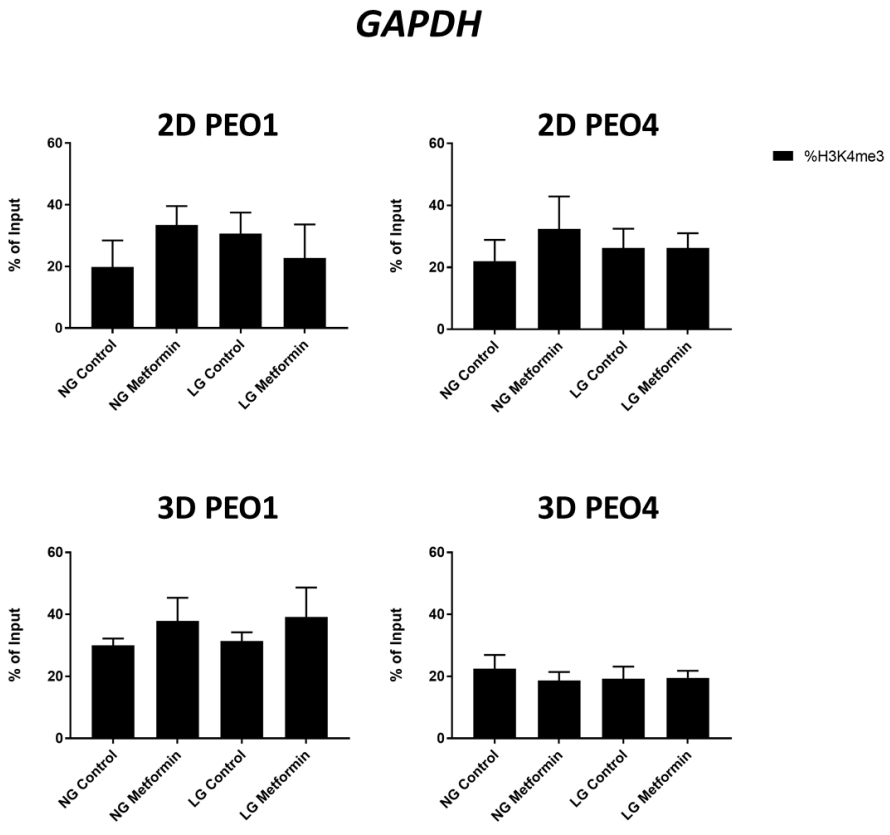

Figure 28. ChIP performed with an antibody specific for H3K4me3 on 2D and 3D PEO1 and PEO4 cells. RT-qPCR was used to analyse the immunoprecipitated DNA with *GAPDH* primers. Statistical analysis by Two-way ANOVA: $p > 0.05$ (n.s.) (n=3 independent cell passages, error bars represent ± S.E.M).

In order to confirm the effectiveness of the TET2 antibody, we sought to establish a positive control region to confirm binding. First, two cell lines, HeLa and HEK293 were identified which according to the Human Protein Atlas, showed TET2 expression. Using western blotting (following the protocol in 3.3.4), the presence of TET2 was confirmed in these cell lines with HEK293 showing a higher level of TET2 protein expression than the HeLa cell line (Figure 29).

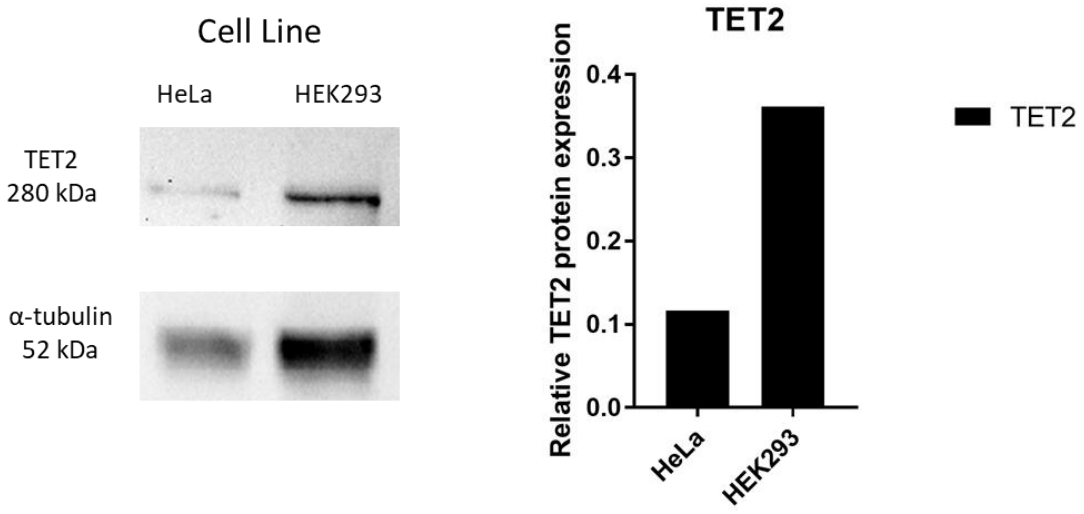

Figure 29. Western blot of TET2 was performed on HeLa and HEK293 cells near confluency.
Western blot analysis was used to evaluate the expression levels of TET2 and α-tubulin levels. Protein bands were quantified using Image J and normalised to α-tubulin (n=1).

After the extraction of chromatin, both cell lines were sonicated for 20 min and the chromatin shearing efficiency was checked on a 1% agarose gel (Figure 30A). After the desired fragment lengths were obtained the chromatin was then validated; we confirmed that chromatin was present in the samples (Figure 30B). The *CCND2* encodes cyclin D2 cell cycle regulator, which plays a role in the regulation of haemopoietic differentiation and cell proliferation. The differential activation may be involved in leukemogenesis (Eisfeld, et al., 2017). TET2 has been shown to bind to the *CCND2* gene so this was used as a potential positive control (Guilhamon, et al., 2013). However, there was no observed TET2 binding on the *CCND2* gene promoter (Figure 30C) or on the CpG island on the *IL6* promoter (Figure 30D). Since we could not confirm TET2 binding in these cell lines, they were not used in further experiments. Unfortunately, we were not successful in determining a positive control for this experiment as we were unable to screen more genes and binding sites due to the pandemic and time constraints.

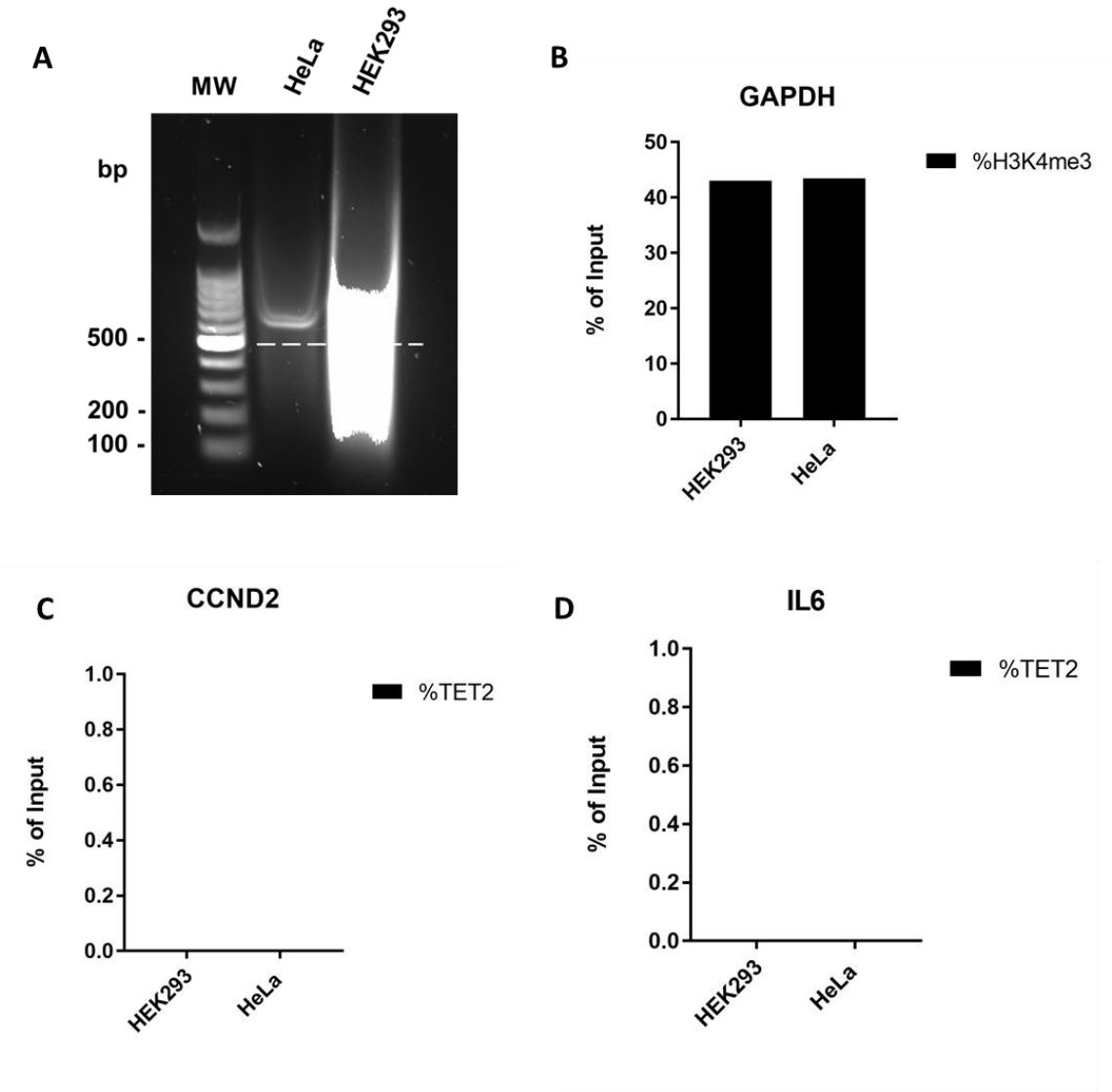

Figure 30. ChIP was performed on HeLa and HEK293 cells using an antibody specific for H3K4me3 or TET2.

Chromatin shearing efficiency was checked on a 1% agarose gel after 20 min of sonication (A). Immunoprecipitated chromatin was then analysed using primers targeting *GAPDH* (B), *CCND2* (C) and *IL6* (D) (n=1).

4.4.3. The use of ChIP to determine transcription factor binding to the promoter of inflammatory cytokines in 2D cells.

As AMPK was activated in the conditions that correlated with the increased inflammatory response, we wanted to investigate if TET2 was involved in directly activating the *IL6* and *IL8* promoter through the AMPK/TET2 pathway. ChIP was conducted on 2D PEO1 and PEO4 cell lines with antibodies against TET2 and the binding was measured on the CpG island in the *IL6* and *IL8* promoter. These sites were chosen, as the binding region of TET2 preferentially associates with CpG-rich regions and CpG islands (Ko, et al., 2013; Ramussen, et al., 2019). On the *IL6* promoter, 2D PEO1 cells showed TET2 binding in the normal glucose control media and higher binding under the low glucose media with metformin condition. The 2D PEO4 cells showed little TET2 binding (Figure 31A). Whereas, on the *IL8* promoter, TET2 binding was seen in all the conditions except the normal glucose control in 2D PEO1 cells (Figure 31B). In 2D PEO4 cells, the normal glucose condition with metformin showed some TET2 binding on the *IL8* promoter.

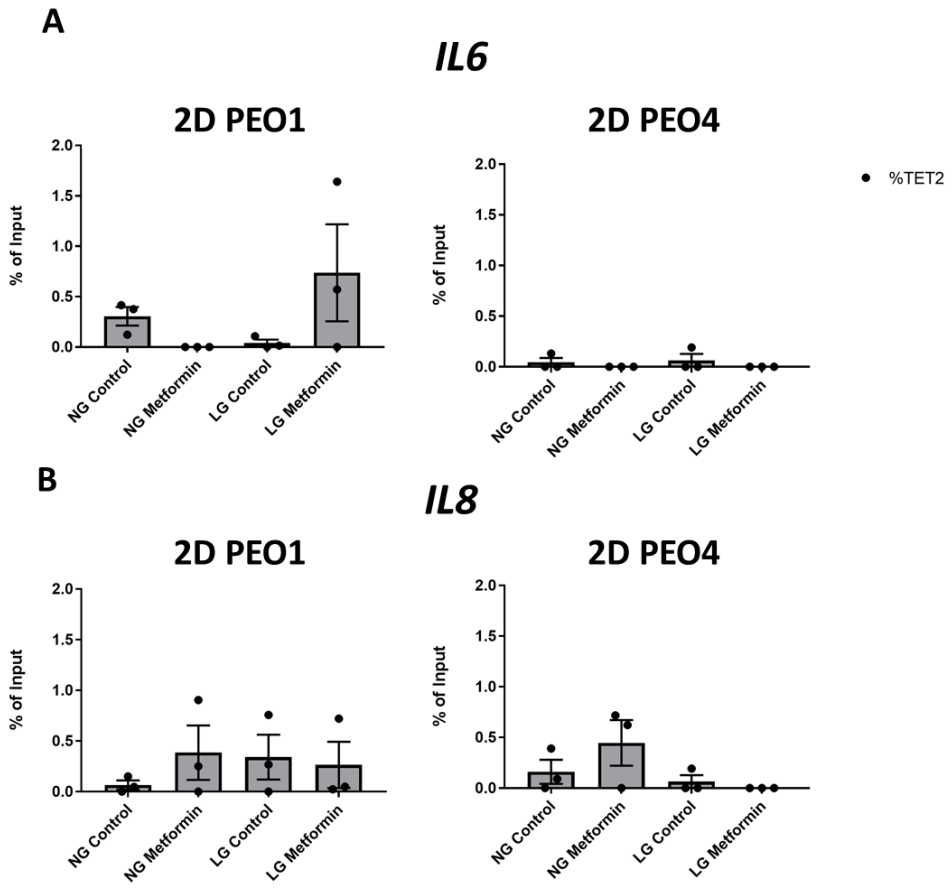

Figure 31. ChIP-qPCR was used to analyse the TET2 enrichment of the CpG island on the *IL6* and *IL8* promoter in 2D PEO1 and PEO4.

2D PEO1 and PEO4 cells were treated with 0.625 mM metformin or ddH_2O (control) in normal glucose (10 mM) and glutamine (2 mM) media (NG) or low glucose (1 mM) and glutamine (2 mM) media (LG). Enrichment of TET2 on the *IL6* (A) and *IL8* (B) promoter were assayed. Statistical analysis by Two-way ANOVA: $p > 0.05$ (n.s.) (n=3 independent cell passages, error bars represent $\pm$ S.E.M).

ATF4 is involved in the ER stress response and the adaptation of cells to metabolic stress such as nutrient depletion (Wortel, et al., 2017). ATF4 binding on the *IL6* and *IL8* promoter were analysed. Binding of ATF4 to the *IL6* promoter in 2D PEO1 was variable under low glucose conditions with metformin (Figure 32A). Furthermore, there did not appear to be much ATF4 binding on the *IL6* promoter in the 2D PEO4 cells or the *IL8* promoter in both 2D PEO1 and PEO4 cell lines (Figure 32B).

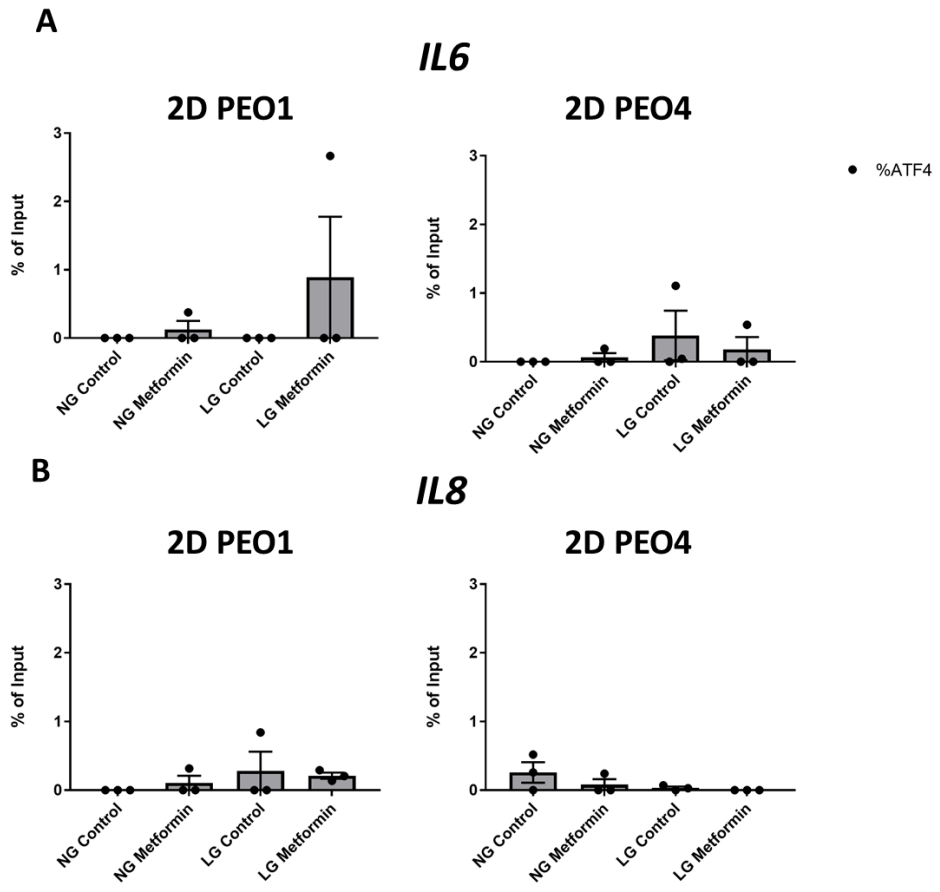

Figure 32. ChIP-qPCR was used to analyse the ATF4 enrichment on the *IL6* and *IL8* promoter in 2D PEO1 and PEO4 cells.

2D PEO1 and PEO4 cells were treated with 0.625 mM metformin or ddH_2O (control) in normal glucose (10 mM) and glutamine (2 mM) media (NG) or low glucose (1 mM) and glutamine (2 mM) media (LG). Enrichment of ATF4 on the *IL6* (A) and *IL8* (B) promoter were assayed. Statistical analysis by Two-way ANOVA: $p > 0.05$ (n.s.) (n=3 independent cell passages, error bars represent $\pm$ S.E.M).

The phosphorylated form of STAT3 can translocate into the nucleus and act as a transcription factor (Marginean, et al., 2021). Under low glucose control conditions pSTAT3 S727 showed some binding on the *IL6* promoter, which was increased under the metformin condition, whereas 2D PEO4 showed little pSTAT3 binding in all conditions (Figure 33A). A similar trend could be seen with the pSTAT3 S727 binding on the *IL6* promoter in 2D PEO4 cells but showed almost no pSTAT3 S727 binding on the *IL8* promoter (Figure 33B).

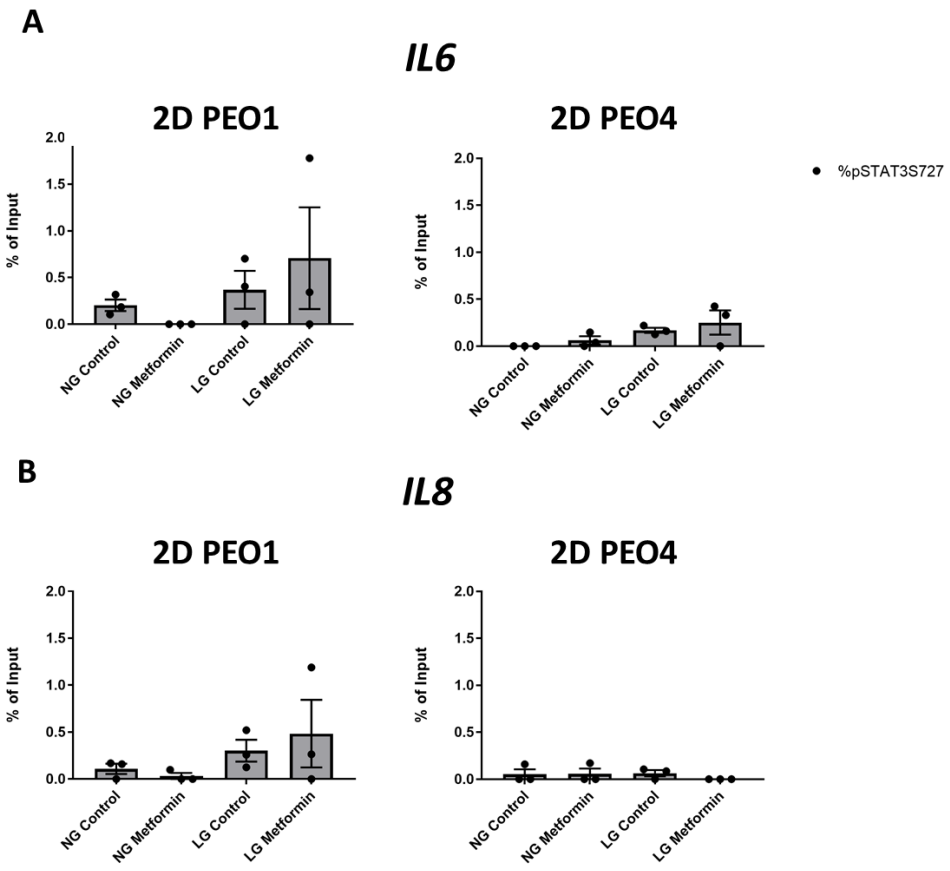

Figure 33. ChIP-qPCR was used to analyse the pSTAT3 S727 enrichment on the *IL6* and *IL8* promoter in 2D PEO1 and PEO4 cells.

2D PEO1 and PEO4 cells were treated with 0.625 mM metformin or ddH_2O (control) in normal glucose (10 mM) and glutamine (2 mM) media (NG) or low glucose (1 mM) and glutamine (2 mM) media (LG). Enrichment of pSTAT3 S727 on the *IL6* (A) and *IL8* (B) promoter were assayed. Statistical analysis by Two-way ANOVA: $p > 0.05$ (n.s.) (n=3 independent cell passages, error bars represent $\pm$ S.E.M).

There did not appear to be much pSTAT3 Y705 binding on the *IL6* promoters in 2D PEO1 and PEO4 cells (Figure 34A). The *IL6* promoter in 2D PEO4 cells showed some pSTAT3 Y705 binding under the normal glucose condition but no binding was seen under the low glucose condition. On the *IL8* promoter, the low glucose control condition showed pSTAT3 Y705 binding in 2D PEO1 cells which was reduced upon the addition of metformin (Figure 34B). The pSTAT3 Y705 binding on the 2D PEO4 *IL8* promoter showed a similar trend as the *IL6* promoter.

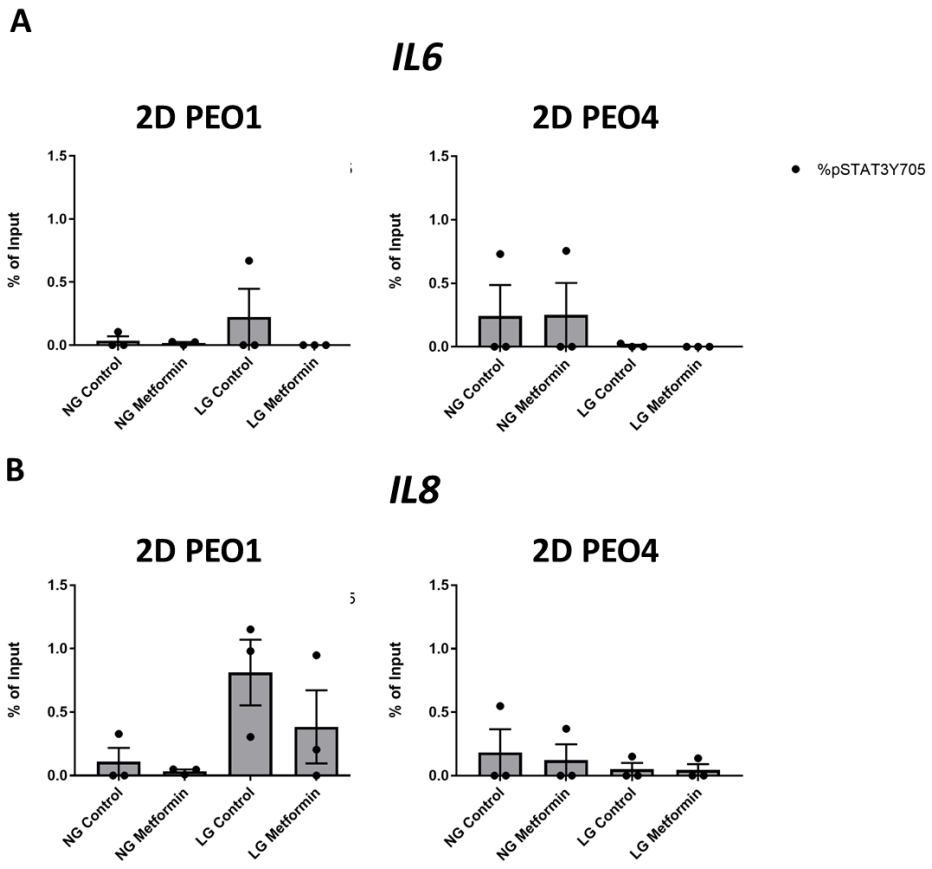

Figure 34. ChIP-qPCR was used to analyse the pSTAT3 Y705 enrichment on the *IL6* and *IL8* promoter in 2D PEO1 and PEO4 cells.

2D PEO1 and PEO4 cells were treated with 0.625 mM metformin or ddH_2O (control) in normal glucose (10 mM) and glutamine (2 mM) media (NG) or low glucose (1 mM) and glutamine (2 mM) media (LG). Enrichment of pSTAT3 Y705 on the *IL6* (A) and *IL8* (B) promoter were assayed. Statistical analysis by Two-way ANOVA: $p > 0.05$ (n.s.) (n=3 independent cell passages, error bars represent $\pm$ S.E.M).

4.4.4. The use of ChIP to determine transcription factor binding to the promoter of inflammatory cytokines in 3D cultures

The *IL6* promoter in 3D PEO1 spheroids showed some TET2 binding under the low glucose condition with and without metformin whereas the 3D PEO4 aggregates showed little TET2 binding (Figure 35A). The *IL8* promoter in 3D PEO1 spheroids showed no TET2 binding except under the normal glucose with metformin condition (Figure 35B). The 3D PEO4 *IL8* promoter shows little TET2 binding under the low glucose control condition which was slightly increased under the low glucose metformin condition.

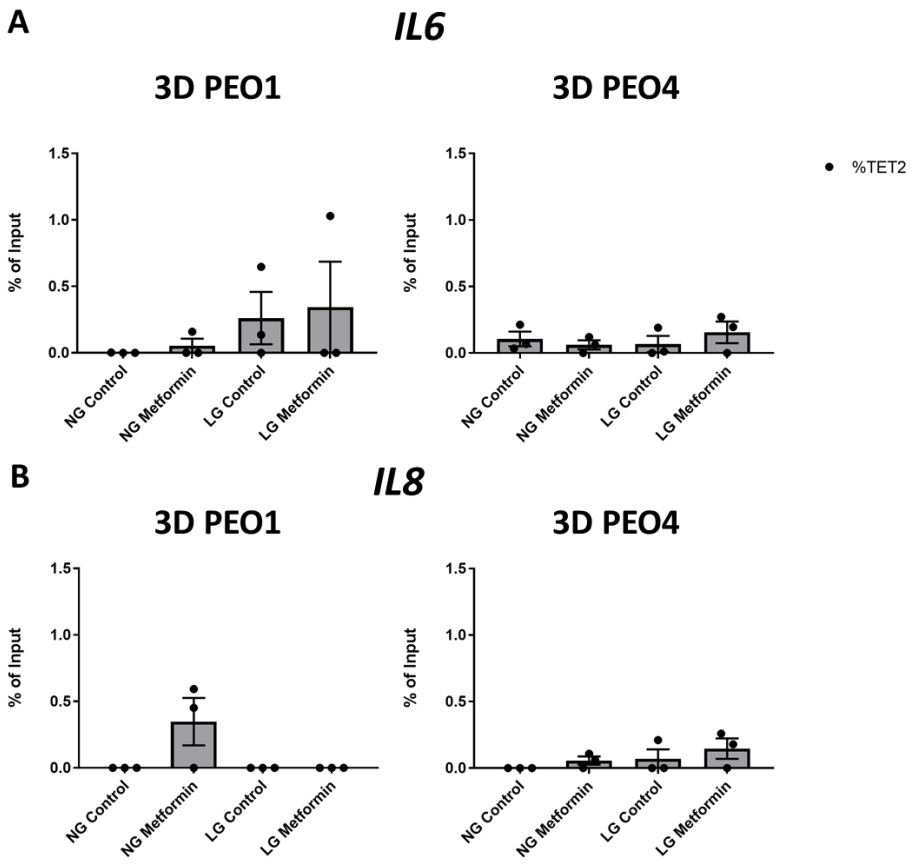

Figure 35. ChIP-qPCR was used to analyse the TET2 enrichment of the CpG island on the *IL6* and *IL8* promoter in 3D PEO1 and PEO4 cells.
3D PEO1 and PEO4 cells were treated with 0.625 mM metformin or ddH_2O (control) in normal glucose (10 mM) and glutamine (2 mM) media (NG) or low glucose (1 mM) and glutamine (2 mM) media (LG). Enrichment of TET2 on the *IL6* (A) and *IL8* (B) promoter were assayed. Statistical analysis by Two-way ANOVA: $p>0.05$ (n.s.) (n=3 independent cell passages, error bars represent $\pm$ S.E.M).

ATF4 appeared to show some binding on the 3D PEO1 *IL6* promoter under the normal glucose condition, one replicate showed binding under the low glucose metformin condition. Little ATF4 binding was seen in the *IL6* promoter in 3D PEO4 aggregates (Figure 36A). However, on the *IL8* promoter, 3D PEO1 spheroids showed ATF4 binding under the normal glucose control condition which increased upon the addition of metformin (Figure 36B). The low glucose metformin also showed a slight increase in ATF4 binding compared to the low glucose control. The 3D PEO4 aggregates also showed little ATF4 binding on the *IL8* promoter in all conditions except the low glucose control condition.

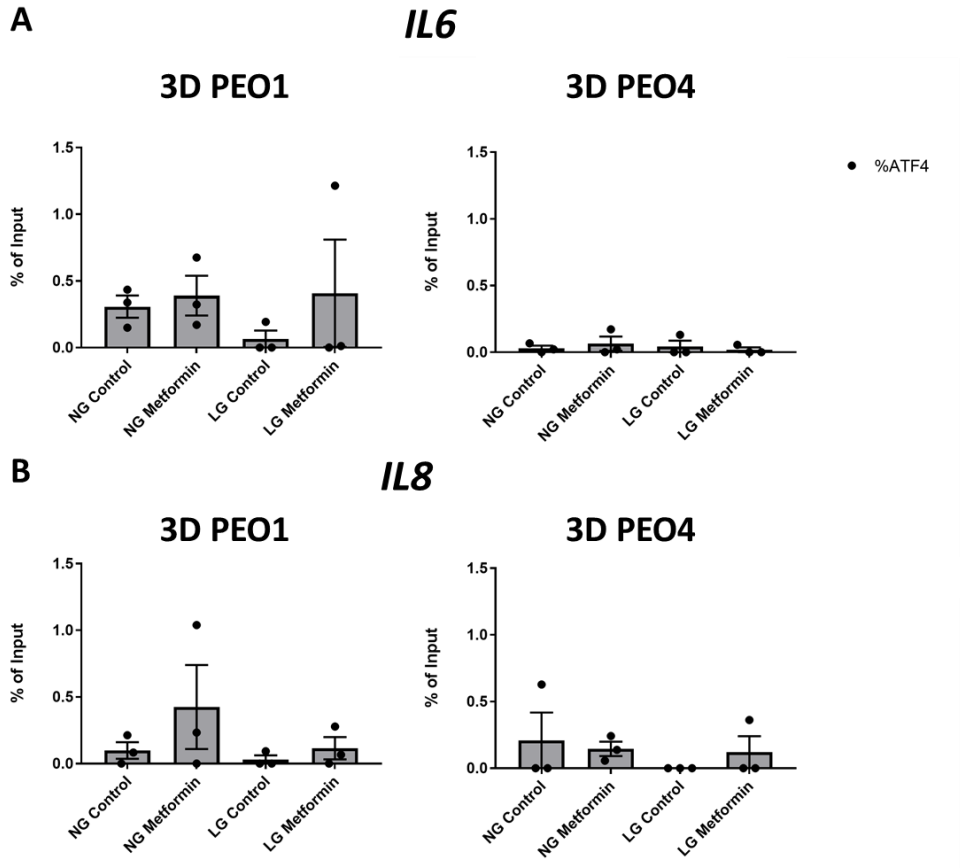

Figure 36. ChIP-qPCR was used to analyse the ATF4 enrichment on the *IL6* and *IL8* promoter in 3D PEO1 and PEO4 cells.

3D PEO1 and PEO4 cells were treated with 0.625 mM metformin or ddH_2O (control) in normal glucose (10 mM) and glutamine (2 mM) media (NG) or low glucose (1 mM) and glutamine (2 mM) media (LG). Enrichment of ATF4 on the *IL6* (A) and *IL8* (B) promoter were assayed. Statistical analysis by Two-way ANOVA: $p > 0.05$ (n.s.) (n=3 independent cell passages, error bars represent $\pm$ S.E.M).

The addition of metformin may increase the binding of pSTAT3 S727 to the *IL6* promoter in 3D PEO1 spheroids whereas in 3D PEO4 aggregates, pSTAT3 S727 binding was observed in the normal glucose condition (Figure 37A). On the *IL8* promoter, the normal glucose condition showed some pSTAT3 binding in the 3D PEO1 cells whereas the low glucose condition showed no binding (Figure 37B). In 3D PEO4 aggregates, the low glucose control condition showed pSTAT3 binding which was diminished upon the addition of metformin.

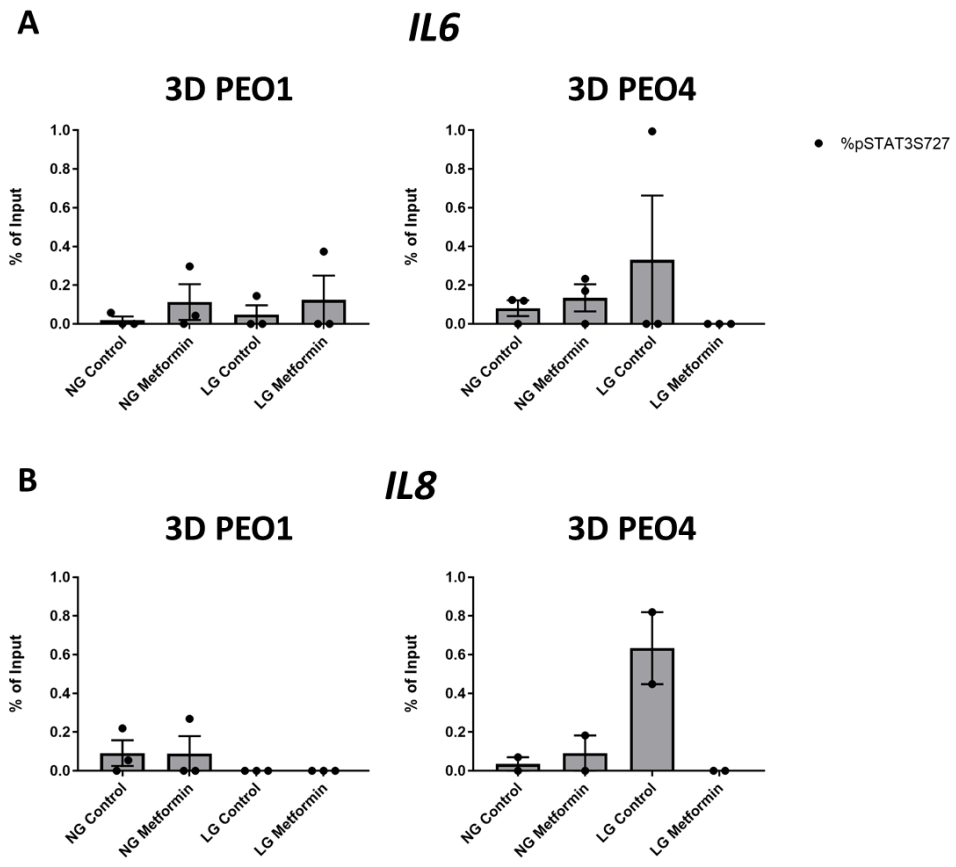

Figure 37. ChIP-qPCR was used to analyse the pSTAT3 S727 enrichment on the *IL6* and *IL8* promoter in 3D PEO1 and PEO4 cells.

3D PEO1 and PEO4 cells were treated with 0.625 mM metformin or ddH_2O (control) in normal glucose (10 mM) and glutamine (2 mM) media (NG) or low glucose (1 mM) and glutamine (2 mM) media (LG). Enrichment of pSTAT3 S727 on the *IL6* (A) and *IL8* (B) promoter were assayed. Statistical analysis by Two-way ANOVA: $p > 0.05$ (n.s.) (n = 2 – 3 independent cell passages, error bars represent $\pm$ S.E.M).

The 3D PEO1 *IL6* promoter showed some pSTAT3 Y705 binding under the normal glucose control condition whereas the other conditions showed little pSTAT3 binding (Figure 38A). The *IL6* promoter in 3D PEO4 aggregates showed little to no pSTAT3 binding in all conditions. The pSTAT3 binding showed a similar pattern in the *IL8* promoter as the *IL6* promoter (Figure 38B). The 3D PEO4 *IL8* promoter showed high pSTAT3 binding in the low glucose metformin condition which was reduced in the control condition. The normal glucose condition showed very little pSTAT3 binding in the 3D PEO4 *IL8* promoter.

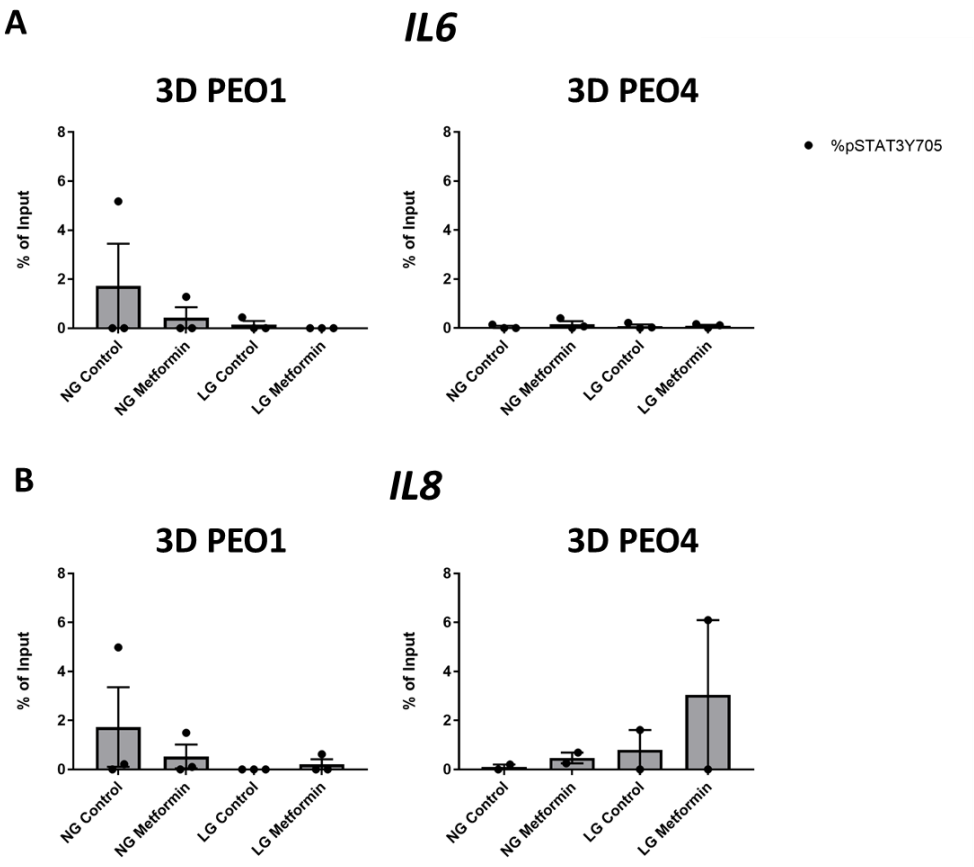

Figure 38. ChIP-qPCR was used to analyse the pSTAT3 Y705 enrichment on the *IL6* and *IL8* promoter in 3D PEO1 and PEO4 cells.

3D PEO1 and PEO4 cells were treated with 0.625 mM metformin or ddH_2O (control) in normal glucose (10 mM) and glutamine (2 mM) media (NG) or low glucose (1 mM) and glutamine (2 mM) media (LG). Enrichment of pSTAT3 Y705 on the *IL6* (A) and *IL8* (B) promoter were assayed. Statistical analysis by Two-way ANOVA: $p > 0.05$ (n.s.) (n=2-3 independent cell passages, error bars represent $\pm$ S.E.M).

4.5. Discussion

It is difficult to come to a solid conclusion from our results as there was variability between the replicates. Additionally, some of the background signal was higher or was comparable to the positive ChIP result, thus, it is difficult to determine if poor enrichment or a false negative is the true result. It is also possible that our protein of interest did not bind to the putative binding site analysed in this experiment. Some adjustments could be made to this experiment including using ChIP-seq to determine putative binding sites followed by ChIP-qPCR to identify the protein enrichment at the binding sites in different experimental conditions. Using ChIP-qPCR alone to screen each binding site is a time consuming and laborious process, it is possible that the binding sites analysed in this experiment may not be the target binding sites. ChIP-seq can also be used to determine the effectiveness of an antibody as many manufacturers make claims of a ChIP validated antibody but results in high failure rate due to poor quality ChIP data (Savic, et al., 2015; Keller, et al., 2021). For this experiment, we looked at the transcription factor binding at 48 h as we wanted to analyse the binding profile preceding the responses at 96 h and 144 h. ChIP provides a snapshot of genomic processes as enzymes are inactivated upon the addition of formaldehyde (Struhl, 2007). A time course experiment could be performed to ensure that transient transcription factor binding is not missed.

Proper controls are essential for the correct interpretation of ChIP data. It can be difficult to find a positive locus bound by the protein of interest that remains unchanged across experimental conditions (Greulich, et al., 2021). A spike-in control involves the use of chromatin that does not originate from our organism of interest along with an antibody that is specific to the aforementioned chromatin being “spiked-in” to each reaction containing our chromatin and antibody targeting our protein of interest. Any variation seen in the ChIP reaction would also be observed in the in spike-in control as the amount of spike-in chromatin is consistent across all samples. Therefore, a normalisation factor can be calculated from the spike-in chromatin and applied to the experimental chromatin to reduce variation between technical replicates and reveal biological differences (Bonhoure, et al., 2014; Hunter, et al., 2019). In addition to biological repeats, technical repeats (performing three separate IP and

detection after sample sonication) can also be considered in order to assess the variability during sample handling (Mukhopadhyay, et al., 2008).

Our results show that in 2D PEO1 cells treated with metformin in low glucose conditions there was some TET2 binding on the *IL6* promoter, which was not seen in the 2D PEO4 cells. In 3D PEO1 cells, one replicate showed TET2 binding whereas the *IL8* promoter showed little TET2 binding in both cell lines in all conditions. This suggests that TET2 may be involved in *IL6* regulation through binding of the CpG island in the promoter but may be transient. The binding of TET2 to the CpG island correlates with the literature where the binding domain, IDAX preferentially binds to CpG-rich regions and CpG islands (Ko, et al., 2013). TET2 has previously been reported to act as a tumour suppressor by repressing inflammation (Cull, et al., 2017; Lv, et al., 2018). However, TET2 has been implicated in the inflammatory response in several studies, such as in mouse macrophage-like cells where TET2 upregulated the pro-inflammatory cytokine *IL1B* through the demethylation of the *TAB2* promoter upon LPS treatment (Liang, et al., 2020). A study by Itoh *et al.,* (2018) showed that, under hypoxia, TET2 bound to and demethylated the *IL6* promoter causing an increase in *IL6* expression in osteosarcoma. In human dental pulp, TET2 may play a role in the LPS-induced expression of cytokines as the silencing of TET2 resulted in the reduction of several cytokines including IL-6 and IL-8 (Wang, et al., 2018). As shown in Chapter 3, AMPK was upregulated in response to low glucose and metformin. The upregulation of AMPK could stabilise TET2, protecting it from degradation (Wu, et al., 2018). TET2 could then bind to the *IL6* promoter and increase its expression.

ATF4 has been reported to show a pro-inflammatory role as knocking down ATF4 led to a decrease in the levels of pro-inflammatory proteins such as IL-1β, IL-6, IL-8 and TNF-α in addition to decreasing the expression of proangiogenic factors *VEGF* and *FGF-2* (Wang, et al., 2012; Deng, et al., 2021; Li, et al., 2021). Both metformin and glucose-deprived conditions can increase the expression of *ATF4* (Quentin, et al., 2012; Terashima, et al., 2013). Our results showed that on the *IL6* promoter in 2D PEO1 cells, one replicate showed ATF4 binding in the metformin treated condition, with low glucose showing higher ATF4 binding. A similar trend was observed with 2D PEO1 cells on the *IL8* promoter but to a lesser degree. However, in the

3D samples, the normal glucose condition showed some ATF4 binding on the *IL8* promoter for both cell lines and the *IL6* promoter for PEO1 cells. Further experiments such as western blotting and knocking down ATF4 will be required to determine what role ATF4 plays on the regulation of the inflammatory response.

The phosphorylation of STAT3 was required for the binding to GAS sequences in the promoters of inflammatory genes. Following treatment with IL-6, pSTAT3 Y705 was recruited to the *IL8* gene promoter without requiring activated NF-κB (Yoshida, et al., 2004). Ox-PAPC and leptin treatment also induced the binding of pSTAT3 Y705 to the GAS sequence in the *IL8* promoter (Gharavi, et al., 2007; Tong, et al., 2008). During cancer cell starvation, the secretion of IL-6 was not associated with STAT3 activation but required the activation of NF-κB (Yoon, et al., 2010; Yoon, et al., 2012). However, pSTAT3 Y705 was required for the proper functioning of NF-κB as a transcription factor in IL-6 induction. Putative binding sites for STAT3 and NF-κB were located next to the start site of the *IL6* promoter, STAT3 and NF-κB may work as a complex due to the overlapping binding site (Yoon, et al., 2012). On the *IL6* promoter, STAT3 was reported to bind and activate transcription (Yoon, et al., 2010). Additionally, PAK1 and pSTAT3 protein were recruited to the *IL6* promoter and played a role in *IL6* expression (Kim, et al., 2019). Our results suggest that the inflammatory response seen in the low glucose metformin treatment in 2D PEO1 cells is independent of pSTAT3 Y705 binding, which also correlates with the lack of pSTAT3 Y705 expression in the western blots. Binding of pSTAT3 S727 was observed in the low glucose metformin condition in 2D PEO1 cells. Phosphorylation of the S727 site has been implicated in the enhancement of STAT3 nuclear transcriptional activity through the interaction with p300 (Lee, et al., 2009; Tesoriere, et al., 2021). It is possible that pSTAT3 S727 is not involved in causing the inflammatory response but is activated as a response to the cytokine. In response to IL-6 stimulation, p300 associates with pSTAT3 S727 – the phosphorylation of S727 at the C-terminal region is required for the p300 driven transcriptional activity of STAT3. The dimerization of STAT3 is not required for the association with p300 (Schuringa, et al., 2001). Additionally, p300 can also acetylate TET2 and enhance its enzymatic activity by stabilising it and inhibiting ubiquitination (Zhang, et al., 2017).

ChIP measures protein association and does not provide information about the function of proteins bound at the genomic region of interest. ChIP is unable to distinguish whether a protein binds to DNA directly or indirectly through protein-protein interactions. Experiments such as transcriptional or genetic analysis are required in order to determine the function of bound proteins (Struhl, 2007).

4.6. Conclusion

Our results showed variation between the replicates which could be due to biological reasons which include weak or indirect binding of proteins or technical limitations such as antibody specificity and variation in cell lysis and chromatin shearing. These factors make ChIP results difficult to interpret. Our results suggest that TET2 may be implicated in the IL-6 response in 2D PEO1 in low glucose metformin condition as this condition showed some TET2 binding. However, the IL-8 response maybe due to a different pathway. Although the *IL6* and *IL8* promoter showed some ATF4 binding t, it is unknown what role ATF4 plays in inflammation here. In 2D PEO1 cells, pSTAT3 Y705 may play a role in *IL8* inflammation but not *IL6* whereas both promoters showed pSTAT3 S727 binding which could be in response to the cytokines produced under the low glucose metformin condition.

Chapter 5

Application of Methylated DNA Immunoprecipitation (MeDIP) to find a link between metabolism and epigenetics in 2D and 3D ovarian cancer cell lines

5.1. Introduction

DNA methylation has a role in processes such as genomic imprinting, X-chromosome inactivation, gene expression, genome stabilisation and embryonic development. DNA methylation involves the addition of a methyl group to the C5 position of the cytosine ring to form 5mC catalysed by DNMTs (Kong, et al., 2016). The TET family of enzymes can demethylate DNA by oxidising 5mC to 5hmC to 5fC and then 5caC. 5fC and 5caC are changed to cytosine by base excision repair via TDG (Pan, et al., 2015). There is a complex relationship between methylation and gene expression. Generally, high levels of gene expression are associated with low promoter methylation (Wagner, et al., 2014). Aberrant DNA methylation is a hallmark of cancer and has been implicated in many types of cancers as tumours are genetically and epigenetically distinct from their tissue of origin (Joyce, et al., 2015; Thienpont, et al., 2016). Changes in DNA methylation involve global hypomethylation and the local hypermethylation of CpG-rich gene promoters. Hypermethylation of promoters can lead to oncogenesis by affecting tumour suppressor genes and interfering with transcription factor binding resulting in transcriptional silencing (Gasche, et al., 2011; Thienpont, et al., 2016). DNA hypomethylation contributes to tumorigenesis by reducing the methylation of highly methylated repetitive sequences i.e., LINE-1 transposons and Alu sequences in addition to causing chromosomal instability, resulting in mitotic dysregulation. Demethylation can also induce the reactivation of certain proto-oncogenes that are normally silenced (Gasche, et al., 2011). Studying DNA methylation will help identify epigenetic events and their role in gene expression and oncogenesis.

To understand the role of 5mC, techniques have been developed to assay 5mC levels and distribution. Techniques involving methylation-sensitive or methylation-specific restriction enzymes biased towards specific restriction motifs can be used. Other techniques use affinity purification of methylation DNA followed by microarray hybridisation or sequencing (Borgel, et al., 2012). Methylated DNA Immunoprecipitation (MeDIP) uses a monoclonal antibody against 5mC to purify methylated DNA. The principle of MeDIP involves the purification of genomic DNA (gDNA) before shearing by sonication (Figure 39). The sheared DNA is then denatured at 95^{o}C to generate single-stranded DNA fragments for improved binding of the antibody. After

immunoprecipitation, the eluted DNA can be used for the analysis of the methylation status using techniques such as RT-qPCR for a single gene resolution or microarray hybridisation or sequencing for whole methylome analysis (Jacinto, et al., 2008; Borgel, et al., 2012).

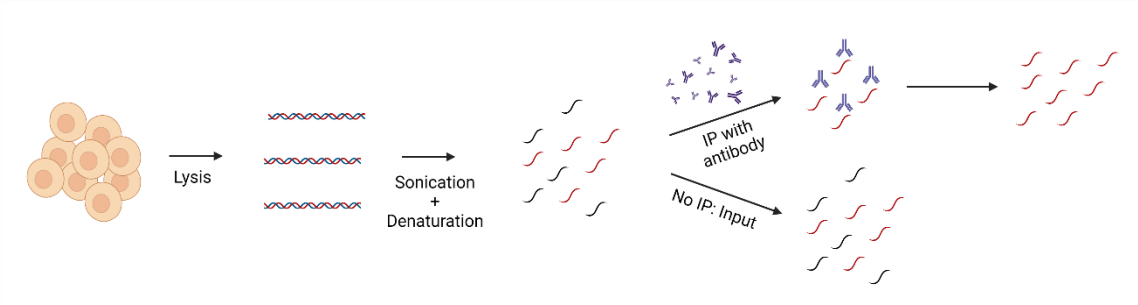

Figure 39. Principles of MeDIP.
DNA is extracted from the cells before sonication and denaturing of double stranded DNA to single stranded DNA. Some sample is not immunoprecipitated, designated as "input" which is used for normalisation. The other samples are immunoprecipitated with a 5mC antibody. Both immunoprecipitated samples and input are then used for downstream applications including RT-qPCR. Created with BioRender.com

Aberrant DNA methylation of inflammatory genes or genes involved in the regulation of inflammation have been implicated in cancer development (Joyce, et al., 2015). The cytokine IL-6 may facilitate tumour proliferation by altering patterns of DNA methylation. IL-6 expression and production are regulated by the methylation of the *IL6* gene promoter. Hypomethylation of the *IL6* gene promoter was associated with increased *IL6* expression in Bechet's disease (Alipour, et al., 2020), rheumatoid arthritis and chronic periodontitis (Nile, et al., 2008; Ishida, et al., 2012; Kobayahi, et al., 2016). Bovine endometrial cells treated with LPS induced the expression of *IL6* and *IL8* mRNA which was regulated by the methylation of the *IL6* and *IL8* promoter. DNA methylation levels at the *IL6* and *IL8* promoter in LPS treated cells showed a decrease at certain sites compared to the control group (Wang, et al., 2018). The expression of *IL8* was controlled by promoter methylation in several diseases. Atypical methylation correlated strongly with the metastatic potential of breast cancer cells (De Larco, et al., 2003). Hypomethylation of the *IL8* promoter was observed in aggressive and chronic periodontitis, in addition to clear cell renal carcinoma (Oliveira, et al., 2009; Andia, et al., 2010; Yoo, et al., 2012). Demethylation of CpG sites in the *IL8* promoter correlated with higher *IL8*

gene expression in osteoarthritic chondrocytes (Takahashi, et al., 2015) and in colorectal cancer patients (Dimberg, et al., 2012) where it was also associated with distant metastasis. These studies suggest that changes in DNA methylation in the *IL6* and *IL8* promoter could affect its expression.

There are only a few studies investigating the effect of metformin on DNA methylation. Metformin decreased the methylation levels of the metformin transporter gene promoters, resulting in higher expression in the liver tissues (García-Calzón, et al., 2017). Metformin may also drive the sensitivity of EOC cancer stem cells to platinum therapy by causing epigenetic changes in the tumour stroma (Brown, et al., 2020). In cancer cells, metformin can induce genome-wide alterations in DNA methylation though the H19/ S-adenosylhomocysteine hydrolase (SAHH) axis. The activation of AMPK resulted in increased levels of let-7 which targeted H19 for degradation. SAHH was freed from sequestration by H19 leading to the hydrolysis of S-adenosylhomocysteine (SAH) – a feedback inhibitor for DNMT3B, resulting in an increase in DNA methylation (Yan, et al., 2015; Zhong, et al., 2017). Supporting this, another study showed that metformin decreased intracellular SAH and altered genome-wide methylation by the AMPK-dependent activation of SAHH in various cell types, including non-cancerous cells. Metformin was able to regulate or influence the DNA methylome by enhancing global DNA methylation as well as site-specific hypermethylation at certain tumour-promoting loci. Metformin can also act as a metabolo-epigenetic regulator by regulating mitochondrial one-carbon metabolism, which is the major metabolic supply of methyl groups for DNA methylation (Cuyàs, et al., 2018).

In addition to affecting DNA methylation, metformin has also been implicated in the regulation of DNA demethylation. The activation of AMPK by metformin and the metabolite α-KG played a role in TET-mediated DNA demethylation in tissue development and regeneration in brown fat (Yang, et al., 2016). As previously discussed, metformin could phosphorylate S99 residue on TET2 mediated by AMPK, preventing its degradation by calpain (Figure 40) (Wu, et al., 2018; Zhang, et al., 2019). TET2 plays a role in DNA demethylation by oxidising 5mC to 5hmC. Hyperglycaemic conditions destabilise TET2 which results in the dysregulation of 5hmC levels

(Wu, et al., 2018). TET2 has been implicated in the inflammatory response by upregulating the expression of proinflammatory cytokines and therefore may play a role in the regulation of *IL6* and *IL8* expression through the DNA demethylation of the promoter (Zhang, et al., 2015; Itoh, et al., 2018; Wang, et al., 2018; Liang, et al., 2020). From these studies, metformin can act as a link between cellular metabolism and DNA methylation and DNA demethylation machinery.

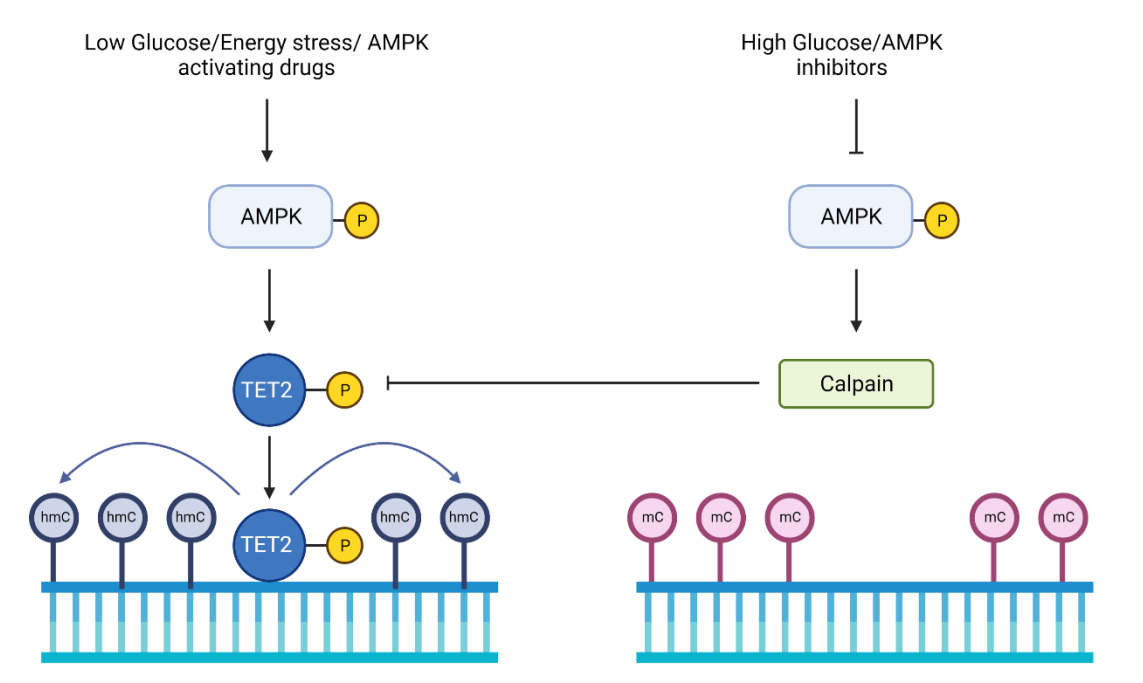

Figure 40. AMPK/TET2 signalling forms the link between metabolism and the epigenome. Under low glucose conditions, AMPK stabilises TET2 through the phosphorylation of the serine 99 residue. In high glucose conditions, calpain degrades TET2 resulting in aberrated regulation of DNA methylation. Figure adapted from (Wu, et al., 2018). Created with BioRender.com

5.2. Aims and Objectives

The effect of metformin and glucose concentration on the levels of DNA methylation on the *IL6* and *IL8* promoter requires further investigation. In unpublished data, we have previously shown that the combination of metformin and low glucose condition resulted in an increase in IL-6 and IL-8 production at 96 h and 144 h in 2D PEO1 cells. Western blotting showed that AMPK was activated under these conditions whereas ChIP indicated that TET2 may bind to the *IL6* promoter. The work carried out in this Chapter was aided by Porvair Ltd. who provided the

gDNA extraction kits, MeDIP columns and reagents as well as providing technical advice. The aims of this chapter were to investigate the DNA methylation status of the *IL6* and *IL8* promoter of 2D and 3D OC cells under experiment conditions and to validate the MeDIP protocol for ovarian cancer research. The objectives were as follows:

1. Optimise the DNA shearing times for DNA extracted from 2D and 3D PEO1 and PEO4 cultures
2. Screen methylated genes as a potential positive control for use to validate the 5mC antibody as well as confirming the presence of methylation in OC samples.
3. Use MeDIP to assay the levels of methylation of the *IL6* and *IL8* promoter under experimental conditions in 2D and 3D PEO1 and PEO4 cultures.

5.3. Methods and Materials

The gDNA extraction kit, 5mC antibody and columns for MeDIP assay were provided by Porvair Ltd.

5.3.1. Treatments

5.3.1.1. 2D cultures

PEO1 and PEO4 cells were seeded at a density of 2 x 10^6 cells in total in a T-75 flask and cultured for 24 h before treatment with 0.625 mM metformin or vehicle (ddH_2O) in LG + Q or NG + Q experimental cell culture media (**Table *1***) for 48 h.

5.3.1.2. 3D cultures

3D cultures of PEO1 and PEO4 cells were prepared via the hanging drop method as described in 2.3.1. A seeding density of 1 x 10^4 cells per spheroid was used. Cells were resuspended in LG + Q or NG + Q experimental cell culture media with 0.625 mM metformin or vehicle (ddH_2O) before seeding on the lid of a 96-well plate. Each treatment condition was prepared in duplicate (approximately 192 spheroids). Spheroids were cultured for 48 h before harvesting.

5.3.2. Genomic DNA extraction

The gDNA extraction was carried out according to the manufacturer's protocol.

5.3.2.1. Cell preparation

5.3.2.1.1. 2D cultures

Cells were washed with PBS and detached by adding 2 mL Accutase and incubation at 37°C for 10 – 20 min. After detaching the cells, 2 – 3 mL of PBS was added to the flask before centrifugation at 200 x g for 5 min at RT. The supernatant was discarded, and the cell pellet was resuspended in 200 µL PBS before transferring to a 1.5 mL centrifuge tube.

5.3.2.1.2. 3D cultures

Spheroids were collected into a 1.5 mL centrifuge tube using a Pasteur pipette before washing with PBS. To facilitate disaggregation, 100 µL of Accutase was added before incubation at 37°C for 10 – 20 min. After incubation, 500 µL of PBS was added and mixed by pipetting to encourage spheroid disaggregation. Samples were centrifuged at 200 x g for 5 min at RT before

discarding the supernatant. The cell pellet was resuspended in 200 µL PBS before transferring into a 1.5 mL centrifuge tube.

5.3.2.2. Cell lysis

To each sample, 10 µL of Proteinase K was added and mixed by pipetting. The DNA Extraction Lysis Buffer was vortexed before use, 200 µL was then added to each sample and pulse vortexed for 30 sec to mix. Samples were incubated for 20 min at 55^{o}C after which, samples were briefly centrifuged to remove liquid from the caps.

5.3.2.3. DNA Capture & Elution

DNA was precipitated by adding 200 µL of 96 – 100% ethanol to each sample before mixing by vortexing. Samples were centrifuged to remove liquid from the caps and loaded into the Chromatrap® DNA Extraction column. The columns were centrifuged at 10,000 x g for 1 min at RT and the flow through was discarded. The columns were then washed by adding 500 µL DNA extraction Wash Buffer 1 to each column and centrifuged at 10,000 x g for 1 min at RT. The flow through was discarded and the columns washed again by adding 500 µL DNA Extraction Wash Buffer 2 to each column before centrifugation at 10,000 x g for 1 min at RT. The flow through was discarded and the columns were dried by centrifuging at maximum speed for 1 min. The columns were then transferred into a 1.5 mL centrifuge tube. To elute the DNA, 200 µL of DNA Extraction Elution Buffer was added to each sample and incubated for 5 min at RT. The columns were centrifuged at maximum speed for 1 min at RT to collect the eluted DNA. To remove contaminating RNA, 1 µL of RNAse A was added to each sample and incubated at 37^{o}C for 1 h.

5.3.3. Determining Genomic DNA shearing efficiency

The extracted DNA samples were quantified using a NanoDrop 1000 and up to 20 µg gDNA was transferred into a 1.5 mL sonication tube in a total volume of 300 µL Sonication Buffer. Genomic DNA was sonicated using a water bath sonicator at 30 sec burst with 30 sec intervals on ice until fragments of 100 – 500 bp were achieved. The sheared DNA was electrophoresed on a 1% agarose gel with 5 µL/50 mL SYBR-Safe DNA gel stain.

5.3.4. Genomic DNA Denaturation

For immunoprecipitation, 500 ng of gDNA was used. Samples were prepared according to **Table *6*** and incubated at 95°C for 10 min. The samples were then immediately transferred to ice and incubated for 10 min.

Table 6. Reagents required for the preparation of samples for gDNA denaturation.
For each IP, 500 ng gDNA is required.

Reagent	Input	Negative (IgG)	5mC
IP Buffer	4 µL	4 µL	4 µL
gDNA	-- µL	-- µL	-- µL
d.H_2O	-- µL	-- µL	-- µL
Total volume		Up to 35 µL	

5.3.5. Immunoprecipitation of sheared DNA

After the denaturation step, DNA was kept on ice to prevent DNA from re-annealing as MeDIP requires the use of single stranded DNA. Reagents were added to each sample according to **Table *7***. The input was set aside at 4°C. The slurries were mixed by pipetting and incubated on ice for 1 h.

Table 7. Preparation of the slurries for immunoprecipitation in the spin column.

Reagents	Negative (IgG)	5mC
Bridging Antibody	2 µL	2 µL
IgG Antibody	2 µL	-
5mC Antibody	-	2 µL
Protease Cocktail Inhibitor	1 µL	1 µL
Total Volume	40 µL	

The Chromatrap® spin columns require washing and activation before use. To each column, 500 µL of IP buffer was added before centrifugation at 4000 x g for 30 sec. The flow through was discarded and the wash step repeated. The columns were centrifuged at top speed for 30 secs to dry the columns. The slurry was added to the Chromatrap® spin column and incubated for 1 hr at 4°C with gentle agitation after which 500 µL of IP buffer was added to each column and centrifuged at 4000 x g for 30 secs. The flow through was discarded and the wash step was repeated three times. The spin columns were centrifuged at top speed for 30 sec to remove any excess liquid. The collection tube was discarded, and the column transferred to a new 1.5 mL collection tube after which 50 µL of Elution buffer was added before incubation at room temperature for 15 min. The columns were centrifuged at top speed for 30 sec to collect the methyl enriched DNA. To each input, 32.5 µL of Elution buffer and 32.5 µL of Neutralisation buffer was added and 50 µL Neutralisation buffer was added to each sample. The samples were mixed before RT-qPCR.

5.3.6. DNA analysis

5.3.6.1. Primer Design

The promoter sequences for *IL6* and *IL8* were obtained from UCSC Genome Browser. MethPrimer (https://www.urogene.org/methprimer) was used to predict CpG Islands (Li & Dahiya, 2002). Primers were analysed using OligoEvaluator™ (Sigma-Aldrich; http://www.oligoevaluator.com) for dimers, hairpin formations and efficiency. A Primer-BLAST search of the primer sequences against the whole genome was performed to check specificity to the region of interest (Ye, et al., 2012).

Table 8. Real time qPCR primers for MeDIP assay.

Target	Primer sequences	Reference
BRDT	F – CCCTTTGGCCTTACCAACTT R – GCCCTCCCTTGAAGAAAAAC	(Borgel, et al., 2012)
TSH2B	F – CAGACATCTCCTCGCATCAA R – GGAGGATGAAAGATGCGGTA	(Borgel, et al., 2012)
H19 ICR	F – GAGCCGCACCAGATCTTCAG R – TTGGTGGAACACACTGTGATCA	(Weber, et al., 2007)
HIST1H2B	F – TGTTTGTTTACTTGGCGAGAC R – GGTTACACAGCACTTTCCAG	(Lisanti, et al., 2012)
IL-6 CpG	F – CCAGGAGAAGATTCCAAAGATGTA R – CGTCGAGGATGTACCGAATTT	(Alipour, et al., 2020)
IL-8 CpG	F – GATAAGGAACAAATAGGAAGTGTG R – TGGCTTTTTATATCATCACCCTAC	(Venza, et al., 2012)

5.3.6.2. Real Time Quantitative Polymerase Chain Reaction (RT-qPCR)

Primers used for RT-qPCR can be found in **Table *8*** and used at a final concentration of 1 µM each with 2.5 µL of input or purified sample and 5 µL of 2 x QuantiFast SYBR® Green (Qiagen; 204056). The cycle conditions used for RT-qPCR were as follows:

95°C – 5 min

95°C – 10 seconds
60°C – 30 seconds
72°C – 30 seconds
} 35 cycles

The melt curve was obtained as follows:

60°C – 1 minute

95°C – 30 seconds

To interpret the qPCR data, locus recovery was calculated as follows:

$$\% \text{ recovery} = 2^{\wedge} (Ct_{input} - Ct_{sample}) * \text{dilution} * 100\%$$

The % recovery for the background (IgG) was subtracted from the % recovery for the sample to calculate an overall % of Input.

5.4. Results

5.4.1. Optimisation of DNA shearing efficiency in OC cell lines

For MeDIP, DNA fragments between 100 – 500 bp were needed so optimising the shearing times for the DNA extracted from PEO1 and PEO4 cells was carried out. DNA was sheared for up to 30 min at the high setting, 30 secs on and 30 secs off with an aliquot of DNA taken every 5 min. Gel electrophoresis was performed on the samples. The results show that majority of the fragments fell between the 100 – 500 bp range at 15 min (Figure 41). At 30 min, most of the fragments fell below 500 bp, thus this amount of time was used for the sonication of experimental samples.

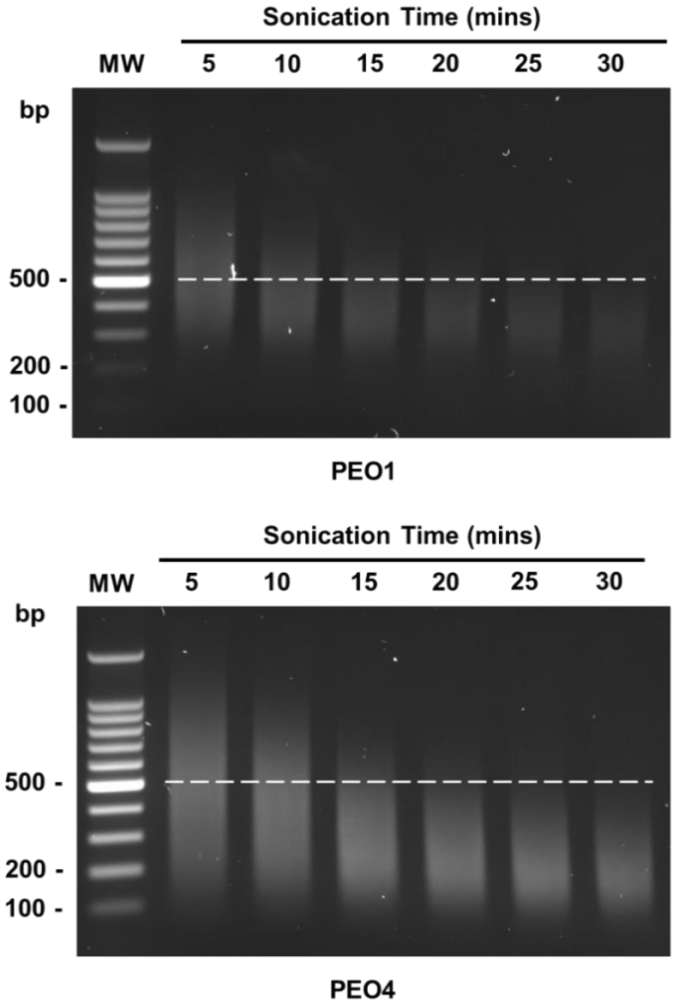

Figure 41. Comparison of DNA shearing efficiency for PEO1 and PEO4 cells, grown under cell culture conditions at confluency (approx. 3 x 10^5 cells/mL).
The fragment range desired (100 – 500 bp) was achieved after 15 min.

We used the same seeding density as for ChIP, 2 x 10^6 cells for 2D cultures and 1 x 10^4 cells per spheroid for 3D cultures to keep experimental conditions consistent. We were able to extract a sufficient amount of DNA for the MeDIP assay at this seeding density. Experimental conditions and treatment can cause changes in morphology and alter the shearing efficiency; therefore, it is important to check the sample on an agarose gel after shearing (Keller, et al., 2021). We performed a gel electrophoresis on the sheared DNA after 30 min of sonication (as established above) at the high setting with 30 secs on and 30 secs off. Although there was a range in fragment sizes after 30 min of shearing, there were enough DNA fragments below 100 – 500 bp for the MeDIP assay (Figure 42).

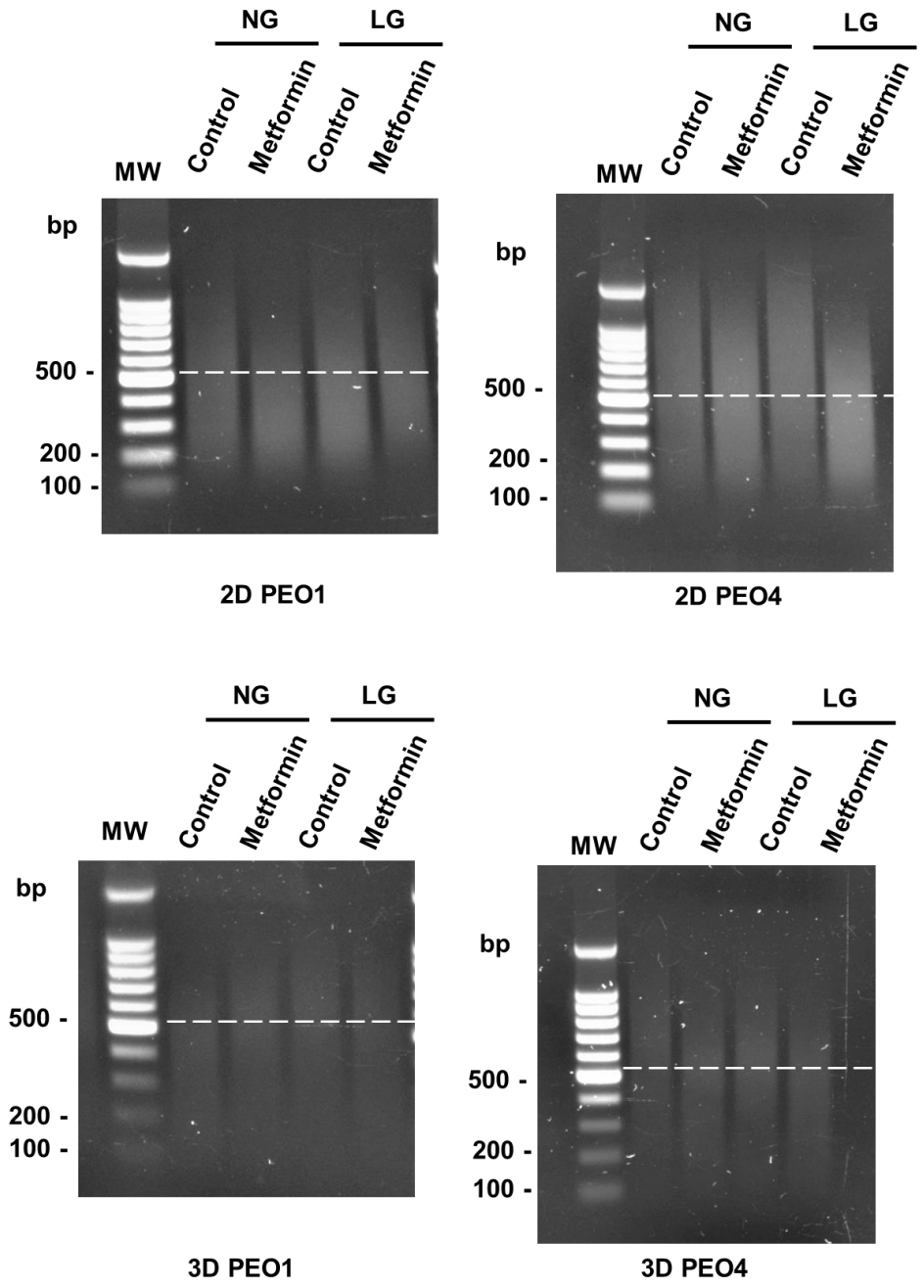

Figure 42. 2D and 3D PEO1 and PEO4 cells were sonicated for 30 min and the DNA shearing efficiency was confirmed using gel electrophoresis.

5.4.2. Determination of a positive control for DNA methylation and validation of DNA samples.

A positive control for methylation was needed in order to validate the efficacy of the 5mC antibody as well as the presence of methylation in our samples. Here we extracted DNA from 3D PEO4 aggregates grown in low glucose conditions treated with and without metformin as an ideal positive control should remain quantitatively unchanged amongst different samples and treatments (Struhl, 2007). We looked at the literature and chose four methylated gene targets as a potential positive control. Bromodomain testis-specific protein (*BRDT*) and Testis/sperm-specific histone 2B (*TSH2B*) are both methylated in somatic cells (Borgel, et al., 2012). *BRDT1* is expressed in the testis and is involved in regulating gene expression to promote spermatogenesis (Chen, et al., 2020). *TSH2B* has been implicated in sperm chromatin organisation (Singleton, et al., 2007). H19/IGF2 Imprinting Control Region (*H19ICR)* is involved in foetal programming and adiposity distribution though DNA methylation (Weber, et al., 2007; Huang, et al., 2012). Histone cluster 1 H2B family member A (*HIST1H2BA*) is expressed in spermatogenic cells and showed high methylation in fibroblasts (Lisanti, et al., 2012; Yao, et al., 2021). Our results showed that the level of methylation in these genes appeared to be affected by the addition of metformin (Figure 43). Despite the methylation levels being on the lower end, *HIST1H2BA* locus was used for further testing as it showed the highest 5mC levels.

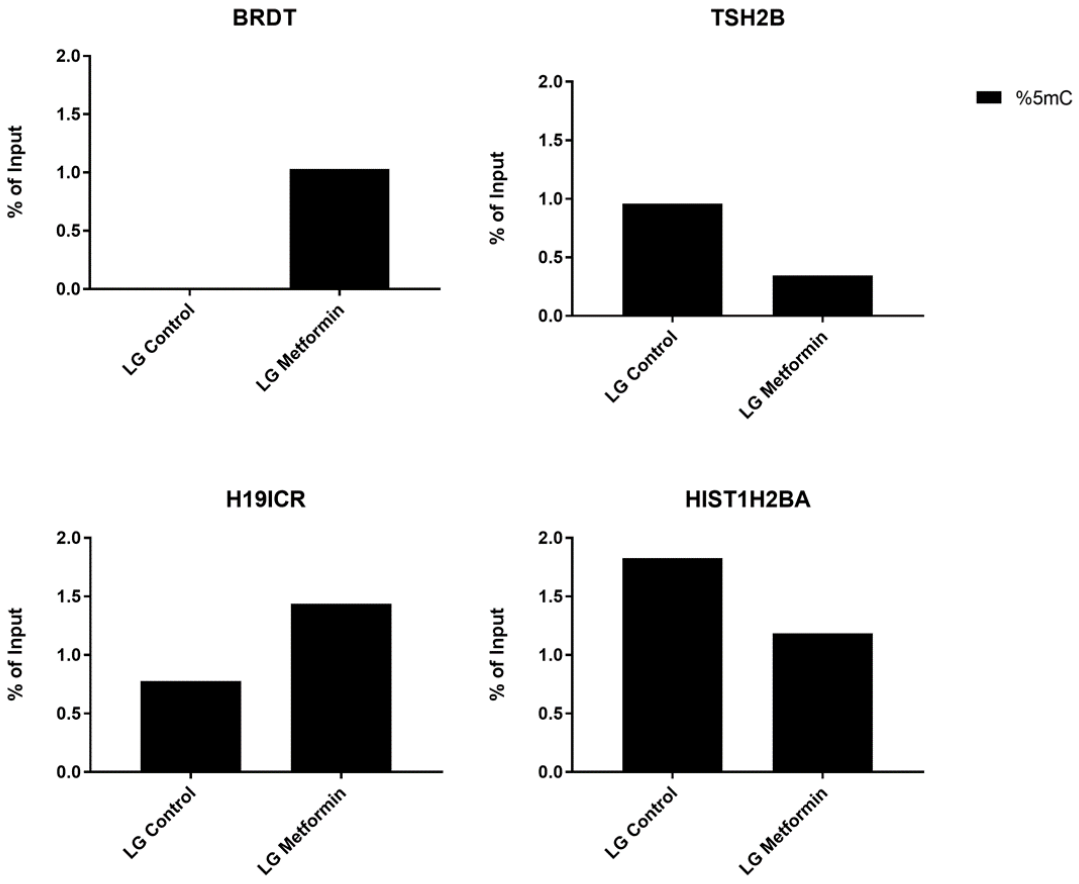

Figure 43. MeDIP assay was performed using 5mC antibody on 3D PEO4 cells in low glucose media treated with and without metformin.
3D PEO4 cells were treated with 0.625 mM metformin or ddH2O (control) in low glucose (1 mM) and glutamine (2 mM) media (LG). Immunoprecipitated DNA was analysed using RT-qPCR with primers targeting *BRDT*, *TSH2B*, *H19ICR* and *HIST1H2BA* (n=1).

As the methylation levels appeared to be on the lower end, we decided to purify the immunoprecipitated DNA from the MeDIP assay to see if the enrichment levels could be improved using the Nucleospin gDNA Clean-up kit (Macherey-Nagel; Cat#740904.50). The purification was carried out following the manufacturer's protocol. The purification of immunoprecipitated DNA did not improve the methylation levels, instead there was a loss of enrichment in all genes analysed (Figure 44). We decided that purification of the immunoprecipitated samples was not necessary.

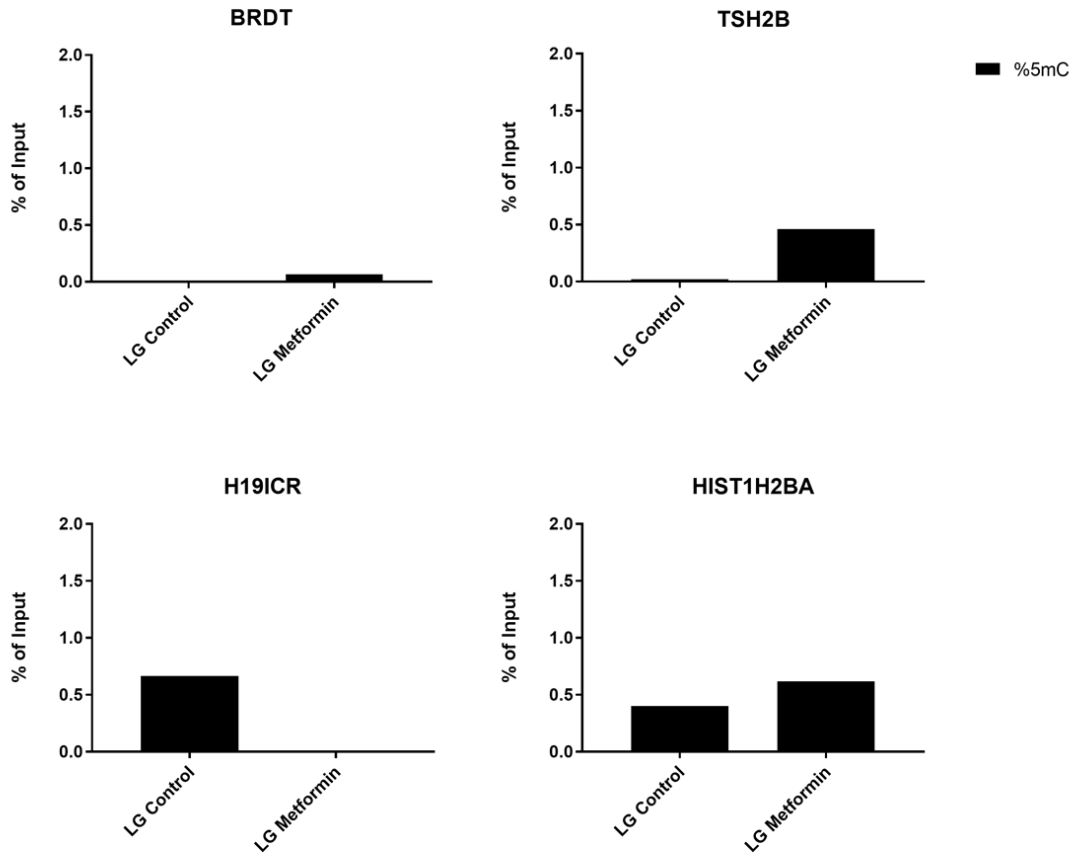

Figure 44. Immunoprecipitated DNA was purified, and RT-qPCR was performed using primers targeting *BRDT*, *TSH2B*, *H19ICR*, *HIST1H2BA*.

Immunoprecipitated DNA from the previous experiment was purified before RT-qPCR was performed (n=1)

HIST1H2BA was used as a positive control to validate the methylation of the immunoprecipitated DNA from our experiment. Our results showed that the levels of methylation remained consistent (~20%) across the different treatments and conditions in 2D PEO1 as well as 3D PEO1 and PEO4 cultures. Variation in the methylation levels between treatments and conditions could be seen in 2D PEO4 cells however this variation was non-significant (Figure 45).

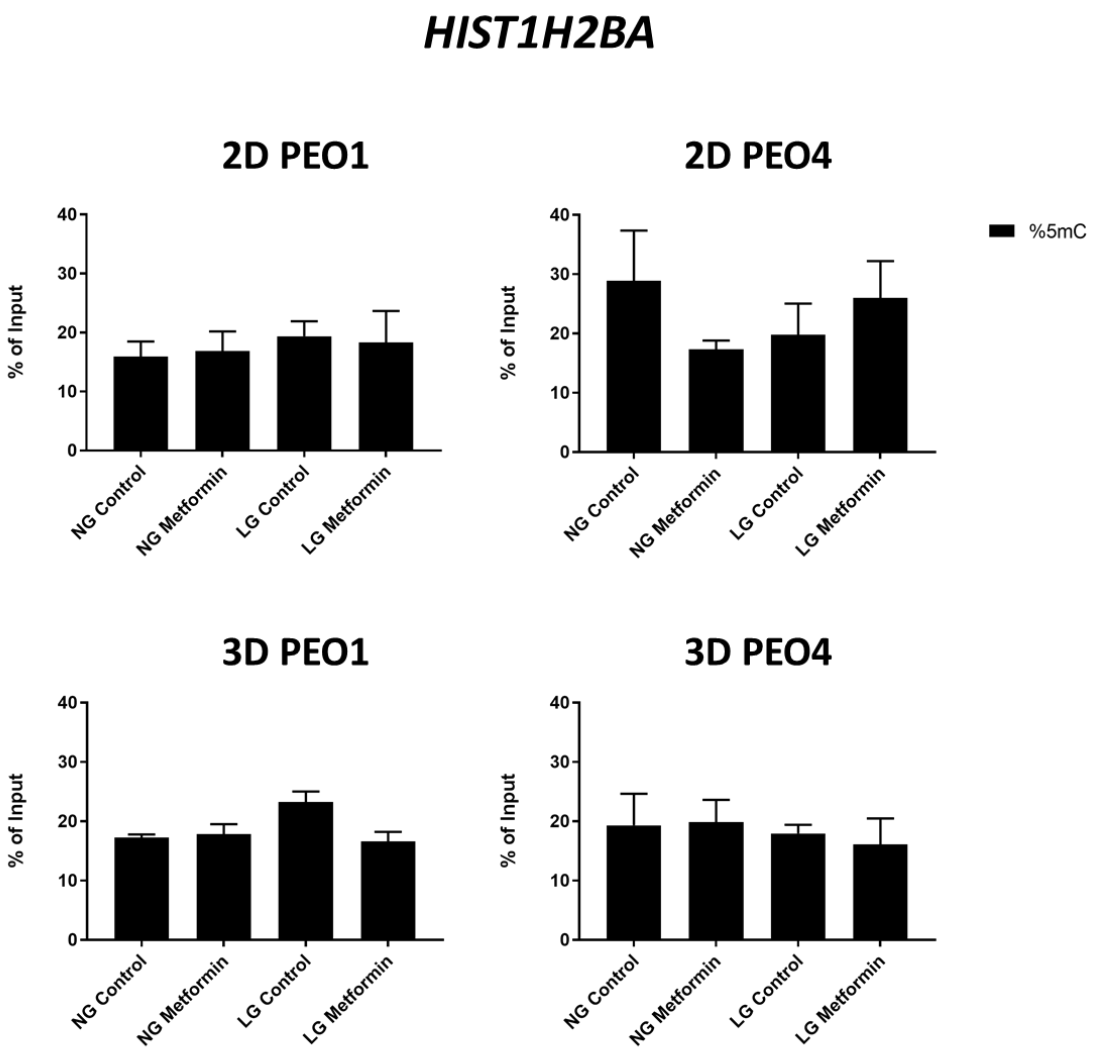

Figure 45. MeDIP-PCR was performed using primers targeting *HIST1H2BA* on DNA extracted from 2D and 3D PEO1 and PEO4 cultures.
2D and 3D PEO1 and PEO4 cells were treated with 0.625 mM metformin or ddH_2O (control) in normal glucose (10 mM) and glutamine (2 mM) media (NG) or low glucose (1 mM) and glutamine (2 mM) media (LG). Statistical analysis by Two-way ANOVA: $p > 0.05$ (n.s.). (n=3 independent cell passages, error bars represent ± S.E.M).

5.4.3. Use of MeDIP assay to analyse the DNA methylation levels of the *IL6* and *IL8* promoter in 2D and 3D ovarian cancer samples

MeDIP assay was performed on DNA extracted from 2D PEO1 and PEO4 samples, qPCR was used to analyse the levels of DNA methylation of the CpG island on the *IL6* and *IL8* promoter.

Our results showed that on the *IL6* promoter, the change in glucose levels or addition of metformin did not significantly alter the levels of methylation in both cell lines (Figure 46A). However, a slight reduction in methylation levels of the normal glucose control condition in PEO1 cells and the low glucose control condition in PEO4 cell lines was observed. The *IL8* promoter show lower levels of methylation compared to the *IL6* promoter. Higher levels of methylation could be observed in the PEO1 cell line compared to the PEO4 (Figure 46B). The addition of metformin appeared to cause a slight increase in methylation of the *IL8* promoter in the normal glucose condition but caused a nonsignificant decrease in methylation in the low glucose condition in 2D PEO1 cells.

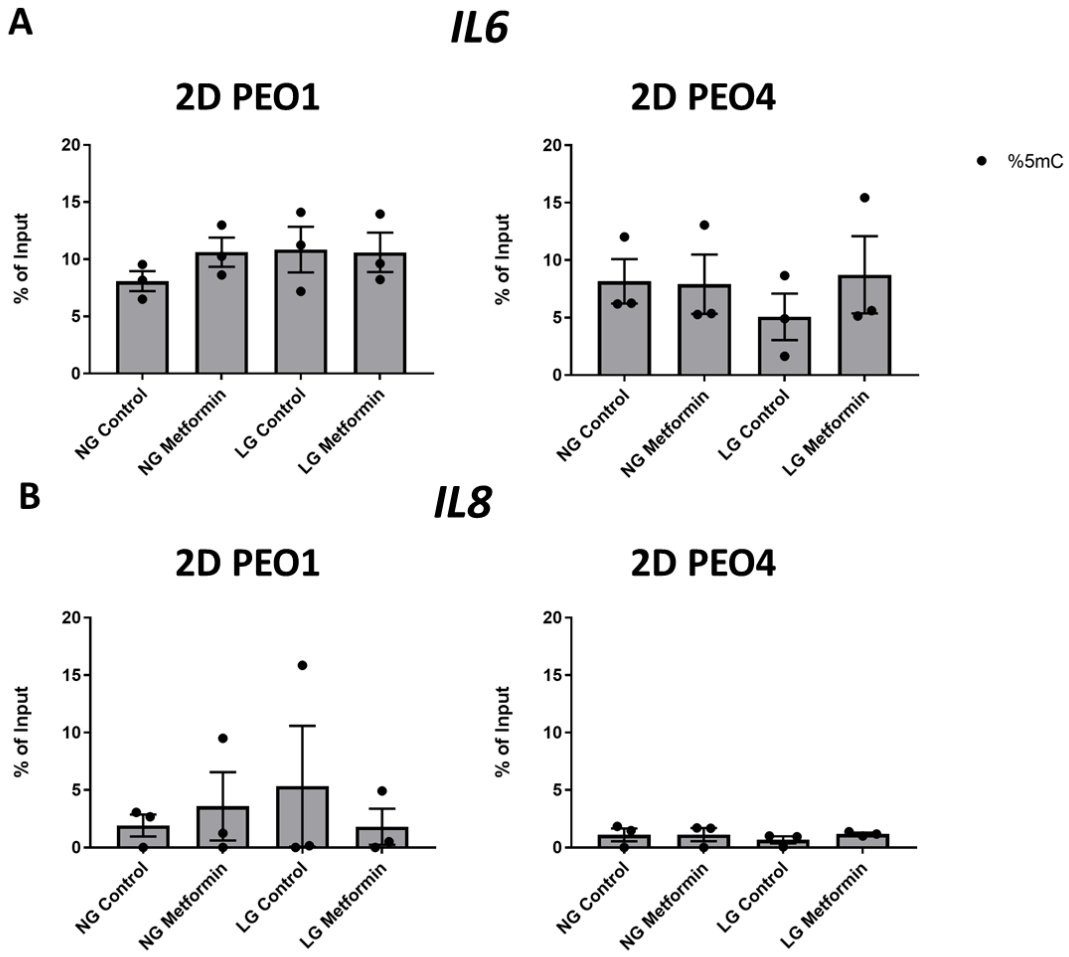

Figure 46. MeDIP-PCR was performed using primers targeting the CpG island on the *IL6* and *IL8* promoter on DNA extracted from 2D PEO1 and PEO4 cultures.
2D PEO1 and PEO4 cells were treated with 0.625 mM metformin or ddH2O (control) in normal glucose (10 mM) and glutamine (2 mM) media (NG) or low glucose (1 mM) and glutamine (2 mM) media (LG). Statistical analysis by Two-way ANOVA: $p > 0.05$ (n.s.). (n = 3 independent cell passages, error bars represent ± S.E.M).

MeDIP assay was also performed on 3D cultures treated with and without metformin in different media conditions. DNA methylation of the CpG island in the *IL6* and *IL8* promoter was analysed using qPCR. Methylation levels of CpG island in the *IL6* promoter did not appear to be affected by the addition of metformin in the normal glucose condition in PEO1 cultures and all glucose conditions in the PEO4 cultures. The low glucose condition caused an increase in methylation levels compared to the normal glucose conditions in PEO1 cultures (Figure 47A).

However, the addition of metformin in the low glucose condition led to a reduction in methylation levels. On the *IL8* promoter, one replicate of the control condition in the PEO1 cultures showed DNA methylation, which was reduced upon the addition of metformin (Figure 47B). In PEO4 cultures, the addition of metformin slightly increased the methylation levels in both glucose conditions.

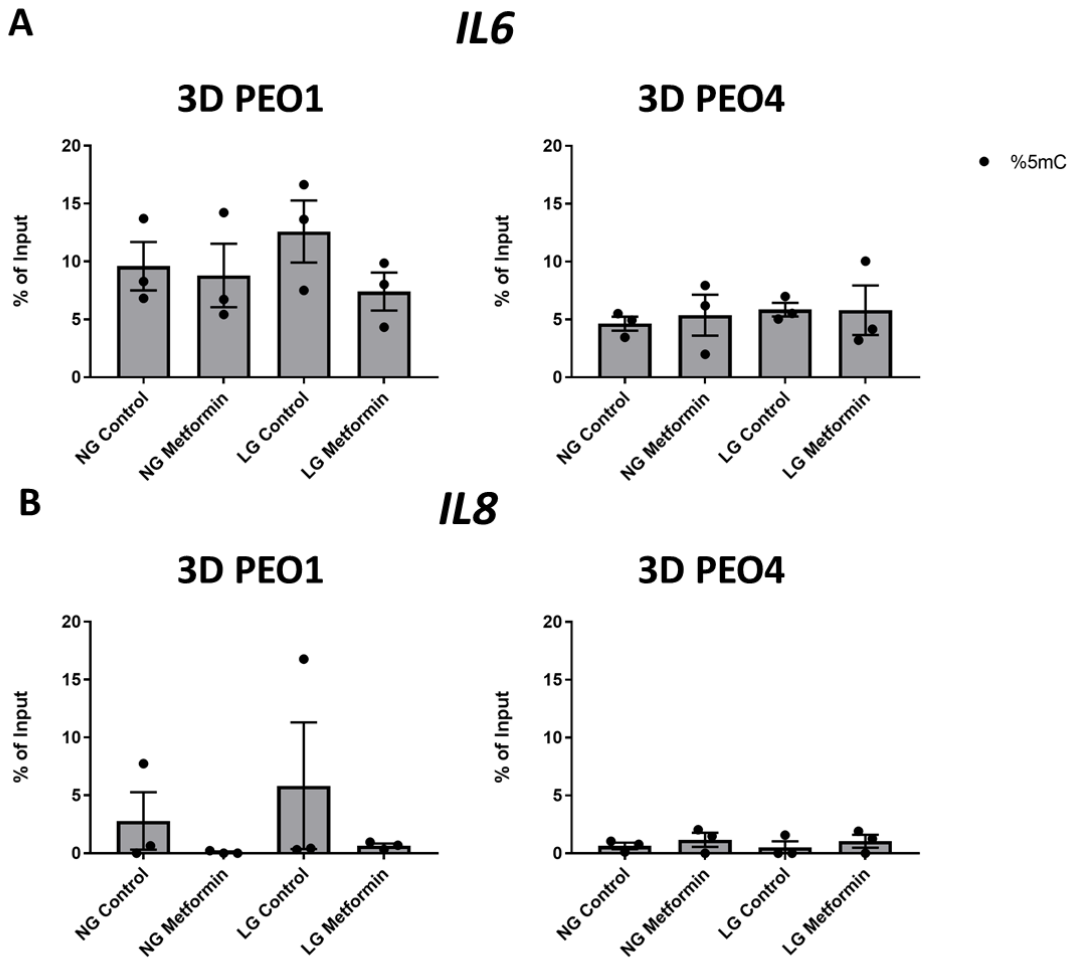

Figure 47. MeDIP-PCR was performed using primers targeting the CpG island on the *IL6* and *IL8* promoter on DNA extracted from 3D PEO1 and PEO4 cultures.
3D PEO1 and PEO4 cells were treated with 0.625 mM metformin or ddH_2O (control) in normal glucose (10 mM) and glutamine (2 mM) media (NG) or low glucose (1 mM) and glutamine (2 mM) media (LG). Statistical analysis by Two-way ANOVA: $p > 0.05$ (n.s.). (n = 3 independent cell passages, error bars represent ± S.E.M).

5.5. Discussion

DNA methylation is dynamic, it is unknown what magnitude of methylation changes play in cancer and how much change is required to facilitate cancer initiation or development (Joyce, et al., 2015). Epigenetic modifications are involved the regulation of cytokines in the inflammatory response during cancer development (Tekpli, et al., 2013). Cytokines themselves can also induce methylation changes in CpGs in the promoters of tumour suppressor genes as well as promoting tumorigenesis through the hypomethylation of oncogenic genes (Gasche, et al., 2011). We aimed to investigate if the AMPK/TET2 axis was responsible in the regulation of the inflammatory response under low glucose treatment with metformin by assaying the levels of DNA methylation of the CpGs at *IL6* and *IL8* promoter under experimental conditions.

Many improvements could be made to this study (discussed below) as due to COVID-19 and time constraints, consumables and reagents for additional experiments were not received in time. Metformin has been implicated in DNA methylation as the activation of AMPK by metformin could modulate DNA methylation machinery (Cuyàs, et al., 2018; Yan, et al., 2020). Glucose has also been involved in causing epigenetic changes including increasing DNA methylation levels (Yu, et al., 2012; Hall, et al., 2018). To better study the demethylating activity of TET2, cells can be treated with 5'-aza-2'-deoxycytidine or 5-azacytidine which are inhibitors of DNA methylation before experimental treatments without being obscured by active DNA methylation (Christman, 2002). The results of the IL-6 and IL-8 ELISA (3.4.1) show that there was a significant cytokine production already at the 48 h time point in 2D PEO1 cells grown in low glucose media with metformin. It is possible that the epigenetic events occurring as a result of experimental treatment may precede this time point. Therefore, the methylation levels of the CpGs on the IL6 and IL8 promoter should be investigated at a shorter time point i.e., 24 h or sooner in order to detect the differences in inflammatory factor gene promoter methylation. The intermediate state of DNA demethylation, 5hmC is a highly abundant epigenetic modification (Tan, et al., 2013). Genome-wide mapping of 5mC and 5hmC using MeDIP-seq and hydroxymethylated DNA immunoprecipitation (hMeDIP) seq respectively can aid in the elucidation of the CpGs involved in the expression of cytokines in the inflammatory response under experiment conditions (Tan, et al., 2013).Our results showed that there were

no significant changes in the level of methylation *IL6* promoter in 2D or 3D PEO1 and PEO4 cells across the different experimental conditions which suggests additional epigenetic control is involved in the expression of IL-6. Similar results were seen in chronic periodontitis patients who showed high expression of *IL6* however no difference in methylation patterns were seen compared to the control group suggesting that the high expression of *IL6* was not associated with methylation status. Samples from both groups showed partial methylation (Stefani, et al., 2013). IL-6 has been reported to increase global 5mC content. The overexpression *IL-6* altered the methylation status of genes associated with tumour progression as well as affecting the expression of *DNMT1* which is involved in DNA methylation (Wehbe, et al., 2006). It is possible that the IL-6 produced by the 2D PEO1 cells in low glucose media with metformin may have influenced the methylation status of the promoter. IL-6 has been reported to increase *DNMT* expression and activity resulting in abnormal levels of methylation (Hodge, et al., 2001; Braconi, et al., 2010; Foran, et al., 2010). Methylated sites could still allow protein complexes to form in order to enhance chromatin remodelling in the vicinity of the *IL6* gene and upregulate its expression (De Larco, et al., 2003).

The *IL8* promoter is not a typical CpG island promoter as it lacks repeat sequences of CpG dinucleotides i.e., CpG islands (Oliveira, et al., 2009; Andia, et al., 2010). Venza *et al.,* (2012) identified six CpG sites in the *IL8* promoter and found that the methylation status of CpG site 5 was involved in *IL8* expression. Despite lacking the numbers to constitute typical CpG islands, they are still a potential target for methylation and epigenetic regulation of *IL8* promoter activity (Andia, et al., 2010). Therefore, we also studied the effect of metformin and glucose concentration on the methylation status of this site. Our results showed highly variable levels of methylation in 2D and 3D PEO1 cultures whereas 2D and 3D PEO4 cultures show low levels of methylation. Tekpli *et al.,* (2013) found similar results in lung cancer cells, that the CpGs at the *IL8* promoter were also unmethylated. Our results showed a reduction in the methylation levels on the 2D PEO1 *IL8* promoter in the low glucose metformin condition compared to the low glucose control which suggests a role of DNA methylation in IL-8 expression. Due to the variation and the low levels of methylation, it is difficult to determine if metformin and glucose has a true effect on DNA methylation on the *IL8* promoter in 2D and 3D PEO1 cultures. It is possible that the hypomethylation of the *IL8* promoter in 2D and 3D PEO4 cultures could result

in the silencing of *IL8* expression. Differing from the epigenetic paradigm where the methylation of promoter CpG island silences gene expression, metastatic breast cancer cell lines showed full methylation of two CpG sites in the *IL8* promoter despite producing high levels of IL-8. The low metastatic cell lines were unmethylated and *IL8* was silenced (De Larco, et al., 2003). It is also possible that methylation marks may be missed due to the CpG sparseness of the *IL8* promoter (Oliveira, et al., 2009; Andia, et al., 2010). The accuracy of MeDIP measurements decrease in regions that have a lower CpG density (Borgel, et al., 2012). MeDIP is also unable to identify individual CpG level methylation (Beck, et al., 2021). Further investigation is required to determine if the low 5mC binding is an indication of an unmethylated state or if it is the absence of sufficient CpG targets in the CpG-poor *IL8* promoter (Andia, et al., 2010; Borgel, et al., 2012).

5.6. Conclusion

We found that metformin and glucose did not affect the methylation status of the CpG island on the *IL6* promoter. The CpG site on the *IL8* promoter was unmethylated and did not appear to be significantly influenced by the experimental conditions. Our data suggests that the high cytokine expression was not associated with the methylation status and that other mechanisms are involved in the regulation of gene transcription. DNA methylation and the modification of histones function both independently and in conjunction to regulate cellular processes to determine the outcomes of biological events. Chromatin condensation and histone modifications should be investigated to elucidate the role they play in the regulation of cytokine expression in experimental media.

Chapter 6

The effect of oncometabolites on cell proliferation and metabolism in ovarian cancer cells

6.1. Introduction

Metabolic reprogramming allows tumours to meet the bioenergetic demands including uncontrolled proliferation as well as other hallmarks of cancer, playing an important role in the malignant transformation of cells (Yong, et al., 2020). To meet the anabolic demands, cancer cells undergo aerobic glycolysis also known as the "Warburg effect", which involves the maintenance of glycolysis at a high rate in the presence of oxygen. Cancer cells utilise glucose and glutamine as their main source of carbon for ATP production (Masamha & LaFontaine, 2018) (Figure 48). This process is thought to be inefficient as OXPHOS produces 34 more ATP molecules from the same molecule of glucose. However, cancer cells often show an increased glucose metabolism which allows maximum growth through faster ATP production and the redistribution of carbons towards the synthesis of nucleotides, proteins, and fatty acids (Nowicki & Gottlieb, 2015). Cancer cells that undergo the Warburg effect can also show dependency on glutamine where they are unable to proliferate without it, known as glutamine addiction (Masamha & LaFontaine, 2018). Proliferating tumour cells can uptake glutamine for energy generation to replenish the TCA cycle (known as anaplerosis). Glutamine can be converted into other non-essential amino acids, purines, and pyrimidines as well as fatty acids for cellular replication. Dependency on glutamine was found to be correlated with cancer invasiveness as low invasive cells are glutamine independent whereas highly invasive cells are glutamine dependent (Yang, et al., 2014).

Rapid proliferating tumour cells will experience intermittent hypoxia as a result of poor vascularisation which can cause cancer cells to become more aggressive, invasive with better metastatic capabilities (Muz, et al., 2015). Free floating spheroids of cancer cells with a diameter > 400 μm show hypoxic and necrotic areas due to oxygen and nutrient gradients resulting in the activation of signalling pathways to maintain cell viability (Riffle & Hegde, 2017). Hypoxia inducible factor 1 (HIF-1) is a regulator of oxygen homeostasis, consisting of two subunits: HIF-1α, which is the subunit that determines HIF-1 activity and HIF-1β. HIF-1α is highly expressed in the later stages of OC and may play an important role in cell proliferation, invasion, angiogenesis, and metastasis (Jin, et al., 2014). Low oxygen partial pressure leads to the activation of hypoxia dependent signalling pathway through the stabilisation of HIF-1α (Semenza, et al., 1991). Stabilisation of HIF-1α results in its translocation into the nucleus

where it can heterodimerise with HIF-1β to form the active HIF-1 transcription factor where it leads to the expression of genes involved in mechanisms such as glucose utilisation, metabolism, and angiogenesis (King, et al., 2006). Although HIF-1α was identified as a key factor in the response to hypoxia, some oncometabolites can induce a state of pseudohypoxia where HIF-1α signalling is activated despite normal oxygen levels resulting in hypoxia-like metabolic changes (Intlekofer, et al., 2015; Laukka, et al., 2016; Dando, et al., 2019; Hayashi, et al., 2019).

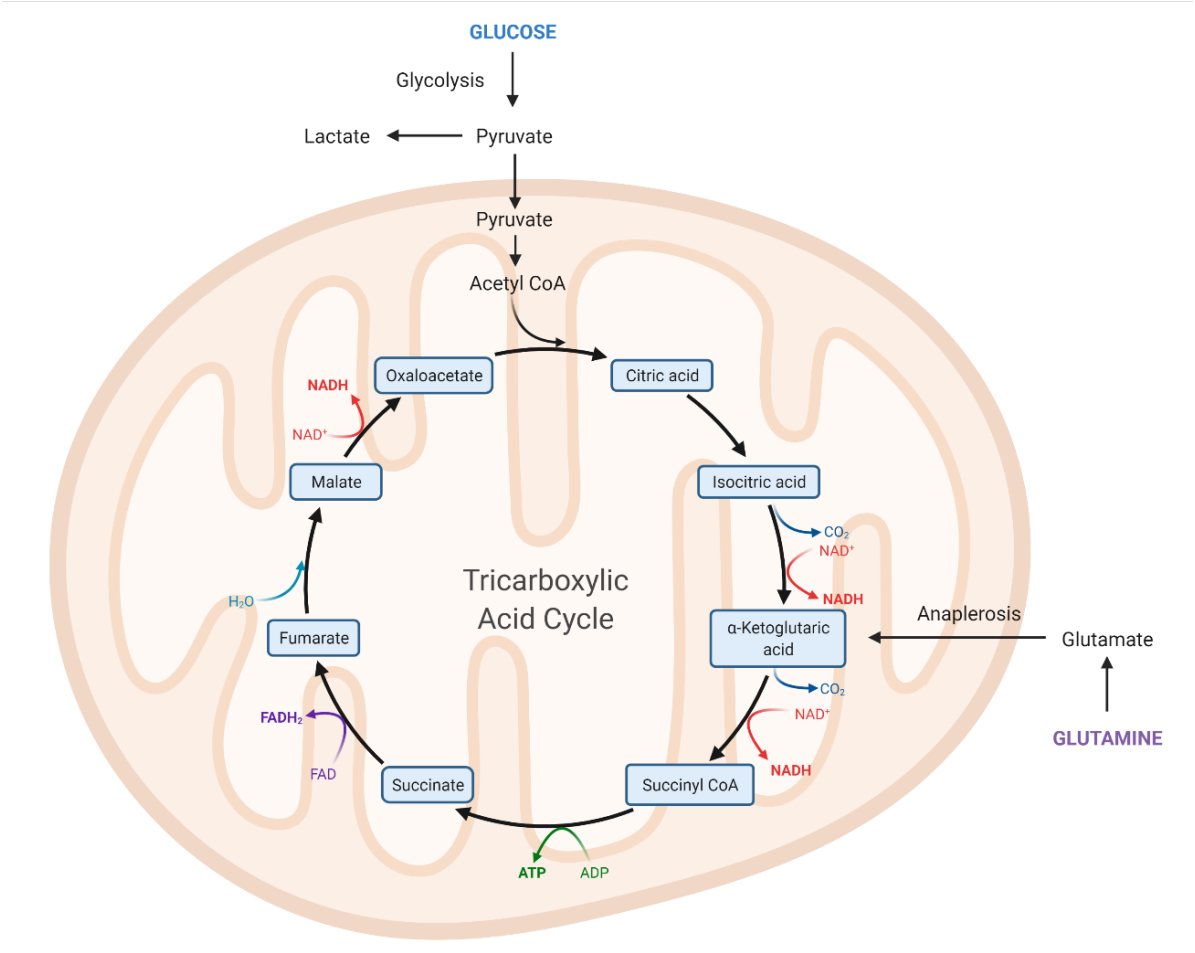

Figure 48. Glucose and glutamine metabolism in cancer cells.
Adapted from "Krebs Cycle" by BioRender.com (2021). Retrieved from https://app.biorender.com/biorender-templates

Oncometabolites are defined as metabolites whose accumulation results in pro-oncogenic capabilities that lead to tumorigenesis (Yong, et al., 2020). Oncometabolites can support tumour repopulations by acting as signalling molecules released by dying cells as well as cells in the tumour microenvironment leading to increased proliferation of therapy resistant cells (Dando, et al., 2019). Oncometabolites can promote tumorigenesis through epigenetic alterations. Well studied metabolites, succinate and 2-HG are structurally similar to α-KG where they share the same acetate with two oxygen atoms linked to C5 used by α-KG to interact with conserved residues in dioxygenases (Xiao, et al., 2012). High levels of intracellular succinate and 2-HG can act as an α-KG competitor to inhibit the TET family of enzymes and their catalysation of DNA demethylation via the hydroxylation of 5mC (Xiao, et al., 2012) (Figure 49). Consequently, this results in genome-wide hypermethylation and alteration of the epigenetic state towards an aggressive tumour phenotype (Terunuma, et al., 2014; Yong, et al., 2020). Studying the effects of oncometabolites on cancer cells can highlight the factors that contribute to the promotion of cancer cell proliferation.

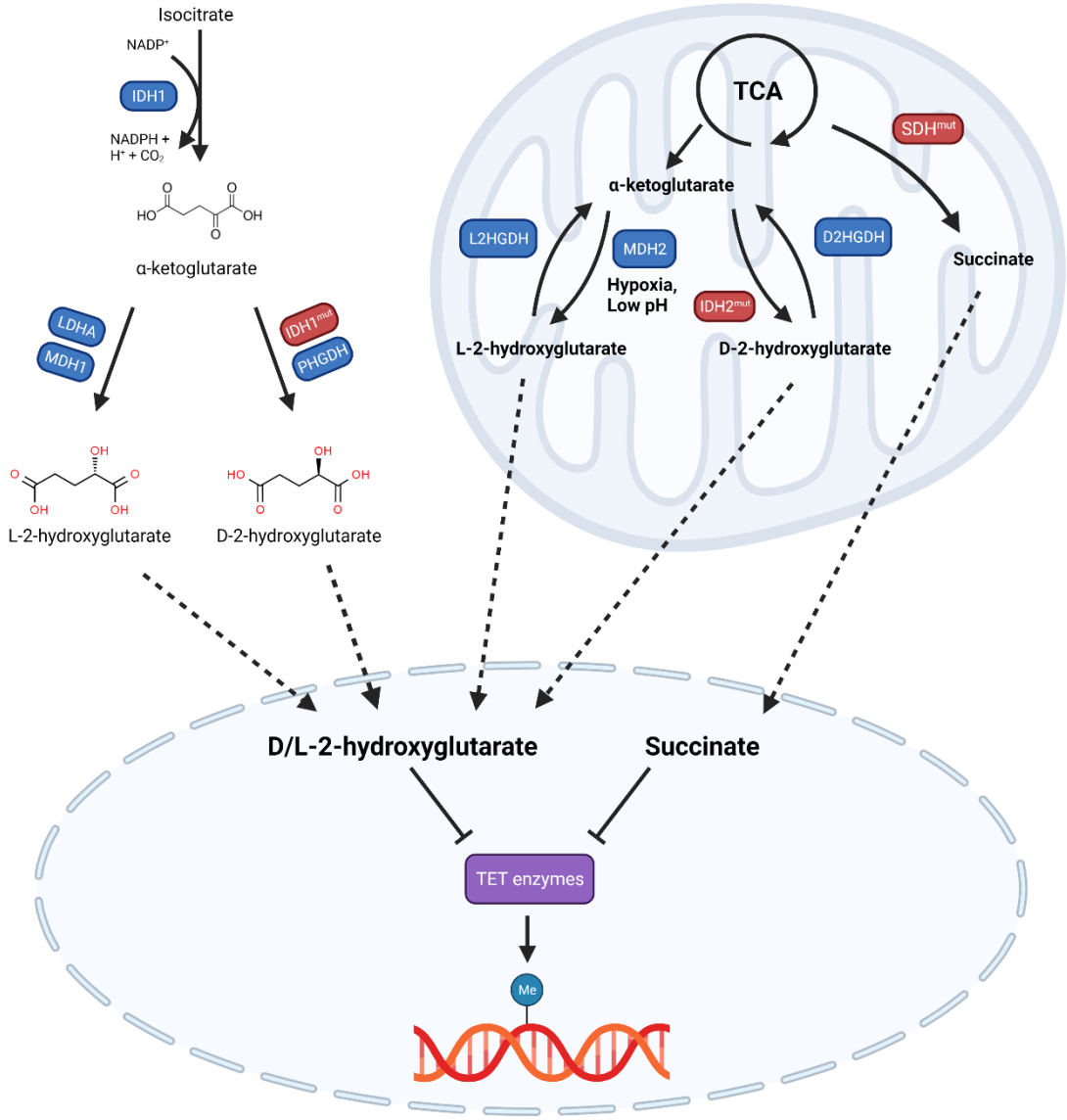

Figure 49. Source of oncometabolites: L-hydroxyglutarate, D-hydroxyglutarate and succinate production and effect on TET enzymes.
Figure adapted from (Samanta & Semenza, 2016). Created with Biorender.com

Succinate is an intermediate metabolite in the TCA cycle that is converted into fumarate, catalysed by the enzyme succinate dehydrogenase (SDH) (Zhao, et al., 2017). SDH is a highly conserved heterotetrametric protein consisting of six subunits encoded by *SDHA, SDHB, SDHC, SDHD, SDHAF1* and *SDHAF2* (Yang, et al., 2013; Tretter, et al., 2016). SDHA and SDHB are catalytic subunits whereas SDHC and SDHD are ubiquinone-binding and membrane-anchorage

subunits (Yang, et al., 2013). *SDHAF1* and *SDHAF2* encodes associated accessory factor (Tretter, et al., 2016). SDH also plays a role in metabolism including electron delivery in substrate level phosphorylation and by functioning as complex II in the electron transport chain (ETC) (Zhao, et al., 2017). To catalyse reactions, SDH requires participation of all subunits, any deleterious mutations in any subunit will result in the destabilisation of the entire enzyme complex and lead to a decrease in SDH activity. B and D subunits are frequently mutated whereas mutations on the A and C subunits occur less frequently (Pozza, et al., 2020). Inactivation of SDH results in the accumulation of its substrate, succinate (Yang & Pollard, 2013). Mutations in SDHB are found at higher frequencies in malignant and metastatic tumours (Tseng, et al., 2018). Knocking down *SDHB* resulted in increased cell proliferation and migration as well as increased acidity, decreased OXPHOS and increased glycolytic activity. The low pH as a result of extracellular acidification from increased glycolysis creates an optimal environment for the activation of proteases which induce ECM degradation and facilitate tumour metastasis (Tseng, et al., 2018). Silencing of *SDHB* facilitated OC cell proliferation, invasion and migration as well as prevented OC cell apoptosis. *SDHB* mRNA and protein levels were downregulated in human ovarian carcinomas compared to normal ovarian epithelium tissues (Chen, et al., 2014). Decreased SDH activity through altered *SDHB* expression was found in OC (Aspuria, et al., 2014). Succinate has been associated with contributing to the complications of certain metabolic diseases by promoting inflammation, oncogenesis, and tumour progression (Zhao, et al., 2017). Malignant prostate cells show an increase in succinate utilisation to drive energy production (Schöpf, et al., 2020). Additionally, succinate is able to stabilise HIF-1α resulting in HIF-1 activity, producing a state of pseudohypoxia (Dando, et al., 2019).

Physiologically, 2-HG exists in two forms: D- and L-2HG, levels of which are usually maintained via the conversion into α-KG by hydroxyglutarate dehydrogenase enzymes, L2HGDH and D2HGDH (Yong, et al., 2020). 2-HG was found in abundance in both primary and metastatic EOC (Fong, et al., 2011). High 2-HG levels have been associated with decreased 5hmC levels due to TET inhibitions, leading to genome-wide hypermethylation (Terunuma, et al., 2014). D-2HG has been implicated in the promotion of stem cell gene expression, the activation of aberrant growth signalling, hypermethylation, blocking differentiation, contributing to cancer initiation and maintenance as well as enhancing cell proliferation, invasion, and migration

(Sullivan, et al., 2016; Colvin , et al., 2016; Seok, et al., 2019). A lack of differentiation can enable cancer cells to retain the ability to proliferate and propagate mutant clones, resulting in tumorigenesis (Yong, et al., 2020). L-2HG appears to be the major form of 2-HG accumulation in response to hypoxia and has been shown to function as a competitive inhibitor of prolyl hydroxylases, promoting HIF-1α accumulation and hypoxic adaptation. D-2HG is a substrate of prolyl hydroxylases, promoting hydroxylation and HIF1α degradation, impeding hypoxic adaption (Intlekofer, et al., 2015). Accumulation of cellular L-2HG in response to reductive stress may initiate a negative feedback loop that limits NADH production by inhibition of the ETC and glycolysis. (Oldham, et al., 2015). L-2HG was found to be more potent than the D-2HG enantiomer in the inhibition of TET enzymes (Xu, et al., 2011). Accumulation of L-2HG levels can also inhibit histone demethylases and increase histone methylation (Sullivan, et al., 2016).

Mutations in IDH1/2 results in the accumulation of D-2HG through the acquisition of a neomorphic enzymatic activity catalysation of α-KG to D-2HG coupled with NADPH oxidation (Figuero, et al., 2010). IDH1/2 mutations have been reported in leukaemia (Ward, et al., 2011) and gliomas (Dang, et al., 2009). However, cancers showing accumulation of 2-HG without *IDH* mutations have also been reported (Han, et al., 2011; Colvin , et al., 2016; Mishra, et al., 2018). In breast cancer, Human D-3-phosphoglycerate dehydrogenase (PHGDH) is regulated by MYC and catalyses the NADH-dependent reduction of α-KG to D-2HG (Fan, et al., 2015). PHDGH may be a source of D-2HG in cancers without IDH mutation. PHDGH is highly expressed in HGSOC and is associated with increased cell proliferation (Fong, et al., 2011; Francavilla, et al., 2017). Additionally, ADHFE1 is involved in the catalysis of α-KG to D-2HG as a result of a coupled reaction with 2-hydroxybutyrate metabolism in breast tumours (Terunuma, et al., 2014). OC also show an increased expression of *ADHFE*1 (Ramakrishna, et al., 2010). Off target, promiscuous activity of LDHA and MDH enzymes on glutamine-derived α-KG can result in the accumulation of L-2HG in mammalian cells (Yong, et al., 2020).

6.2. Aims and objectives

Oncometabolites succinate and D-/L-2HG have been reported to increase cell proliferation through the inhibition of TET family of enzymes, resulting in alterations in the epigenetic

landscape. In HGSOC, succinate and D-/L-2HG levels were reported to be higher than normal cells. We wanted to see whether OC with different metabolic dependencies showed different responses to the oncometabolite: we used SKOV3, which are glutamine-dependent (Masamha & LaFontaine, 2018) and OVCAR3, which are glutamine-independent (Yang, et al., 2014). Additionally, we also wanted to explore whether OC cells with varying resistance to chemotherapy responded differently to oncometabolites , so we used the chemosensitive PEO1 and chemoresistant PEO4 cell lines. These cell lines were derived from cells which were cultured from the same patient at different stages of EOC progression (Langdon, et al., 1988). Therefore, our aims of this study are to investigate the effect oncometabolites and the tumour environment has on 2D and 3D OC cell viability and proliferation. Our objectives were as follows:

1. Assay cell viability and proliferation of 2D OC cell treated with varying concentrations of succinate and D-/L-2HG in cell culture conditions using MTT assay and CyQuant assay respectively at 24 h, 48 h and 72 h.
2. Perform CyQuant assay on OC cells that showed a response to oncometabolite at different seeding densities and restricted media conditions.
3. Investigate the effect of oncometabolite on the formation and size of OC spheroids

6.3. Methods and Materials

6.3.1. Treatments

Dimethyl succinate (Cat#W239607), Diethyl fumarate (Cat#D95654-5G), DMOG (Cat#400091-50MG) and L-2HG (Cat#90790) were purchased from Merck. D-2HG (Cat#S7873-SEL) was purchased from SelleckChem via Stratech. Dimethyl succinate and diethyl fumarate were made up as a stock solution of 100 mM in RNase free water and both D-2HG and L-2HG were kept in a stock solution of 500 mM in RNase free water. DMOG was made up as a stock solution at a concentration of 500 mM in DMSO (Merck; Cat#D5879-1L-M). Experimental media conditions can be found in **Table *1***. For DMOG, succinate and fumarate, concentrations between 0 - 1 mM were used and for D-2HG and L-2HG, concentrations between 0 – 10 mM were used.

6.3.1.1. 2D cell line

Cells were seeded at cell densities dependent on the experiment in a 96-well plate. After 24 h, cell culture media was removed and replaced with media with varying concentrations of treatment. Cells were treated for up to 72 h.

6.3.1.2. 3D cell line

Oncometabolite treatment was added to the cell suspension before preparation of the droplets. Spheroids were monitored and cultured for up to 8 days.

6.3.1.2.1. Spheroid staining

To stain the spheroid membranes for fluorescent microscopy, cells were collected by centrifugation at 500 x g for 10 min and resuspended at a density of 1 x 10^6 cells/mL in serum free cell culture media. To the cell suspension, 5 µL of 1 mM Vybrant™ DiO Cell-Labeling Solution (Invitrogen; Cat#V22886) was added. Cell suspension was mixed by pipetting and incubated in the dark for 20 min at 37°C. The labelled suspension was centrifuged at 500 x g for 5 min. The supernatant was removed and resuspended in serum free media to wash. The wash step was repeated two more times. Spheroids were prepared in cell culture media with treatment according to the hanging drop method mentioned in 2.3.1. To stain the nuclei, spheroids were collected using a bulb pipette into black walled, clear bottom 96-well plates (Corning; Cat#3340) containing 100 µL of 20 µM Hoechst 33342. Spheroids were incubated in the staining solution in the dark for 30 min at 37°C. The stained spheroids were imaged using the Olympus Fluorescent Microscope (IX51).

6.3.2. MTT (3-(4,5-Dimethyl-2-thiazolyl)-2,5-diphenyl-2H-tetrazolium bromide) Assay

A stock solution of MTT (Merck; Cat#M2128) at 5 mg/mL in PBS was diluted to 0.5 mg/mL with cell culture medium. The MTT/media solution was added at 50 µL to each well and incubated at cell culture conditions for 2 h. The MTT/media solution was then removed, and the purple formazan crystals were dissolved in 100 µL of DMSO and incubated at room temperature for 15 min. Samples were analysed on a microplate reader at 570 nm.

6.3.3. CyQuant Assay

After treatment, the culture media was removed from the wells of the 96-well plate and washed with PBS before being frozen at -70^{o}C until ready to run the assay. The plates were thawed at room temperature and the DNA content was measured using the CyQuant cell proliferation assay kit (Invitrogen; Cat#C7026) following the manufacturer's instruction. CyQuant GR dye/cell lysis buffer was added at a volume of 100 µL to each well and incubated at room temperature for 5 min in the dark. Samples were mixed and transferred to a black 96-well half-area plate (Corning Costar, Corning, NY, USA). A standard curve with concentrations ranging from 10 ng/mL to 1 µg/mL was generated using λDNA which was provided with the kit. The fluorescence of the samples was measured using a microplate reader at 485 nm excitation and 530 nm emission.

6.4. Results

6.4.1. Effect of oncometabolites on cell proliferation and viability of 2D OC cells in normal cell culture conditions

In order to determine the effect of D-2HG, L-2HG and succinate on the viability of OC cells, MTT assays were performed after 24 h of treatment. Our results show there was no significant changes in OC cells that were treated with the oncometabolites when compared to the vehicle control (Figure 50). OVCAR3 cells treated with succinate appear to show an increase in cell viability at a concentration of 0.0625 mM but were unaffected by 2-HG. SKOV3 cells showed a non-significant dose-dependent decrease in cell viability upon the addition of 2-HG whereas succinate did not appear to show a clear effect. In PEO1 cells, the different concentrations of D-2HG and succinate showed a similar trend. The addition of L-2HG to PEO4 cells showed a non-significant increase in cell viability at 5 mM as well as a dose dependent increase upon the addition of succinate which plateaus after 0.125 mM.

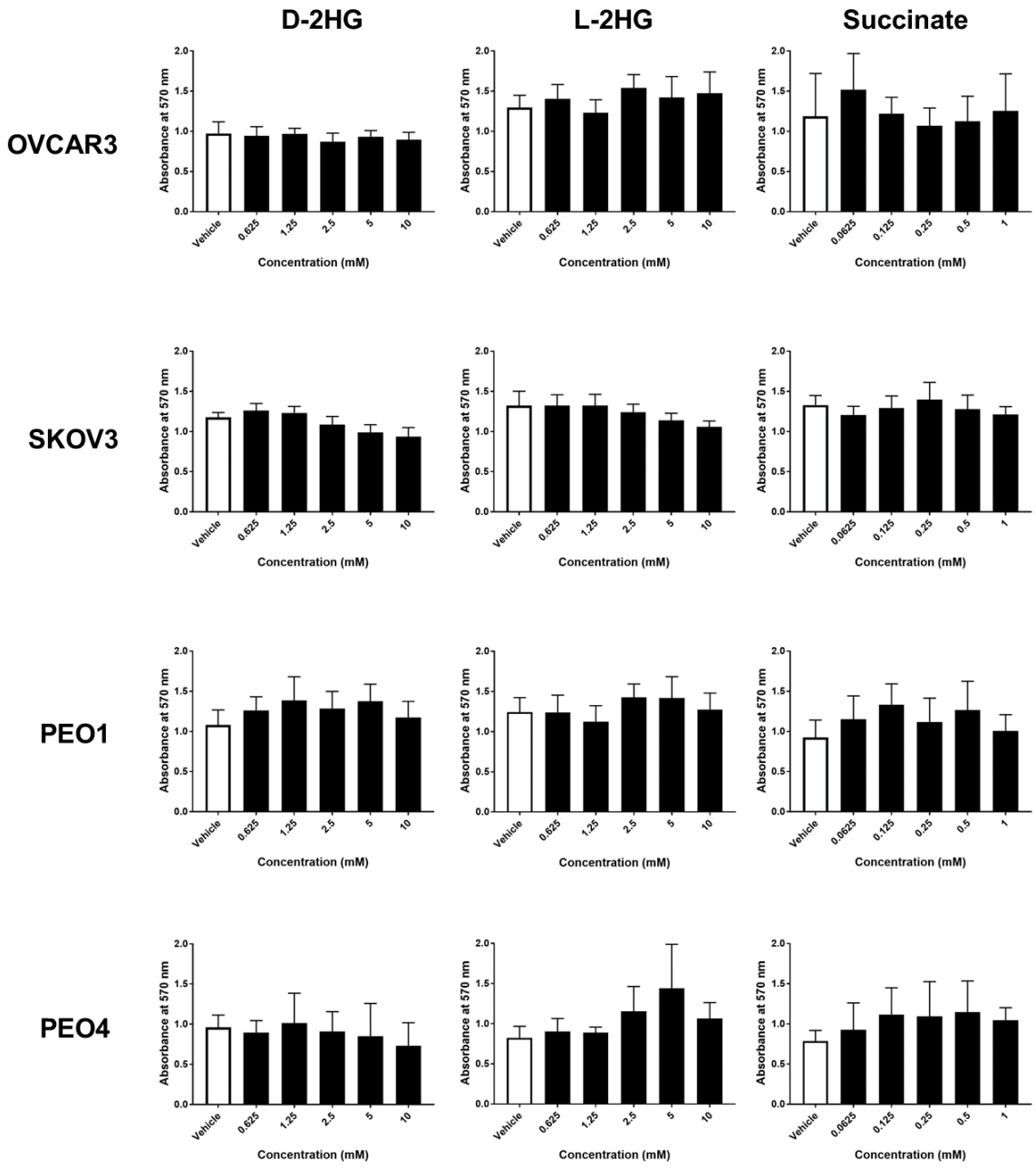

Figure 50. MTT cell viability assay in OVCAR3, SKOV3, PEO1 and PEO4 cells treated with D-2HG or L-2HG or succinate for 24 h.

Cells were seeded at 1 x 10^5cells/mL into wells of a 96-well plate. Cells were treated with 10, 5, 2.5, 1.25, 0.625 mM D/L-2HG or 1, 0.5, 0.25, 0.125, 0.0625 mM succinate. Error bars represent ± S.E.M (One-way ANOVA $p > 0.05$ (n.s.); n= 4 - 5 biological replicates).

Another well studied oncometabolite, fumarate, is produced as a result of mutations in the genes encoding fumarate hydratase (*FH*) leading to an accumulation of fumarate (Shanmugasundaram, et al., 2014). Fumarate is also structurally similar to α-KG and reported to inhibit the TET family of enzymes (Laukka, et al., 2016). We assayed the effect of fumarate on OC cell viability and found that fumarate appeared to reduce viability in all cell lines (Figure 51). Fumarate appeared to reduce OVCAR3 cell viability at concentrations over 0.125 mM, but this effect was not significant. A significant reduction in SKOV3 cell viability was observed when treated with fumarate at concentrations of 0.25 mM and over (0.25 mM; $p < 0.05$, 0.5 mM; $p < 0.001$, 1 mM; $p < 0.0001$). The addition of fumarate reduced PEO1 cell viability, showing a significant reduction at 1 mM ($p < 0.05$). PEO4 cells appear be sensitive to fumarate treatment, showing a significant reduction in cell viability even at the lowest concentration, 0.0625 mM (0.125 mM – 1 mM - $p < 0.0001$). We did not undergo further experiments with fumarate as *FH* mutations did not appear to be common in OC patients (Ylisaukko-oja, et al., 2006; Zhang, et al., 2020).

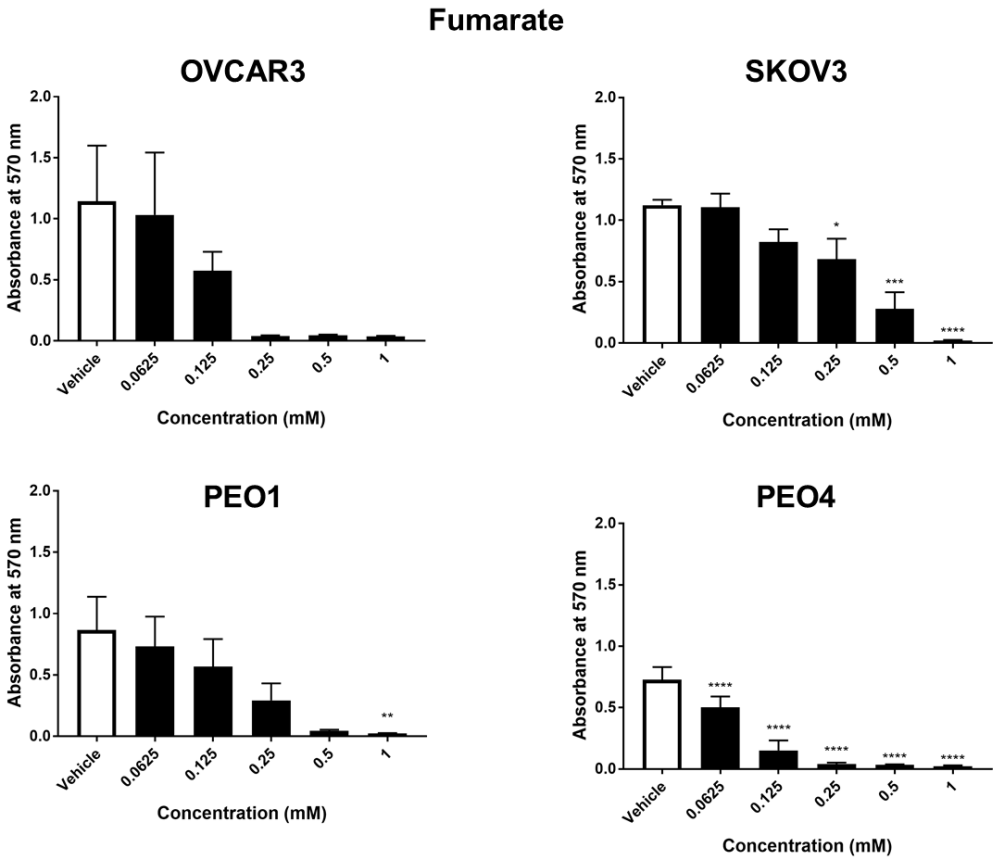

Figure 51. MTT cell viability assay in OVCAR3, SKOV3, PEO1 and PEO4 cells treated with fumarate for 24 h.

Cells were seeded at 1 x 10^5 cells/mL into wells of a 96-well plate. Cells were treated with 1, 0.5, 0.25, 0.125, 0.0625 mM fumarate. Error bars represent ± S.E.M (One-way ANOVA $p < 0.05$ (*), $p < 0.01$ (**), $p < 0.001$ (***), $p < 0.0001$ (****); n = 4 independent cell passages).

Next, we wanted to investigate if oncometabolites had an effect on cell proliferation. Tetrazolium salt MTT is reduced to purple formazan crystals in metabolically active cells by mitochondrial dehydrogenases- mainly SDH (Rai, et al., 2018). As mentioned above, SDH activity is reduced in OC as a result of reduced *SDHB* expression (Aspuria, et al., 2014).. Therefore, the CyQuant assay, which quantifies cell proliferation indirectly though measuring cellular DNA content, without relying on metabolic activity, was used to validate the MTT results. Oncometabolites did not appear to have a significant effect on OC cell proliferation. However, a non-significant increase in cell proliferation can be seen in SKOV3 and PEO1 cells treated with D-2HG at 72 h (Figure 52) and PEO1 cells treated with L-2HG at 72 hr (Figure 53). Succinate also appeared to cause a non-significant increase in cell proliferation at 72 h in

SKOV3 and PEO1 cells (Figure 54). There were no major differences in the trend seen between MTT and CyQuant.

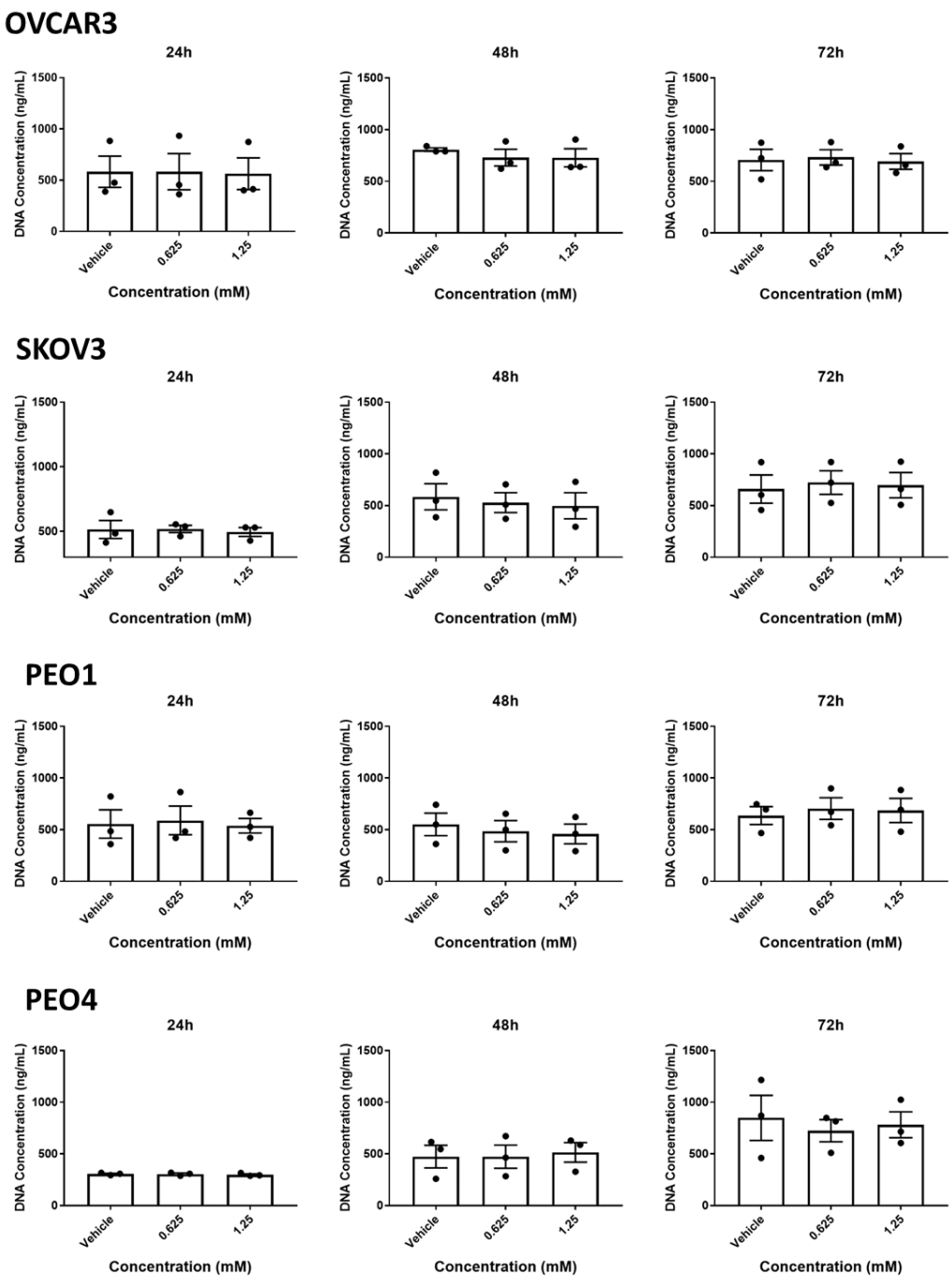

Figure 52. CyQuant cell proliferation assay in OVCAR3, SKOV3, PEO1 and PEO4 cells treated with D 2 hydroxyglutarate (2-HG) for 24, 48 or 72 h.

Cells were seeded at 1 x 10^5 cells/mL into wells of a 96-well plate. Cells were treated with 1.25 mM and 0.625 mM D-2HG.. Error bars represent ± S.E.M (One-way ANOVA $p > 0.05$ (n.s.); n = 3 independent cell passages).

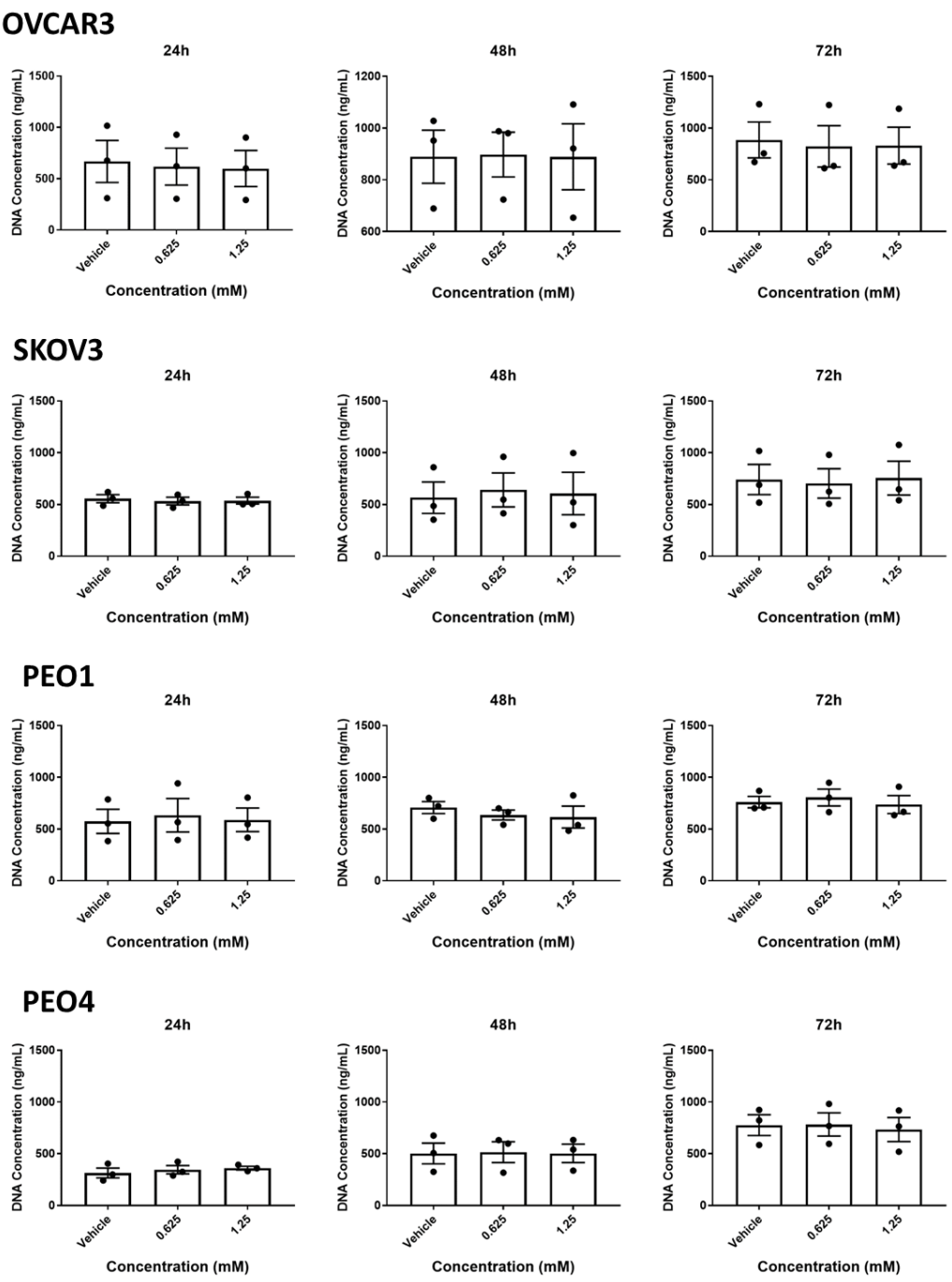

Figure 53. CyQuant cell proliferation assay in OVCAR3, SKOV3, PEO1 and PEO4 cells treated with L-2 hydroxyglutarate (2-HG) for 24, 48 or 72 h.

Cells were seeded at 1 x 10^5 cells/mL into wells of a 96-well plate. Cells were treated with 1.25 mM and 0.625 mM L-2HG. Error bars represent ± S.E.M (One-way ANOVA $p > 0.05$ (n.s.); n = 3 independent cell passages).

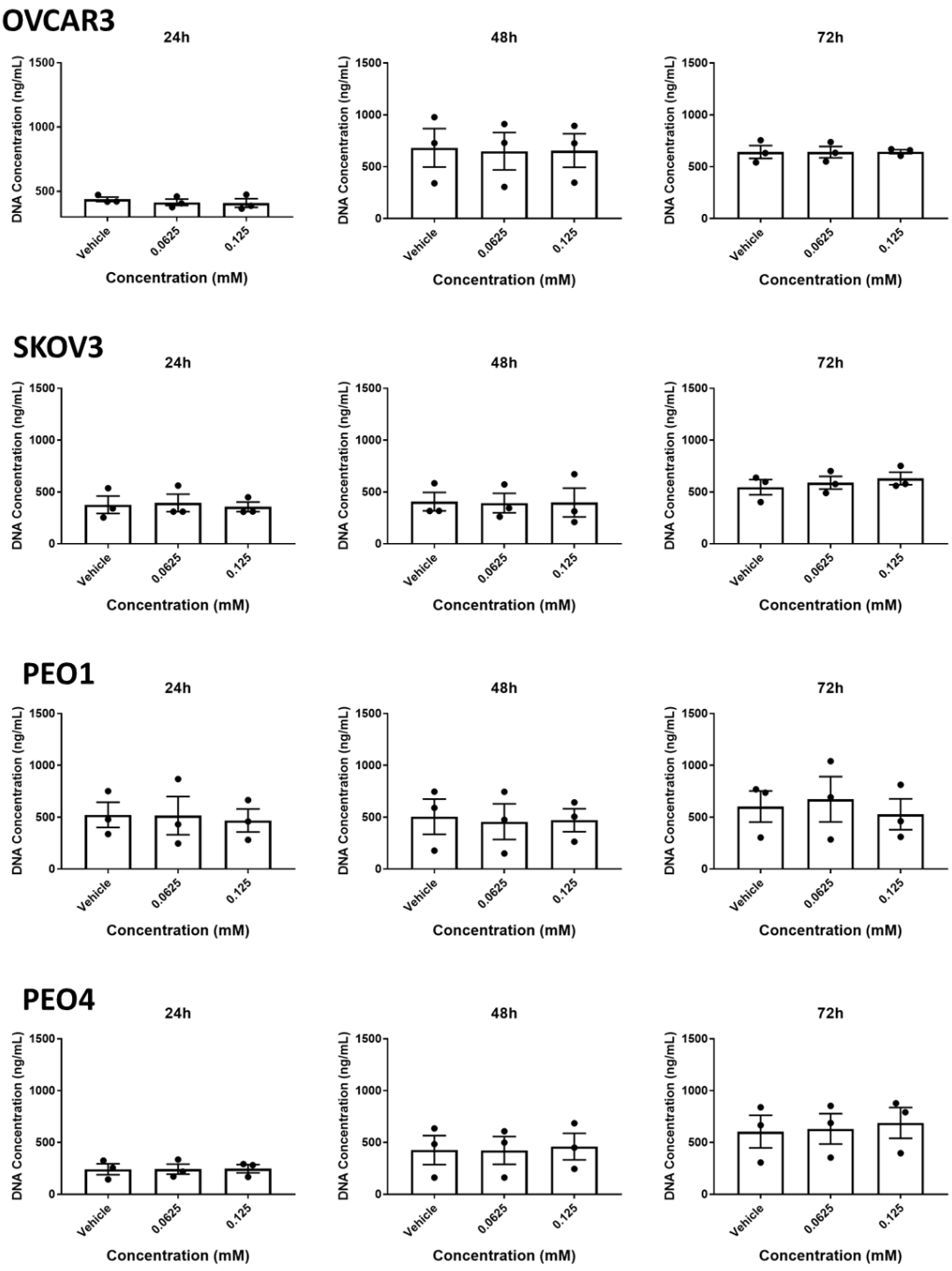

Figure 54. CyQuant cell proliferation assay in OVCAR3, SKOV3, PEO1 and PEO4 cells treated with succinate for 24, 48 or 72 h.

Cells were seeded at 1 x 10^5 cells/mL into wells of a 96-well plate. Cells were treated with 0.125 mM and 0.0625 mM succinate. Error bars represent ± S.E.M (One-way ANOVA $p > 0.05$ (n.s.); n = 3 independent cell passages).

6.4.2. Effect of succinate treatment in restricted media conditions and cell density on the growth and viability of OC cells.

As succinate appeared to show a more noticeable effect, we investigated whether succinate could facilitate cell proliferation under restricted media conditions. The conditions we used were normal cell culture conditions (10 mM glucose and 2 mM glutamine), restricted glucose conditions (1 mM glucose) with glutamine (1 mM glucose and 2 mM glutamine) and with lactate (1 mM glucose, 2 mM glutamine and 10 mM lactate) to represent physiologically relevant conditions in the malignant EOC ascites such as hypoglycaemia and high levels of lactate (Fong, et al., 2011; Kipps, et al., 2013). Succinate did not appear to cause a significant effect in OC cells in restricted media conditions (Figure 55). At 48 h, succinate caused a non-significant increase in cell proliferation at the restricted glucose condition and the restricted glucose with 2 mM glutamine condition at 72 h in OVCAR3 cells. SKOV3 treated with succinate showed a non-significant increase in cell proliferation at the restricted glucose and 2 mM glutamine condition at 48 h and the restricted glucose condition at 72 h. At 72 h, PEO1 cells treated with succinate at the low glucose condition showed a non-significant decrease in cell growth. PEO4 cells appeared to be unaffected by the addition of succinate in different media conditions.

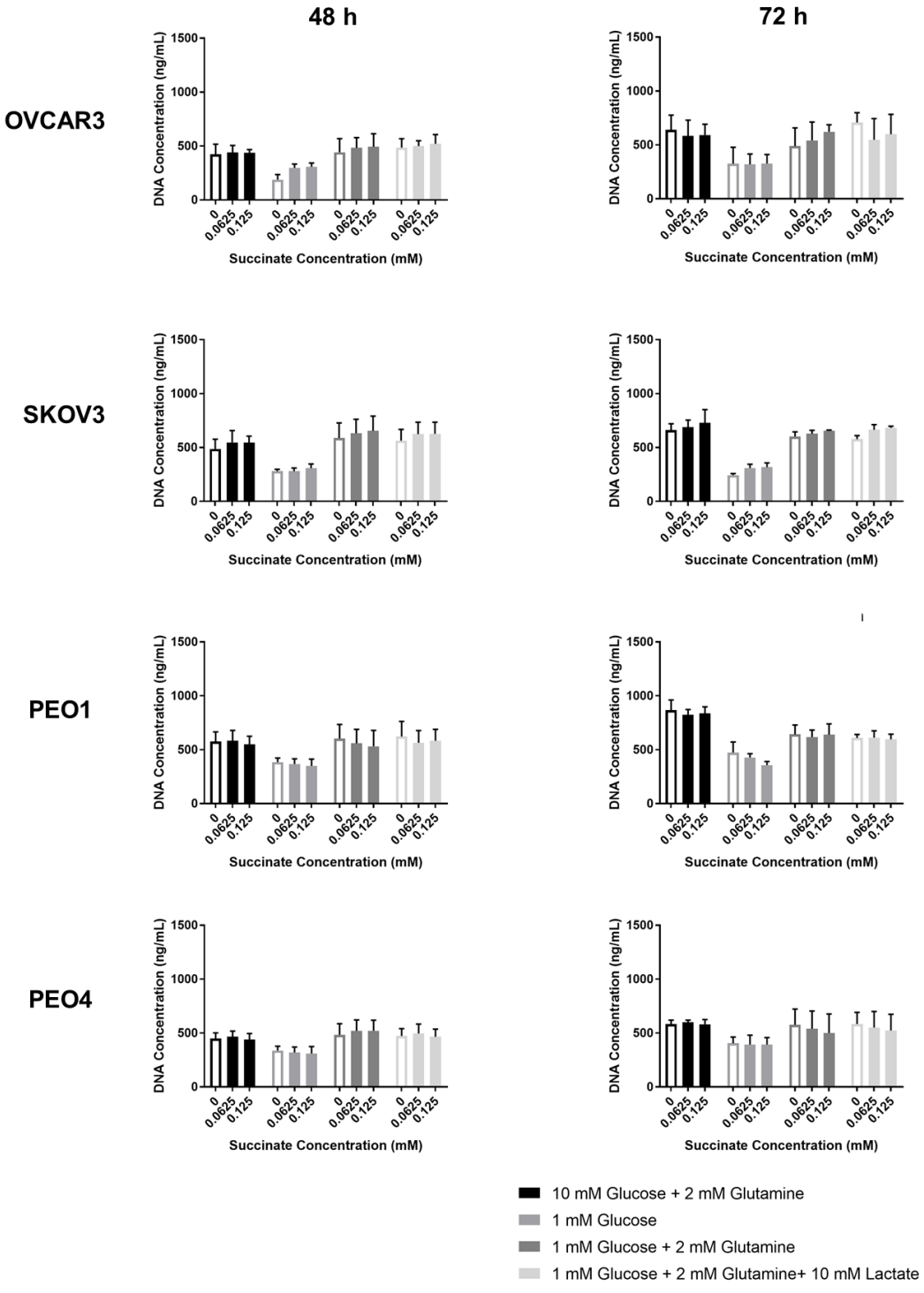

Figure 55. CyQuant cell proliferation assay in OVCAR3, SKOV3, PEO1 and PEO4 cells treated with succinate for 48 or 72 h.

Cells were seeded at 1 x 10^5 cells/mL into wells of a 96-well plate. Cells were treated with 0 (vehicle – ddH_2O) – 0.125 mM succinate. Error bars represent ± S.E.M (One-way ANOVA $p > 0.05$ (n.s.); n = 3 independent cell passages).

Since a treatment of 72 h is prolonged, there is a possibility that the cells reach over confluence and become quiescent which is associated with changes in metabolism including decreased glutamine consumption as well as decreased aspartate and alanine synthesis (Coloff, et al., 2016). Therefore, OC cells were seeded at different densities before treatment with succinate for 72 h (Figure 56). At the highest cell density, succinate appeared to cause an increase in cell viability in OVCAR3 cells when compared to the vehicle. In SKOV3 cells, succinate also caused a non-significant increase in cell viability at 10,000 cells and 2,500 cells. However, a significant increase in cell viability was seen at 0.5 mM and 2 mM at 2,500 cells ($p < 0.05$). The highest dose of succinate (2 mM) caused a non-significant decrease in cell viability at 5,000 and 1,000 cells. The addition of succinate appeared to reduce the cell viability of PEO1 cells in a dose dependent manner at a density of 5,000 cells. Similarly, succinate caused a dose-dependent decrease in cell viability in PEO4 cells at 5,000 cells with the higher doses of succinate (1 mM and 2 mM) causing a significant decrease in cell viability ($p < 0.05$). These results suggest that cell density does have an effect on OC response to succinate.

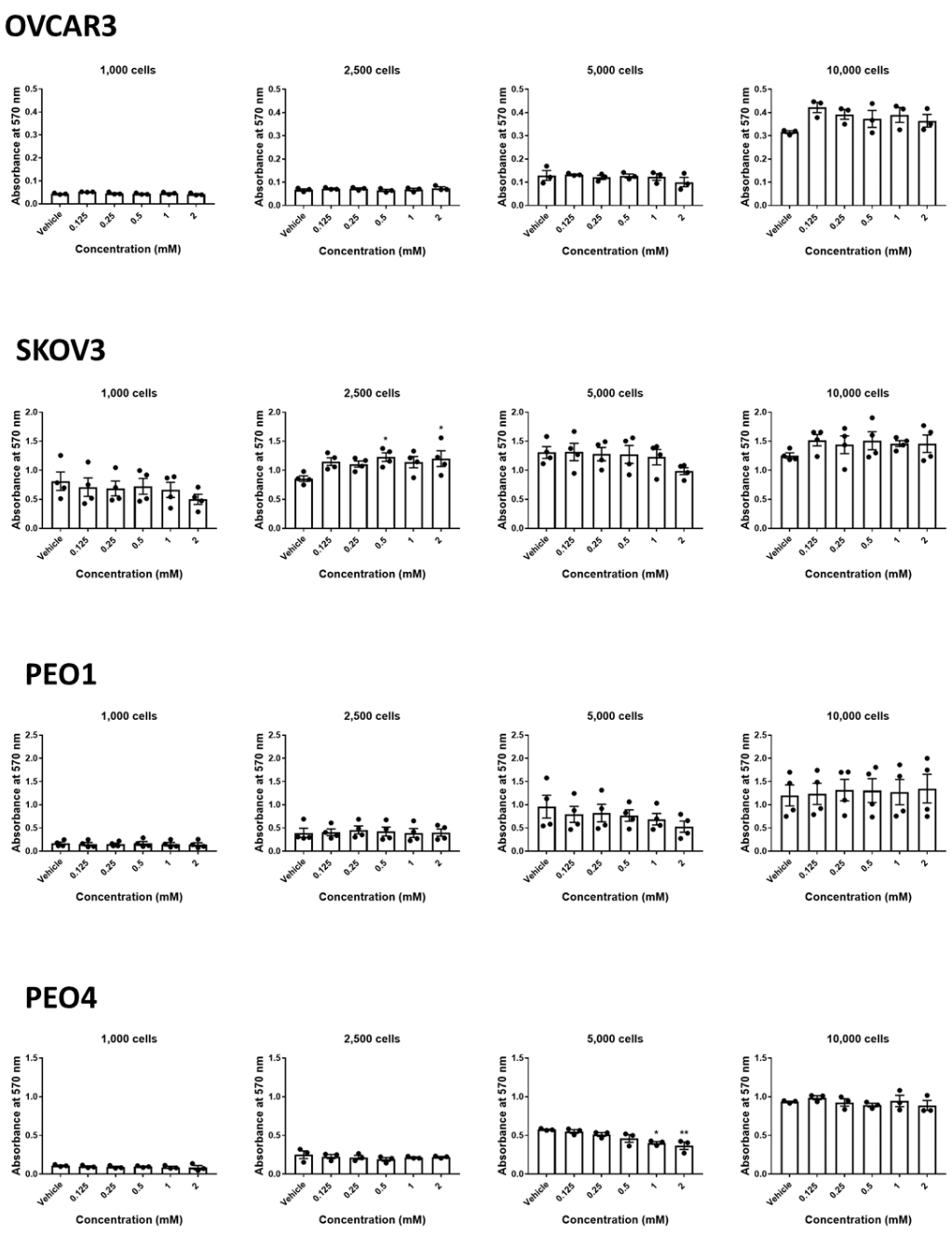

Figure 56. MTT assay was performed on OVCAR3, SKOV3, PEO1 and PEO4 cells at varying cell densities and concentrations of succinate.

Cells were seeded so that each well contained 100 µL of 10,000, 5,000, 2,500 or 1,000 cells in total. After 24 h, cells were exposed to succinate at concentrations of 0.125 mM, 0.25 mM, 0.5 mM, 1 mM, and 2 mM for 72 h to which an MTT assay was performed afterwards. Absorbance was measured at 570 nm as a correlation of cell proliferation. Error bars ± S.E.M, (One-way ANOVA, $p < 0.05$ (*), $p < 0.01$ (**) n = 3 - 4 independent cell passages).

SKOV3 cells are highly dependent on glutamine – termed “glutamine-addicted”, whereas OVCAR3 cells are less dependent on glutamine (Yang, et al., 2014). We wanted to investigate if SKOV3 could utilise succinate to facilitate growth in glutamine restricted conditions. Our results show that the removal of glutamine reduced the growth of SKOV3 cells however, the higher concentrations of succinate (1 mM and 2 mM) could significantly increase the cell viability under glucose only conditions ($p < 0.05$) (Figure 57). No clear trend was observed in OVCAR3 cells treated with succinate in the different glutamine conditions suggesting that SKOV3 could metabolise succinate for growth when glutamine is depleted.

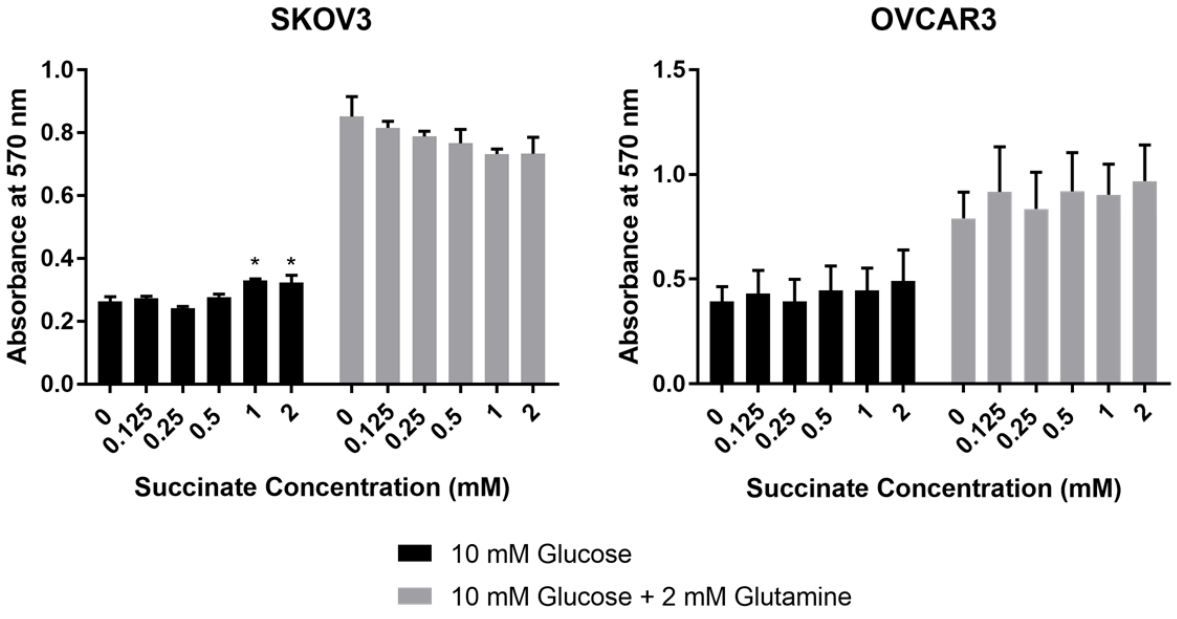

Figure 57. MTT assay was performed on SKOV3 and OVCAR3 treated with succinate in media containing glucose and with or without glutamine.
Cells were seeded from a 2.5 x 10^4 cells/mL suspension. After 24 h, cells were cultured in media containing 10 mM glucose with or without 2 mM glutamine in addition to succinate treatment at concentrations of 0.125 mM, 0.25 mM, 0.5 mM, 1 mM, and 2 mM for 72 h to which an MTT assay was performed afterwards. Absorbance was measured at 570 nm as a correlation of cell proliferation. Error bars ± S.E.M, (One-way ANOVA, $p < 0.05$ (*), n = 4 independent cell passages).

Succinate was reported to be able to stabilise HIF-1α through the inhibition of α-KG-dependent HIF-α prolyl hydroxylase (PHD) (Selak, et al., 2005). DMOG is also able to stabilise HIF-1α through the inhibition of HIF PHDs (Singh, et al., 2020). OC cells were treated with DMOG to

investigate if the response to succinate may be regulated through HIF. DMOG did not cause a significant effect in OVCAR3 or PEO4 cells (Figure 58). In SKOV3 cells, DMOG caused a significant decrease in MTT activity at 1 mM concentration ($p < 0.01$). DMOG appeared to cause a significant increase in cell viability at 0.0625 mM concentration in PEO1 cells ($p < 0.05$). Although the results of DMOG treatment did not correlate with the succinate treatment, this does not rule out the role of HIF-1α in the OC cell response to succinate. Differences in these results could be due to the responsiveness of OC cells to either treatment or how well they permeate through the cellular membrane.

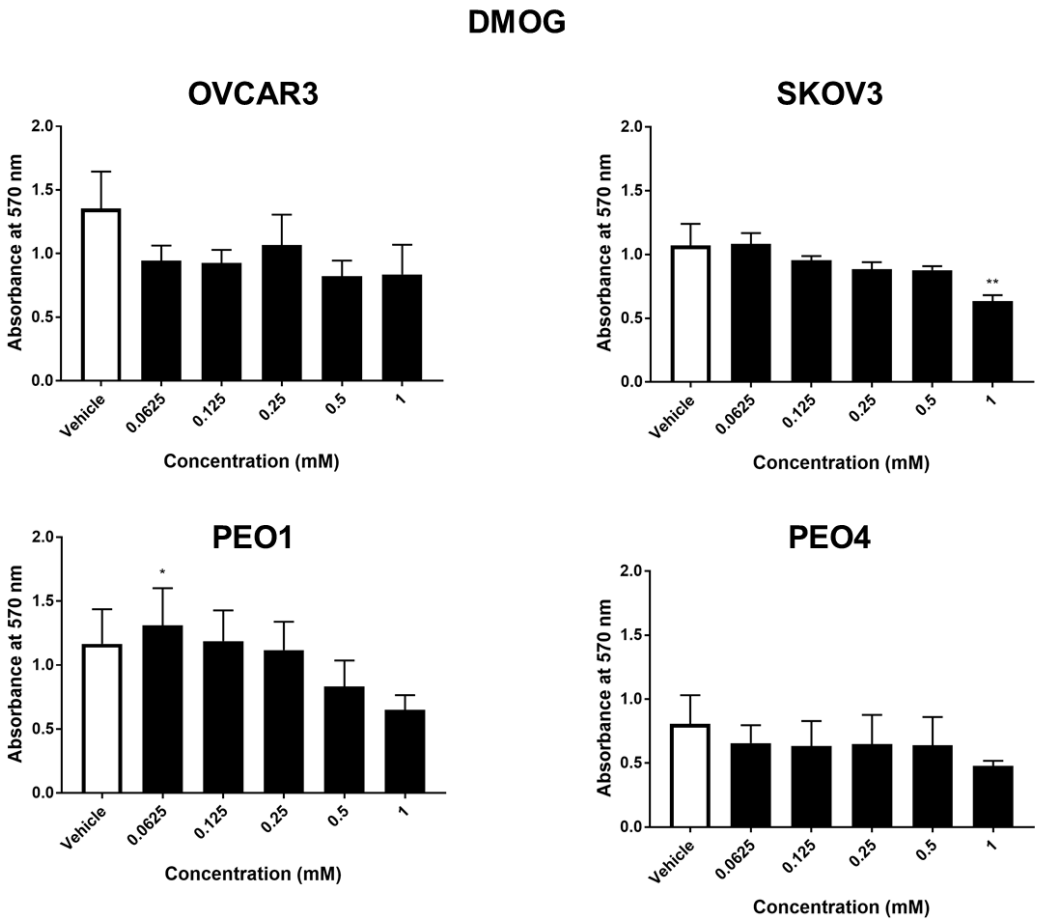

Figure 58. MTT cell proliferation assay in OVCAR3, SKOV3, PEO1 and PEO4 cells treated with DMOG for 24 h.

Cells were seeded at 1 x 10^5 cells/mL into wells of a 96-well plate. Cells were treated with 1, 0.5, 0.25, 0.125, 0.0625 mM DMOG. Error bars represent ± S.E.M (One-way ANOVA $p < 0.05$ (*), $p < 0.01$ (**); n= 4 independent cell passages).

6.4.3. Effect of succinate on the growth of 3D OC spheroid size and morphology.

Spheroids above 400 μM in diameter develop a hypoxic core which in turn activate signalling pathways in order to maintain cell viability (Riffle & Hegde, 2017). Hypoxia has also been reported to result in the accumulation of succinate which could promote cell growth (Chinopoulos, 2013; Gu, et al., 2020). First, we looked at how readily our OC cell lines formed spheroids by making 3D cultures using the hanging drop method. We found that OVCAR3 and PEO4 cells formed loose clusters of multicellular aggregates that were easily disaggregated, whereas SKOV3 and PEO1 cells formed more compact spheroids (Figure 59). Since it is difficult to quantify the diameter of multicellular aggregates, we decided to carry out succinate treatment on only PEO1 and SKOV3 cells.

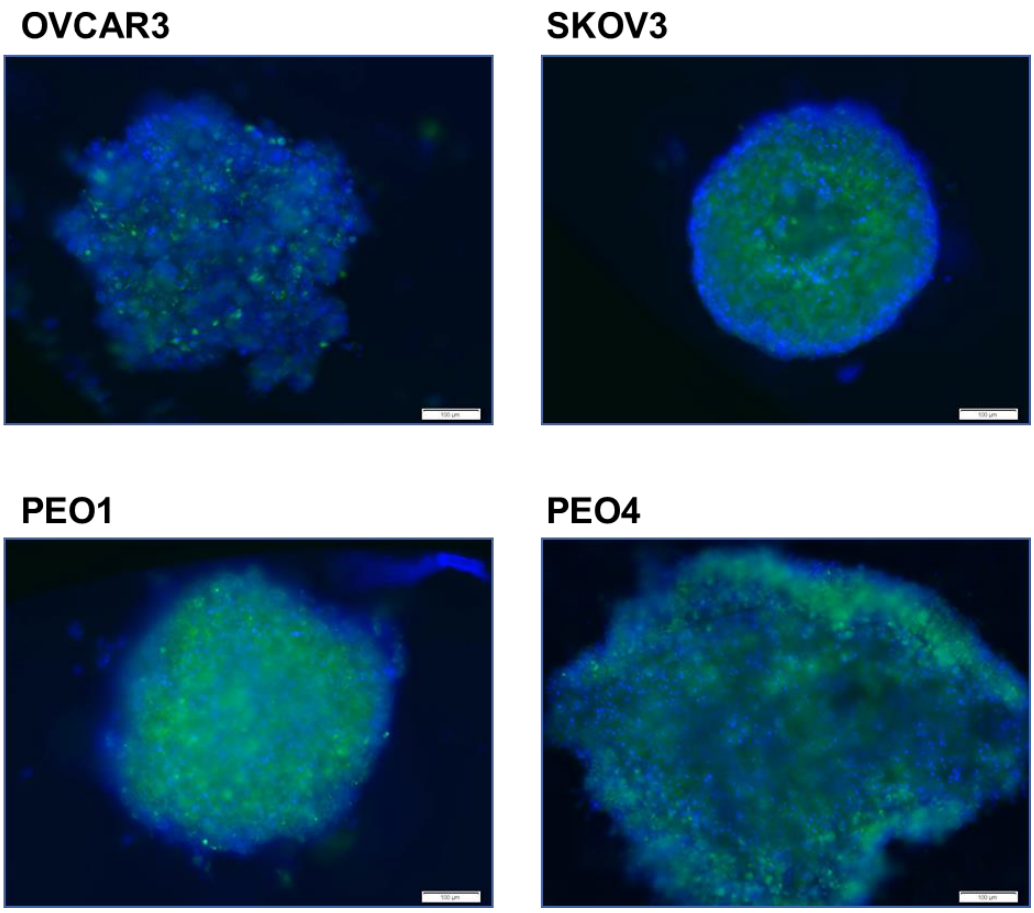

Figure 59. Fluorescent microscopy of 3D OVCAR3, SKOV3, PEO1 and PEO4 spheroids.
OC cells were seeded at 5000 cells on a petri plate and allowed to grow for 72 h. Spheroid membrane was stained with Vybrant™ DiO Cell-Labeling Solution and the nuclei were stained with Hoechst 33342. Spheroids were imaged using the Olympus Fluorescent Microscope (IX51) (Scale bar = 100µM).

From the 2D experiment, 1 mM succinate was used in the treatment media of the SKOV3 and PEO1 spheroids. The results showed that succinate caused a non-significant increase in SKOV3 spheroid diameter at time points, 24 h and 72 h (Figure 60). Whereas in PEO1 cells, succinate appeared to reduce spheroid diameter size at 24 h but had no effect on the spheroid diameter at 48 h and 72 h. In both cell lines, the spheroid diameter reduced in size across the different time points, possibly as a result of spheroid compaction. Succinate also did not appear to alter spheroid morphology across the different time points in both cell lines.

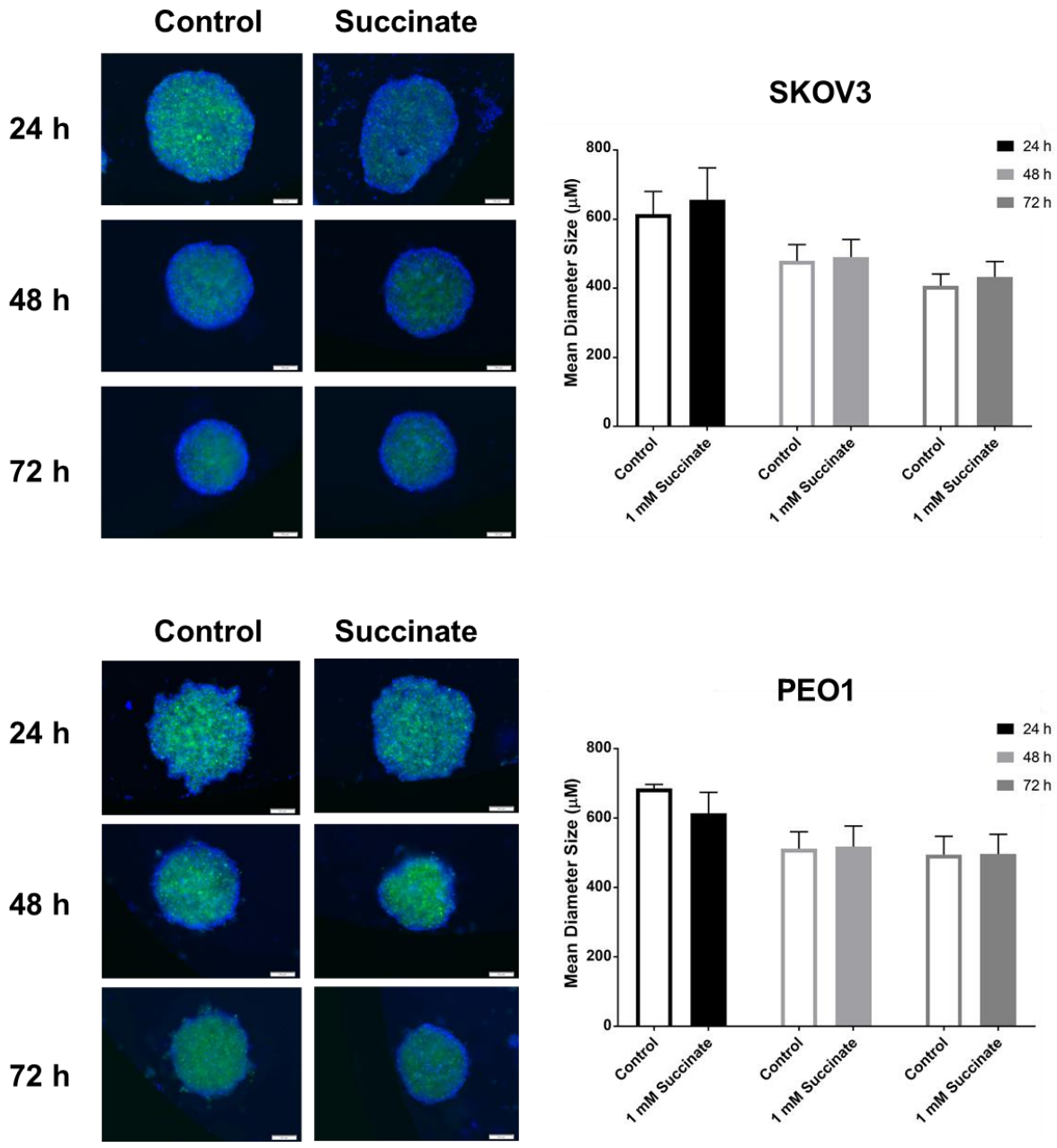

Figure 60. Comparison of spheroid diameter size in 3D SKOV3 and PEO1 treated with 1 mM succinate. SKOV3 and PEO1 cells were seeded at $5x10^3$ cells with 1 mM succinate on a Petri dish, size was monitored after 24 h, 48 h and 72 h. Spheroid membranes were stained with Vybrant™ DiO Cell-Labeling Solution and the nuclei were stained with Hoechst 33342 (Scale bar = 100µM) (Two-way ANOVA, $p > 0.05$ (n.s.), n = 3 independent cell passages).

Long term effects of succinate treatment on spheroid morphology were investigated in SKOV3 and PEO1 spheroids. Spheroids show an overall decrease in diameter as a result of spheroid

compaction in both cell lines and treatment (Figure 61). Succinate did not cause a noticeable change in size in SKOV3 and PEO1 spheroids at day 4 and 7. In SKOV3 spheroids, succinate treatment caused cells to shed around the outside perimeter of the spheroid at day 7 and 8 compared to the control which had a solid, compact perimeter. This effect was seen in in PEO1 spheroids at day 8 in both control and succinate treated spheroids with succinate treated spheroids showing a more pronounced effect.

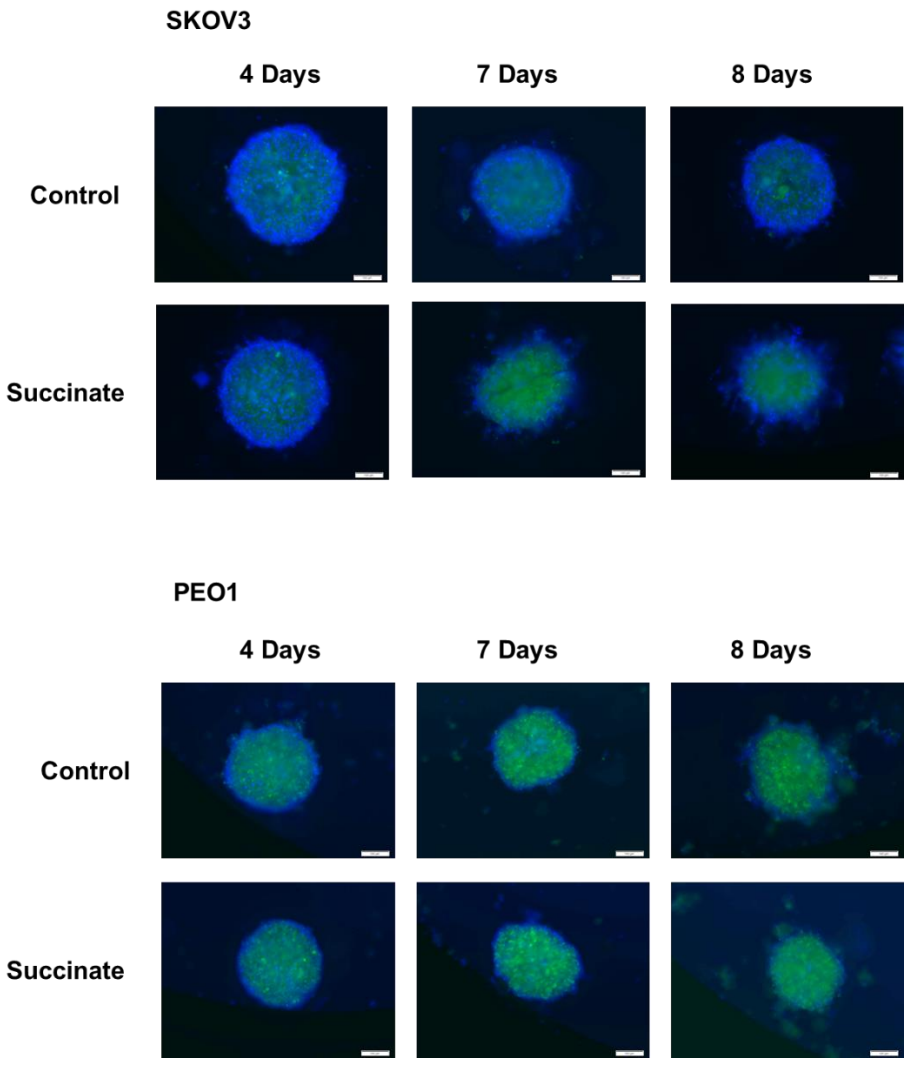

Figure 61. 3D SKOV3 and PEO1 cells were treated with 1 mM succinate for up to 8 days.
SKOV3 and PEO1 cells were seeded at $5x10^3$ cells with 1 mM succinate on a Petri dish, size was monitored after 4 days, 7 days and 8 days, with 10 µL of media containing 1 mM succinate added every 2 days. Spheroid membrane was stained with Vybrant™ DiO Cell-Labeling Solution and the nuclei were stained with Hoechst 33342 (Scale bar = 100µM; n = 3 independent cell passages).

6.5. Discussion

The accumulation of 2-HG can enhance cell proliferation and was associated with TET2 enzyme activity inhibition as well as reduced levels of 5hmC, CpG island and histone hypermethylation (Shim, et al., 2014; Sullivan, et al., 2016; Seok, et al., 2019). In primary fibroblasts, even low concentrations of 2-HG were sufficient to facilitate cell proliferation and induce epigenetic changes (Dvořák, et al., 2017). The D-2HG enantiomer was widely reported to be the enantiomer involved in influencing cell proliferation and viability (Terunuma, et al., 2014; Chan, et al., 2015; Chen, et al., 2016; Sullivan, et al., 2016; Seok, et al., 2019). Our results showed that neither D-2HG or L-2HG had a significant effect on the cell viability and proliferation of the OC cell line. Similar results were seen in a study using mesenchymal stromal cells where D-2HG did not appear to affect proliferation (Liu, et al., 2021). Exogenous L-2HG also did not exhibit a significant effect in colorectal cancer (Colvin , et al., 2016). D-2HG could be contributing to oncogenesis though increased invasion and migration as well as producing proinflammatory cytokines including IL-6, RANTES, IP-10 and IL-8 in order to recruit T-cells, macrophages, dendritic cells, and neutrophils (Chen, et al., 2016; Han, et al., 2018). Recruitment of immune cells results in prolonged inflammation which further drives neoplasia (Han, et al., 2018). Conversely, D-2HG has also been shown to inhibit ATP synthase and reduce cell proliferation and viability, promoting cell cycle arrest and apoptosis (Bralten, et al., 2011; Fu, et al., 2015; Su, et al., 2018). Whilst D-2HG was able to drive oncogenesis through epigenetic alterations, accumulation of the oncometabolite on a cellular level can be metabolically disadvantageous especially in cells which do not have the capacity to export D-2HG (Bunse, et al., 2018). The accumulation of L-2HG resulted in the suppression of anti-tumour immunity and regulated immune cell function and infiltration in the tumour microenvironment in pancreatic cancer cells (Gupta, et al., 2021). Despite being a more potent inhibitor than D-2HG to TET enzymes, leukemic transformation appeared to be specific to D-2HG (Xu, et al., 2011; Losman, et al., 2013). Further studies should be carried on investigating whether 2-HG facilitates or inhibits OC cancer progression. As both enantiomers appear to influence the immune response, exploring the link between the epigenetic alterations caused by 2-HG on OC cytokine production could be carried out.

Succinate has been associated with contributing to the complications of specific metabolic diseases by promoting inflammation, oncogenesis, and tumour progression as well as stimulating STAT3 which can lead to tumorigenesis (Zhao, et al., 2017). Our results showed that succinate did not have an effect on proliferation or viability in OC cells under normal cell culture conditions but when seeded at lower density (2,500 cells), the glutamine dependent SKOV3 cells showed a significant increase in cell viability when treated with 0.5 mM and 2 mM succinate in cell culture conditions. However, this effect was not seen in the follow up experiment whereby only the SKOV3 cells in glutamine deprived conditions showed a significant increase in viability when treated with 1 mM and 2 mM succinate. These results suggest that the highly invasive SKOV3 cells are able to metabolise succinate to promote cell viability when glutamine is lacking. Glutamine is essential for anaplerosis in highly invasive cells; however, succinate could replace glutamine as a substrate for anaplerosis when glutamine is lacking (Yang, et al., 2014; Sant'Anna-Silva, et al., 2021). In prostate cancer, succinate uptake from the tumour environment resulted in an anaplerotic effect and stimulated amino acid metabolism including methionine, argininosuccinate and aspartate (Sant'Anna-Silva, et al., 2021). Succinate utilisation has been reported to promote growth and viability in several carcinomas such as uterine endometrial (Gu, et al., 2020), ovarian (Chen, et al., 2014) and prostate (Weber, et al., 2018). However, succinate could also increase tumorigenic potential through the increase in migration, invasion, and colony formation without affecting the rate of proliferation (Sant'Anna-Silva, et al., 2021). In some of our results, we saw that succinate caused a decrease in cell viability at certain cell densities. PEO4 cells seeded at 5,000 cells showed a significant decrease in cell viability upon treatment with 1 mM and 2 mM succinate. This decrease may be due to the activation of the HIF-1α pathway by succinate which then induced apoptosis (Yang, et al., 2020). Treatment with DMOG also showed that, stabilisation of HIF-1α can lead to cytotoxicity as seen with SKOV3 cells treated with 1 mM DMOG. In pheochromocytoma cells, HIF-1α stabilisation was seen after treatment with 1 mM DMOG and higher concentrations of DMOG also resulted in the reduction in cell viability (Singh, et al., 2020).

Solid tumours often exhibit hypoxic regions which can cause tumour cells to undergo metabolic reprogramming to enable hypoxic tumour cells to survive and proliferation to outcompete

untransformed cells. Hypoxia-induced changes in tumour cell metabolism can lead to the production of oncometabolites including succinate (Kes, et al., 2020). 3D spheroids exhibit hypoxic and apoptotic/necrotic areas formed as a result of oxygen and nutrient gradients. Spheroids of a diameter of approximately 200 - 300 µM exhibit a proliferating zone at the surface with a normoxic quiescent zone in the middle and hypoxic zone in the core. Spheroids of approximately 500 µM in diameter show necrotic areas (Däster, et al., 2017). The OC spheroids formed in our experiment showed a diameter of above 400 µM and may produce succinate as a result of hypoxia (Chinopoulos, 2013; Flores, et al., 2018); however, the exogenous succinate did not significantly induce cell proliferation through the increase of spheroid diameter size. Mutations in *SDHB* results in the accumulation of succinate (Gu, et al., 2020). The silencing of *SDHB* in neuroblastoma 3D cultures also resulted in no significant differences in spheroid diameter compared to the wild type control (D'Antongiovanni, et al., 2017).

In hereditary leiomyomatosis and renal cell cancer cells, fumarate accumulation correlated with an increase in cell proliferation as a result of chronic proliferative signalling by disrupting cellular iron signalling (Kerins, et al., 2017). Our results showed that fumarate had a cytotoxic effect on OC cells with the chemoresistant PEO4 being the most sensitive to fumarate treatment. At low concentrations, fumarate was reported to have a cytoprotective role through the activation of the NRF2 pathway (Saidu, et al., 2017). High concentrations of fumarate resulted in oxidative stress and subsequent cytotoxicity by decreasing nuclear translocation of NRF2, therefore reducing the production of downstream targets (Saidu, et al., 2017; Saidu, et al., 2018). KRAS mutated cells appear to be more sensitive to fumarate treatment compared to cells without the mutation (Saidu, et al., 2018). SKOV3 and OVCAR3 cell lines show wild type KRAS (Nakayama, et al., 2008); whereas PEO1 cells do not appear to express *KRAS* (Coscia, et al., 2016). The KRAS status of PEO4 is unknown but it is possible this may be the reason behind the different sensitivities between the OC cell lines. We did not pursue fumarate further as it showed little clinical relevance to OC (Ylisaukko-oja, et al., 2006; Zhang, et al., 2020).

6.6. Conclusion

In this chapter, we investigated the effect of oncometabolites, succinate and D-L-2HG on the cell viability and proliferation in OC cells at various cell densities and media compositions. We found that both enantiomers of 2-HG did not significantly affect the viability or proliferation of OC cells. Succinate appeared to promote the viability of 2D glutamine dependent SKOV3 cells seeded at 2,500 cells under glutamine deprived conditions suggesting that succinate could replace glutamine as a substrate for anaplerosis. In 3D cultures, succinate did not influence the spheroid diameter size. Oncometabolites could influence tumorigenesis by influencing the immune response, cell migration, invasion, and colony formation through alterations in the epigenetic landscape which is an area which could be explored further.

Chapter 7

Concluding Discussion

EOC patients initially respond well to treatment but will often show recurrence with chemoresistant tumours (Ozols, 2005). Novel approaches to identify strategies for the treatment of cancer involves targeting cancer metabolism and the epigenome (Pollak, 2012; Cheng, et al., 2019). This study aimed to elucidate the effect of the dysregulated cancer metabolism on OC growth as well as the efficacy of metformin treatment in OC cells with a focus on epigenetics. We used both 2D and 3D models of HGSOC in this study as the 3D models best recapitulates the free-floating aggregates found in the ascites of OC patients (Bilandzic & Stenvers, 2014).

7.1. Cancer metabolism

In order to survive the harsh tumour microenvironment with limited nutrients, cancer cells may adapt by undergoing metabolic reprogramming from anaerobic to aerobic glycolysis, and vice versa, in order to synthesise protein, nucleic acids, and lipids to maintain rapid proliferation. The imbalance between glucose supply and consumption rate in tumour cells results in low levels of extracellular glucose, creating a metabolically restrictive local environment (Li & Simon, 2020). The reduced glucose concentration can affect the efficacy of anti-cancer drugs, such as metformin, which has been widely studied in the repurposing to treat cancer (Menendez, et al., 2012). Both glutamine and glucose can support cancer growth by driving the TCA cycle for energy generation (Yang, et al., 2014). Tumour-derived metabolites ("oncometabolites") from the TCA cycle provide a microenvironment that favours disease progression (Li & Simon, 2020). The presence of oncometabolites in the ascites of OC patients are implicated in the dysregulation of post-translational modifications, metabolic and alterations in cancer cells and facilitate tumorigenesis (Dando, et al., 2019). TET2 is a tumour suppressor that regulates the DNA methylome. First shown by Wu *et al.,* (2018); low glucose or AMPK agonists, such as metformin, were reported to stabilise TET2 through the activation of AMPK (Wu, et al., 2018; Zhang, et al., 2019). TET2 is degraded in hyperglycaemic conditions which leads to the dysregulation of 5hmC, compromising its tumour suppressive function (Wu, et al., 2018). Oncometabolites 2-HG and succinate can also lead to epigenetic aberrations through the competitive inhibition of TET2 due to structural similarities with TET2 substrate, α-KG (Xiao, et al., 2012). Thus, TET2 acts as a link between epigenetics and metabolism.

7.2. Metformin repurposing

Maximum approved daily dose of metformin for the treatment of diabetes is 2.5g (35 mg/kg bodyweight). Following a therapeutic dose, plasma concentrations of metformin are between 40 µM and 70 µM, as it reaches the liver through the portal vein. Systemic plasma concentrations are reduced to 10 µM – 40 µM after hepatic uptake (He & Wondisford, 2015). Anti-cancer effects of metformin have previously been observed at non-physiological and clinically irrelevant concentrations, poorly reflecting the *in vivo* scenario (Menendez, et al., 2012). Several studies have shown that under physiological hypoglycaemic conditions, cancer cells were more sensitive to metformin treatment and required lower concentrations of metformin to reduce cell viability (Wahdan-Alaswad, et al., 2013; Bikas, et al., 2015). Glucose concentrations in the ascites of OC patients were <3.3 mM which is considered hypoglycaemic (Kipps, et al., 2013; Tourkmani, et al., 2018). Cancer cells undergo apoptotic cell death as a result of metformin in glucose starved tumour environment (Menendez, et al., 2012). Püschel *et al.,* (2020) reported that metformin promoted the release of IL-6 and IL-8 under cellular starvation. However, the concentrations of metformin used in the study were supra-physiological (1 and 10 mM) (Püschel, et al., 2020). We found that treatment with a therapeutic concentration of metformin (0.625 mM) in hypoglycaemic conditions resulted in the release of IL-6 and IL-8 in the chemosensitive PEO1 cells. As chronic inflammation plays an important role in OC metastasis through chemotaxis, this result made us question whether metformin was suitable to be repurposed for the treatment of OC (Lo, et al., 2011; Nieman, et al., 2011).

In Chapter 3, we aimed to investigate the pathway involved in the inflammatory response seen in chemosensitive OC cells treated with a chronic, therapeutic concentration of metformin under hypoglycaemic conditions. Hypoglycaemia did potentiate the cytotoxic effect of metformin in both chemosensitive PEO1 and chemoresistant PEO4 cells, showing a reduction in cell viability and growth; however, the reduction was more prominent in PEO1 cells. This may be due to PEO4 cells not expressing the metformin transporters *OCT3* and *OCTN1*, making them less sensitive to the anti-proliferative effects of metformin as a result of reduced drug uptake (Coscia, et al., 2016; Jackson, et al., 2017). To overcome this, future experiments could

include the use of phenformin, which does not require receptor-mediated uptake. We also observed a significant increase in IL-6 and IL-8 expression in the metformin treated PEO1 cells in low glucose media over a 48 h, 96 h and 144 h. This response was independent of JAK/STAT3 signalling but may involve AMPK/TET2 as the combination of metformin and hypoglycaemia strongly activated AMPK. The stabilisation of TET2 through the stabilisation of AMPK could result in binding to the promoter of inflammatory genes and activation of their expression (Itoh, et al., 2018; Wang, et al., 2018; Wu, et al., 2018). A similar trend was observed in the 3D aggregates, though the effect was not significant.

Although culturing OC cells in low glucose did enhance the efficacy and cytotoxicity of metformin, the hypoglycaemic nature of the local OC environment may be detrimental as induction of inflammatory cytokines could worsen the cancer, possibly causing the emergence of chemoresistant tumours (Savant, et al., 2018). Colony formation and invasive capabilities of cancer cells when treated with metformin will need to be studied to see whether this increases the metastatic potential of chemosensitive cells. Co-treatment with cisplatin should also be investigated to see if resistance to chemotherapy is affected under physiological conditions.

7.2.1. Epigenetics

Epigenetics and the microenvironment play a role in regulating genes which drive inflammatory changes in cancer (Raghuraman, et al., 2016). Metabolism also regulates epigenetic modifications as metabolites can affect the activity of enzymes that modify the genome (Lu & Thompson, 2012; Wong, et al., 2017). We wanted to validate the role of AMPK/TET2 pathway in IL-6 and IL-8 expression by exploring TET2 binding using ChIP as well as TET2 activity indirectly through assaying levels of DNA methylation using MeDIP. ChIP is a widely used assay that investigates protein-DNA interactions for the mapping of transcription factors on the genome or specific locus. Similarly, MeDIP is a technique that assays the levels of 5mC (methylation mark) as DNA methylation is usually associated with gene silencing (Collas, 2010). In collaboration with Porvair Ltd., who provided the ChIP and MeDIP kits as well as technical assistance, transcription factor binding and DNA methylation levels on the promoter of inflammatory genes in response to metformin treatment in low glucose were investigated.

Both assays were column-based which shows many advantages over bead-based matrices including better protein-DNA pull down, better enrichment as well as fewer processing steps therefore reducing the chance of technical errors and target loss (Chernukhin, et al., 2011). Optimisation of both assays was undertaken to ensure maximal antibody binding and better enrichment. Results of the ChIP assay in Chapter 4 showed variation between biological replicates making it difficult to reach a solid conclusion. However, results suggest that the IL-6 response may be regulated by TET2 in 2D PEO1 cells treated with metformin in low glucose media. TET2 binding t on the *IL6* promoter was observed in one replicate of the 3D PEO1 spheroids so it is unclear if TET2 does play a role in *IL6* expression. IL-8 expression may not require TET2 binding but may still be influenced by AMPK activation. Studies have reported the role of AMPK in the upregulation of IL-8 expression (Tang, et al., 2011; Ko, et al., 2015). ER stress regulator, ATF4 is upregulated by metformin and hypoglycaemia and has been reported to bind directly to the *IL6* and *IL8* promoter to exert a proinflammatory effect (Quentin, et al., 2012; Terashima, et al., 2013; Iwasaki, et al., 2014; Püschel, et al., 2020). In this study, ATF4 did not appear to bind to the promoter of the inflammatory genes under low glucose and metformin conditions and may not be involved in its expression.

TET2 plays a role in DNA demethylation through the oxidation of 5mC to 5hmC (Pan, et al., 2015). By assaying 5mC, we found that DNA methylation levels of the CpG island were not influenced by experimental conditions in either 2D or 3D HGSOC cell lines (Chapter 5). The *IL8* promoter appeared to be unmethylated and was not significantly influenced by experimental conditions. These results suggests that other mechanisms of epigenetic regulation are involved in *IL6* and *IL8* gene transcription in metformin treated PEO1 cells cultured under physiological conditions. DNA methylation and histone modifications can influence each other, therefore future studies should focus on the effect of metformin on the histone marks on the promoter of inflammatory genes under different concentrations of glucose (Cedar & Bergman, 2009).

7.3. Oncometabolites

Cancer cells alter their metabolism in order to maximise nutrient utilisation to meet bioenergetic and biosynthetic demands (Li & Simon, 2020; Yong, et al., 2020). Rapid glucose

consumption may result in a hypoglycaemic microenvironment through the Warburg effect, producing elevated levels of lactate as a by-product (Wise & Thompson, 2010). The combination of hypoglycaemia and high lactate levels facilitate disease progression as a result of metabolic stress due to limited nutrient supply as well as unfavourable pH levels (Li & Simon, 2020). The dysregulation of the TCA cycle can also produce high levels of metabolites that can induce oncogenesis. In Chapter 6, the effect of the oncometabolites 2-HG, succinate, and fumarate on OC cancer cell proliferation was investigated.

Chapter 6 showed that in HGSOC cell lines, oncometabolites 2-HG and succinate had little effect on viability and proliferation as well as spheroid size under tissue culture conditions. Oncometabolite treatment under physiological conditions (hypoglycaemic and increased lactate) also showed little change in proliferation. This suggests that the aforementioned oncometabolites could influence tumorigenesis through other means such as regulating the immune response, cell migration as well as colony formation and invasive capabilities (Sant'Anna-Silva, et al., 2021). We also found that in the highly invasive and glutamine addicted SKOV3 cell line, the reduced proliferation may be due to high seeding density causing cells to become quiescent as a response to over-confluency. Quiescent cells are dormant and non-proliferative that can be a result of contact inhibition and restriction of nutrients (Lagies, et al., 2020). We saw that when SKOV3 cells were sub-confluent, succinate did show significantly higher MTT activity compared to the control. Additionally, under glutamine depleted conditions, SKOV3 cells may be able to use exogenous succinate as a substitute for glutamine in anaplerosis to facilitate cell proliferation (Yang, et al., 2014; Sant'Anna-Silva, et al., 2021). No significant changes in cell viability were observed in the glutamine independent OVCAR3 cells, signifying that utilisation of succinate may be a marker of highly invasive cells.

Although fumarate has been shown to have a pro-proliferative effect in hereditary leiomyomatosis and renal cell cancer cells (Kerins, et al., 2017), fumarate showed a cytotoxic effect in all HGSOC cell lines analysed in this study. High fumarate concentrations were reported to cause oxidative stress and subsequent cytotoxicity through the decrease of NRF2 (Saidu, et al., 2017; Saidu, et al., 2018). Our study showed that the chemoresistant HGSOC cell

line, PEO4 was the most sensitive to cytotoxic effect of fumarate treatment. Further studies will be required in order to determine if fumarate treatment causes any off-target effects before being considered as a potential candidate as an anti-cancer agent.

7.4. Limitations

Due to COVID-19, the lockdown period resulted in the loss of many samples, as chromatin is only stable for a few months at -80^{o}C (Haring, et al., 2007). The pandemic also affected logistics and the reduced workforce of manufacturers and suppliers meant that laboratory supplies and consumables were delayed. The combination of extended sample recollection and delays with supplies meant that many planned experiments could not be completed before the deadline. This study aimed to establish a link between epigenetics and metabolism in OC progression through investigating the proinflammatory effect of metformin. There are many areas which could be improved which will be discussed below.

In cancer research, many experiments are performed on 2D cell cultures *in vitro* which are simple and relatively low in cost in terms of maintenance (Kapałczyńska, et al., 2018). However, 2D cultures cannot recapitulate the complexity and heterogeneity of tumours *in vivo* resulting in loss of signals that are involved in the maintenance of cellular processes (Zanoni, et al., 2016). To better improve clinical relevance, this study was carried out in cell lines grown as 3D spheroids which expose cells to conditions such as hypoxia and heterogenous distribution of nutrients similar to that of OC tumours and free-floating multicellular aggregates *in vivo* (Liao, et al., 2014; Zanoni, et al., 2016; Cavo, et al., 2020). Primary cultures would be the most appropriate model, since they contain populations of the different cell types that appear in the source tissue but were not used here due to difficulties with isolation and culturing during the pandemic in addition to a shorter life span of cells (Kapałczyńska, et al., 2018). 3D cell line models were better suited for the long-term treatments used in our study.

Though the ChIP results implied the presence of TET2 and ATF4 binding, it would be beneficial to perform western blotting using antibodies against TET2 and ATF4 to confirm their

expression and to assess whether experimental conditions affected their protein levels. Alternative techniques such as RT-qPCR could be used to further corroborate the results and indicate whether the response is at a genetic level or post-translation. Knockdown/silencing studies using siRNAs will better help us understand the contribution of the genes involved in the metformin response and the mechanism of action.

As discussed in Chapter 4 and Chapter 5, the variability within experiments could be improved with more replicates if more time was available. It is also possible that our protein of interest did not bind to the putative binding site in this study, or that the antibody was not suitable for our experiment (more so in the case of the ChIP assay). Using ChIP-seq and MeDIP-seq can help identify possible binding sites for our protein of interest and for ChIP, ChIP-seq can be used to validate and determine the effectiveness of the antibody. For MeDIP, pre-treatment with DNA methylation inhibitors, 5'-aza-2'-deoxycytidine or 5-Azacytidine would provide a better idea of TET2 activity under different experimental conditions without being masked by active methylation by DNMTs. It would also be useful to carry out a time course experiment to help us understand the changes in epigenetic alterations that precede the inflammatory response.

With regards to TET2 activity, a dot blot assay to quantify amounts of 5hmc and 5mC or an ELISA used to measure TET2 activity could be considered in order to determine if oncometabolites do indeed exhibit an inhibitory effect on TET2 in HGSOC cells. Additionally, these experiments would further verify if the AMPK/TET2 pathway is involved in the inflammatory response observed in chemosensitive OC cells during hypoglycaemia and treatment with metformin. These techniques are future experiments that should be considered in order to help us better understand the role of TET2 in regulating cellular responses as a result of dysregulated cancer metabolism.

7.5. Concluding remarks

In conclusion, TET2 may be an important link between cancer metabolism, tumour microenvironment and epigenetics in OC tumorigenesis. The repurposing of metformin is

attractive due to showing anti-cancer effects in a wide range of cancer types. We show that the anticancer effect may be cell type and context dependent as metformin treatment may worsen the prognosis of OC under physiological condition by increasing inflammation. This mechanism may involve AMPK activation and TET2 binding but the expression of inflammatory genes may involve other epigenetic alterations besides DNA methylation. We also found that under restricted glutamine conditions, glutamine-addicted, highly invasive OC cells are able to use oncometabolite, succinate to facilitate cell growth. Though we could not establish the effect oncometabolites had on TET2, there are many studies that explore and discuss the connection between metabolism and epigenetics. Overall, the data highlights the importance of the physiological tumour microenvironment on the efficacy of certain treatments and in the facilitation of cancer growth and proliferation which is regulated by epigenetic mechanisms.

Bibliography

Ahluwalia, A. et al., 2001. DNA methylation and ovarian cancer. I. Analysis of CpG island hypermethylation in human ovarian cancer using differential methylation hybridisation. *Gynecol Oncol,* 82(2), pp. 261 - 268.

Alipour , S. et al., 2020. Methylation status of interleukin-6 gene promoter in patients. *Reumatol Clin.,* 16(3), p. 229–234.

Alipour, S. et al., 2020. Methylation status of interleukin-6 gene promoter in patients with Behçet's disease. *Reumatol Clin (Engl Ed),* 16(3), pp. 229-234.

Andia, D. C. et al., 2010. DNA Methylation Status of the IL8 Gene Promoter in Aggressive Periodontitis. *Journal of Peridontology,* 81(9), pp. 1336-1341.

Antequera, F., Boyes, J. & Bird, A., 1990. High Levels of De Novo Methylation and Altered Chromatin Structure at CpG Islands in Cell Lines. *Cell,* Volume 62, pp. 503 - 514.

Arts, J. et al., 2007. R306465 is a novel potent inhibitor of class I histone deacetylases with broad-spectrum antitumoral activity against solid and haematological malignancies.. *Br J Cancer,* Volume 97, p. 1344–1353.

Aspuria, P.-J.P. et al., 2014. Succinate dehydrogenase inhibition leads to epithelial-mesenchymal transition and reprogrammed carbon metabolism. *Cancer & Metabolism,* Volume 2, p. 21.

Balch, C. et al., 2009. Minireview: Epigenetic Changes in Ovarian Cancer. *Endocrinology,* Volume 150, pp. 4003-4011.

Balch, C., Huang, T. H., Brown, R. & Nephew, K., 2004. The epigenetics of ovarian cancer drug resistance and resensitisation. *AJOG Reviews,* Volume 191, pp. 1552 - 1572.

Balch, C. et al., 2007. Antimitogenic and chemosensitizing effects of the methylation inhibitor zebularine in ovarian cancer. *Mol Cancer Ther,* Volume 4, p. 1505–1514.

Bar, D. et al., 2016. The effect of metabolic comorbidities and commonly used drugs on the prognosis of patients with ovarian cancer. *Eur J Obstet Gynecol Reprod Biol,* Volume 207, pp. 227-231.

Barnholtz-Sloan, J. S. et al., 2003. Ovarian cancer: changes in patterns at diagnosis and relative survival over the last three decades. *American Journal of Obstetrics and Gynecology,* 189(4), pp. 1120-1127.

Barski, A. et al., 2007. High-Resolution Profiling of Histone Methylations in the Human Genome. *Cell,* 129(4), pp. 823-837.

Beck, D., Maamar, M. B. & Skinner, M. K., 2021. Genome-wide CpG density and DNA methylation analysis method (MeDIP, RRBS, and WGBS) comparisons. *Epigenetics,* Volume 11, pp. 1-13.

Bergström, J., Fürst, P., Norée, L. O. & Vinnars, E., 1974. Intracellular free amino acid concentration in human muscle tissue. *J Appl Physiol,* 36(6), pp. 693-7.

Berishaj, M., Gao, S. P., Ahmed, S. & et al. , 2007. Stat3 is tyrosine phosphorylated through interleukin-6/glycoprotein 130/Janus kinase pathway in breast cancer. *Breast Cancer Res,* Volume 9, p. R32.

Bharti, S. K. et al., 2017. Metabolomic characterization of experimental ovarian cancer ascitic fluid. *Metabolomics,* Volume 13, p. 113.

Bikas, M. et al., 2015. Glucose-deprivation increases thyroid cancer cells sensitivity to metformin. *Endocrine-Related Cancer,* 22(6), p. 919–932.

Bilandzic, M. & Stenvers, K. L., 2014. Assessment of Ovarian Cancer Spheroid Attachment and Invasion of Mesothelial Cells in Real Time. *J. Vis. Exp,* Volume 87, p. e51655.

Bizjak, M., Malavašič, P., Pirkmajer, S. & Pavlin, M., 2019. Comparison of the effects of metformin on MDA-MB-231 breast cancer cells in a monolyer and in tumour spheroid as a function of nutrient concentrations. *Biochemical and Biophysical Research Communications,* 515(2), pp. 296-302.

Bodmer, M. et al., 2011. Use of metformin and the risk of ovarian cancer: A case-control analysis. *Gynaecologic Oncology ,* Volume 123, pp. 200 - 204.

Bonhoure, N. et al., 2014. Quantifying ChIP-seq data: a spiking method providing an internal reference for sample-to-sample normalization. *Genome Res.,* Volume 24, pp. 1157-1168.

Borgel, J., Guibert, S. & Weber, M., 2012. Methylated DNA Immunoprecipitation (MeDIP) from Low Amounts of Cells. In: N. Engel, ed. *Genomic Imprinting: Methods and Protocols (Methods in Molecular Biology).* Totowa, NJ: Humana Press, pp. 149-158.

Botwell, D. D. L., 2010. The genesis and evolution of high-grade serous ovarian cancer. *Nature Reviews Cancer,* Volume 10 , pp. 803 - 808.

Braconi, C., Huang, N. & Patel, T., 2010. MicroRNA-dependent regulation of DNA methyltransferase-1 and tumor suppressor gene expression by interleukin-6 in human malignant cholangiocytes. *Hepatology,* 51(3), pp. 881-90.

Bralten, L. B. C. et al., 2011. IDH1 R132H decreases proliferation of glioma cell lines in vitro and in vivo. *Ann Neurol.,* 69(3), pp. 455-463.

Brancher , S. et al., 2020. Metformin use and lung cancer survival: a population-based study in Norway. *British Journal of Cancer,* Volume 124, pp. 1018-1025.

Brat, D. J., Bellail, A. C. & Van Meir, E. G., 2005. The role of Interleukin-8 and its receptors in gliomagenesis and tumoral angiogenesis. *Neuro-oncol,* Volume 7, pp. 122-133.

Browning, L. et al., 2018. IL-6 and ovarian cancer: inflammatory cytokines in promotion of metastasis. *Cancer Manag Res.,* Volume 10, p. 6685–6693.

Brown, J. R. et al., 2020. Phase II clinical trial of metformin as a cancer stem cell–targeting agent in ovarian cancer. *JCI Insight,* 5(11), p. e133247.

Bunse, L. et al., 2018. Suppression of antitumor T cell immunity by the oncometabolite (R)-2-hydroxyglutarate. *Nature Medicine,* Volume 24, p. 1192–1203.

Burleson, K. M., Boente, M. P., Panbuccian, S. E. & Skubitz, A. P. N., 2006. Disaggregation and invasion of ovarian carcinoma ascites spheroids. *Journal of Translational Medicine,* Volume 4, p. 6.

Cancer Research UK, 2014. *Ovarian Cancer Statistics.* [Online]
Available at: http://www.cancerresearchuk.org/health-professional/cancer-statistics/statistics-by-cancer-type/ovarian-cancer#heading-Six
[Accessed 17 January 2018].

Cavo, M. et al., 2020. A synergic approach to enhance long-term culture and manipulation of MiaPaCa-2 pancreatic cancer spheroid. *Scientific Reports,* Volume 10, p. 10192.

Cedar, H. & Bergman, Y., 2009. Linking DNA methylation and histone modification: patterns and paradigms. *Nature Reviews Genetics,* Volume 10, p. 295–304.

Cepeda, V. et al., 2007. Biochemical mechanisms of cisplatin cytotoxicity. *Anticancer Agents Med Chem.,* Volume 7, p. 3–18.

Cerezo, M. et al., 2013. Metformin Blocks Melanoma Invasion and Metastasis Development in AMPK/p53-Dependent Manner. *Mol Cancer Ther,* 12(8), pp. 1605-1615.

Chan, S. M. et al., 2015. Isocitrate dehydrogenase 1 and 2 mutations induce BCL-2 dependence in acute myeloid leukemia. *Nat Med.,* 21(2), p. 178–184.

Chapman-Rothe, N. et al., 2013. Chromatin H3K27me3/H3K4me3 histone marks define gene sets in high-grade serous ovarian cancer that distinguish malignant, tumour-sustaining and chemo-resistant ovarian tumour cells.. *Oncogene,* 32(38), pp. 4586-4592.

Cheaib, M. & Simon, M., 2013. Dynamic chromatin remodelling of ciliate macronuclear DNA as determined by an optimised chromatin immunoprecipitation (ChIP) method for Paramecium tetraurelia. *Applied Microbiology and Biotechnology,* Volume 97, pp. 2661-2670.

Chen, E. C. et al., 2015. Targeted Disruption of Organic Cation Transporter 3 Attenuates the Pharmacologic Response to Metformin. *Mol Pharmacol,* 88(1), p. 75–83.

Cheng, Y. et al., 2019. Targeting epigenetic regulators for cancer therapy: mechanisms and advances in clinical trials. *Signal Transduction and Targeted Therapy,* Volume 4, p. 62.

Chen, J. et al., 2016. The oncometabolite R-2-hydroxyglutarate activates NF-κB-dependent tumor-promoting stromal niche for acute myeloid leukemia cells. *Scientific Reports,* Volume 6, p. 32428.

Chen, L. et al., 2020. BRDT promotes ovarian cancer cell growth. *Cell Death & Disease,* Volume 11, p. 1021.

Chen, L. et al., 2014. Succinate dehydrogenase subunit B inhibits the AMPK-HIF-1α pathway in human ovarian cancer in vitro. *Journal of Ovarian Research,* Volume 7, p. 115.

Chen, T. et al., 2003. Establishment and Maintenance of Genomic Methylation Patterns in Mouse Embryonic Stem Cells by Dnmt3a and Dnmt3b. *Mol Cell Biol. ,* 23(16), pp. 5594-5605.

Chernukhin, I. et al., 2011. BioVyon Protein A, an alternative solid-phase affinity matrix for chromatin immunoprecipitation. *Analytical Biochemistry,* 412(2), pp. 183-188.

Chiang, J., Karlan, B. Y., Cass, I. & Baldwin, R. L., 2006. BRCA1 promoter methylation predicts adverse ovarian cancer prognosis. *Gynecologic Oncology,* 101(3), pp. 403-410.

Chinopoulos, C., 2013. Which way does the citric acid cycle turn during hypoxia? The critical role of α-ketoglutarate dehydrogenase complex. *Special Issue: Brain Energy Metabolism: Bioenergetics of Neurological Disease and Aging,* 91(8), pp. 1030-1043.

Christman, J. K., 2002. 5-Azacytidine and 5-aza-2'-deoxycytidine as inhibitors of DNA methylation: mechanistic studies and their implications for cancer therapy. *Oncogene,* Volume 21, p. 5483–5495.

Chung, J., Uchida, E., Grammar, T. C. & Blenis, J., 1997. STAT3 Serine Phosphorylation by ERK-Dependent and Independent Pathways Negatively Modulates its Tyrosine Phosphorylation. *Molecular and Cellular Biology,* 17(11), pp. 6508-6516.

Collas, P., 2010. The Current State of Chromatin Immunoprecipitati. *Mol Biotechnol,* Volume 45, p. 87–100.

Coloff, J. L. et al., 2016. Differential Glutamate Metabolism in Proliferating and Quiescent Mammary Epithelial Cells. *Cell Metabolism,* 23(5), pp. 867-880.

Colvin , H. et al., 2016. Oncometabolite D-2-Hydroxyglurate Directly Induces Epithelial-Mesenchymal Transition and is Associated with Distant Metastasis in Colorectal Cancer. *Sci Rep,* Volume 6, p. 36289.

Corney, D. C. et al., 2010. Frequent Downregulation of miR-34 Family in Human Ovarian Cancers. *Clin Cancer Res,* Volume 16, pp. 1119-1128.

Coscia, F. et al., 2016. Intregrative proteomic profiling of ovarian cancer cell lines reveals precursor cell associated with proteins and functional status. *Nat Commun.,* Volume 7, p. 12645.

Cull, A. H. et al., 2017. Tet2 restrains inflammatory gene expression in macrophages. *Experimental Hematology,* Volume 55, pp. 56-70.e13.

Cuyàs, E. et al., 2018. Metformin regulates global DNA methylation via mitochondrial one-carbon metabolism. *Oncogene,* Volume 37, p. 963–970.

Dando, I. et al., 2019. Oncometabolites in cancer aggressiveness and tumour repopulation. *Biol. Rev.,* Volume 94, p. 1530–1546.

Dang, L. et al., 2009. Cancer-associated IDH1 mutations produce 2-hydroxyglurate. *Nature,* 462(7274), p. 739.

D'Antongiovanni, V. et al., 2017. The microenvironment induces collective migration in SDHB-silenced mouse pheochromocytoma spheroids. *Endocrine-Related Cancer,* 24(10), p. 555–564.

Däster, S. et al., 2017. Induction of hypoxia and necrosis in multicellular tumor spheroids is associated with resistance to chemotherapy treatment. *Oncotarget,* 8(1), p. 1725–1736.

De Larco, J. E. et al., 2003. Atypical methylation of the interleukin-8 gene correlates strongly with the metastatic potential of breast carcinoma cells. *Proc Natl Acad Sci U S A. ,* 100(24), p. 13988–13993.

DeBerardinis, R. J. et al., 2007. Beyond aerobic glycolysis: transformed cells can engage in glutamine metabolism that exceeds the requirement for protein and nucleotide synthesis. *Proc Natl Acad Sci U S A,* 104(49), pp. 19345 - 19350.

Deng, X., He, Y., Miao, X. & Yu, B., 2021. ATF4-mediated histone deacetylase HDAC1 promotes the progression of acute pancreatitis. *Cell Death & Disease ,* Volume 12, p. 5.

Denkert, C. et al., 2006. Mass Spectrometry–Based Metabolic Profiling Reveals Different Metabolite Patterns in Invasive Ovarian Carcinomas and Ovarian Borderline Tumors. *Cancer Res,* 66(22), pp. 10795-804.

Desoize, B. & Jardillier, J., 2000. Multicellular resistance: a paradigm for clinical resistance?. *Crit Rev Oncol Hematol,* 36(2-3), pp. 193-207.

Dimberg, J. et al., 2012. DNA promoter methylation status and protein expression of interleukin-8 in human colorectal adenocarcinomas. *Int J Colorectal Dis.,* 27(6), p. 709–714.

Du, J. et al., 2005. AICAR stimulates IL-6 production via p38 MAPK in cardiac fibroblasts in adult mice: A possible role for AMPK,. *Biochemical and Biophysical Research Communications,* 337(4), pp. 1139-1144.

Dvořák, A. et al., 2017. Background levels of neomorphic 2-hydroxyglutarate facilitate proliferation of primary fibroblasts. *Physiol Res,* 66(2), pp. 293-304.

Eisfeld, A. et al., 2017. Mutations in the CCND1 and CCND2 genes are frequent events in adult patients with t(8;21)(q22;q22) acute myeloid leukemia. *Leukemia,* 31(6), p. 1278–1285.

Elloul, S. et al., 2010. Mesenchymal-to-epithelial transition determinants as characteristics of ovarian carcinoma effusions. *Clin Exp Metastasis,* Volume 27, p. 161–172.

Ersoy, C. et al., 2008. The effect of metformin treatment on VEGF and PAI-1 levels in obese type 2 diabetic patients. *Diabetes Res. Clin. Pract,* Volume 81, pp. 56-60.

Esparza-López, J. et al., 2019. Metformin reverse mesenchymal phenotype of primary breast cancer cells through STAT3/NF0kB pathways. *BMC Cancer,* Volume 19, p. 728.

Esteller, M., 2008. Epigenetics in cancer. *N Engl J Med,* Volume 358, p. 1148–1159.

Fan, J. et al., 2015. Human Phosphoglycerate Dehydrogenase Produces the Oncometabolite D-2-Hydroxyglutarate. *ACS Chem Biol. ,* 10(2), pp. 510 - 516.

Ficz, G. & Gribben, J. G., 2014. Loss of 5-hydroxymethylcytosine in cancer: Cause or consequence?. *Genomics,* 104(5), pp. 352 - 357.

Figuero, M. E. et al., 2010. Leukaemic IDH1 and IDH2 mutations results in a hypermethylated phenotype, disrupt TET2 function and impair haematopoietic differentiation. *Cancer Cell,* 18(6), pp. 553 - 567.

Flores, R. E. et al., 2018. Mycoplasma infection and hypoxia initiate succinate accumulation and release in the VM-M3 cancer cells. *Biochimica et Biophysica Acta (BBA) - Bioenergetics,* 1859(9), pp. 975-983.

Fong, M. Y., McDunn, J. & Kakar, S. S., 2011. Identification of Metabolites in the Normal Ovary and Their Transformation in Primary and Metastatic Ovarian Cancer. *PLoS ONE,* 6(5), p. e19963.

Foran, E. et al., 2010. Upregulation of DNA methyltransferase-mediated gene silencing, anchorage-independent growth, and migration of colon cancer cells by interleukin-6. *Mol Cancer Res,* 8(4), pp. 471-81.

Fornes, O. et al., 2020. JASPAR 2020: update of the open-access database of transcription factor binding profiles. *Nucleic Acids Res,* 48(D1), pp. D87-D92.

Francavilla, C. et al., 2017. Phosphoproteomics of Primary Cells Reveals Druggable Kinase Signatures in Ovarian Cancer. *Cell Report ,* 18(13), pp. 3242 - 3256.

Fu, S. et al., 2011. Phase 1b-2a study to reverse platinum resistance through use of a hypomethylating agent, azacitidine, in patients with platinum-resistant or platinum-refractory epithelial ovarian cancer. *Cancer,* 117(8), pp. 1661-1669.

Fu, X. et al., 2015. 2-Hydroxyglutarate Inhibits ATP Synthase and mTOR Signaling. *Cell Metab.,* 22(3), p. 508–515.

Fu, X. et al., 2015. 2-Hydroxyglutarate Inhibits ATP Synthase and mTOR Signalling.. *Cell Metab,* 22(3), pp. 508-515.

Gade, P. & Kalvakolanu, D. V., 2012. Chromatin Immunoprecipitation Assay as a Tool for Analyzing Transcription Factor Activity.. In: A. Vancura, ed. *Transcriptional Regulation. Methods in Molecular Biology (Methods and Protocols).* New York, NY: Springer, pp. 85-104.

García-Calzón, S. et al., 2017. Diabetes medication associates with DNA methylation of metformin transporter genes in the human liver. *Clinical Epigenetics,* Volume 9, p. 102.

Gasche, J. A., Hoffmann, J., Boland, R. & Goel, A., 2011. Interleukin-6 promotes tumorigenesis by altering DNA methylation in oral cancer cells. *Carcinogenesis,* 129(5), pp. 1053-1063.

Gharavi, N. M. et al., 2007. Role of the JAK/STAT Pathway in the Regulation of Interleukin-8 Transcription by Oxidized Phospholipids in Vitro and in Atherosclerosis in Vivo. *Lipids and Liproproteins,* 282(43), pp. 31460-31468.

Gifford, G. et al., 2004. The acquisition of hMLH1 methylation in plasma DNA after chemotherapy predicts poor survival for ovarian cancer patients. *Clin. Cancer Res.,* Volume 10, p. 4420–4426.

Gong, F. et al., 2017. Epigenetic silencing of TET2 and TET3 induces an EMT-like process in melanoma. *Oncotarget,* 8(1), pp. 315-328.

Gotlieb, W. H. et al., 1998. Intraperitoneal pressures and clinical parameters of total paracentesis for palliation of symptomatic ascites in ovarian cancer.. *Gynecol Oncol.,* 71(3), pp. 381-385.

Gotlieb, W. H. et al., 2008. In vitro metformin anti-neoplastic activity in epithelial ovarian cancer. *Gynaecologic Oncology,* 110(2), pp. 246 - 250.

Grant, C. E., Bailey, T. L. & Stafford Noble, W., 2011. FIMO: Scanning for occurrences of a given motif. *Bioinformatics,* 27(7), pp. 1017-1018.

Gravel, S. et al., 2014. Serine Deprivation Enhances Antineoplastic Activity of Biguanides. *Cancer Res,* 74(24), pp. 7521-7533.

Gregory, R. I. & Shiekhattar, R., 2005. MicroRNA biogenesis and cancer. *Cancer Res,* Volume 65, pp. 3509-3512.

Greulich, F., Mechtidou, A., Horn, T. & Uhlenhaut, N. H., 2021. Protocol for using heterologous spike-ins to normalize for technical variation in chromatin immunoprecipitation. *STAR Protocols,* 2(3), p. 100609.

Grisham, R. N., 2016. Low-Grade Serous Carcinoma of the Ovary. *Oncology (Williston Park),* 30(7), pp. 650 - 652.

Gu, C. et al., 2020. Melatonin alleviates progression of uterine endometrial cancer by suppressing estrogen/ubiquitin C/SDHB-mediated succinate accumulation. *Cancer Letters,* Volume 476, pp. 34-47.

Gui, D. Y. et al., 2016. Environment Dictates Dependence on Mitochondrial Complex I for NAD+ and Aspartate Production and Determines Cell Sensitivity to Metformin. *Cell Metabolism,* 24(5), pp. 716-727.

Guilhamon, P. et al., 2013. Meta-analysis of IDH-mutant cancers identifies EBF1 as an interaction partner for TET2. *Nat Commun. ,* Volume 4, p. 2166.

Guo, H. et al., 2019. Reversal of obesity-driven aggressiveness of endometrial cancer by metformin. *American Journal of Cancer Research,* 9(10), pp. 2170-2193.

Gupta, V. K. et al., 2021. Hypoxia-Driven Oncometabolite L-2HG Maintains Stemness-Differentiation Balance and Facilitates Immune Evasion in Pancreatic Cancer. *Cancer Res,* 81(15), pp. 4001-4013.

Gu, T. P. et al., 2011. The role of Tet3 DNA dioxygenase in epigenetic reprogramming by oocytes. *Nature,* 477(7366), pp. 606-610.

Hall, E. et al., 2018. The effects of high glucose exposure on global gene expression and DNA methylation in human pancreatic islets. *Molecular and Cellular Endocrinology,* Volume 472, pp. 57-67.

Hamedi, B. et al., 2018. Combination of Metformin and Chemotherapy decreases the Recurrence Rates of Epithelial Ovarian Cancers: A randomised Clinical Trial. *International Journal of Cancer Management,* 11(7), p. e11621.

Handy, D. E., Castro, R. & Loscalzo, J., 2011. Epigenetic Modifications: Basic Mechanisms and Role in Cardiovascular Disease. *Circulation,* 123(19), pp. 2145 - 2156.

Han, J. et al., 2018. Elevated d-2-hydroxyglutarate during colitis drives progression to colorectal cancer. *PNAS,* 115(5), pp. 1057-1062.

Han, L. et al., 2011. High glucose promotes pancreatic cancer cell proliferation via the induction of EGF expression and transactivation of EGFR. *PLoS One,* 6(11), p. e27074.

Haring, M. et al., 2007. Chromatin immunoprecipitation: optimization, quantitative analysis and data normalization. *Plant Methods,* 3(11).

Hasnain, S. Z. et al., 2012. The interplay between endoplasmic reticulum stress and inflammation. *Immunol Cell Biol.,* 90(3), pp. 260-270.

Hayashi, Y., Yokota, A., Harada, H. & Huang, G., 2019. Hypoxia/pseudohypoxia-mediated activation of hypoxia-inducible factor-1α in cancer. *Cancer Sci.,* 110(5), p. 1510–1517.

Helmlinger, G. et al., 2002. Acid production in glycolysis-impaired tumors provides new insights into tumor metabolism. *Clinical Cancer Research,* Volume 8, p. 1284–1291.

He, L. & Wondisford, F. E., 2015. Metformin Action: Concentrations Matter. *Cell Metabolism ,* 21(2), pp. 159-162.

Henriksen, J. H., Stage, J. G., Schlichting, P. & Winkler, K., 1980. Intraperitoneal pressure: ascitic fluid and splanchnic vascular pressures, and their role in prevention and formation of ascites.. *Scand J Clin Lab Invest.,* 40(6), pp. 493-501.

Herrera, C. A. et al., 2002. Expression of metastasis-related genes in human epithelial ovarian tumors. *Int J Oncol,* Volume 20, pp. 5-13.

He, W. P. et al., 2015. Decreased expression of H3K27me3 in human ovarian carcinomas correlates with more aggressive tumor behavior and poor patient survival. *Neoplasma,* 62(6), pp. 932-7.

Hill, P. W. S., Amouroux, R. & Hajkova, P., 2014. DNA demethylation, Tet proteins and 5-hydroxymethylcytosine in epigenetic reprogramming: An emerging complex story. *Genomics,* 104(5), pp. 324-333.

Hilvo, M. et al., 2016. Accumulated metabolites of hydroxybutyric acid serve as diagnostic and prognostic biomarkers of ovarian high-grade serous carcinomas. *Cancer Res.,* 76(4), p. 796–804.

Hodeiba, M. et al., 2017. Metformin and phenformin inhibit cell proliferation and alter metabolism in high-grade serous ovarian cancer (HGSC). *Gynaecologic Oncology ,* 145(Supplement 1), p. 119.

Hodge, D. R. et al., 2001. Interleukin-6 Regulation of the Human DNA Methyltransferase (HDNMT) Gene in Human Erythroleukemia Cells. *Accelerated Publication,* 276(43), pp. 39508-39511.

Huang, N. et al., 2009. Metformin inhibits TNF-a induced IkB kinase phosphorylation, IkB-a degradation and IL-6 production in endothelial cells through PI3K-dependent AMPK phosphorylation. *International Journal of Cardiology,* Volume 134, pp. 169-175.

Huang, R. et al., 2012. DNA methylation of the IGF2/H19 imprinting control region and adiposity distribution in young adults. *Clinical Epigenetics,* Volume 4, p. 21.

Huang, Y. et al., 2014. Distinct roles of the methylcytosine oxidases Tet1 and Tet2 in mouse embryonic stem cells. *PNAS,* 111(4), pp. 1361-1366.

Huang, Y. & Rao, A., 2014. Connections between TET proteins and aberrant DNA modification in cancer. *Trends Genet. ,* 30(10), pp. 464-474.

Hudson, L. G., Zeineldin, R. & Stack, M. S., 2008. Phenotypic plasticity of neoplastic ovarian epithelium: unique cadherin profiles in tumor progression. *Clin. Exp. Metastasis,* Volume 25, pp. 643-655.

Hunter, A. L. et al., 2019. An improved method for quantitative ChIP studies of nuclear receptor function. *Journal of Molecular Endocrinology ,* 62(4), pp. 169-177.

Hyler, A. R. et al., 2018. Fluid shear stress impacts ovarian cancer cell viability, subcellular organisation, and promotes genomic instability. *PLoS One,* 13(3), p. e0194170.

Intlekofer, A. M. et al., 2015. Hypoxia Induces Production of L-2-Hydroxxyglutarate. *Cell Metabolism,* 22(2), pp. 304 - 311.

Iorio, M. et al., 2007. MicroRNA Signatures in Human Ovarian Cancer. *Cancer Research,* Volume 67, pp. 8699-8707.

Ip, C. K. et al., 2016. Stemness and chemoresistance in epithelial ovarian carcinoma cells under shear stress. *Scientific Reports,* Volume 6, p. 26788.

Ishida, K. et al., 2012. Interleukin-6 Gene Promoter Methylation in Rheumatoid Arthritis and Chronic Periodontitis. *Translational Periodontology,* 83(7), pp. 917-925.

Itoh, H. et al., 2018. TET2-dependent IL-6 induction mediated by the tumour microenvironment promotes tumour metastasis in osteosarcoma. *Oncogene,* 37(22), pp. 2903-2920.

Ito, S. et al., 2011. Tet proteins can convert 5-methylcytosine to 5-formylcytosine and 5-carboxylcytosine. *Science,* 333(6047), pp. 1300 - 1303.

Ivarsson, K. et al., 2000. Upregulation of interleukin-8 and polarized epithelial expression of interleukin-8 receptor A in ovarian carcinomas. *Acta Obstet Gynecol Scand,* Volume 79, pp. 777-784.

Iwanicki, M. P. et al., 2011. Ovarian Cancer Spheroids Use Myosin-Generated Force to Clear the Mesothelium. *Cancer Discovery ,* 1(2), pp. 144 - 157.

Iwasaki, Y. et al., 2014. Activating Transcription Factor 4 Links Metabolic Stress to Interleukin-6 Expression in Macrophages. *Diabetes,* 63(1), pp. 152-161.

Izutsu, N. et al., 2008. Epigenetic modification is involved in aberrant expression of class III β-tubulin, TUBB3, in ovarian cancer cells. *Int J Oncol,* Volume 32, pp. 1227-1235.

Jacinto, F. V., Ballestar, E. & Esteller, M., 2008. Methyl-DNA immunoprecipitation (MeDIP): hunting down the DNA methylome. *Biotechniques,* 44(1), pp. 35, 37, 39.

Jackson, A. L. et al., 2017. Phenformin has anti-tumorigenic effects in human ovarian cancer cells and in an orthotopic mouse model of serous ovarian cancer. *Oncotarget,* 8(59), pp. 100113-100127.

Jackson, A. L. et al., 2017. Phenformin has anti-tumorigenic effects in human ovarian cancer cells in an orthotopic mouse model of serous ovarian cancer. *Oncotarget,* 8(59), pp. 100113-100127.

Javeshghani, S. et al., 2012. Carbon source and myc expression influence the antiproliferative actions of metformin. *Cancer Res,* 72(23), pp. 6257 - 6267.

Jin, G. et al., 2017. Combination curcumin and (−)-epigallocatechin-3-gallate inhibits colorectal carcinoma microenvironment-induced angiogenesis by JAK/STAT3/IL-8 pathway. *Oncogenesis,* Volume 6, p. e384.

Jin, K. L. et al., 2008. Expression profile of histone deacetylases 1, 2 and 3 in ovarian cancer tissues. *Journal of Gynecologic Oncology,* 19(3), pp. 185-190.

Jin, Y. et al., 2014. Pathological and prognostic significance of hypoxia-inducible factor 1α expression in epithelial ovarian cancer: a meta-analysis. *Tumor Biology,* Volume 35, p. 8149–8159.

Johnson, D. E., O'Keefe, R. A. & Grandis, J. R., 2018. Targeting the IL-6/JAK/STAT3 signalling axis in cancer. *Nature Reviews: Clinical Oncology,* 15(4), pp. 234 - 248.

Jones, P. A., 2012. Functions of DNA methylation: islands, start sites, gene bodies and beyond. *Nature Reviews Genetics,* 13(7), pp. 484 - 492.

Jones, P. A., Issa, J.-P. J. & Baylin, S., 2016. Targeting the cancer epigenome for therapy. *Nature Epigenetics,* Volume 17, pp. 630-642.

Joyce, B. T. et al., 2015. Longitudinal Study of DNA Methylation of Inflammatory Genes and Cancer Risk. *Cancer Epidemiol Biomarkers Prev.,* 24(10), pp. 1531-1538.

Kafer, G. R. et al., 2016. 5-Hydroxymethylcytosine marks sites of DNA damage and promotes genome stability. *Cell Reports,* Volume 14, pp. 1283-1292.

Kajbaf, F., De Broe, M. E. & Lalau, J., 2015. Therapeutic Concentrations of Metformin: A Systematic Review. *Clinical Pharmacokinetics,* Volume 55, p. 439–459.

Kalkat, M. et al., 2017. MYC Deregulation in Primary Human Cancers. *Genes (Basel),* 8(6), p. 151.

Kantak, S. S. & Kramer, R. H., 1998. E-cadherin Regulates Anchorage-independent Growth and Survival in Oral Squamous Cell Carcinoma Cells. *Cell Biology and Metabolism,* 273(27), pp. 16953-16961.

Kapałczyńska, M. et al., 2018. 2D and 3D cell cultures – a comparison of different types of cancer cell cultures. *Arch Med Sci.,* 14(4), p. 910–919.

Kassim, S. K. et al., 2004. Vascular endothelial growth factor and interleukin-8 are associated with poor prognosis in epithelial ovarian cancer patients. *Clinical Biochemistry,* 37(5), pp. 363-369.

Kellenberger, L. D. et al., 2010. The Role of Dysregulated Glucose Metabolism in Epithelial Ovarian Cancer. *Journal of Oncology,* Volume 2010, p. 514310.

Keller, C. A. et al., 2021. Effects of sheared chromatin length on ChIP-seq quality and sensitivity. *G3,* 11(6), p. jkab101.

Kent, W. J. et al., 2002. The human genome browser at UCSC. *Genome Res.,* 12(6), pp. 996-1006.

Kerins, M. J. et al., 2017. Fumarate Mediates a ChronicProliferative Signal in FumarateHydratase-Inactivated Cancer Cells byIncreasing Transcription and Translationof Ferritin Genes. *Molecular and Cellular Biology,* 37(11), pp. e00079-17.

Kes, M. M. G., Van den Bossche, J., Griffioen, A. W. & Huijbers, E. J. M., 2020. Oncometabolites lactate and succinate drive pro-angiogenic macrophage response in tumors. *Biochimica et Biophysica Acta (BBA) - Reviews on Cancer,* 1874(2), p. 188427.

Khoja, H., Smejkal, G., Krowczynska, A. & Herlihy, J. D., 2019. *Optimizing Sample Fixation and Chromatin Shearing forImproved Sensitivity and Reproducibility of ChromatinImmunoprecipitation,* Woburn, Massachusetts: Covaris Application Note.

Kim, J., Choi, H., Kim, S. & Lee, D., 2019. The PAK1-Stat3 Signaling Pathway Activates IL-6 Gene Transcription and Human Breast Cancer Stem Cell Formation. *Cancers,* 11(10), p. 1527.

Kim, J. et al., 2012. High-grade serous ovarian cancer arises from fallopian tube in a mouse model. *PNAS,* 109(10), pp. 3921 - 3926.

King, A., Selak, M. A. & Gottlieb, E., 2006. Succinate dehydrogenase and fumarate hydratase: linking mitochondrial dysfunction and cancer. *Oncogene,* Volume 25, p. 4675–4682.

Kinnaird, A., Zhao, S., Wellen, K. E. & Michelakis, E. D., 2016. Metabolic control of epigenetics in cancer. *Nature Reviews Cancer,* Volume 16, pp. 694-707.

Kipps, E., Tan, D. S. P. & Kaye, S. B., 2013. Meeting the challenge of ascites in ovarian cancer: new avenues for therapy and research. *Nature Reviews Cancer,* Volume 13, pp. 273 - 282.

Kiraly, O. et al., 2015. Inflammation-Induced Cell Proliferation Potentiates DNA Damage-Induced Mutations In Vivo. *PLoS Genet.,* 11(2), p. e1004901.

Klymenko, Y. et al., 2017c. Heterogeneous Cadherin Expression and Multicellular Aggregate Dynamics in Ovarian Cancer Dissemination.. *Neoplasia,* 19(7), pp. 549-563.

Klymenko, Y. et al., 2017a. Cadherin composition and multicellular aggregate invasion in organotypic models of epithelial ovarian cancer intraperitoneal metastasis.. *Oncogene,* 36(42), pp. 5840-5851.

Klymenko, Y., Kim, O. & Stack, M. S., 2017b. Complex Determinants of Epithelial: Mesenchymal Phenotypic Plasticity in ovarian Cancer. *Cancers,* 9(8), p. E104.

Klymenko, Y. et al., 2018. Modeling the effect of ascites-induced compression on ovarian cancer multicellular aggregates. *Dis Model Mech.,* 11(9), p. dmm034199.

Kobayahi, T., Ishida, K. & Yoshie, H., 2016. Increased expression of interleukin-6 (IL-6) gene transcript in relation to IL-6 promoter hypomethylation in gingival tissue from patients with chronic periodontitis. *Archives of Oral Biology ,* Volume 69, pp. 89-94.

Koch, A. E. et al., 1992. Interleukin-8 as a Macrophage-Derived Mediator of Angiogenesis. *Science,* 258(5089), pp. 1798-1801.

Ko, H. et al., 2015. Regulation of Cigarette Smoke Induction of IL-8 in Macrophages by AMP-activated Protein Kinase Signaling. *Journal of Cellular Physiology,* 230(8), pp. 1781-1793.

Kohli, R. M. & Zhang, Y., 2013. TET enzymes, TDG and the dynamics of DNA demethylation. *Nature,* 502(7472), pp. 472 - 479.

Kohn, S. et al., 2013. Anti-inflammatory mechanism of metformin and its effect in intestinal inflammation and colitis-associated colon cancer. *Gastroentrology ,* 29(3), pp. 502-510.

Ko, M. et al., 2013. Modulation of TET2 expression and 5-methylcytosine oxidation by the CXXC domain protein IDAX. *Nature,* Volume 497, p. 122–126.

Kong, L. et al., 2016. A primary role of TET proteins in establishment and maintenance of De Novo bivalency at CpG islands. *Nucleic Acids Research,* 44(18), p. 8682–8692.

Kroemer, G. & Pouyssegur, J., 2008. Tumour Cell Metabolism: Cancer's Achilles' Heel. *Cancer Cell,* 13(6), pp. 472 - 482.

Kryczek, I. et al., 2000. IL-6 production in ovarian carcinoma is associated with histiotype and biological characteristics of the tumour and influences local immunity. *Br J Cancer,* 82(3), pp. 621-628.

Kumar, S. et al., 2014. Metformin intake associates with better survival in ovarian cancer: A case control study. *Cancer,* 119(3), pp. 555 - 562 .

Kurman, R. J. & Shih, I.-M., 2010. The Origin and Pathogenesis of Epithelial Ovarian Cancer- a Proposed Unifying Theory. *Am J Surg Pathol.,* 34(3), pp. 433-443.

Kwon, M. et al., 2010. Derepression of CLDN3 and CLDN4 during ovarian tumorigenesis is associated with loss of repressive histone modifications. *Carcinogenesis,* 31(6), p. 974–983.

Labidi-Galy, S. I. et al., 2017. High grade serous ovarian carcinomas originate in the fallopian tube. *Nature Communications,* Volume 8, p. 1093.

Lagies, S. et al., 2020. Cells grown in three-dimensional spheroids mirror in vivo metabolic response of epithelial cells. *Communications Biology,* Volume 3, p. 246.

Lal-Nag, M. et al., 2017. A High-Throughput Screening Model of the Tumor Microenvironment for Ovarian Cancer Cell Growth. *SLAS Discovery,* 22(5), p. 494–506.

Lamkin, D. M. et al., 2009. Glucose as a prognostic factor in ovarian carcinoma. *Cancer,* 115(5), p. 1021–1027.

Langdon, S. P. et al., 1988. Characterization and Properties of Nine Human Ovarian Adenocarcinoma Cell Lines. *CANCER RESEARCH,* Volume 48, pp. 6166-6172.

Laukka, T. et al., 2016. Fumarate and Succinate Regulate Expression of Hypoxia-inducible Genes via TET Enzymes. *J Biol Chem. ,* 291(8), pp. 4256-4265.

Lee, C. et al., 2009. MicroRNA Profiling of BRCA1/2 Mutation-Carrying and Non-Mutation-Carrying High-Grade Serous Carcinomas of Ovary. *PLoS One,* 4(10), p. e7314.

Lee, D. J. et al., 2019. Impact of metformin on disease control and survival in patients with head and neck cancer: a retrospective cohort study. *Journal of Otolaryngology - Head & Neck Surgery,* Volume 48, p. 34.

Lee, H. et al., 2009. Persistently Activated Stat3 Maintains Constitutive NF-κB Activity in Tumors. *Cancer Cell,* 15(4), pp. 283-293.

Lee, J. M. et al., 2013. A three-dimensional microenvironment alters protein expression and chemosensitivity of epithelial ovarian cancer cells in vitro. *Laboratory Investigation,* Volume 93, p. 528–542.

Lee, M. et al., 2019. Targeting STAT3 and oxidative phosphorylation in oncogene-addicted tumours. *Redox Biology,* Volume 25, p. 101073.

Lee, P. S. et al., 2010. Elevated MAL expression is accompanied by promoter hypomethylation and platinum resistance in epithelial ovarian cancer. *Int. J. Cancer,* Volume 126, p. 1378–1389.

Lega, I. C. et al., 2013. Association Between Metformin Therapy and Mortality After Breast Cancer. *Diabetes Care,* 36(10), pp. 3018-3026.

Lehmann, U. et al., 2002. Promoter hypermethylation of the death-associated protein kinase gene in breast cancer is associated with the invasive lobular subtype.. *Cancer Res.,* Volume 62, p. 6634–6638.

Leidgens, V. et al., 2017. Stattic and metformin inhibit brain tumour initiating cells by reducing STAT3 phosphorylation. *Oncotarget,* 8(5), pp. 8250-8263.

Lengyel, E., 2010. Ovarian Cancer Development and Metastasis. *The American Journal of Pathology,* 177(3), pp. 1053-1064.

Liang, Y. et al., 2020. TET2 promotes IL-1β expression in J774.1 cell through TLR4/MAPK signaling pathway with demethylation of TAB2 promoter. *Molecular Immunology,* Volume 126, pp. 136-142.

Liao, J. et al., 2014. Ovarian Cancer Spheroid Cells with Stem Cell-Like Properties Contribute to Tumor Generation, Metastasis and Chemotherapy Resistance through Hypoxia-Resistant Metabolism. *PLoS One,* 7(9), p. e84941.

Liao, J. et al., 2014. Ovarian Cancer Spheroid Cells with Stem Cell-Like Properties Contribute to Tumour Generation, Metastasis and Chemotherapy Resistance through Hypoxia-Resistant Metabolism. *PLOS ONE,* 9(1), p. e84941.

Li, A. et al., 2021. ATF4-mediated GDF15 suppresses LPS-induced inflammation and MUC5AC in human nasal epithelial cells through the PI3K/Akt pathway. *Life Sciences,* Volume 275, p. 119356.

Li, F. & Simon, M. C., 2020. Cancer Cells Don't Live Alone: Metabolic. *Developmental Cell,* Volume 54, pp. 183-195.

Li, H. & Zhang, R., 2013. Role of EZH2 in Epithelial Ovarian Cancer: From Biological Insights to Therapeutic Target.. *Front Oncol. ,* 13(3), p. 47.

Li, L. C. & Dahiya, R., 2002. MethPrimer: designing primers for methylation PCRs. *Bioinformatics,* 18(11), pp. 1427-31.

Li, L. et al., 2016. Epigenetic inactivation of CpG demethylase TET1 as a DNA methylation feedback loop in human cancer. *Scientific Reports,* Volume 6, p. 26591.

Li, M. et al., 2009. Integrated analysis of DNA methylation and gene expression reveals specific signalling pathways associated with platinum resistance in ovarian cancer. *BMC Medical Genomics ,* Volume 2, p. 34.

Lin, B. et al., 2015. Global analysis of H3K4me3 and H3K27me3 profiles in glioblastoma stem cells and identification of SLC17A7 as a bivalent tumor suppressor gene. *Oncotarget.,* 6(7), p. 5369–5381.

Lin, C. et al., 2013. Metformin enhances cisplatin cytotoxicity by suppressing signal transducer and activator of transcription 3 activity indepdently of the liver kinase B1-AMP activated protein kinase pathway. *Am J Respir Cell Mol Biol,* 49(2), pp. 241-250.

Lio, C.-W.et al., 2016. Tet2 and Tet3 cooperate with B-lineage transcription factors to regulate DNA modification and chromatin accessibility. *eLife,* Volume 5, p. e18290.

Lisanti, S., von Zglinicki, T. & Mathers , J. C., 2012. Standardization and quality controls for the methylated DNA immunoprecipitation technique. *Epigenetics,* 7(6), pp. 615-625.

Liu, L. et al., 2021. The oncometabolite R-2-hydroxyglutarate dysregulates the differentiation of human mesenchymal stromal cells via inducing DNA hypermethylation. *BMC Cancer,* Volume 21, p. 36.

Li, Y. et al., 2009. Azacitidine enhances sensitivity of platinum-resistant ovarian cancer cells to carboplatin through induction of apoptosis. *Am J Obstet Gynecol,* 200(177), p. e1–e9.

Lo, C. et al., 2011. IL-6 Trans-Signalling in Formation and Progression of Malignant Ascites in Ovarian Cancer. *Therapeutics, Targets and Chemical Biology,* 71(2), pp. 424 - 436.

Long, X. et al., 2016. IL-8, a novel messenger to cross-link inflammation and tumor EMT via autocrine and paracrine pathways (Review). *Int J Oncol,* Volume 48, pp. 5-12.

Lord, S. R. et al., 2020. Transcriptomic analysis of human primary breast cancer identifies fatty acid oxidation as a target for metformin. *British Journal of Cancer,* Volume 122, p. 258–265 .

Losman, J. et al., 2013. (R)-2-Hydroxyglutarate is Sufficient to Promote Leukemogenesis and its Effects are Reversible. *Science,* 339(6127), p. 10.1126/science.1231677.

Lu, C. & Thompson, C. B., 2012. Metabolic Regulation of Epigenetics. *Cell Metabolism ,* 16(1), pp. 9 - 17 .

Lu, T., Bankhead III, A., Ljungman, M. & Neamati, N., 2019. Multi-omics profiling reveals key signalling pathways in ovarian cancer controlled by STAT3. *Theranostics,* 9(19), pp. 5478-5496.

Lv, L. et al., 2018. Vpr Targets TET2 for Degradation by CRL4VprBP E3 Ligase to Sustain IL-6 Expression and Enhance HIV-1 Replication. *Molecular Cell,* 70(5), pp. 961-970.e5.

Lyko, F. & Brown, R., 2005. DNA methyltransferase inhibitors and the development of epigenetic cancer therapies. *J Natl Cancer Inst,* Volume 97, p. 1498–1506.

Macciò, A. & Madeddu, C., 2012. Inflammation and ovarian cancer. *Cytokine,* 58(2), pp. 133-147.

MacKenzie, E. D. et al., 2007. Cell-Permeating α-Ketaglutarate Derivatives Alleviate Pseudohypoxia in Succinate Dehydrogenase-Deficient Cells. *American Society for Microbiolog,* 27(9), pp. 3282-3289.

Ma, L. et al., 2019. Low glucose and metformin-induced apoptosis of human ovarian cancer cells is connected to ASK1 via mitochondrial and endoplasmic recticulum stress-associated pathways. *Journal of Experimental & Clinical Cancer Research,* 38(1), p. 77.

Mancini, S. J. et al., 2017. Activation of AMP-activated protein kinase rapidly suppresses multiple pro-inflammatory pathways in adipocytes including IL-1 receptor-associated kinase-4 phosphorylation. *Molecular and Cellular Endocrinology,* Volume 440, pp. 44-56.

Marginean, E. C. et al., 2021. Phosphorylated transducer and activator of transcription-3 (pSTAT3) immunohistochemical expression in paired primary and metastatic colorectal cancer. *Translational Oncology,* 14(2), p. 100996.

Marsh, D. J., Shah, J. S. & Cole, A. J., 2014. Histones and Their Modifications in Ovarian Cancer – Drivers of Disease and Therapeutic Targets. *Front Oncol.,* Volume 4, p. 144.

Masamha, C. P. & LaFontaine, P., 2018. Molecular targeting of glutaminase sensitizes ovarian cancercells to chemotherapy. *J Cell Biochem.,* Volume 119, p. 6136–6145.

Matre, P. et al., 2016. Inhibiting glutaminase in acute myeloid leukemia: metabolic dependency of selected AML subtypes. *Oncotarget.,* 7(48), pp. 79722-79735.

Mattaini, K. R., Sullivan, M. R. & Vander Heiden, M. G., 2016. The importance of serine metabolism in cancer. *J Cell Biol.,* 214(3), pp. 249-257.

Matte, I., Bessette, P. & Piché, A., 2017. Ascites in Ovarian Cancer Progression: Opportunities for Biomarker Discovery and New Avenues for Target Therapies. In: L. Rodrigo, ed. *Ascites - Physiopathology, Treatment, Complications and Prognosis.* EU: InTech, pp. 145 - 163.

Menendez, J. A., Alarcón, T. & Joven, J., 2014. Gerometabolites: The pseudohypoxic aging side of cancer oncometabolites. *Cell Cycle,* 13(5), pp. 699-709.

Menendez, J. A. et al., 2012. Metformin is synthetically lethal with glucose withdrawal in cancer cells. *Cell Cycle,* 11(15), pp. 2782-2792.

Mezzanzanica, D., Canevari, S., Cecco, L. D. & Bagnoli, M., 2011. miRNA control of apoptotic programs: focus on ovarian cancer. *Expert Rev. Mol. Diagn.,* Volume 11, p. 277–286.

Mills, G. B. et al., 1990. Ascitic Fluid from Human Ovarian Cancer Patients Contains Growth Factors Necessary for Intraperitoneal Growth of Human Ovarian Adenocarcinoma Cells. *J. Clin. Invest. ,* Volume 86, pp. 851-855.

Mishra, P. et al., 2018. ADHFE1 is a breast cancer oncogene and induces metabolic reprogramming. *J Clin Invest,* 128(1), pp. 323-340.

Miska, E. A., 2005. How microRNAs control cell division, differentiation, and death. *Curr Opin Genet Dev ,* Volume 5, p. 563–8.

Moser, T. L. et al., 1996. Evidence for preferential adhesion of ovarian epithelial carcinoma cells to type I collagen controlled by the α2β1 integrin. *Int. J. Cancer,* Volume 67, pp. 695-701.

Mukhopadhyay, A., Deplancke, B., Walhout, A. J. M. & Tissenbaum, H. A., 2008. Chromatin immunoprecipitation (ChIP) coupled to detection by quantitative real-time PCR to study transcription factor binding to DNA in Caenorhabditis elegans. *Nat Protoc.,* 3(4), p. 698–709.

Murdoch, C., Monk, P. N. & Finn, A., 1999. Cxc chemokine receptor expression on human endothelial cells. *Cytokine,* Volume 11, pp. 704-712.

Muz, B., de la Puente, P., Azab, F. & Kareem-Azab, A., 2015. The role of hypoxia in cancer progression, angiogenesis, metastasis and resistance to therapy. *Hypoxia (Auckl),* Volume 3, pp. 83 - 92.

Myerburg, M. M. et al., 2010. AMPK Agonists Ameliorate Sodium and Fluid Transport and Inflammation in Cystic Fibrosis Airyway Epithelial Cells. *Am J Respir Cell Mol Biol,* Volume 42 , pp. 676-684.

Nakajima, H. & Kunimoto, H., 2014. TET2 as an epigenetic master regulator for normal and malignant haematopoiesis. *Cancer Sci,* Volume 105, pp. 1093-1099.

Nakamichi, N. et al., 2013. Involvement of carnitine/organic cation transporter OCTN1/SLC22A4 in gastrointestinal absorption of metformin. *J Pharm Sci,* 102(9), pp. 3407-3417.

Nakayama, N. et al., 2008. KRAS or BRAF mutation status is a useful predictor of sensitivity to MEK inhibition in ovarian cancer. *Br J Cancer,* 99(12), p. 2020–2028.

Natanzon, Y., Goode, E. I. & Cunningham, J. M., 2017. Epigenetics in ovarian cancer. *Seminars in Cancer Biology,* S1044-579X(17), pp. 30062 - 7.

National Academies of Sciences, Engineering, and Medicine, 2016. *Ovarian Cancers: Evolving Paradigms in Research and Care..* Washington (DC): National Academies Press (US).

Nerstedt, A. et al., 2010. AMP-activated protein kinase inhibits IL-6-stimulated inflammatory response in human liver cells by suppressing phosphorylation of signal transducer and activator of transcription 3 (STAT3). *Diabetologia,* Volume 53, pp. 2406-2416.

Ness, R. B. et al., 2000. Factors Related to Inflammation of the Ovarian Epithelium and Risk of Ovarian Cancer. *Epidemiology,* 11(2), pp. 111 - 117.

Nguyen, H. T., Tian, G. & Murph, M. M., 2014. Molecular epigenetics in the management of ovarian cancer: are we investigating a rational clinical promise?. *Frontiers in Oncology,* 4(71), pp. 1 - 12.

Nieman, K. M. et al., 2011. Adipocytes promote ovarian cancer metastasis and provide energy for rapid tumor growth. *Nature Medicine,* Volume 17, p. 1498–1503.

Nile, C. J. et al., 2008. Methylation status of a single CpG site in the IL6 promoter is related to IL6 messenger RNA levels and rheumatoid arthritis. *Rheumatoid Arthritis Basic Science Studies,* 58(9), pp. 2686-2693.

Nilsson, M. B., Langley, R. R. & Fidler, I. J., 2005. Interleukin-6 secreted by human ovarian carcinoma cells is a potent proangiogenic cytokine. *Cancer Res,* 65(23), pp. 10794-10800.

Nowicki, S. & Gottlieb, E., 2015. Oncometabolites: tailoring our genes. *FEBS Journal ,* 282(15), pp. 2796-2805.

Oldham, W. M., Clish, C., Yang, Y. & Loscalzo, J., 2015. Hypoxia-mediated increases in L-2-hydroxyglutarate coordinate the metabolic response to reductive stress. *Cell Metab.,* 22(2), pp. 291-303.

Oliveira, N. F. P. et al., 2009. DNA methylation status of the IL8 gene promoter in oral cells of smokers and non-smokers with chronic periodontitis. *Journal of Clinical Periodontology ,* 36(9), pp. 719-725.

O'Neill, L. P., VerMilyea, M. D. & Turner, B. M., 2006. Epigenetic characterization of the early embryo with a chromatin immunoprecipitation protocol applicable to small cell populations. *Nature Genetics,* Volume 38, p. 835–841.

Ono, R. et al., 2002. LCX, leukaemia-associated protein with a CXXC domain, is fused to MLL in acute myeloid leukaemia with trilineage dysplasia having t(10;11)(q22;q23). *Cancer Res.,* Volume 62, pp. 4075-4080.

Ooi, S. K., O'Donnell, A. H. & Bestor, T. H., 2009. Mammalian cytosine methylation at a glance. *J Cell Sci,* 122(Pt 16), pp. 2787-2791.

Owen, M. R., Doran, E. & Halestrap, A. P., 2000. Evidence that metformin exerts its anti-diabetic effects through inhibition of complex I of the mitochondrial respiratory chain. *Biochem. J,* Volume 348, pp. 607 - 614.

Ozols, R. F., 2005. Treatment goals in ovarian cancer. *Int J Gynecol Cancer,* 15(Suppl. 1), pp. 3-11.

Paley, P. J. et al., 1997. Vascular endothelial growth factor expression in early stage ovarian carcinoma. *Cancer,* 80(1), pp. 98-106.

Pan, F., Weeks, O., Yang, F. & Xu, M., 2015. The TET2 interactors and their links to hematological malignancies. *IUBMB Life,* 67(6), pp. 438-445.

Paulsen, M. & Ferguson-Smith, A. C., 2001. DNA methylation in genomic imprinting, development, and disease. *J Pathol.,* 195(1), pp. 97-110.

Pavlova, N. N. & Thompson, C. B., 2016. The Emerging Hallmarks of Cancer Metabolism. *Cell Metab.,* 23(1), pp. 27 - 47 .

Penson, R. T. et al., 2000. Cytokines IL-1beta, IL-2, IL-6, IL-8, MCP-1, GM-CSF and TNFalpha in patients with epithelial ovarian cancer and their relationship to treatment with paclitaxel. *Int J Gynecol Cancer,* 10(1), pp. 33-41.

Pfeifer, G. P., Kadam, S. & Jin, S.-G., 2013. 5-hydroxymethylcytosine and its potential roles in development and cancer. *Epigenetics Chromatin,* Volume 6, p. 10.

Plumb, J. A. et al., 2003. Pharmacodynamic Response and Inhibition of Growth of Human Tumor Xenografts by the Novel Histone Deacetylase Inhibitor PXD101. *Mol Cancer Ther,* 2(8), pp. 721-8.

Plumb, J. A. et al., 2000. Reversal of drug resistance in human tumor xenografts by 2'-deoxy-5-azacytidine-induced demethylation of the hMLH1 gene promoter. *Cancer Res,* Volume 60, p. 6039–6044.

Pollak, M. N., 2012. Investigating Metformin for Cancer Prevention and Treatment: The End of the Beginning. *Cancer Discovery,* Volume 2, pp. 778-790.

Pourgholami, M. H., Ataie-Kachoie, P., Badar, S. & Morris, D. L., 2013. Minocycline inhibits malignant ascites of ovarian cancer through targeting multiple signalling pathways. *Gynaecologic Oncology,* 129(1), pp. 113-119.

Pozza, E. D. et al., 2020. Regulation of succinate dehydrogenase and role of succinate in cancer. *Seminars in Cell & Developmental Biology,* Volume 98, pp. 4-14.

Püschel, F. et al., 2020. Starvation and antimetabolic therapy promote cytokine release and recruitment of immune cells. *PNAS,* 117(18), pp. 9932-9941.

Quentin, T., Steinmetz, M., Poppe, A. & Thoms, S., 2012. Metformin differentially activates ER stress signalling pathways without indicing apoptosis. *Disease models & mechanisms,* 5(2), pp. 259-269.

Raghuraman, S. et al., 2016. The Emerging Role of Epigenetics in Inflammation and Immunometabolism. *Trends in Endocrinology and Metabolism ,* 27(3), pp. 782-795.

Rai, Y. et al., 2018. Mitochondrial biogenesis and metabolic hyperactivation limits the application of MTT assay in the estimation of radiation induced growth inhibition. *Scientific Reports,* Volume 8, p. 1531.

Ramakrishna, M. et al., 2010. Identification of Candidate Growth Promoting Genes in Ovarian Cancer through Integrated Copy Number and Expression Analysis. *PLos ONE,* 5(4), p. e9983.

Ramalingam, P., 2016. Morphologic, Immunophenotypic and Molecular Features of Epithelial Ovarian Cancer. *Oncology (Williston Park),* 30(2), pp. 166 - 176.

Ramussen, K. D. et al., 2019. TET2 binding to enhancers facilitates transcription factor recruitment in hematopoietic cells. *Genome Res.,* 29(4), p. 564–575.

Rasmussen, K. D. & Helin, K., 2016. Role of TET enzymes in DNA methylation, development, and cancer. *Genes Dev.,* 30(7), pp. 733-750.

Rattan, R. et al., 2011. Metformin Suppresses Ovarian Cancer Growth and Metastasis with Enhancement of Cisplatin Cytotoxicity In Vivo. *Neoplasia,* 13(5), pp. 483-491.

Rawluszko-Wieczorek, A. A., Siera, A. & Jagodzinski, P. P., 2015. TET proteins in cancer: Current "state of the art". *Critical Reviews in Oncology/Hematology ,* 96(3), pp. 425-436.

Rego, D. F. et al., 2015. Effects of metformin on head and neck cancer: a systematic review. *Oral Oncol.,* 51(5), pp. 416-22.

Riffle, S. & Hegde, R. S., 2017. Modeling tumor cell adaptations to hypoxia in multicellular tumor spheroids. *J Exp Clin Cancer Res.,* Volume 36, p. 102.

Rizzo, S. et al., 2010. Ovarian Cancer Stem Cell–Like Side Populations Are Enriched Following Chemotherapy and Overexpress EZH2. *Mol Cancer Ther,* 10(2), p. 325–35.

Rogalska, A. et al., 2018. Hyperglycaemia-Associated Dysregulation of O-GlcNAcylation and HIF1A reduces anticancer action of metformin in ovarian cancer cells (SKOV-3). *Int J Mol Sci,* 19(9), p. 2750.

Romero, I. L. et al., 2012. Relationship of Type II Diabetes and Metformin Use to Ovarian Cancer Progression Survival and Chemosensitivity. *Ostet Gynecol,* 119(1), pp. 61 - 67.

Rosen, D. G. et al., 2009. Ovarian cancer: pathology, biology and disease models. *Front Biosci,* Volume 14, pp. 2089 - 2102 .

Saidu, N. E. B. et al., 2018. Dimethyl fumarate is highly cytotoxic in KRAS mutated cancer cells but spares non-tumorigenic cells. *Oncotarget,* 9(10), p. 9088–9099.

Saidu, N. E. B. et al., 2017. Dimethyl Fumarate Controls the NRF2/DJ-1 Axis in Cancer Cells: Therapeutic Applications. *Mol Cancer Ther,* 16(3), pp. 529-539.

Saini, U. et al., 2017. Elevated STAT3 expression in ovarian cancer ascites promotes invasion and metastasis: a potential therapeutic target. *Oncogene,* 36(2), pp. 168-181.

Samanta, D. & Semenza, G. L., 2016. Serine Synthesis Helps Hypoxic Cancer Stem Cells Regulate Redox. *Cancer Res.,* 76(22), pp. 6458-6462.

Sans, M. et al., 2017. Metabolic Markers and Statistical Prediction of Serous Ovarian Cancer Aggressiveness by Ambient Ionization Mass Spectrometry Imaging. *Cancer Res.,* 77(11), pp. 2903-2913.

Sant'Anna-Silva, A. C. et al., 2021. Succinate Anaplerosis Has an Onco-Driving Potential in Prostate Cancer Cells. *Cancers,* 13(7), p. 1727.

Saraei, P., Asadi, I., Kakar, M. & Moradi-Kor, N., 2019. The beneficial effects of metformin on cancer prevention and therapy: a comprehensive review of recent advances. *Cancer Manag Res.,* Volume 11, p. 3295–3313.

Savant, S. S., Sriramkumar, S. & O'Hagan, H. M., 2018. The Role of Inflammation and Inflammatory Mediators in the Development, Progression, Metastasis, and Chemoresistance of Epithelial Ovarian Cancer. *Cancers,* 10(8), p. 251.

Savic, D. et al., 2015. CETCh-seq: CRISPR epitope tagging ChIP-seq of DNA-binding proteins. *Genome Res.,* Volume 10, pp. 1581-1589.

Schöpf, B. et al., 2020. OXPHOS remodeling in high-grade prostate cancer involves mtDNA mutations and increased succinate oxidation. *Nature Communications,* Volume 11, p. 1487.

Schuringa, J., Schepers, H., Vellenga, E. & Kruijer, W., 2001. Ser727-dependent transcriptional activation by association of p300 with STAT3 upon IL-6 stimulation. *FEBS Letters,* 495(1-2), pp. 71-76.

Sciacovelli, M. & Frezza, C., 2016. Oncometabolites: Unconventional triggers of oncogenic signalling cascades. *Free Radic Biol Med.,* Volume 100, pp. 175-181.

Secrist, J. P., Zhou, X. & Richon, V. M., 2003. HDAC inhibitors for the treatment of cancer. *Curr. Opin. Investig. Drugs,* Volume 4, p. 1422–1427.

Seeber, L. M. S. & van Diest, P. J., 2012. Epigenetics in Ovarian Cancer. *Methods Mol Biol,* Volume 863, pp. 253 - 269.

Seidel, H. M. et al., 1995. Spacing of palindromic half sites as a determinant of selective STAT (signal transducers and activators of transcription) DNA binding and transcriptional activity. *Proc Natl Acad Sci U S A,* 92(7), pp. 3041-3045.

Selak, M. A. et al., 2005. Succinate links TCA cycle dysfunction to oncogenesis by inhibiting HIF-α prolyl hydroxylase. *Cancer Cell,* 7(1), pp. 77-85.

Semenza, G. L., Nejfelt, M. K., Chi, S. M. & Antonarakis, S. E., 1991. Hypoxia-inducible nuclear factors bind to an enhancer element located 3' to the human erythropoietin gene. *Proc Natl Acad Sci U S A,* 88(13), pp. 5680-4.

Seok, J. et al., 2019. The oncometabolite d-2-hydroxyglutarate induces angiogenic activity through the vascular endothelial growth factor receptor 2 signaling pathway. *Int J Oncol.,* 54(2), pp. 753-763.

Shackelford, D. B. & Shaw, R. J., 2009. The LKB1-AMPK pathway: metabolism and growth control in tumour suppression. *Nat Rev Cancer,* 9(8), pp. 563 - 575.

Shank, J. J. et al., 2012. Metformin targets ovarian cancer stem cells in vitro and in vivo. *Gynecol Oncol,* 127(2), pp. 390 - 397.

Shanmugasundaram, K. et al., 2014. The Oncometabolite Fumarate Promotes Pseudohypoxia Through Noncanonical Activation of NF-κB Signaling. *THE JOURNAL OF BIOLOGICAL CHEMISTRY,* 289(35), p. 24691–24699.

Shaw, R. J. et al., 2005. The Kinase LKB1 Mediates Glucose Homeostasis in Liver and Therapeutic Effects of Metformin. *Science,* 310(5754), pp. 1642-1646.

Shen-Gunther, J. & Mannel, R. S., 2002. Ascites as a Predictor of Ovarian Malignancy. *Gynaecologic Oncology,* Volume 87, pp. 77 - 83.

Shield, K., Ackland, M. L., Ahmed, N. & Rice, G. E., 2008. Multicellular spheroids in ovarian cancer metasases: Biology and pathology. *Gynaecologic Oncology ,* Volume 113, pp. 143 - 148 .

Shield, K. et al., 2007. α2β1 integrin affects metastatic potential of ovarian carcinoma spheroids by supporting disaggregation and proteolysis. *J Carcinog.,* Volume 6, p. 11.

Shim, E. et al., 2014. L -2-Hydroxyglutarate: An Epigenetic Modifier and Putative Oncometabolite in Renal Cancer. *Cancer Discovery,* Volume 4, pp. 1290-1298.

Siegel, R. L., Miller, K. D. & Jemal, A., 2018. Cancer Statistics. *CA CANCER J CLIN,* Volume 68, pp. 7 - 30.

Singh, A., Wilson, J. W., Schofield, C. J. & Chen, R., 2020. Hypoxia-inducible factor (HIF) prolyl hydroxylase inhibitors induce autophagy and have a protective effect in an in-vitro ischaemia model. *Scientific Reports,* Volume 10, p. 1597.

Singleton, S. et al., 2007. Testis/sperm-specific histone 2B in the sperm of donors and subfertile patients: variability and relation to chromatin packaging. *Human Reproduction,* 22(3), p. 743–750.

Sivalingam, V. N. et al., 2020. Hypoxia and hyperglycaemia determine why some endometrial tumours fail to respond to metformin. *British Journal of Cancer,* Volume 122, pp. 62-71.

Skinner, H. et al., 2021. Addition of Metformin to Concurrent Chemoradiation in Patients With Locally Advanced Non-Small Cell Lung Cancer: The NRG-LU001 Phase 2 Randomized Clinical Trial. *JAMA Oncol.*

Smolle, E., Taucher, V. & Haybeck, J., 2014. Malignant Ascites in Ovarian Cancer and the Role of Targeted Therapeutics. *Anticancer Research,* 34(4), pp. 1553 - 1561.

Sodek, K. L., Ringuette, M. J. & Brown, T. J., 2009. Compact spheroid formation by ovarian cancer cells is associated with contractile behavious and an invasive phenotype. *Int. J. Cancer,* Volume 124, pp. 2060-2070 .

Sorge, S. et al., 2020. ATF4-Induced Warburg Metabolism Drives Over-Proliferation in Drosophila. *Cell Rep.,* 31(7), p. 107659.

Steele, N., Finn, P., Brown, R. & Plumb, J. A., 2009. Combined inhibition of DNA methylation and histone acetylation enhances gene re-expression and drug sensitivity in vivo. *British Journal of Cancer,* Volume 100, p. 758–763.

Stefani, F. A. et al., 2013. Expression, polymorphism and methylation pattern of interleukin-6 in periodontal tissues. *Immunobiology,* Volume 218, p. 1012–1017.

Stewart, D. J., 2007. Mechanisms of resistance to cisplatin and carboplatin. *Crit Rev Oncol Hematol.,* Volume 63, p. 12–31.

Strathdee, G. et al., 2005. Demethylation of the MCJ gene in stage III/IV epithelial ovarian cancer and response to chemotherapy. *Gynecologic Oncology,* 97(3), pp. 898-903.

Struhl, K., 2007. Interpreting Chromatin Immunoprecipitation Experiments. In: D. Zuk, ed. *Evaluating Techniques in Biochemical Research..* Cambridge: Cell Press, pp. 29-33.

Sullivan, L. B., Gui, D. Y. & Vander-Heiden, M. G., 2016. Altered metabolite levels in cancer: implications for tumour biology cancer therapy. *Nat Rev Cancer,* 16(11), pp. 680-693.

Sun, Y. et al., 2017. Genome-Wide STAT3 Binding Analysis after Histone Deacetylase Inhibition Reveals Novel Target Genes in Dendritic Cells. *J Innate Immun.,* 9(2), p. 126–144.

Su, R. et al., 2018. R-2HG Exhibits Anti-tumor Activity by Targeting FTO/m6A/MYC/CEBPA Signaling. *Cell,* 172(1-2), p. 90–105.e23..

Tahiliani, M. et al., 2009. Conversion of 5-Methylcytosine to 5-Hydroxymethylcytosine in Mammalian DNA by MLL Partner TET1. *Science,* 324(5929), pp. 930-935.

Takahashi, A. et al., 2015. Epigenetic regulation of interleukin-8, an inflammatory chemokine, in osteoarthritis. *Osteoarthritis and Cartilage,* 23(11), pp. 1946-1954.

Takai, N. et al., 2006. A novel histone deacetylase inhibitor, Scriptaid, induces growth inhibition, cell cycle arrest and apoptosis in human endometrial cancer and ovarian cancer cells.. *Int J Mol Med,* Volume 17, p. 323–329.

Tanaka, Y. O. et al., 2016. Differentiation of epithelial ovarian cancer subtypes by use of imaging and clinical data: a detailed analysis. *Cancer Imaging ,* Volume 16, p. 3.

Tang, G. et al., 2011. Novel role of AMP-activated protein kinase signalling in cigarette smoke induction of IL-8 in human lung epithelial cells and lung inflammation in mice. *Free Radical Biology and Medicine,* 50(11), pp. 1492-1502.

Tang, M., Etokidem, E. & Lai, K., 2016 . The Leloir Pathway of Galactose Metabolism – A Novel Therapeutic Target for Hepatocellular Carcinoma. *Anticancer Research,* 36(12), pp. 6265-6271.

Tan, L. et al., 2013. Genome-wide comparison of DNA hydroxymethylation in mouse embryonic stem cells and neural progenitor cells by a new comparative hMeDIP-seq method. *Nucleic Acids Research,* 41(7), p. e84.

Tan, X. et al., 2015. Metformin suppresses pancreatic tumour growth with inhibition of NF-kB/STAT3 inflammatory signalling. *Pancreas,* 44(4), pp. 636-647.

Tekpli, X. et al., 2013. DNA methylation at promoter regions of interleukin 1B, interleukin 6, and interleukin 8 in non-small cell lung cancer. *Cancer Immunol Immunother,* Volume 62, p. 337–345.

Terashima, J. et al., 2013. An aryl hydrocarbon receptor induces VEGF expression through ATF4 under glucose deprivation in HepG2. *BMC molecular biology,* Volume 14, p. 27.

Terunuma, A. et al., 2014. MYC-driven accumulation of 2-hydroglutarate is associated with breast cancer prognosis. *J Clin Invest.,* 124(1), pp. 398 - 412.

Tesoriere, A., Dinarello, A. & Argenton, F., 2021. The Roles of Post-Translational Modifications in STAT3 Biological Activities and Functions. *Biomedicines,* 9(8), p. 956.

Thienpont, B. et al., 2016. Tumour hypoxia causes DNA hypermethylation by reducing TET activity. *Nature,* Volume 537, pp. 63-68.

Tian, Y. et al., 2017. Global changes of 5-hydroxymethylcytosine and 5-methylcytosine from normal to tumour tissues are associated with carcinogenesis and prognosis in colorectal cancer. *J Zhejiang Univ Sci B,* 18(9), pp. 747-756.

Timmermans, M. et al., 2018. No improvement in long-term survival for epithelial ovarian cancer patients: A population-based study between 1989 and 2014 in the Netherlands. *Eur J Cancer.,* Volume 88, pp. 31-37.

Tong, K. et al., 2008. Leptin induces IL-8 expression via leptin receptor, IRS-1, PI3K, Akt cascade and promotion of NF-κB/p300 binding in human synovial fibroblasts. *Cellular Signalling,* 20(8), pp. 1478-1488.

Tourkmani, A. M. et al., 2018. Hypoglycemia in Type 2 Diabetes Mellitus patients: A review article. *Diabetes & Metabolic Syndrome: Clinical Research & Reviews,* 12(5), pp. 791-794.

Tretter, L., Patocs, A. & Chinopoulous, C., 2016. Succinate, an intermediate in metabolism, signal transduction, ROS, hypoxia, and tumorigenesis. *Biochimica et Biophysica Acta (BBA) - Bioenergetics,* 1857(8), pp. 1086-1101.

Tseng, P. et al., 2018. Decreased succinate dehydrogenase B in human hepatocellular carcinoma accelerates tumor malignancy by inducing the Warburg effect. *Scientific Reports,* Volume 8, p. 3081.

Tucker, D. W. et al., 2018. Epigenetic Reprogramming Strategies to Reverse Global Loss of 5-Hydroxymethylcytosine, a Prognostic Factor for Poor Survival in High-grade Serous Ovarian Cancer. *Clin Cancer Res,* Volume 24, pp. 1389-1401.

Tucker, D. W., Wang, T. & Zhang, X., 2015. Prognostic values of 5-hmC, 5-mC and TET2 in epithelial ovarian cancer. *Archives of Gynaecology and Obstetrics,* 292(4), pp. 891-897.

Uhlen, M. et al., 2017. A pathology atlas of the human cancer transcriptome. *Science,* 357(6352), p. eaan2507.

van Baal, J. O. A. M. et al., 2018. Development of Peritoneal Carcinomatosis in Epithelial Ovarian Cancer: A Review. *Journal of Histochemistry & Cytochemistry,* 66(2), p. 67 –83.

Veatch, A. L., Carson, L. F. & Ramakrishnan, S., 1994. Differential expression of the cell-cell adhesion molecule E-cadherin in ascites and solid human ovarian tumor cells. *International Journal of Cancer,* 58(3), pp. 393-399.

Venza, I. et al., 2012. PGE2 induces interleukin-8 derepression in human astrocytoma through coordinated DNA demethylation and histone hyperacetylation. *Epigenetics,* 7(11), p. 1315–1330.

Vincent, E. E. et al., 2015. Differential effects of AMPK agonists on cell growth and metabolism. *Oncogene,* Volume 34, p. 3627–3639.

Wagner, J. R. et al., 2014. The relationship between DNA methylation, genetic and expression inter-individual variation in untransformed human fibroblasts. *Genome Biol.,* 15(2), p. R37.

Wahdan-Alaswad, R. et al., 2013. Glucose promotes breast cancer aggression and reduces metformin efficacy. *Cell Cycle,* 12(24), pp. 3759-3769.

Wallbilich , J. J. et al., 2017. High Glucose-mediated STA3 Activation in Endometrial Cancer Is Inhibited by Metformin. *PLoS One,* 12(1), p. e0170318.

Wang, J. et al., 2018. LPS-induces IL-6 and IL-8 gene expression in bovine endometrial cells “through DNA methylation”. *Gene,* Volume 677, pp. 266-272.

Wang, S., Lei, K., Liu, J. & Jia, Y., 2017. Continuous use of metformin can improve survival in type 2 diabetic patients with ovarian cancer. *Medicine (Baltimore),* 96(29), p. e7605.

Wang, X. et al., 2018. DNA methylcytosine dioxygenase ten-eleven translocation 2 enhances lipopolysaccharide-induced cytokine expression in human dental pulp cells by regulating MyD88 hydroxymethylation. *Cell and Tissue Research,* Volume 373, p. 477–485.

Wang, Y. et al., 2012. The Unfolded Protein Response Induces the Angiogenic Switch in Human Tumor Cells through the PERK/ATF4 Pathway. *Cancer Res,* Volume 72, pp. 5396-5406.

Wang, Y. et al., 2010. Autocrine production of interleukin-6 confers cisplatin and paclitaxel resistance in ovarian cancer cells. *Cancer Letters,* 295(1), pp. 110-123.

Wang, Y. et al., 2011. Autocrine production of interleukin-8 confers cisplatin and paclitaxel resistance in ovarian cancer cells. *Cytokine,* 56(2), pp. 365-375.

Wang, Y. et al., 2013. STAT3 activation in response to IL-6 is prolonged by the binding of IL-6 receptor to EGF receptor. *PNAS,* 110(42), pp. 16975-16980.

Warburg, O., Wind, F. & Negelein, E., 1927. The metabolism of tumours in the body. *J Gen Physiol.,* Volume 8, pp. 519 - 530 .

Ward, P. S. et al., 2011. The common feature of leukaemia-associated IDH1 and IDH2 mutations is a neomorphic enzyme activity that converts α-ketoglutarate to 2-hydroxyglutarate. *Cancer Cell,* 17(3), pp. 225 - 234.

Ware, M. J. et al., 2016. Generation of Homogenous Three-Dimensional Pancreatic Cancer Cell Spheroids Using an Improved Hanging Drop Technique. *TISSUE ENGINEERING: Part C,* 22(4), pp. 312 - 322.

Weber, A. et al., 2018. Succinate Accumulation Is Associated with a Shift of Mitochondrial Respiratory Control and HIF-1α Upregulation in PTEN Negative Prostate Cancer Cells. *Int. J. Mol. Sci.,* 19(7), p. 2129.

Weber, M. et al., 2007. Distribution, silencing potential and evolutionary impact of promoter DNA methylation in the human genome. *Nature Genetics,* Volume 39, pp. 457-466.

Wehbe, H. et al., 2006. Interleukin-6 Contributes to Growth in Cholangiocarcinoma Cells by Aberrant Promoter Methylation and Gene Expression. *Cancer Res,* Volume 66, pp. 10517-10524.

Wilcox, C. B. et al., 2005. High-resolution methylation analysis of the BRCA1 promoter in ovarian tumors. *Cancer Genet Cytogenet,* Volume 159, pp. 114-122.

Willows, R. et al., 2017. Phosphorylation of AMPK by upstream kinases is required for activity in mammalian cells. *Biochem J,* 474(17), pp. 3059-3073.

Wise, D. R. et al., 2008. Myc regulates a transcriptional program that stimulates mitochondrial glutaminolysis and leads to glutamine addiction. *Proc Natl Acad Sci U S A,* 105(48), pp. 18782 - 18787.

Wise, D. R. & Thompson, C. B., 2010. Glutamine Addiction: A New Therapeutic Target in Cancer. *Trends Biochem Sci,* 35(8), pp. 427 - 433.

Wong, C. C., Qian, Y. & Yu, J., 2017. Interplay between epigenetics and metabolism in oncogenesis: mechanisms and therapeutic approaches. *Oncogene,* Volume 36, p. 3359–3374.

Wortel, I. M. N., van der Meer, L. T., Killberg, M. S. & van Leeuwen, F. N., 2017. Surviving StressL Modulation of ATF4-Mediated Stress Responses in Normal and Malignant Cells. *Trends Endocrinol Metab.,* 28(11), pp. 794-806.

Wu, D. et al., 2018. Glucose-regulated phosphorylation of TET2 by AMPK reveals a pathway linking diabetes to cancer. *Nature,* Volume 559, pp. 637-641.

Xiao, M. et al., 2012. Inhibition of α-KG-dependent histone and DNA demethylases by fumarate and succinate that are accumulated in mutations of FH and SDH tumor suppressors. *Genes Dev. ,* 26(12), pp. 1326-1338.

Xu, L. & Fidler, I. J., 2000. Interleukin 8: An Autocrine Growth Factor for Human Ovarian Cancer. *Oncology Research,* Volume 12, p. 97–106.

Xu, S. et al., 2018. Metformin Suppresses TUmour Progression by Inactivating Stromal Fibroblasts in Ovarian Cancer. *Mol Cancer Ther.,* 17(6), pp. 1291-1302.

Xu, W. et al., 2011. Oncometabolite 2-Hydroxyglutarate Is a Competitve Inhibitor of α-Ketoglutarate-dependent Dioxygenases. *Cancer Cell,* 19(1), pp. 17 - 30.

Yang, H. et al., 2008. MicroRNA expression profiling in human ovarian cancer: miR-214 induces cell survival and cisplatin resistance by targeting PTEN. *Cancer Res,* Volume 68, pp. 425-433.

Yang, L. et al., 2014. Metabolic shifts toward glutamine regulate tumor growth, invasion and bioenergetics in ovarian cancer. *Mol Syst Biol.,* 10(5), p. 728.

Yang, M. & Pollard, P. J., 2013. Succinate: A New Epigenetic Hacker. *Cancer Cell,* 23(6), pp. 709-711.

Yang, M., Soga, T. & Pollard, P. J., 2013. Oncometabolites: linking altered metabolism with cancer. *J Clin Invest.,* 123(9), pp. 3652-3658.

Yang, N. et al., 2008. MicroRNA Microarray Identifies Let-7i as a Novel Biomarker and Therapeutic Target in Human Epithelial Ovarian Cancer. *Cancer Res,* Volume 68, pp. 10307-10314.

Yang, Q. et al., 2016. AMPK/α-Ketoglutarate Axis Dynamically Mediates DNA Demethylation in the Prdm16 Promoter and Brown Adipogenesis. *Cell Metabolism,* 24(4), pp. 542-554.

Yang, Q. et al., 2020. Metabolic changes during malignant transformation in primary cells of oral lichen planus: Succinate accumulation and tumour suppression. *Journal of Cellular and Molecular Medicine,* 24(2), pp. 1179-1188.

Yang, X. et al., 2021. Metformin Antagonizes Ovarian Cancer Cells Malignancy Through MSLN Mediated IL-6/STAT3 Signaling. *Cell Transplantation,* Volume 30, p. 09636897211027819.

Yan, J. et al., 2020. Insulin and Metformin Control Cell Proliferation by Regulating TDG-Mediated DNA Demethylation in Liver and Breast Cancer Cells. *Molecular Therapy Oncolytics,* Volume 18, pp. 282-294.

Yan, L. et al., 2015. Regulation of tumor cell migration and invasion by the H19/let-7 axis is antagonized by metformin-induced DNA methylation. *Oncogene,* 34(23), pp. 3076-84.

Yao, L. et al., 2021. Quantitative proteomic biomarkers from extracellular vesicles of human seminal plasma in the differential diagnosis of azoospermia. *Clin Transl Med.,* 11(5), p. e423.

Ye, J. et al., 2012. Primer-BLAST: A tool to design target-specific primers for polymerase chain reaction.. *BMC Bioinformatics,* Volume 13, p. 134.

Yin, X. & Xu, Y., 2016. Structure and Function of TET Enzymes. In: A. Jeltsch & R. Jurkowska, eds. *DNA Methyltransferases - Role and Function.* s.l.:Springer, pp. 275-302.

Ylisaukko-oja, S. K. et al., 2006. Germline fumarate hydratase mutations in patients with ovarian mucinous cystadenoma. *European Journal of Human Genetics,* Volume 14, p. 880–883.

Yong, C., Stewart, G. D. & Frezza, C., 2020. Oncometabolites in renal cancer. *Nature Reviews Nephrology,* Volume 16, p. 156–172.

Yoo, K., Park, Y. & Chang, S., 2012. DNA hypomethylation of interleukin 8 in clear cell renal cell carcinoma. *Oncology Letters,* 5(1), pp. 39-42.

Yoon, S. et al., 2010. STAT3 transcriptional factor activated by reactive oxygen species induces IL6 in starvation-induced autophagy of cancer cells. *Autophagy,* 6(8), pp. 1125-1138.

Yoon, S. et al., 2012. NF-κB and STAT3 cooperatively induce IL6 in starved cancer cells. *Oncogene,* Volume 31, p. 3467–3481.

Yoshida, Y. et al., 2004. Interleukin 1 Activates STAT3/Nuclear Factor-κB Cross-talk via a Unique TRAF6- and p65-dependent Mechanism. *Mechanisms of Signal Transduction,* 279(3), pp. 1768-1776.

Yu, C. et al., 2002. STAT3 activation is required for interleukin-6 induced transformation in tumor-promotion sensitive mouse skin epithelial cells. *Oncogene,* Volume 21, p. 3949–3960.

Yu, X. et al., 2012. High levels of glucose induce “metabolic memory” in cardiomyocyte via epigenetic histone H3 lysine 9 methylation. *Molecular Biology Reports,* Volume 39, p. 8891–8898.

Zand, B. et al., 2016. Role of Increased n-acetylaspartate levels in cancer. *J Natl Cancer Inst,* 108(6), p. djv426.

Zanoni, M. et al., 2016. 3D tumor spheroid models for in vitro therapeutic screening: a systematic approach to enhance the biological relevance of data obtained. *Sci Rep,* Volume 6, p. 19103.

Zebrowski, B. K. et al., 1999. Markedly elevated levels of vascular endothelial growth factor in malignant ascites. *Ann Surg Oncol,* 6(4), pp. 373-8.

Zhang, J. et al., 2016. Tet3-Mediated DNA Demethylation Contributes to the Direct Conversion of Fibroblast to Functional Neuron.. *Cell Rep,* 17(9), pp. 2326-2339.

Zhang, L., Li, P., Wang, T. & Zhang , X., 2015. Prognostic values of 5-hmC, 5-mC and TET2 in epithelial ovarian cancer. *Archives of Gynaecology and Obstetrics,* 29(4), pp. 891-897.

Zhang, L. et al., 2020. Fumarate hydratase FH c.1431_1433dupAAA (p.Lys477dup) variant is not associated with cancer including renal cell carcinoma. *Human Mutation,* Volume 41, p. 103–109.

Zhang, Q. et al., 2015. Tet2 is required to resolve inflammation by recruiting Hdac2 to specifically repress IL-6. *Nature,* Volume 525, pp. 389-393.

Zhang, R. et al., 2015. Inhibitory effects of metformin at low concentration on epithelial-mesenchymal transition of CD44+CD117+ ovarian cancer stem cells. *Stem Cell Res Ther,* Volume 6 , p. 262.

Zhang, S. et al., 2008. Identification and Characterisation of Ovarian Cancer-initiating Cells from Primary Human Tumours. *Cancer Res,* 68(11), pp. 4311 - 4320.

Zhang, T. et al., 2019. Phosphorylation of TET2 by AMPK is indispensable in myogenic differentiation. *Epigenetics & Chromatin,* Volume 12, p. 32.

Zhang, T. et al., 2013. Identification of potential biomarkers for ovarian cancer by urinary metabolomic profiling. *J Proteome Res,* 4(12), pp. 505-12.

Zhang, Y. W. et al., 2017. Acetylation enhances TET2 function in protecting against abnormal DNA methylation during oxidative stress. *Mol Cell.,* 65(2), p. 323–335.

Zhao, T., Mu, X. & You, Q., 2017. Succinate: An initiator in tumorigenesis and progression. *Oncotarget,* 8(32), p. 53819–53828.

Zheng, J., Santoni, G., Xie, S. & Lagergren, J., 2021. Improved prognosis in gastric adenocarcinoma among metformin users in a population-based study. *Br J Cancer,* Volume 125, pp. 277 - 283.

Zhong, T. et al., 2017. Metformin alters DNA methylation genome-wide via the H19/SAHH axis. *Oncogene,* Volume 36, p. 2345–2354.

Zhuang, Y., Chan, D. K., Haugrud, A. B. & Miskimins, W. K., 2014. Mechanisms by which low glucose enhances the cytotoxicity of metformin to cancer cells both in vitro and in vivo. *PLoS One ,* 9(9), p. e108444.